HAFNIUM ISOTOPE EVIDENCE ON THE SOURCES OF GRENVILLIAN DETRITAL ZIRCON DEPOSITED AT THE GREAT UNCONFORMITY

by

AARON L. HANTSCHE

B.S., University of Texas at Austin, 2013

A thesis submitted to the

Faculty of the Graduate School of the

University of Colorado in partial fulfillment

of the requirement for a degree of

Master of Science

Department of Geological Sciences

2015

This thesis entitled:

Hafnium Isotope Evidence on the Sources of Grenvillian Detrital Zircon
Deposited at the Great Unconformity

written by Aaron L. Hantsche

has been approved for the Department of Geological Sciences

Dr. G. Lang Farmer

Dr. Shemin Ge

Date:

The final copy of this thesis has been examined by the signatories, and we find that both the content and the form meet acceptable presentation standards of scholarly work in the above mentioned discipline

Hantsche, Aaron L., (M.Sc., Geological Sciences)

Hafnium Isotope Evidence on the Sources of Grenvillian Detrital Zircons Deposited at the Great Unconformity

Thesis directed by Dr. G. Lang Farmer

ABSTRACT

Detrital zircon U-Pb ages are commonly used to assess the provenance of siliciclastic sediments. However, in Cambrian siliciclastic units in North America, such determinations are limited by the wide spatial distribution of Proterozoic crystalline basement rocks with similar U-Pb ages. In this study, combined U-Pb and Hf isotopic data were obtained from 1.0 to 1.3 Ga, so called "Grenvillian", detrital zircons in sedimentary rocks from central North America, in order to better define the geographic source locations and sediment transport directions after the breakup of the Mesoproterozoic supercontinent Rodinia. The whole-rock radiogenic isotopic compositions of granitic rocks from a 1.086 ± 0.02 Ga anorthosite-charnockite-mangerite-granite (AMCG) suite in Sonora, Mexico were used to identify the petrogenetic nature of these Grenville-age crustal intrusions. Additionally, Hf isotopic compositions were determined for zircon from this suite of samples to help complete the existing Hf isotope database for potential sources of Grenvillian detrital zircon. All samples have low measured ε_{Hf} values ranging from -25.5 to -21.1 and are determined to have crystallized from a melt that incorporated a large component of Paleoproterozoic crust of the Yavapai/Mazatzal Province that underlies portions of northwestern Mexico. These data and existing isotopic data for other 1.0 Ga to 1.3 Ga rocks throughout North America were applied to determine the provenance of Grenvillian detrital zircon found in four Neoproterozoic and Cambrian basal sandstone units from the central U.S. Three of these samples were are from fluvial to shallow marine depositional environments, and

are interpreted to be deposited after the breakup of Rodinia during the transgression of the early Paleozoic Sauk Sea; the fourth sample is a Neoproterozoic injectite sandstone that is interpreted as a pre-Sauk Sea sedimentary unit. The easternmost sample, the Cambrian Lamotte Sandstone in southeastern Missouri, is observed to contain a major zircon population of ~1.1 Ga with a narrow range of Hf isotopic compositions that range from ε_{Hf} = -27.4 to -20.0. Samples from basal sandstones from Colorado drill cores have a broad Grenvillian age peak from 1.0 – 1.3 Ga, accompanied by peaks at ~1.4 and ~1.7 Ga. The Grenvillian detrital zircon in these samples exhibit a wide range of ε_{Hf} that falls in the wide range of values also observe in the nearby Neoproterozoic Tava Sandstone Injectites (ε_{Hf} = -42.5 to -14.4). The Lamotte Sandstone in the east potentially originated from a limited catchment area in the Southern Appalachian Mountains, while western basal sandstones incorporated zircon from multiple sources, such as the Southern Appalachians, the Adirondacks, the Llano Uplift, the Franklin Mountains, and local felsic intrusions. Interestingly, Flathead sandstone from central Wyoming is dominated by ~1.7 Ga zircons with a distinct absence of Grenvillian zircon, indicating that the supply of Grenvillian zircon from the south and east had been shut off to this region. Broadly, the observed increase in range of U-Pb and ε_{Hf} values with westward geographic position is interpreted to be the result of the mixing of multiple zircon sources with westward sediment transport. The presence or absence of Grenvillian detrital zircon in basal sandstones provides information of the relative timing and paleogeography of Laurentia during the Cambrian. The absence of Grenvillian zircon is unique in these sandstones, and requires some type of sediment transport barrier, such as a topographic structural high of the proposed Paleozoic Transcontinental Arch, or a potential oceanic barrier, such as the Sauk Sea. These observation will require additional detrital zircon data from other North American basal sandstones to confirm and establish the sedimentation controls of Laurentian cross-continent zircon transport.

ACKNOWLEDGEMENTS

The education and research I have accomplished at the University of Colorado have helped to craft my strengths as a geologist, a research scientist, and a teacher. Despite all the effort that I have put into this, I wouldn't be where I am today without the guidance, assistant, and support of my advisor, my teachers, my colleagues, and my friends.

I would first like to thank my advisor, Lang Farmer. Somehow, Lang managed to repeatedly explain isotope geology, detrital zircon provenance, and the tectonic history of North America, to me without making me feel like an idiot. His patience, instruction, and willingness to share his knowledge with me has taught me invaluable lessons about life as an instructor and researcher. By the end of my stint in Boulder, I have finally been convinced that I possess a grain of knowledge about isotope systematics, analytical techniques, and the tectonic significance of detrital zircon provenance studies.

Additionally, I would like to thank Dr. David Budd and Dr. Chuck Stern for taking the time out of their schedules to review my thesis, and I appreciate their insights toward improving it and their feedback during my defense.

Thanks to Christine Siddoway at Colorado College, who provided samples and feedback for this project. She also brought Lang and I out to see the Tava Sandstone Injectite near Manitou Springs, which was the first time I have ever seen sedimentary intrusions – very cool!

In no particular order, I would like to thank the following people: Craig Jones, for much of my knowledge of tectonic history of the Western U.S., Alan Seeling, for providing samples of previously unstudied basal sandstones from the Denver-Julesburg Basin, Becky Flowers and Jim Metcalf, for the use of their lab for all stages of mineral separation, Dr. Lupe Espinosa Maldonado and Dr. Jose-Luis Rodriguez Castañeda, for guiding Lang and I through the desert of Sonora, Mexico, Mark Winternheimer, for supplying samples of the Lamotte Sandstone in Missouri, Emily Verplanck, for her help training my to use the TIMS facility at CU, Dr. George Gehrels, Mark Pecha, and the lab team at the University of Arizona, for teaching me to use the laser ablation systems and mass spectrometers, Paul Boni, for graciously letting me crush rocks in his workspace, Amanda Howard, for her previous work and help with error ellipses, Mary Krause, Kevin Mahan, Joe Smyth, Peter Molnar, Nathan Niemi, Marin Clark, Chris Fedo, and anyone else who helped with my thesis work.

It is important to consider my background when coming to CU, so I'd like to give some credit to a few people from the University of Texas. Particularly, I would like to thanks Dr. Mark Cloos, for teaching me the basics of how to conduct a research project and how to produce high quality scientific work. Thanks to Dr. Bill Carlson, who gave me a strong background in petrology, which I transferred to teaching both mineralogy and petrology. Lastly, among others, thanks to Marin Trautman, Paul Betka, Nolan Townsend, Randy Marrett, and Whitney Behr.

Thanks to my friends and colleagues who helped create a fun environment both at school and in the mountains: Josh Johnson and Jacky Baughman, my officemates, classmates, and skimates, Derek Weller, who revamped the Mineralogy lab with me, Cailey Condit, who also thinks about Proterozoic Laurentia on a daily basis, Jess Stanley, for teaching me to use heavy liquids, and all my friends I met here in Boulder.

I'd like to thank my mom, dad, sister, and the rest of my family for their support of my slowly advancing education. My sister spent a whole summer in Boulder, and I felt like it went by so fast. My parents each took trips to visit me, and I was glad for the opportunity to show them the beauty of the Northern Front Range. Thanks to my whole family for all that they've given me over the years!

And of course, I would be remiss to not save a big thank you for Sara Burk. We have been through very tough times, but the last two years have seen us get stronger together. This woman supported me in my hours and hours of late night thesis writing, figure making, and reference checking, with hardly a complaint. Coffee, food, rides – anything I needed to get my work done – she was there for me. Thank you so much for the continuous support through my Master's work. I love you, Sara!

TABLE OF CONTENTS

LIST OF TABLES

LIST OF FIGURES

Introduction

The formation and subsequent break up of Precambrian supercontinents is a poorly understood aspect of Earth's evolution, principally because of the lack of an extensive geologic record preserving information on how these processes were initiated and how they evolved through time. For example, in the case of the Mesoproterozoic to Neoproterozoic supercontinent Rodinia, few sedimentary rocks are preserved from the time of Rodinia stability (~1.1 to 0.78 Ga) from which the paleogeography of the stable continent can be inferred (Li et al., 2008). Instead extensive sedimentary successions are mainly preserved from the period during, and subsequent to, the breakup of Rodinia in the Neoproterozoic and Cambrian, when sediments were deposited at and above the so-called "Great Unconformity" (Sloss, 1963; Sloss, 1988; Fedo and Cooper, 2001; Spencer et al., 2014). These sedimentary rocks do, however, provide an opportunity to address aspects of the disaggregation of Rodinia, such as whether, and where, topographically high rift flanks were produced at the loci of continental separation, how changes in the topography of Rodinia affected the size and orientation of surface river systems, and the history of marine transgression onto these fragments through time. Information on these issues can be obtained from sedimentary rocks through an assessment of their original depositional settings and, in the case of siliciclastic sedimentary rocks, by understanding the sources (provenance) of the detrital sediments.

Laurentia, which comprises present day North America, is one of the most extensively studied continental fragments produced during the disassembly of Rodinia. Studies of preserved Neoproterozoic and Cambrian sedimentary rocks have concluded that river systems during this period were dominantly oriented from east to west (present coordinates) during this entire time period, suggesting that the paleoslope on the developing continent was from east to west despite the fact that rifting occurred along every margin of the continent and must have resulted in multiple localized areas of higher elevation (Rainbird et al., 1997; 2012; Stewart et al., 2001; Whitmeyer and Karlstrom, 2007). The primary evidence supporting east to west sediment transport comes from detrital zircon U-Pb age determinations from

Neoproterozoic and Cambrian sedimentary rocks, principally from western portions of Laurentia. These siliciclastic units include a significant age population of 1.0 Ga to 1.3 Ga zircon grains ("Grenvillian zircon") which are typically interpreted to be derived from the erosion at eastern margin of the Laurentian continent, which, at the this time, was comprised in part of Mesoproterozoic igneous and metamorphic rocks associated with the so-called Grenville Orogeny (Hynes and Rivers, 2010). If true, this suggests that the highlands associated with the Grenville Orogeny remained a principal site erosion and sediment production during the breakup of Rodinia, despite the likelihood that other margins of Laurentia were also sites of surface elevation increases during this time.

The present study was undertaken to test whether Grenvillian detrital zircon in Cambrian sandstones in western Laurentia were all derived from the same source regions at the eastern margin of the continent. A source region for detrital zircon is defined herein as the original source of igneous and/or metamorphic zircons that were later incorporated into surface sediments. Detrital zircon U-Pb and Hf isotopic data are employed to determine the zircon sources, using the basic concept that if potential sources of Grenvillian zircon can be distinguished on the basis of these combined data sets, then it should be possible to better spatially resolve the provenance of Grenvillian detrital zircon grains. There are two basic requirements for such a study. First, there must be sufficient isotopic data from zircon in potential Grenvillian source rocks and, second, isotopic data from Grenvillian detrital zircon must be obtained. This project incorporates both activities. Igneous zircon Hf isotopic data were lacking for Mesoproterozoic intrusions in Northern Mexico, therefore, in the second chapter of this thesis, petrographic analyses and radiogenic isotopic data are used to assess the genetic source of ~1.1 Ga anorthosites and granitic rocks from Sonora, Mexico which are part of an anorthosite-charnockite-mangerite-granite (AMCG) suite. Igneous zircon U-Pb age and Hf isotopic data were obtained as part of this study for use in detrital zircon provenance analysis.

The third thesis chapter uses U-Pb ages and Hf isotopic data from zircon in Grenvillian igneous and metamorphic rocks in northern Sonora and from other 1.0-1.3 Ga basement rocks in Laurentia culled from the literature to assess the provenance of Grenvillian detrital zircon found in Neoproterozoic to Cambrian basal sandstones. These provenance determinations are used to suggest that Grenvillian detrital zircon in these rocks were obtained from both the southern and eastern portions of the continent, providing new insights on the paleogeography of the Laurentian continent. .

To provide the necessary context for the next two chapters, a basic review of pertinent aspects of the geologic evolution of Laurentia is given in the following text, along with a review of both zircon U-Pb and Hf isotopic systematics.

Geologic Setting and Background

The Mesoproterozoic supercontinent Rodinia was assembled from 900 to 1300 Ma, when Paleoproterozoic and Archean continental fragments were sutured together around the central block of Laurentia (Li et al., 2008). One of these sutures is associated with the Grenville Orogeny, which dominated eastern Laurentian geological activity from 1.0-1.3 Ga and is recorded in North America by the Grenville Province, an accretionary terrane that extends from eastern Canada to the southeast United States (van Schmus et al., 1993; Whitmeyer and Karlstrom, 2007; Hynes and Rivers, 2010). A contemporaneous accretionary terrane, exposed in Llano Uplift in central Texas, also exists on the southern margin of Laurentia (Whitmeyer and Karlstrom, 2007). Mesoproterozoic crustal intrusions in southwest Laurentia such as the Franklin Mountains in west Texas, the Little Hatchet Mountains in New Mexico, the Pikes Peak Batholith in Colorado, and an AMCG suite in Sonora, Mexico, were all intruded contemporaneously with the Grenville Orogeny but within existing Laurentian Paleoproterozoic crust (Anderson and Silver, 1981; Smith et al., 1999; Whitmeyer and Karlstrom, 2007; Amato and Mack, 2012; this study).

Rodinia remained a stable supercontinent until ~0.78 Ga when rifting began along the western margin of Laurentia (Li et al., 2008). Rifting along the southern and eastern margins of Laurentia began later, between 0.62-0.55 Ga (Thomas, 1991; 2011; Whitmeyer and Karlstrom, 2007). Weathering and erosion during the long period of Rodinia stability exposed Proterozoic and Archean basement rocks, removing most siliciclastic sedimentary rocks that might have been present prior to rifting during the late Neoproterozoic (Li et al., 2008).

During and after rifting, sedimentary sequences began to accumulate on the western continental margin, with accommodation space developing as a result of thermal subsidence along the rift flanks (Fedo and Cooper, 2001). The continental transgression of the Sauk Sea during this time influenced the deposition and preservation of marine sediments deposited directly over the exposed cratonal basement rocks in the latest Proterozoic and early Cambrian (Fedo and Cooper, 2001). The contact between shallow marine sandstones and exposed crystalline basement corresponds to the so-called Great Unconformity in a large portion of the western and midcontinent regions (Sloss, 1963). The distribution and thickness of the Sauk Sequence, the basal sedimentary package beginning with the shallow marine sandstones of the Sauk Sea transgression, has been long known (Sloss, 1960, 1963), but the source for the sediments has been speculative until recent advancements in U-Pb detrital zircon geochronology (Rainbird et al., 1997; Stewart et al., 2001; Gehrels et al., 2011; Schoenborn et al., 2012; Gehrels and Pecha, 2014; Howard et al., 2015; this study).

Sedimentologic data and previous detrital zircon provenance analyses are consistent with a general east-to-west paleoflow direction for Laurentian fluvial systems during the early Cambrian, with highlands at the eastern margin of the continent representing the ultimate source of siliciclastic sediments comprising basal sandstones in the central and western continent (Rainbird et al., 1997; Gehrels and Pecha, 2014). The eastern highlands were either a) the result of uplift associated with the development of a rifted margin at or near the time of sediment transport, or b) topography remaining from the Grenville orogeny (Lambiase and Bosworth, 1995). However, while many workers have favored Grenville Province in easternmost Laurentia for Grenvillian detrital zircon (Rainbird et al., 1992; 1997; 2012; Stewart et al., 2001; Gehrels and Pecha, 2014), other potential sources for zircon of this age do exist along the southern and western margins of Laurentia (Anderson and Silver, 1981; Van Schmus et al, 1993; Whitmeyer and Karlstrom, 2007; Howard et al., 2015). One goal of this study is to assess the potential role of these sources in providing detrital zircon found in on-craton basal sandstones of the Great Unconformity through the use of zircon U-Pb and Hf isotope systematics.

U-Th-Pb Systematics

Dating zircons using the U-Th-Pb isotopic system relies on the facts that uranium substitutes readily into the zircon ($ZrSiO_4$) crystalline structure and subsequently undergoes radioactive decay, with the two isotopes of uranium, ^{235}U and ^{238}U, decaying through an extensive decay chain to two different isotopes of lead, ^{207}Pb and ^{206}Pb (Gehrels, 2014). The zircon crystallization age can be determined solely from Pb isotopic measurements, with no need to measure the parent isotopic composition (Hiess et al., 2012). Using laser ablation mass spectrometry and standard-bracketing techniques, isotopes ^{204}Pb (stable), ^{206}Pb (from ^{238}U with a half-life of 4.47 Ga), ^{207}Pb (from ^{235}U with a half-life of 0.70 Ga, and ^{208}Pb (from ^{232}Th with a half-life of 14.01 Ga) can be measured to produce a U-Pb age (Jaffey et al., 1971; Gehrels 2014)). With one ratio based on the U decay system ($^{206}Pb^*/^{207}Pb^*$), the crystallization age from the ratios can be found by comparison to the concordia derived by solving for *t* in the following formula using Wetherill (1956).

$$\frac{^{206}Pb*}{^{207}Pb*} = \left(\frac{1}{137.82}\right) * \frac{(e^{\lambda_{235}t} - 1)}{(e^{\lambda_{238}t} - 1)}$$

Zircons are highly resistant to both physical and chemical weathering and can survive multiple sedimentary cycles. The routine preservation of detrital zircon in sandstones, for example, allow the zircon crystallization ages to be used to assess the zircon provenance. Though zircon U-Pb ages have been used in provenance studies for decades, the more recent development of rapid *in situ* analytical techniques, such as laser ablation inductively coupled plasma mass spectrometry (ICPMS), has rendered U-Pb age determinations in individual zircon grains quick and routine (Fedo et al., 2003; Gehrels, 2014). Using analyses of multiple detrital zircons (>100 grains) in siliciclastic sedimentary sample, it is now possible to fully identify both major and minor zircon age populations such rocks. The U-Pb detrital zircon age spectra generated in such a fashion can be used to define potential crustal source regions for these grains (Fedo et al., 2003).

Lu-Hf Systematics

Hafnium isotopic analyses of zircon have also become more routine over the past decade, again because of the development of in situ analysis techniques such as laser ablation multicollector-ICPMS (Blichert-Toft and Albarede, 1997; Scherer et al., 2007). In general, variations in the isotopic composition of Hf in terrestrial rocks and minerals occur due to the β decay of ^{176}Lu, a heavy rare earth element (HREE) to ^{176}Hf, a transition metal with a half-life of ~37.1 Ga (Patchett, 1983). Chemical differences cause differentiation during partial melting from a given source, however isotopic fractionation does not occur due to the high atomic weight of these nuclides (Vervoort and Patchett, 1996). During partial melting of mantle material, Lu preferentially stays in the residual rock, particularly if it is garnet bearing, similar to the Sm-Nd system (Vervoort and Patchett, 1996). The resulting depleted mantle has a higher Lu/Hf ratio than the extracted melt, resulting more rapid growth of the ^{176}Hf/^{177}Hf ratio in the mantle than in the crust, generating two distinct isotopic reservoirs (Vervoort and Patchett, 1996 Vervoort and Blichert-Toft, 1999). Derivation of zircon from melt extracted from the mantle will therefore have high ε_{Hf}, while zircon derived from the melting of older crustal material will have lower ε_{Hf} values (Scherer et al., 2007). An ε_{Hf} value corresponds to the ^{176}Hf/^{177}Hf ratio of a sample to the ^{176}Hf/^{177}Hf of the Chondritic Uniform Reservoir (CHUR) as follows:

$$\varepsilon_{Hf} = \left(\frac{\left(\frac{^{176}Hf}{^{177}Hf}\right)_{Sample}}{\left(\frac{^{176}Hf}{^{177}Hf}\right)_{CHUR}} - 1\right) * 1000$$

As a silicate melt begins to crystallize, another stage of internal chemical fractionation occurs as zircon preferentially incorporate Hf at weight percent levels, and Lu is excluded (Stevenson and Patchett, 1990; Amelin et al., 1999). The low Lu/Hf ratios, typically ≈ 0.002, incorporated by zircon makes Hf isotopic evolution negligible in zircon, as very little radiogenic Hf is produced in situ (Amelin et al., 1999; Kinny and Maas, 2003). Because the $^{176}Hf/^{177}Hf$ does not change significantly over time, detrital zircon will retain the Hf isotopic composition of the reservoir they crystallized from at the time of extraction (Scherer et al., 2007). Patchett (1983) showed that Hf isotopic composition is highly unlikely to be reset after crystallization, even in highly discordant zircon. The use of the Hf isotopic system in zircon is supported by the stability of the mineral and isotopic composition through geologic time and conditions. Importantly, Hf composition of individual crystals from a single melt also appear homogenous, allowing for the isotopic characterization of crystalline rocks as zircon sources for detrital zircon (Blichert-Toft and Albarede, 1997; Morel et al., 2008). With relatively fast and easy analyses, the higher spatial resolution of detrital zircon provenance studies provided by the combination of the Hf isotopic system with U-Pb ages demonstrates that zircon Hf isotopic ratios should be determined whenever possible for detrital studies (Andersen, 2003; Gehrels and Pecha, 2014).

Chapter Two

Radiogenic isotopic characterization of ~1.08 Ga anorthosites and granites from Sonora, Mexico

Introduction

Determining the origin of anorthosites and related igneous rocks (AMCG suite) remains an issue of active research, both in terms of how the magmas leading to the production of these rocks were generated, and why AMCG suite rocks were so were extensively produced worldwide at ~1.0 Ga to 1.3 Ga (Hynes and Rivers, 2010). Regardless of their exact mode of origin, isotopic data from AMCG rocks, including the anorthosites, clearly demonstrate that their parental magmas interacted extensively with older continental crust through which the magmas traversed prior to their final emplacement. As a result, anorthosites can serve as probes of the age and composition of deep continental crust that is not accessible for direct study (Farmer and DePaolo, 1983; 1984).

In North America, AMCG rocks are also critical to studies of the paleogeography of continental regions, as inferred from detrital zircon U-Pb ages and Hf isotopic compositions in siliciclastic sedimentary rocks, because many such rocks contain prominent detrital zircon ~1.1 Ga age populations. The AMCG rocks are a potential source of zircon in this age range, so the distribution and zircon fertility of these rocks is critical to understanding how and where detritus carrying zircon was transported, eroded, and deposited on the North American landscape through time.

In this study, we pursue both of these aspects of AMCG rock through a radiogenic isotopic study of ~1.1 Ga anorthosites and related igneous rocks found in northern Sonora, Mexico. Whole-rock Sm-Nd and Rb-Sr isotopic compositions were obtained in order to identify the source of the parent magma, and potentially identify the composition of any crustal material by the intrusions. Single zircon U-Pb ages and Hf isotopic compositions were obtained to confirm the crystallization age of these intrusions and to provide information on the isotopic compositions expected for Grenvillian detrital zircon derived from AMCG suite rocks in Sonora (Chapter 3).

Geologic Background

The Precambrian geologic history of Laurentia involves the accretion and subsequent disaggregation of multiple crustal blocks through time, with the blocks constituting the North American portions of Laurentia being identifiable through U-Pb zircon age determination and whole rock Nd isotopic data (Bennett and DePaolo, 1987; Whitmeyer and Karlstrom, 2007). In general, Archean crustal provinces are restricted to the northern portions of North America, while various Proterozoic crustal provinces, including the Paleoproterozoic Yavapai, Mazatzal, and Mojave Provinces, are found in the southern and western regions of the continent (Whitmeyer and Karlstrom, 2007). Of the Paleoproterozoic terranes, the Yavapai and Mazatzal Provinces are accretionary terranes that trend northwest-southwest across the entire midcontinent and are mutually distinguishable on the basis of their crystallization ages (1.7-1.8 Ga [Yavapai] versus 1.6-1.7 Ga [Mazatzal] (Van Schmus et al, 1993). The Mojave Province is interpreted as the product of the interaction of juvenile Paleoproterozoic crust with material derived from the Archean Wyoming Craton (Bennett and DePaolo, 1987). This province has distinctly lower measured ε_{Nd} values than the Yavapai and Mazatzal Provinces despite containing Paleoproterozoic igneous rocks with similar U-Pb crystallization ages (Bennett and DePaolo, 1987).

All three Paleoproterozoic provinces are present in Sonora, Mexico (Figure 2.1), although their geographic extent and relative dispositions are disputed (Van Schmus et al., 1993; Iriondo and Premo, 2003; Iriondo et al., 2004; Farmer et al., 2005). For example, some workers suggest that the Mojave Province, which is exposed in the so-called Caborca block in northern Sonora (Figure 2.1), was juxtaposed with Yavapai and Mazatzal terranes along the proposed left-lateral Mojave-Sonora megashear during the Mesozoic (Anderson and Silver, 2005). Others have suggested that the relative dispositions of the Paleoproterozoic terranes in Sonora have not been modified since their original juxtaposition during the construction of the Rodinian supercontinent (Iriondo and Premo, 2003; Iriondo et al. 2004; Farmer et al., 2005; Amato et al., 2009). In addition, although existing geochronologic and isotopic data reveal that the Mojave Province underlies the areas around the towns of Quitovac and Caborca (Figure 2.1), the overall

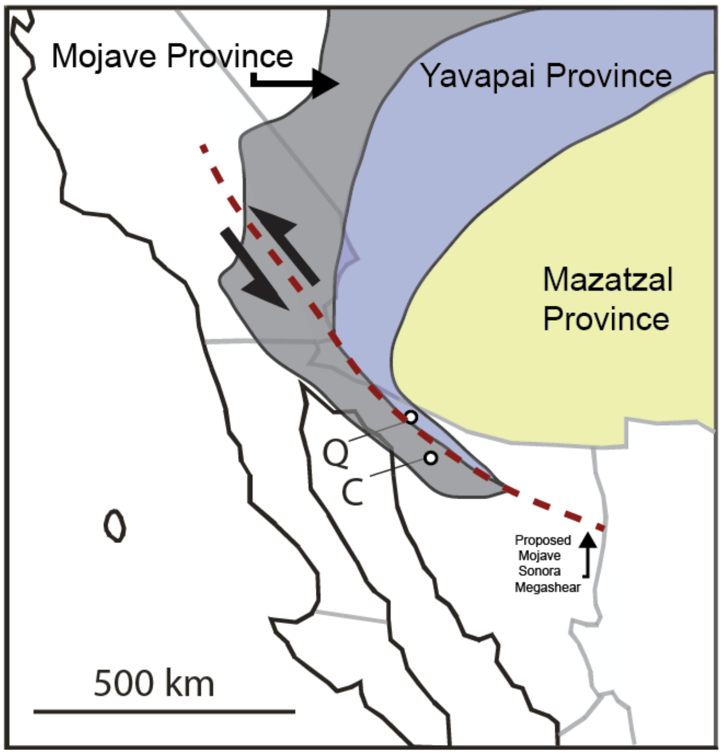

Figure 2.1. Cartoon of Proterozoic crustal provinces in Sonora, Mexico and outline of proposed Mojave Sonora Megashear. C = Caborca, Q = Quitovac. Modified from Farmer et al., 2005.

extent of the Mojave province in Sonora is not known (Iriondo et al., 2004; Farmer et al., 2005; Amato et al, 2009).

One method of better determining the distribution of Paleoproterozoic basement terranes in Sonora is through a comprehensive study of the isotopic compositions of Mesoproterozoic (~1.1 Ga) AMCG suite, igneous rocks exposed in the region. Elsewhere, AMCG rocks have been shown to contain a large proportion of preexisting crustal material (Bybee and Ashwal, 2015). If this is the case for AMCG rocks in Sonora, then the nature and distribution of unexposed Paleoproterozoic rocks can be inferred from the initial isotopic compositions of these AMCG samples.

To assess the isotopic compositions of Mesoproterozoic AMCG suite rocks in Sonora, Mexico, ten samples of previously unanalyzed Mesoproterozoic anorthosite and granite samples were collected for whole-rock Sm-Nd and Rb-Sr isotopic analyses by isotope dilution - thermal ionization mass spectrometry (ID-TIMS). These data are used to assess the origin of the parental magmas to the AMCG suite rocks and to further map the extent of Paleoproterozoic basement provinces in the subsurface beneath northern Sonora. In addition, individual zircon crystals were collected from four of these samples for U-Pb age determinations and Hf isotopic analysis.

Sample Descriptions

Each sample collected was approximately 2-5 kg in size and was selected from fresh interior rock obtained as far distant from zones of obvious alteration (fractures, faults, etc.) as possible. Nevertheless, most of the samples showed evidence of minor weathering.

The location, field exposure, and petrographic features of each sample is described below. Sample locations are listed in Table 2.1 and located on Figure 2.2. Samples QTV-1, QTV-2, QTV-3, and CP-3 are the only samples that yielded zircon for U-Pb and Hf analysis.

Table 2.1. List of sample locations for granites and anorthosites from Sonora, Mexico.

Field Area	Sample Name	Location (m)
Quitovac		
	13S-QTV-1	0325265 E 3467365 N
	13S-QTV-2	0325432 E 3467265 N
	13S-QTV-3	0325432 E 3467265 N
Sonoyta		
	13S-SNY-1	0317564 N 3527612 E
Sierra Pinta		
	13S-SP-1	0311560 E 3453864 N
Cerro Rajon		
	13S-CR-1	0409399 E 3361162 N
	13S-CR-2	0411790 E 3355591 N
Cerro Prieto		
	13S-CP-1	0431064 E 3366024 N
	13S-CP-2	0431917 E 3362357 N
	13S-CP-3	0431824 E 3362955 N

GPS data from UTM Zone 12N.

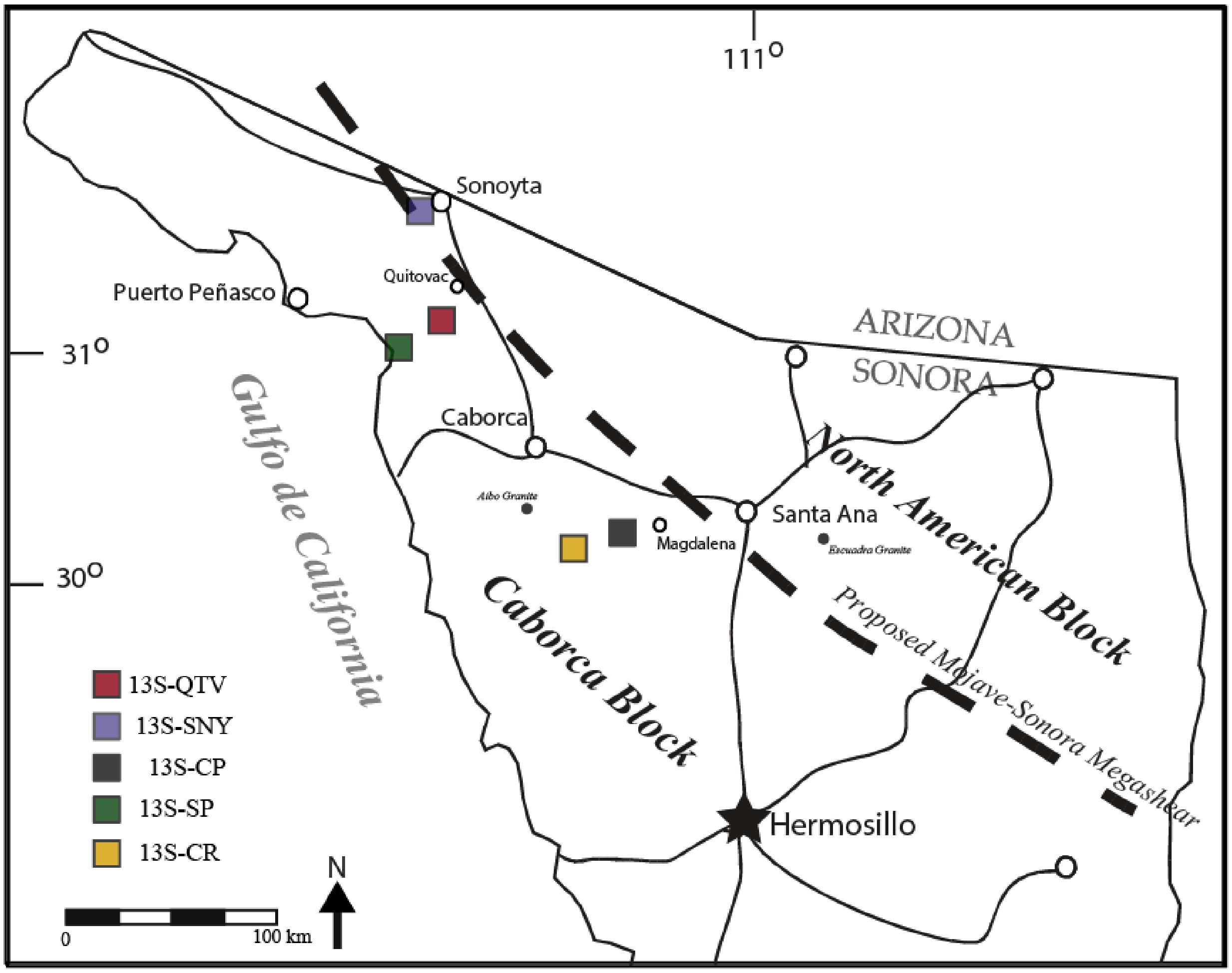

Figure 2.2. Map of Sonora, Mexcio, with sample locations indicated. GPS locations in Table 2.1. Aibo Granite location from Farmer et al., 2005. Escuadra Granite location from Amato et al., 2009. Map modified from Farmer et al., 2005.

13S-QTV (1, 2, 3)

Three AMCG suite samples were obtained from the Sierritas Blancas located ~20 km southwest of Quitovac, Sonora, Mexico (Fig. 2.2). Sample 13S-QTV-1 is from the Sierritas Blancas anorthosite, for which a ~1.1 Ga zircon U-Pb age is already available (Enriquez-Castillo et al., 2009). QTV-1 is from a ~20 m thick black anorthosite intrusive dike and consists of adcumulate anorthosite with largely unweathered plagioclase grains. A Michael Levy test for plagioclase gave an average extinction angle of ~12°, suggesting a more albitic plagioclase composition. Sparse, secondary sericite is present with interstitial quartz between larger plagioclase crystals. Plagioclase twinning shows minor deformation by the deflection of laminar twins and weak deformation banding (Figure 2.3A). Partially oxidized opaque minerals are common.

Samples QTV-2 and -3 were obtained from locations ~10m apart in the Murietta granite in the Sierritas Blancas. QTV-2 is less weathered and exhibits a bright pink color in outcrop due to large perthitic microcline crystals (Figure 2.3C). Sample QTV-3 displays a reddish brown hue, likely due to weathering as evidence by the widespread growth of sericite on most of the large feldspar crystals. Both samples contain perthitic microcline as the primary potassic feldspar (Figure 2.3D). Potassic feldspar crystals are much larger than either quartz or other mineral phase in the rocks. The primary mafic phase in both samples is biotite, which is commonly associated with opaque minerals. Plagioclase is present as a minor phase in both of these samples. These samples do not contain micrographic quartz exhibited by the nearby Aibo Granite to the southeast (Anderson and Silver, 1981).

13S-SNY-1

Sample SNY-1 was collected from an anorthosite body exposed at Sonoyta, Sonora, near the US international border (Fig 2.2). The anorthosite body is exposed in multiple hills ~ 4 km west of Sonoyta. The sample obtained is strongly weathered. Plagioclase grains have been almost completely altered to sericite (Figure 2.3B) although remnant twinning and crystal boundaries are visible in some grains.

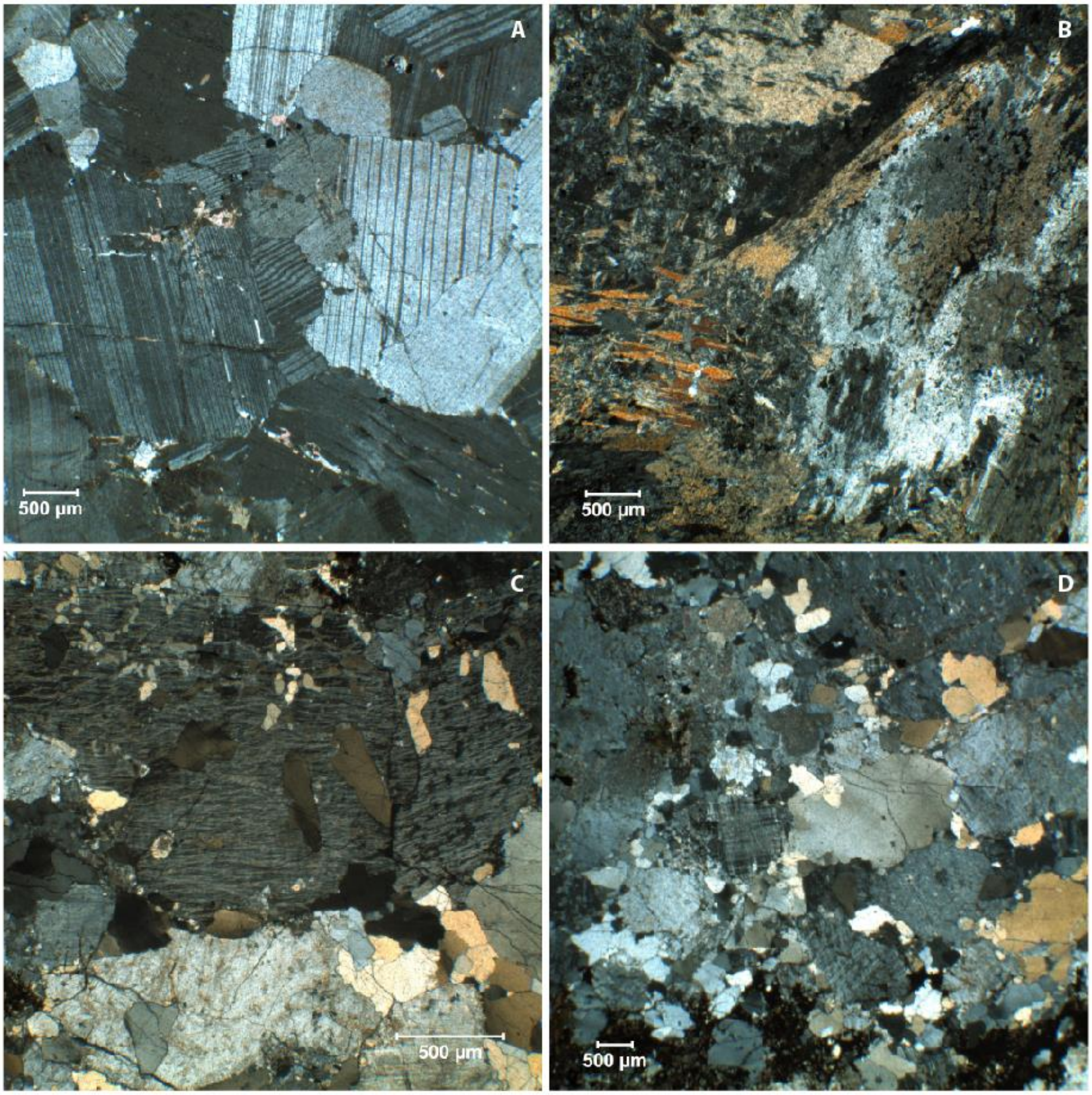

Figure 2.3. Photomicrographs of samples of anorthosite from Quitovac and Sonoyta, Mexico. A) QTV-1 anorthosite with weak deformation seen in albite twins; B) SNY-1 weathered anorthosite with sericitic alteration and oxide overprinting; C) QTV-2 granite with perthitic K-feldspar, quartz, and biotite assemblage; D) QTV-3 granite with microcline and equigranular texture.

13S-SP-1

Sample 13S-SP-1 was obtained from an anorthosite body exposed in Sierra Pinta, located ~50 km southeast of Puerto Peñasco and ~10 km from the eastern shore of the Gulfo de California (Figure 2.2). The anorthosite is exposed along the Sierra Pinta crest and adjacent small drainages. The sample itself is composed of large (up to 3 cm) white plagioclase grains exhibiting an orthocumulate texture filled in with interstitial secondary chlorite. The rock is extensively weathered, and sericite has replaced most of the plagioclase grains and chlorite is found in most of the interstices. Remnant lamellar twinning in the plagioclase is still evident in cross polarized light (Figure 2.4A).

13S-CR-2

Sample 13S-CR-2 was collected near Cerro Rajon, Sonora, Mexico, near the Bamori Complex of Anderson and Silver (1981), on a hill composed primarily of previously unstudied, weathered anorthosite (Fig. 2.2). Petrographically, the sample contains remnant plagioclase creating an adcumulate texture that has been mostly replaced by sericite.

13S-CP (1-3)

The first two of these samples was obtained from a previously unstudied anorthosite intrusion located ~20 km east of Cerro Raton near the town of Magdalena (Fig. 2.2). CP-1 is a pyroxene- and plagioclase-rich rock with a moderate degree of weathering and sericite replacement exposed at Rancho de San Antonio. The plagioclase forms an adcumulate texture. Pyroxene crystals have been mostly replaced by amphibole, though remnant clinopyroxene can be seen in the interior of amphibole grains (Figure 2.4B). Many replacement crystals still exhibit ~90°/90° cleavage, but are length slow, which suggests clinopyroxene replacement by amphibole. CP-2 is from an anorthosite intrusion exposed at Rancho de Santa Niña (Fig. 2.2). In thin section, this rock appears weathered and shows replacement of plagioclase grains by chlorite and sericite.

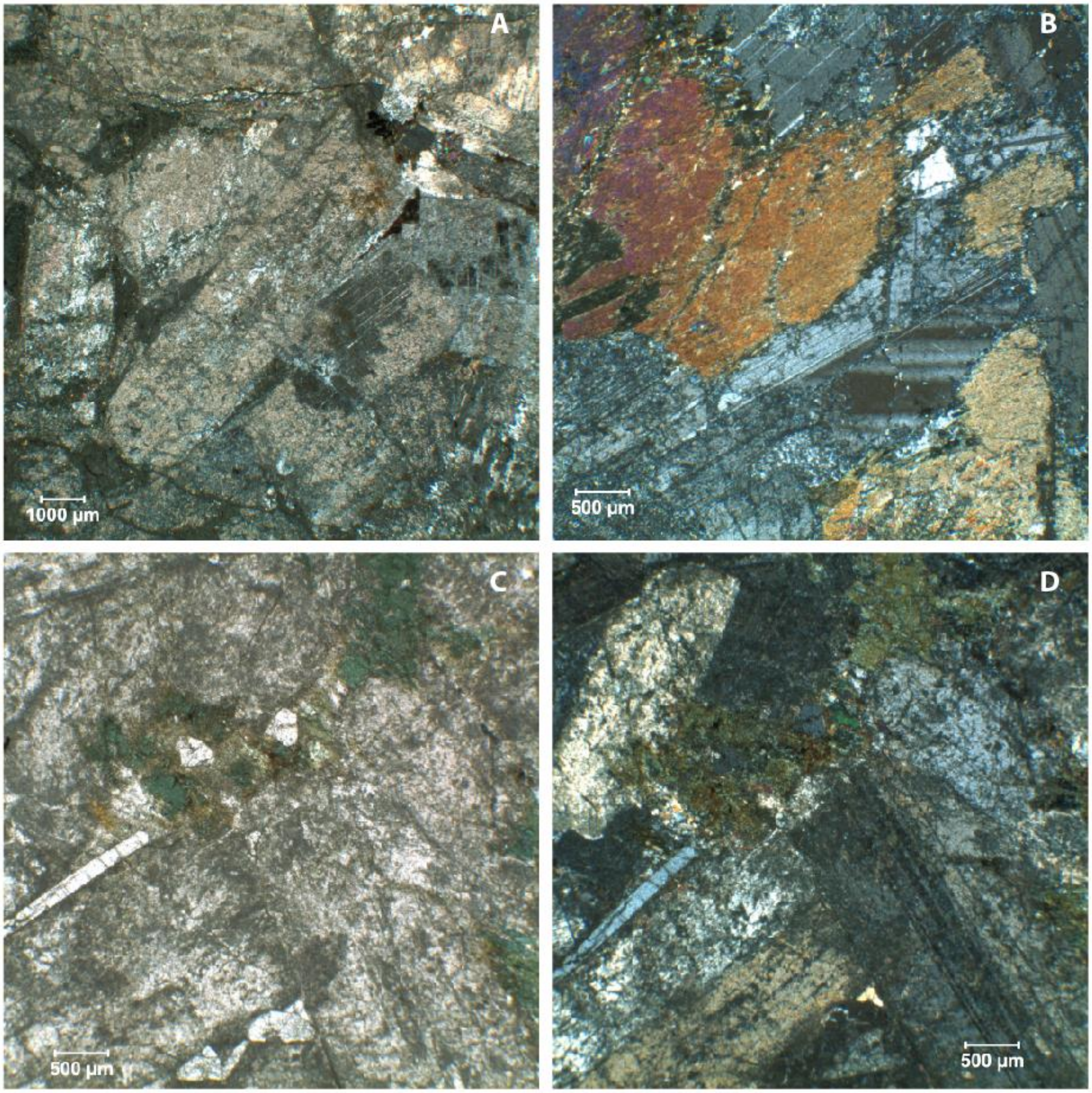

Figure 2.4. Photomicrographs of samples of anorthosite from south and east of Caborca, Mexico. A) SP-1 anorthosite with plagioclase mostly replaced by sericitization; B) CP-1 anorthosite with pyroxene overprinting; C) CP-3 weathered anorthosite with actinolite and scapolite in plane polarize light. D) CP-3 under cross polarize light for feldspar identification

The third sample, 13S CP-3, is from an anorthosite body exposed ~2 km to the north of Rancho de Santa Margarita (Fig. 2.2). This sample has a similar mineralogy to CP-2, but contains actinolite grains that have not been chloritized. Plagioclase still shows strong sericitization and an adcumulate texture. Biotite crystals can be seen spatially associated with the actinolite, though these were not visible in hand sample. Actinolite may be a replacement of primary clinopyroxene grains but no residual clinopyroxenes are preserved. Euhedral scapolite crystals are present, notably near the actinolite and biotite crystals (Figure 2.4C- PPL and 2.4D - XPL). Small (~150 μm) cross cutting calcite veins can be seen in thin section.

Methods

Physical Separation

All crushing and mineral separation was performed at the University of Colorado at Boulder. Rocks were broken into small fragments and crushed in a jaw crusher to pebble size. A split of this material was saved for whole-rock dissolution. The rest of the sample was then crushed in a disk mill and sifted through a 600 μm sieve. Disk mill plates were moved closer together until all grains passed through the sieve. Both jaw crusher and disk mill were cleaned thoroughly with wire brush and air hose between each sample.

Due to small sample size and projected low zircon yield, anorthosite samples were hand washed to remove clay-sized particles. Crushed sample was placed in a bucket and submerged in water with soap to prevent flocculation of clays. Sample was repeatedly agitated and allowed to settle for ten seconds before water and suspended load was decanted. Samples were air dried on drying racks.

For the granite samples (QTV-2, 3), a Wilfley table was tilted at 20° and water flow rates were adjusted so that ~10% of each sample was sorted into the heaviest bin. Care was taken to clean the Wilfley table after each sample using water and air to remove residual grains. Samples were air dried.

Magnetic Separation

Preliminary magnetic separation was done using a hand magnet to remove the bulk of the magnetic minerals from the sample. A Frantz magnetic separator was used in two stages: prior to heavy liquid separation and after heavy liquid separation. Samples were fed into the Frantz separator slowly, with the tilt at 20° and the current set at 0.35 A. The magnetic portion was removed, and the sample was processed again at 20° but with the current at 0.6 A. The nonmagnetic portion from this step was used for heavy liquid separation in lithium metatungstate ($\rho = 2.85$ g/cm^3) discussed below. After heavy liquid separation, the remaining sample was fed through the Frantz until the non-magnetic portion was small enough to pick zircons by hand under binocular microscopes. The final separation parameters were 20° at 1.0 A, 20° at 1.4 A, and decreasing slopes down to 1° until sufficiently sorted. All separates were retained in individual containers.

Heavy Liquid Separation

For each sample, 10 ml of crushed sample was put into a 50 ml test tube. Multiple tubes were required for most samples, and the total number varied depending on amount of sample and zircon fertility. These test tubes were then filled to 45 ml with lithium metatungstate (LMT) at a density of 2.85 g/cm^3. Test tubes were shaken and centrifuged to accelerate density separation.

After density separation, the heavy minerals in the bottom of the test tube were frozen in place using liquid nitrogen. The floating mineral separate was dumped into filter paper, rinsed in distilled deionized H_2O (DDI H_2O), and dried at room temperature overnight. The heavy separate was thawed and rinsed into a different filter before drying. LMT was recovered by multiple stages of filtering and evaporated until solution was measured at the original density.

Methylene iodide (MEI), at a density of ~ 3.3 g/cm^3, was used in small volume constriction tubes for low yield or poorly separated samples. MEI was poured in a test tube, with the constriction tube inside of it. Sample was then poured inside the constriction tube and allowed to settle. Light minerals were separated by plugging the small hole in the constriction tube and removing it from the test tube. Both separates were rinsed with acetone.

Whole-Rock Dissolution

Splits of each sample from the initial crushing stage of separation were powdered using a shatterbox. The shatterbox was cleaned by crushing of pure quartz sand for five minutes. While wearing gloves, powdered sand was removed and the alumina-ceramic puck and shatterbox interior were blown with compressed air. A pre-contamination sample was run and cleaned in the same manner. Pea-sized pieces of the sample were then pulverized for five minutes. Sample was dumped on to clean aluminum foil and funneled directly into glass storage container. New gloves were used for each sample to reduce risk of powder contamination.

Samples were then cut down to ~0.5 g for dissolution by pouring the powder between two sheets of weighing paper and dividing the sample repeatedly. Excess sample was returned to the glass container, while the sample for dissolution was stored in a small glass vial and sample weight was recorded. Sample was mixed in a 30 ml beaker with 4N HNO_3 and concentrated HF and allowed to sit for 24 hours. Sample was then dried down using a hot plate and mixed with $HClO_4$. After 24 hours, sample was again dried down, and remaining solid was dissolved in 1.5 N HCl and stored in 30 ml polyurethane vials.

Column Chemistry

Prior to column chemistry, each sample was split into two aliquots: spiked and unspiked. Unspiked aliquots were poured out into 30 ml beakers and dried on a hot plate. Spike samples were poured into 30 ml beakers and then spiked with internal standards for Rb, Sr, and Nd-Sm before being dried down. All aliquot weights and spike weights were recorded. Column chemistry was carried out following a method modified from Farmer et al. (1991). After column chemistry, samples were added to a rhenium filament in 1 ml aliquots. The concentration of each aliquot added depended on the element being analyzed and the expected concentration. For example, for Rb, ~1/300 of each sample was added; for Sm, the entire sample was used.

TIMS

A 6-collector, Thermo-Finnigan thermal ionization mass spectrometer was used to measure all Rb, Sr, Sm, and Nd for whole-rock samples at the University of Colorado at Boulder. Samples were loaded on rhenium filaments using HNO_3 (Sm, Nd) or HCl + H_3PO_4 (Rb, Sr). Direct measurements of unspiked samples were made for the radiogenic isotopic composition of $^{143}Nd/^{144}Nd$ (Table 2.2).

LA-ICP-MS

Zircon separates were sent to the Arizona LaserChron Center at the University of Arizona in Tucson. Analytical methods for LaserChron analyses can be found in the analytical methods appendix of Gehrels and Pecha (2014). U-Pb measurements were made using a Thermo Element2 single collector ICP-MS (Inductively Coupled Plasma – Mass Spectrometer). U-Pb data can be found in Appendix A, Table A-1. Analyses that are >20% discordant or >5% reverse discordant are not included in the results or interpretation.

For Hf isotopic analyses, zircon were ablated using a Photon Machines Analyte G2 excimer laser coupled to a Nu Instruments HR-MC-ICPMS (High Resolution – Multicollector- Inductively Coupled Plasma – Mass Spectrometer). Hf data can be seen in Appendix A, Table A-3.

Results

Zircon U-Pb ages and Hf isotopic compositions

Sufficient zircon for U-Pb and Hf isotopic analyses were isolated from only four samples including both anorthosite and granites samples from Quitovac (QTV 1-3) and the anorthosite from Rancho de Santa Margarita (CP-3). U-Pb condordia diagrams are shown in Figure 2.5.

Table 2.2. Radiogenic Isotopic data for intrusive rocks from Sonora, Mexico.

Sample	[Sr]	[Rb]	$^{87}Rb/^{86}Sr$	$^{87}Sr/^{86}Sr$ (m)	[Sm]	[Nd]	$^{147}Sm/^{144}Nd$	$^{143}Nd/^{144}Nd$ (m)	$^{147}Sm/^{144}Nd$ (i)	$^{143}Nd/^{144}Nd$ (i)	ε_{Nd} (i)
13S-CP-2	-	-	-	-	1.508 ± 0.001	6.019 ± 0.002	0.1552 ± 0.0001	0.512126 ± 0.000014	0.1541 ± 0.0001	0.511005 ± 0.000014	-4.15 ± 0.14
13S-CP-3	289.950 ± 0.041	11.954 ± 0.001	0.11916 ± 0.00002	0.714409 ± 0.000011	0.763 ± 0.001	3.289 ± 0.004	0.1437 ± 0.0002	0.512031 ± 0.000026	0.1427 ± 0.0002	0.510993 ± 0.000026	-4.39 ± 0.26
13S-CR-2	369.358 ± 0.085	5.143 ± 0.001	0.04024 ± 0.00001	0.710441 ± 0.000011	-	-	-	-	-	-	-
13S-QTV-1	-	-	-	-	14.765 ± 0.002	73.925 ± 0.007	0.1237 ± 0.0001	0.511909 ± 0.000014	0.1228 ± 0.0001	0.511015 ± 0.000014	-3.95 ± 0.14
13S-QTV-2	111.588 ± 0.005	194.085 ± 0.06	5.02658 ± 0.00028	0.801439 ± 0.000011	11.959 ± 0.001	62.372 ± 0.032	0.1188 ± 0.0001	0.511903 ± 0.000017	0.1179 ± 0.0001	0.511045 ± 0.000017	-3.37 ± 0.17
13S-QTV-3	142.095 ± 0.016	300.514 ± 0.005	6.1120 ± 0.00069	0.812075 ± 0.000026	16.497 ± 0.008	83.778 ± 0.010	0.1220 ± 0.0006	0.511881 ± 0.000013	0.1211 ± 0.0006	0.511000 ± 0.000013	-4.26 ± 0.13
13S-SNY-1	37.824 ± 0.001	.6927 ± 0.005	0.05293 ± 0.00038	0.707735 ± 0.000007	0.876 ± 0.001	3.201 ± 0.002	0.1697 ± 0.0001	0.512374 ± 0.000135	0.1685 ± 0.0001	0.511149 ± 0.000135	-1.35 ± 1.35
13S-SP-1	237.914 ± .015	23.435 ± 0.001	0.28467 ± 0.00002	0.713063 ± 0.000008	3.273 ± 0.001	14.017 ± 0.004	0.1446 ± 0.0001	0.512099 ± 0.000009	0.1436 ± 0.0001	0.511055 ± 0.000009	-3.19 ± 0.09

Rb-Sr and Sm-Nd isotopic data for whole-rock samples presented in this study. Concentrations in parts per million. (m) refers to measured values; (i) refers to inital values calculated at 1.1 Ga. Errors reported at 2σ.

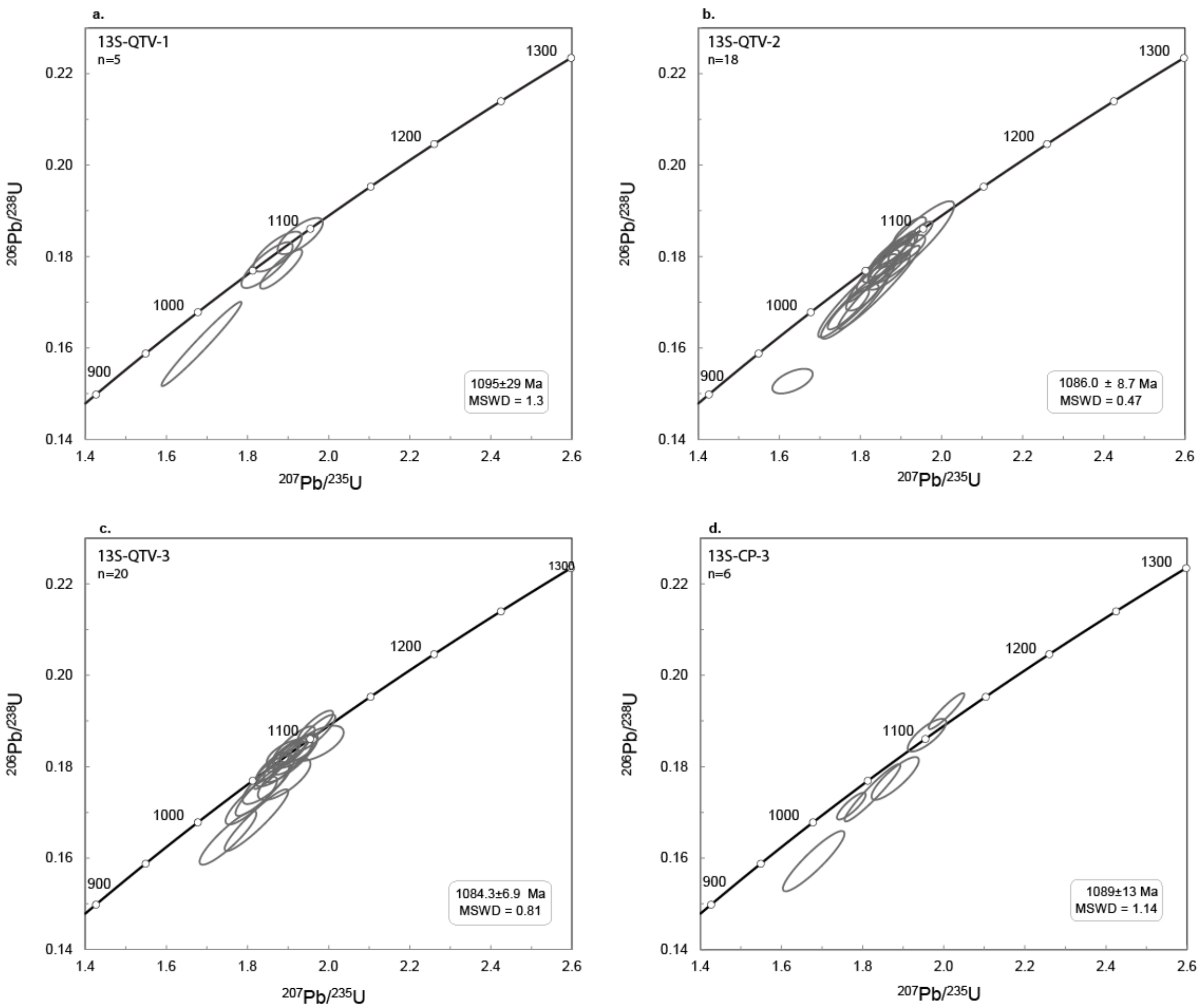

Figure 2.5. Concordia diagrams of zircon ages for intrusive samples from Sonora, Mexico. Error ellipses for each data point at 1-sigma (68.3%) confidence. Ages < 90% concordant were discarded. All analyses performed at Arizona Laserchron Center in Tucson, Arizona.

The U-Pb ages for the Quitovac samples QTV1-3 were all identical within error (QTV-1, 1095 ± 29 Ma, n=5, figure 2.5a; QTV-2, 1086 ± 8.7 Ma, n = 18; figure 2.5b; QTV-3, 1084.3 ± 6.9 Ma, n = 20; figure 2.5c). All ages are within error of zircon U-Pb ages for these rocks reported by Enriquez-Castillo et al. (2009). The zircon Hf isotopic compositions of these samples are also identical within error (Figure 2.6). QTV-1, -2, and -3 have median $\varepsilon_{Hf}(0)$ = -24.7 ± 1.5 (n = 5), -23.4 ± 1.8 (n = 15), and -24.3 ± 1.9 (n = 14), respectively.

Sample CP-3 has a U-Pb age of 1089 ± 13 Ma (n = 6; figure 2.5d). The Hf composition ranges from $\varepsilon_{Hf}(0)$ = -22.4 to -25.1, with a median of -23.5 and an average 2σ error of ± 1.3 (n = 3). One zircon was measured with a concordant age at 1435.5 ± 25.1 Ma, likely the result of measurement of a xenocrystic zircon core.

Whole Rock Sm-Nd and Rb-Sr Measurements

The Sm-Nd isotopic analyses produce in an isochron corresponding to an age of 1.117 ± 0.17 Ga with an initial $^{143}Nd/^{144}Nd$ = 0.51100 ± 0.00015 and MSWD = 2.4 (Table 2.2; Figure 2.7). Sample 13S-SNY-1 has been included on the graph, but excluded from the isochron calculation due to the large analytical uncertainty for this measurement. All samples have similar isotopic compositions, regardless of composition, displayed by the ε_{Nd} (T) at a model age of 1.1 Ga, in Figure 2.8. The Quitovac anorthosite and granite samples range from ε_{Nd} = -3.37 to -4.26 and have the low $^{147}Sm/^{144}Nd$ ratios from 0.118 to 0.123. The anorthosite sample (13S-QTV-1) has ε_{Nd} (1100 Ma) in between the values of the two granite samples. The sample from Sonoyta (13S-SNY-1) had the highest ε_{Nd} = -1.35, but also the highest $^{147}Sm/^{144}Nd$ ratio at 0.169. The anorthosites (13S-CP-2, 3) from Cerro Prieto, south of Caborca, have ε_{Nd} (1100 Ma) = -4.15 to -4.39.

These samples also produce a Rb-Sr isochron that gives an age of 1.21 ± 110 Ga, which overlaps the U-Pb zircon age of ~1.1 Ga (Figure 2.9). These data (Table 2.2) plot to form a low accuracy “pseudochron” with MSDW = 695 and an initial Sr isotopic composition of $^{87}Sr/^{86}Sr$ = 0.709549 ± 0.0051.

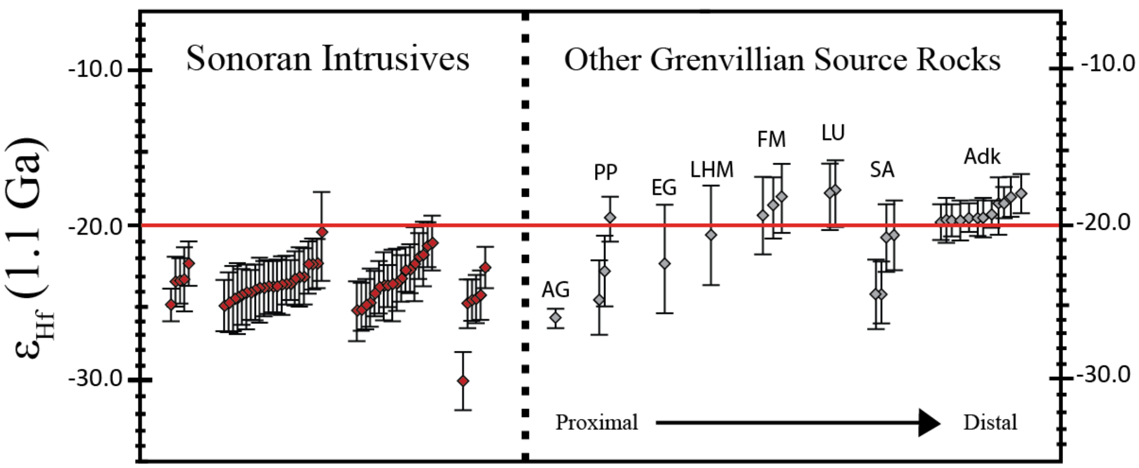

Figure 2.6. Rank order diagram of Hf isotopic composition of zircon from Grenville age igneous rocks from Sonora, Mexico. Sonoran Intrusives include samples from Quitovac, Sonora, Mexico (13S-QTV) and near Caborca (13S-CP-2). Red line denotes "high" and "low" ε_{Hf} at ε_{Hf}(i) = -20. Other Grenvillian source rocks: AG = Aibo Granite; PP = Pikes Peak Batholith; EG = Escuadara Granite; LHM = Little Hatchet Mountains; FM = Franklin Mountains; LU = Llano Uplift; SA= Southern Appalachian gneisses; modified from Howard et al (2015). Adk = Adirondacks; from Bickford et al (2010).

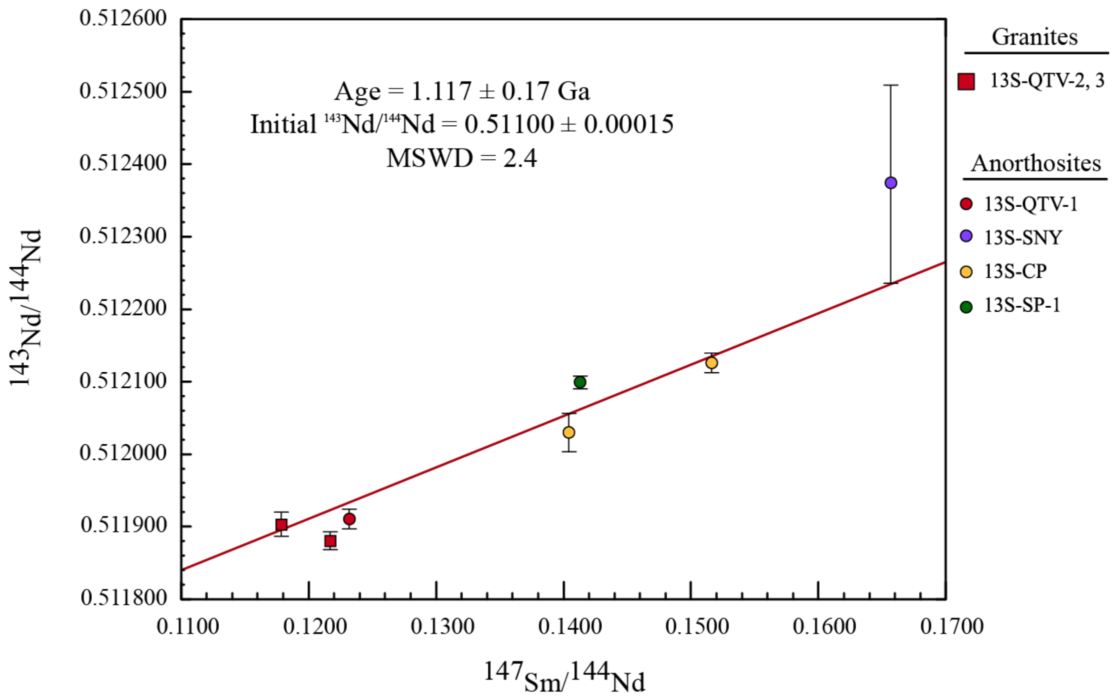

Figure 2.7. Sm-Nd isochron diagram for whole-rock analyses of intrusive rocks from Sonora, Mexico. Available data from seven samples listed in Table 2.2. Error bars for $^{147}Sm/^{144}Nd$ smaller than symbols.

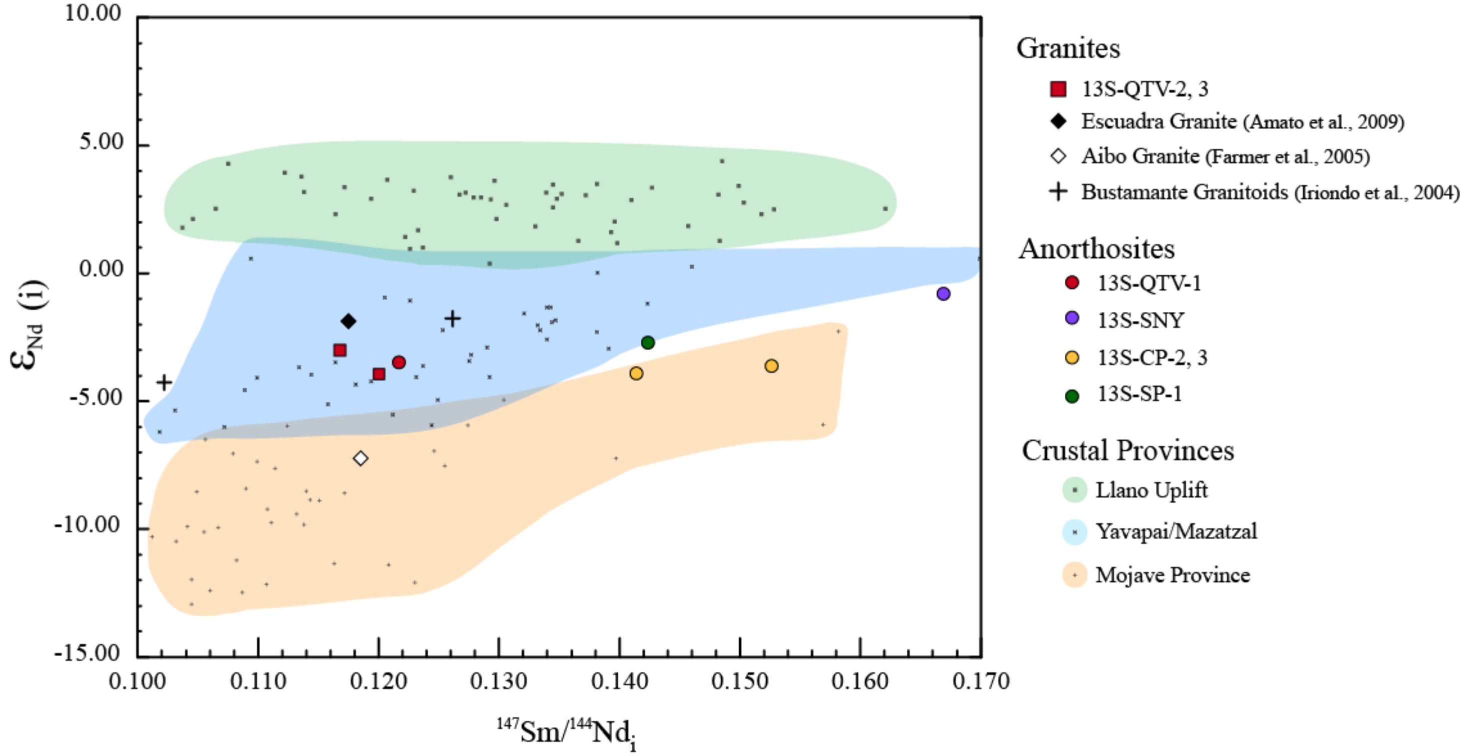

Figure 2.8. Isochron diagram showing ε_{Nd} at 1.1 Ga for whole-rock analyses of intrusive rocks from Sonora, Mexico. Basement rock data from previous studies included for comparison. Llano Uplift data from Patchett and Ruiz, 1989. Yavapai/Mazatzal data from DePaolo, 1981; Bennett and DePaolo, 1987; Nelson and DePaolo, 1985; Kempton et al., 1990; Nealy and Unruh, 1991. Mojave Province data from Nelson and DePaolo, 1985; Bennett and DePaolo, 1987; Barovich et al., 1989.

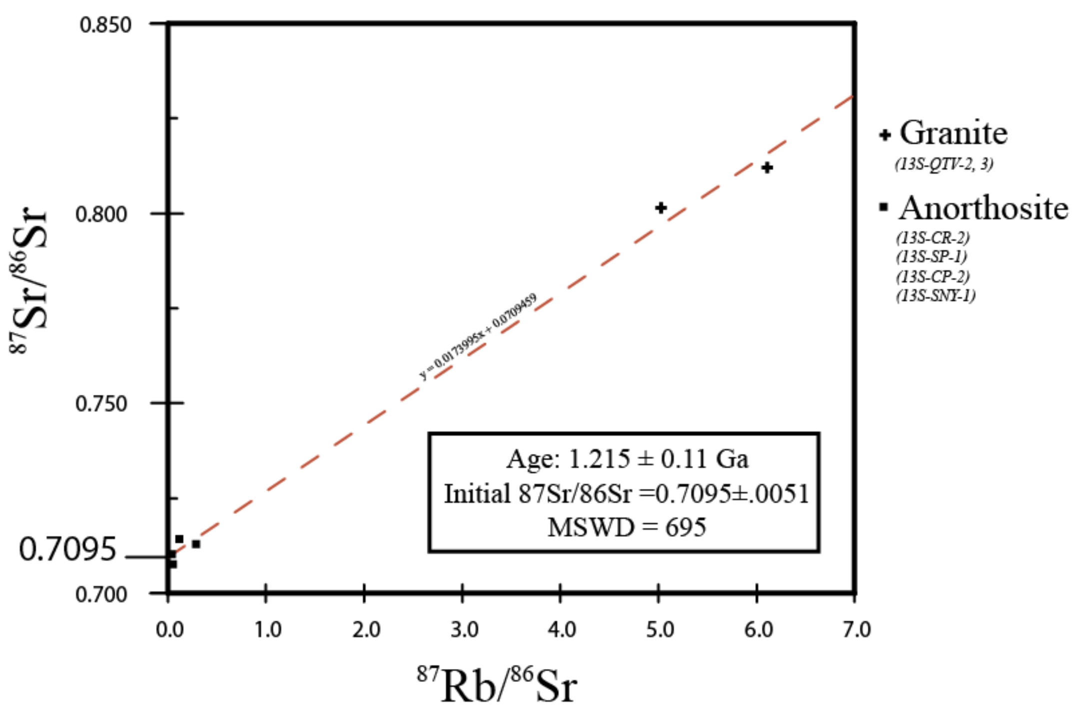

Figure 2.9. Rb-Sr isochron plot with available data from six samples listed in Table 2.2. Error bars smaller than symbols.

Discussion

Ages

The new age determinations for the granitic rocks sampled here demonstrate that the Sonoran granites and anorthosites crystallized contemporaneously at ~1.09 Ga. This age is consistent with measured ages for other Mesoproterozoic granitic rocks in the region, including the Aibo Granite, the Escuadra Granite, and other Quitovac-area granitic rocks (Anderson and Silver, 1981; Amato et al., 2009; Iriondo et al., 2009). The coeval emplacement of these regional intrusions indicates that broad areas of northern Sonora were affected by AMCG suite magmatism.

Isotopic Data

The fact that the analyzed granitic rocks and anorthosites plot on the same Nd and Sr isochrons indicate that all of these rocks crystallized from parental magmas with similar, homogenous, Sr and Nd isotopic compositions. This observation supports models for the formation of AMCG suites involving the production of both anorthosites and granitic rocks from the same parental magmas. Unfortunately the limited data set obtained in this study does not allow any further speculation on the exact relationship between the two lithologies. We can use the available isotopic data to assess possible sources of these parental magmas. Most models for the origin of AMCG rocks involve the injection of mafic magmas into the continental crust, followed by extensive crustal interaction (Turner et al., 1992; Emslie et al., 1994; Duchesne et al., 1999; Bybee and Ashwal, 2015). The large degree of crustal interaction, potentially through assimilation-fractional crystallization (AFC) processes, can obscure evidence of an original mafic magma is obscured (Bybee and Ashwal, 2015). If mafic magmas were involved in the production of these rocks, it is not apparent in the isotopic data for the Sonoran AMCG rocks, given that the ε_{Nd} (T) values and the initial $^{87}Sr/^{86}Sr$ ratio from the Sonoran AMCG samples overlap the values expected for intermediate composition crust of the Yavapai/Mazatzal Province at ~1.1 Ga (Figure 3.8; Bennett and DePaolo, 1987; Famer, 1992; Farmer et al., 2005b). The ε_{Nd} (T) values are much lower than expected for juvenile mantle derived igneous rocks at this time, such as the rocks from the Llano Uplift (Figure 3.8; Patchett and Ruiz, 1989). The conclusion is that both the Nd and Sr in the AMCG suite rocks in Sonora were largely inherited from the underlying Precambrian basement.

Implications for the distribution of Mojave Province crust

Existing models of the geographic extent of the Mojave Province in Sonora, Mexico are based largely on the distribution of the Aibo Granite, south of Caborca, Sonora, which has a significantly lower ε_{Nd} (T) value than other AMCG suite rocks in Sonora (Iriondo et al., 2004; Farmer et al., 2005; Molina-Garza and Iriondo, 2007; Amato et al., 2009). The data presented here supports the conclusion that the extent of the Mojave Province is, in fact, restricted to the Caborca area. Anorthosite sample 13S-CP-2, from east of the Aibo Granite sample location, has a Nd isotopic composition similar to that of Yavapai/Mazatzal Province crust (Iriondo et al., 2004; Amato et al., 2009). Isotopic data from samples 13S-QTV-1, 2, and 3, shows that Yavapai/Mazatzal crust likely exists to the southwest of Quitovac as well. Previous analyses of AMCG suite rocks northwest of Quitovac suggest that these rocks were either derived from and/or interacted extensively with Yavapai/Mazatzal crust (Iriondo et al., 2004). All samples overlap within error in ε_{Nd} with Yavapai/Mazatzal Province crust or crustal derivatives, such as the Escuadra Granite to the east of Caborca (Amato et al., 2009).

Characterization for Detrital Zircon Analysis

These intrusions have ε_{Hf} values that are similar to measured values for the Aibo Granite and Escuadra granites in Sonora, Mexico, despite differences in the Nd isotopic characteristics (Figure 2.6; Amato et al., 2009; Howard et al., 2015). All of these plutons exhibit the same U-Pb ages (~1.08 Ga) and have ε_{Hf} values between -20 and -26, suggesting isotopic similarity of these intrusions over a large geographic region, allowing them to be characterized for detrital zircon provenance determinations. While the granitic samples have a high zircon fertility, few zircon were recovered from anorthosites in this study, consistent with anorthosites from Canadian AMCG suites (McLelland et al., 2004). This suggests that the granitic rocks, but not anorthosites, of the ~1.08 AMCG suite in present day Sonora, Mexico could have contributed to the load of Grenvillian detrital zircon present in Neoproterozoic and Cambrian sandstones in the western United States. Grenville-age granitic rocks are known to have a high zircon fertility compared to other intrusions, so even smaller volume exposures of these granitic plutons may have played a critical role in zircon contribution (Dickinson, 2008).

Conclusions

Isotopic study of several samples from a ~1.08 Ga AMCG suite in northwest Mexico yielded genetic interpretations on the source of the intrusions. The major contributions are:

1. Isotopic data demonstrate that northwestern Sonora, Mexico underwent widespread AMCG suite magmatism that resulted in the contemporaneous crystallization of granite and anorthosite intrusions around 1.089 Ga.

2. The ε_{Nd} data suggest that a major crustal component was involved during the generation of the parental magma that produced the AMCG intrusive suite. The observed crustal signature is consistent with derivation from intermediate crust of the Yavapai/Mazatzal Province, both to the north and east of the Mojave-derived Aibo Granite near Caborca.

3. The AMCG suite in northwestern Mexico, as well as other regional 1.08-1.09 Ga granites (Aibo and Escuadra), have similar Hf isotopic composition and U-Pb ages. While low zircon yield from anorthosites suggests little contribution to the sedimentary record, exposed granitic rocks from this suite could have played a large role in zircon supply to siliciclastic units during the Neoproterozoic and Cambrian.

Chapter Three

Provenance of Grenvillian detrital zircon from intracratonal basal sandstones in North America

Introduction

Sediment provenance studies commonly compare U-Pb ages of detrital zircon in siliciclastic sedimentary rocks with igneous zircon in exposed crystalline rocks to determine the sediment source. However, when broad tracts of crust share the same age, it is difficult to resolve the distinct geographic source of the detrital zircon in this fashion. For example, the U.S. and Mexican portions of North America are comprised principally of Paleoproterozoic to Mesoproterozoic basement rocks, making detailed provenance determinations difficult for zircon of these ages despite a nearly ubiquitous occurrence in Phanerozoic siliciclastic sedimentary rocks (Stewart et al., 2001; Thomas, 2001; Fedo et al., 2003). One approach towards better defining the sources of detrital zircons is to combine U-Pb ages with Hf isotopic analyses in cases where the Hf isotopic compositions of zircon from coeval source rocks vary regularly with geographic position. In North America, it has been demonstrated that regular spatial variations exist in the Hf isotopic compositions of 1.0 Ga to 1.3 Ga ("Grenvillian") basement rocks in North America and can be used to refine the provenance of Grenvillian detrital zircon (Howard et al., 2015). This study takes advantage of this observation and uses U-Pb ages and Hf isotopic data to assess the provenance of such Grenvillian detrital zircon from Neoproterozoic to Cambrian sandstones deposited at or near the so-called "Great Unconformity", which is a non-depositional and/or erosional surface exposed around the world that represents a time gap of over one billion years (Sloss, 1963; Peters and Gaines, 2012). The goal of the study is to use the abundances and provenance determinations of Grenvillian zircons to determine 1) if and where rift-generated topographic highlands were located in Laurentia during the deposition of these sediments, 2) the paleogeography and direction(s) of sediment transport, and 3) the orientation and timing of marine transgressions across the Laurentian continent during and just after the breakup of Rodinia.

Geologic Background

The Great Unconformity is a surface of non-deposition and/or erosion separating Precambrian basement rocks from overlying Neoproterozoic to Cambrian sandstones and is exposed in virtually every continent on Earth. Although the exact circumstances involved in the production of this global unconformity are poorly understood, there is an increasing recognition of its importance in Earth history. Recent studies, for example, suggest that exposure of unweathered crystalline rocks along the unconformity and subsequent flooding of the continents after the breakup of the supercontinent Rodinia may have influenced ocean chemistry and increased the available nutrients for the expansion of biomineralizing marine phyla associated with the “Cambrian Explosion” (Peters and Gaines, 2012).

In North America, basal sandstones deposited along the Great Unconformity are exposed from at western craton margin and across the midcontinent into the central United States (Fig. 3.1). These Neoproterozoic to Cambrian sedimentary rocks include the middle member of the Wood Canyon Formation (California), the Tapeats Sandstone (Arizona), the Sawatch Sandstone (Colorado), the El Arpa Formation (Sonora, Mexico), the Flathead Sandstone (Wyoming), the Lamotte Sandstone (Missouri), the Mt. Simon Sandstone (Ohio, Michigan, Illinois), the Van Horn Formation (Texas), the Riley Formation (TX), and the Reagan Sandstone (Oklahoma and Kansas) (McElroy, 1965; Bell, 1970; Hereford, 1977; Houseknecht and Ethridge, 1978; Fedo and Cooper, 2001,; Stewart et al., 2001; Stewart et al., 2002; Gehrels et al., 2011. Lovell and Bowen, 2013; Cullen, 2014; Gehrels and Pecha, 2014; Siddoway and Gehrels, 2014; Spencer et al., 2014). These sedimentary units are part of so-called “Sauk” sedimentary sequences that were deposited during the mid- to late-Cambrian marine transgression onto the Laurentian continent that resulted in the epicontinental Sauk Seaway (Sloss, 1963; 1988). All of the sandstones listed above are stratigraphically equivalent and represent sediments originally deposited in shallow marine or fluvial depositional environments. The depositional age of the sandstones becoming progressively younger toward the craton interior due to the progressive inundation of the continent by the Sauk Sea from the southwest to northeast during the Cambrian (Sloss, 1963; 1988; Fedo and Cooper, 2001).

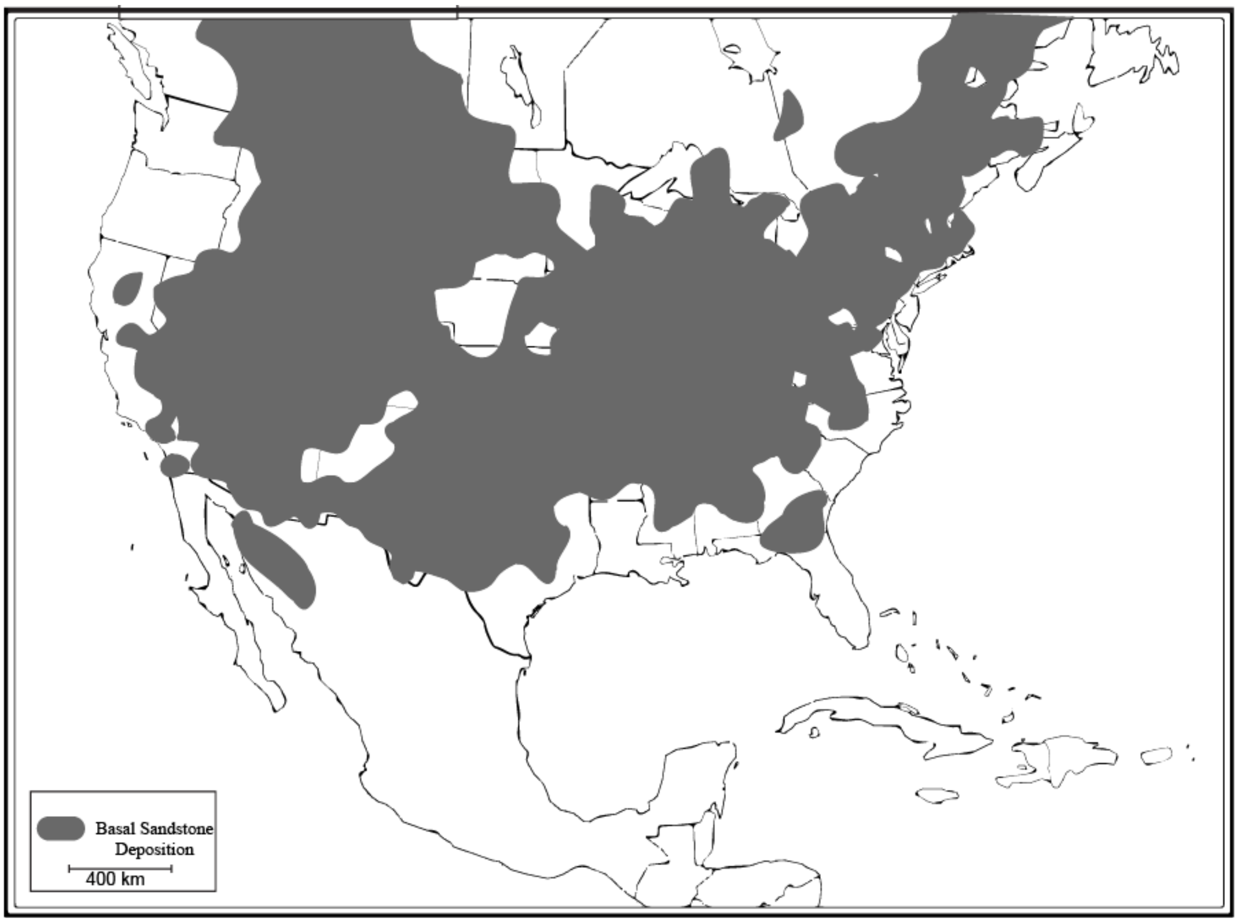

Figure 3.1. Cartoon map showing regional extent of basal sandstone deposition. Modified from Stewart et al., 2002 and Peters and Gaines, 2012.

An important aspect of the Great Unconformity for the purpose of detrital zircon provenance determinations is that it represents a surface from which older sedimentary material had been stripped prior to the deposition of overlying sandstones, minimizing the possibility that detrital zircons in these sedimentary units were derived from recycling of previously deposited detritus. In addition, because the U-Pb ages of zircons from the underlying crystalline rocks can be directly measured, detrital zircons in the basal sandstones derived from the local basement sources can be readily identified. As a result, it should be possible to assess which areas of the Laurentia continent were exposed and actively exhuming just after the breakup of Rodinia from detrital zircon studies of the basal sandstones, and what the general sediment transport directions across the continent were during this time interval.

Detrital zircon U-Pb age spectra are available for many of the basal "Sauk Sequence" sandstones in North America, and show dominant age populations at 1.0-1.3 Ga, 1.4 Ga, and 1.7 Ga, all which corresponds to the ages of Paleoproterozoic crust that comprises much of the southern portions of the continent, as well as subordinate zircon populations derived from Archean crust (Thomas, 2001; Stewart et al., 2001; Gehrels et al., 2011; Gehrels and Pecha, 2014; Howard et al., 2015). The zircons with ages between 1.0 to 1.3 Ga are termed "Grenvillian" zircon and are of principal interest in this study. Grenvillian detrital zircons are common in Neoproterozoic and Cambrian sandstones, so common, in fact, that some authors have termed this sedimentation event the "Grenville Flood" and have suggested that sediment shed from the highlands along the eastern continental margin of Laurentia were fluvially transported and deposited across the continent to the west (Rainbird et al., 1992; 1997; 2012; Mueller et al., 2007). One impetus for this study is to use detrital zircon U-Pb and Hf isotopic data from basal Sauk Sequence sandstones to test this hypothesis. An important issue is the fact that Grenvillian crystalline rocks are not restricted geographically to the Grenville Province in easternmost Laurentia where largely juvenile accreted terranes of intrusive and metamorphic rocks span the eastern boundary of North America, from southeastern

Canada to the southeastern United States (Figure 3.2; van Schmus et al., 1993; Whitmeyer and Karlstrom, 2007). Basement crystalline rocks of similar age can also be found to the southwest as part of the accretionary terranes currently exposed in the Llano Uplift in Texas. In addition, ~1.1 Ga granitic rocks and anorthosites are found as intrusions within Paleoproterozoic crust throughout southwest North America (Anderson and Silver, 1974; 1981; Karlstrom and Bowring, 1988; Karlstrom and Whitmeyer, 2007; Howard et al., 2015; this study). Previous work has demonstrated that despite similar crystallization ages, zircon from these geographically distinct Grenvillian rocks have different Hf isotopic compositions (Bickford et al., 2010; Howard et al., 2015). As a result, the combined U-Pb and Hf isotopic datasets of Grenvillian detrital zircon can be used to better resolve the geographic location of their sources.

Samples

In order to assess the provenance of detrital zircon found in basal Sauk sandstones across North America, U-Pb ages and Hf isotopic composition were obtained from sandstones at four locations across the midcontinent (Fig. 3.2). General descriptions of each unit sampled are provided below.

Lamotte Sandstone

The mid- to upper- Cambrian Lamotte Sandstone outcrops in the St. Francois Mountains in southeastern Missouri, where it unconformably overlies ~1.48 Ga Proterozoic basement of the Eastern Granite-Rhyolite Terrane (Menuge et al., 2002). The Upper Lamotte Sandstone is a moderately-to-well sorted, quartz-dominated sandstone (Houseknecht and Ethridge, 1978) that ranges in thickness from 7 to 30 m, and is locally more feldspathic and more poorly sorted towards the basal contact (Houseknecht and Ethridge, 1978). Previous workers suggested that the lowermost portions of the Lamotte Sandstone represent detritus derived from local ~1.48 Ga basement via a braided stream system that drained eastward from a highland to the west (present day coordinates), thought to be the ancestral St. Francois Mountains (Houseknecht and Ethridge, 1978). As the continent was inundated by the Sauk Sea there was a gradual shift from a braided-stream depositional setting to a shallow marine environment, as evidenced by a shift

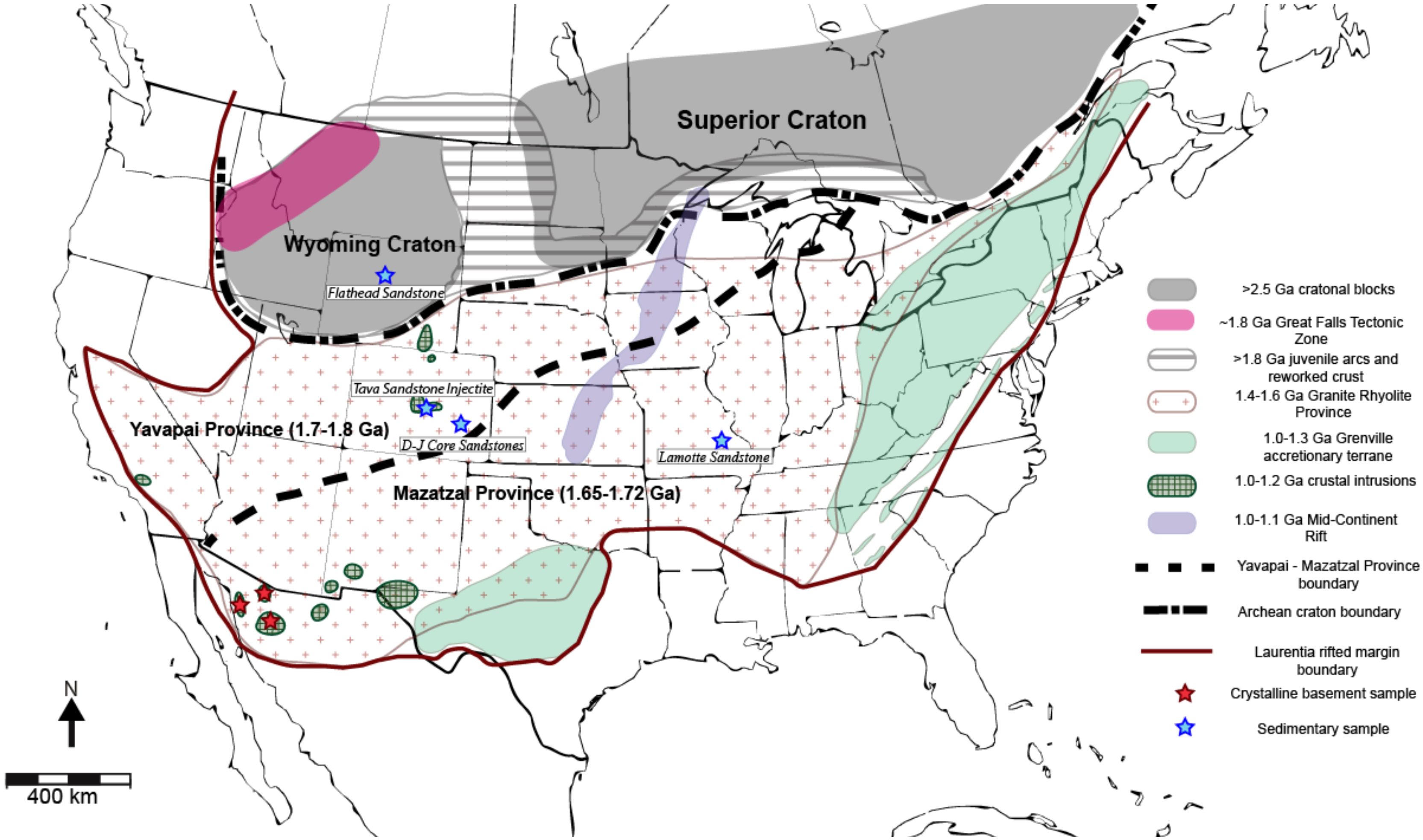

Figure 3.2. Cartoon map indicating the extent of North American crystallne basement rock and cratonal boundaries. Laurentian rifted margin boundary after the break up of Rodinian supercontinent. Stars indicate samplesv from this study; Crystalline basement samples discussed in Ch.2. Basement ages and regional extent from Reed (1993) and Whitemeyer and Karlstrom (2007). Political map from the Cartographic Research Lab at the University of Alabama.

to the deposition of well-sorted quartz sands interpreted to have been derived from continental sources in the Canadian Shield to the north (Ojakangas, 1963; Houseknecht and Ethridge, 1978). As the marine transgression proceeded, siliclastic sedimentation transitioned to the deposition marine of carbonates that now comprise the late-Cambrian Bonneterre Formation (Houseknecht and Ethridge, 1978).

To assess the provenance of the Lamotte Sandstone, two samples of the upper Lamotte sandstone were provided by Summit Proppants, L.L.C. from a proppant sand quarry near Farmington, Missouri (Figure 3.2). Both samples consists of uncemented quartz sands, with modal quartz contents of >95%. Quartz grains are well-rounded and define a narrow size range from 0.5 mm to 0.7 mm. The two samples both yielded very small amounts of heavy minerals and as a result zircons from the two samples were combined for subsequent analyses; zircons were well rounded and clear, approximately 100-200 µm (long-axis), with generally no inclusions or visible radiation damage.

Flathead Sandstone

The upper Cambrian Flathead Sandstone is a regionally extensive, unconformable basal sandstone in Wyoming, North Dakota, and Montana (Bell, 1970). It is commonly divided into an upper and lower unit. The lower unit is a cross-stratified, well-cemented, poorly sorted, medium to coarse grained quartzite (Bell and Middleton, 1978; Beebee and Cox, 1998). This unit gradually transitions into interbedded sandstone-shale-siltstone sedimentary units that comprise its upper portion (Bell and Middleton, 1978). Sedimentary structures indicate both fluvial and shallow marine depositional environments as the shoreline responded to a marine transgression and to gradually increasing water depths (Beebee and Cox, 1998). The Flathead Sandstone is conformably overlain by the late Cambrian Gros Ventre Formation that is composed of shales and limestone (Bell and Middleton, 1978).

Detrital zircon U-Pb age determinations exist for both upper and lower Flathead Sandstone in the Bighorn Basin in northern Wyoming (May et al., 2013). At this locality, sandstone from near the basal contact contains a large ~2891 Ma detrital zircon population at, with a smaller peak at ~1785 Ma (May et al., 2013). The upper Flathead sandstone sample has identical age peaks, but the peak at ~1785 Ma forms the dominant population (May et al., 2013).

In this study, samples of the Flathead Sandstone were taken from the eastern Owl Creek Mountains in central Wyoming, southeast of the Bighorn Basin. The Archean basement of the eastern Owl Creek Mountains upon with the sandstone was deposited is composed of a ~2.9 Ga bimodal intrusive suite which was metamorphosed at ~2.75 Ga and then intruded by a ~2.6 Ga peraluminous granite (Mueller et al., 1985; Frost et al., 2006). One sample (14WY-FH-1) was obtained from the portions of the unit within 10m of the basal contact with the Archean granite and is a well-cemented quartzite with well-rounded to sub-rounded, poorly sorted quartz grains. The lower Flathead sample yielded insufficient zircon for analysis. A second sandstone sample (14WY-FH-2) was taken near the upper contact of the Flathead Sandstone with the late Cambrian Gros Ventre shale and consists of fine grained, well-sorted, and well-rounded quartz grains. Zircons from this sample are pink, very fine grained (~100 μm), generally euhedral to subhedral, and show little to no visible radiation damage.

Colorado Basal Sauk Sequence Sandstones

Early Paleozoic sedimentary rocks are preserved throughout Colorado, both in outcrop and in the subsurface (Johnson, 1944; MacLachlan, 1961; Myrow et al., 2003). Preserved Cambrian sandstone outcrops are restricted geographically to central Colorado in the form of the Sawatch Formation which is interpreted as a transgressive marine deposit that includes large-scale, glauconite-rich, tidally influenced, subaqueous marine dune deposits (Myrow et al., 2003). U-Pb detrital zircon spectra for this unit are already available and were not analyzed for this study (Siddoway and Gehrels, 2014). While the Sawatch Sandstone represents the basal Sauk Sequence in central Colorado, new cores from the Denver-Julesburg Basin sample a basal sandstone of unknown age which are described and analyzed here. Additionally, samples of a Neoproterozoic sandstone injectite unit representing the sediment composition prior to the breakup of Rodinia, the Tava Sandstone, were provided for this study by Dr. Christine Siddoway.

Denver-Julesburg (D-J) Basin

Material from three cores drilled through the Paleozoic sedimentary sequence into crystalline rocks were provided for this study by Nighthawk Energy, LLC. These cores, named Jackson Hole, Big Sky, and Taos, are located within 6 km of each other in northern Lincoln County and southern Washington County, Colorado (Figure 3.2). The granitic basement of the Big Sky core is ~1458 ± 14.3 Ma from zircon U-Pb ages (A. Seeling, personal communication). Detailed descriptions of the cores were generated as part of this study and two different lithofacies were identified in each of the studied cores (Appendix B). The first is characterized by homogenous, cross-bedded quartz-dominated (>95%), medium grain sandstone (Figure 3.3A). Quartz grains are sub-rounded and poorly- to moderately-sorted in these sections. Lag deposits with a high abundance of granule to pebble size clasts occur between cross-bedded sections and at facies transitions. Glauconite is present in these sands and can range in modal abundance from 0% up to 15%, giving some hand samples a pale green hue. Samples with low glauconitic components are generally quartz cemented. Samples with a higher glauconitic component have a carbonate cement that completely supports the quartz grains in some areas. Carbonate replacement yields a patchy distribution of widely spaced quartz grains in a carbonate cement in some areas (Figure 3.3B). The glauconite in these samples forms distinct, irregularly shaped grains which are larger than the majority of the quartz grains. Calcite, shown in Figure 3.3B, may have selectively replaced preexisting feldspar grains.

The second lithofacies found in the D-J core samples is a heterolithic, quartz-rich (>60%), glauconitic, fine-grain sandstone. This facies is characterized by interbedded, dark green, glauconite-rich and white, quartz dominated layers. Individual mineral grains are dominantly cemented by carbonate with a variable hematite component, creating a red appearance (Figure 3.3C). Glauconite in these samples is present both as individual grains and as a very fine-grained interstitial cement. Very fine-grained glauconitic mud drapes occur on irregular boundaries interpreted as paleosurfaces formed during episodes

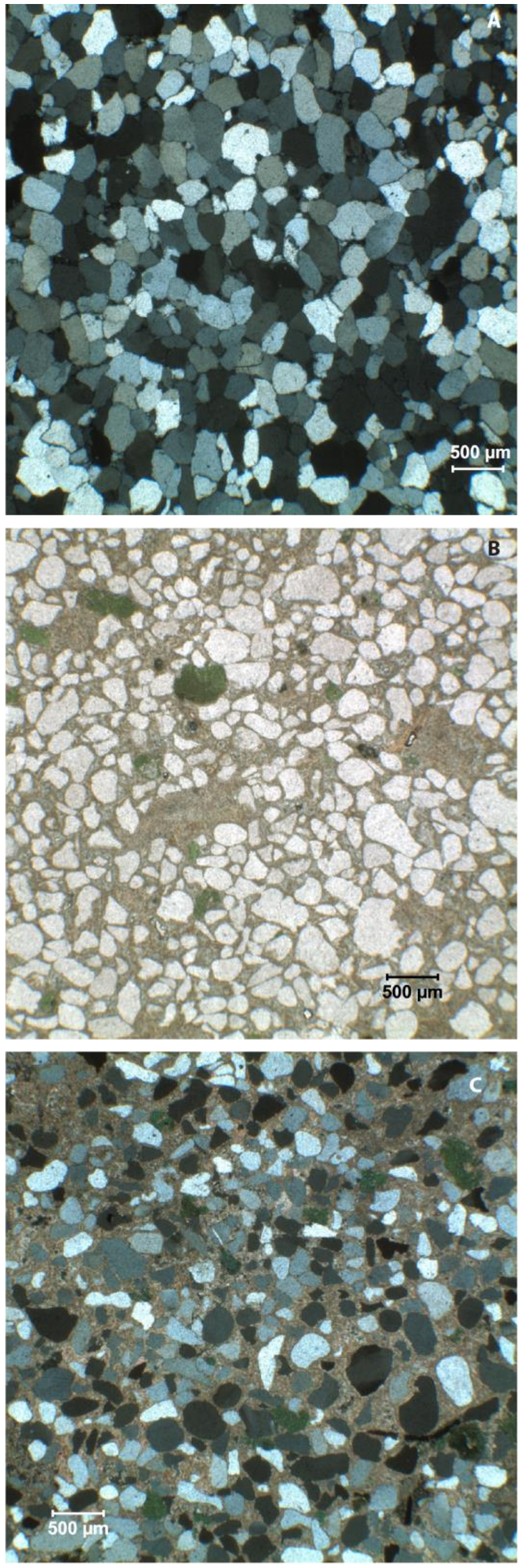

Figure 3.3. Photomicrographs of samples from basal sandstone cores in Lincoln County, Colorado. A) JH-1 quartzarenite wih little to no cement, uniform gray in hand sample; B) BS-3 in plane polrized light with calcite-cemented quartz-rich sandstone with glauconite graines. C) CP-3 weathered anorthosite with actinolite and scapolite in plane polarized light.

of subaerial exposure. Infrequently, this facies contain rip-up clasts of both quartz-rich and glauconite-rich material, though no storm deposits are evident in the cores. Sections of this facies contain abundant, large (~1-3 cm) hematite nodules. Parallel laminations and wavy laminations are present, but are disturbed by various degrees of bioturbation and downward burrowing. Additionally, the second facies occasionally exhibits pedogenic-like overprinting due to weathering processes that obscure any primary sedimentary structures.

Though no absolute age has been determined for the samples of basal sandstones in this study, the glauconitic sandstone in the D-J cores is overlain by Ordovician carbonates and is certainly lower Paleozoic in age (A. Seeling, personal communication). The sandstones in these cores are lithologically and stratigraphically similar to the Cambrian Sawatch Sandstone (Myrow, 1998; Myrow et al., 2003).

Eight samples were taken for this study, and six of these were from Facies 1. Three samples were taken from the Big Sky Core, at depths of 8204.1 feet (BS-3), 8203.8 feet (BS-2), and 8183.4 feet (BS-1), all from Facies 1. Three samples were taken from the Taos Core, at depths of 8153.1 feet (T-1), 8152.9 feet (T-2), and 8119.4 feet, with the T-1 and T-2 from Facies 1 and T-3 from Facies 2. Two samples were taken from the Jackson Hole Core, at depths of 8396.5 feet (JH-1) and 8372.1 feet (JH-2), both from Facies 1. Of these samples only two (14CO-BS-3 and 14CO-T-3) yielded enough zircon for isotopic analysis, though some zircon were recovered from the remaining six samples from the Taos (14CO-T), Big Sky (14CO-BS), and Jackson Hole (14CO-JH) cores. These zircon were combined for the purposes of isotopic analyses (14CO-Core).

Tava Sandstone Injectite

The Tava Sandstone is a regionally extensive Neoproterozoic sandstone injectite that is found in dikes and sills in the Proterozoic basement rocks along the Ute Pass Fault Zone through central Colorado, USA (Siddoway and Gehrels, 2014). These sandstone dikes were first recognized by Vitanage (1954) and mapped more extensively by Harms (1965). The Tava Sandstone is a fine grained quartz arenite with well-rounded quartz grains supporting isolated quartz aggregates and pebbles (Siddoway and Gehrels, 2014). Thin-section analysis indicated that elongate grains formed a fabric aligned parallel to dike walls and interpreted to have formed during emplacement (Vitanage, 1954). These sandstone injectites are interpreted to record the composition of the last vestige of Neoproterozoic sedimentation prior to the continental inundation of the Sauk Sea (Siddoway and Gehrels, 2014).

Three grain mounts from samples of separate injectite bodies previously analyzed for U-Pb isotopic ages were used in this study (Host - SH324-HO [n=79], Body - SH324-BD [n=89], Vein - SH324-VE [n=79]; Siddoway, unpublished data). U-Pb ages from zircon from the Tava Sandstone are characterized by three distinct age populations at ~1.7 Ga, ~1.4 Ga, and ~1.1 Ga (Siddoway and Gehrels, 2014). The ~1.1 Ga peak is characterized by a broad age distribution from 0.97 to 1.33 Ga. The Tava Sandstone zircons also include a subordinate population of Archean age grains (Siddoway and Gehrels, 2014).

Methods

Physical separation

All crushing and mineral separation was performed at the University of Colorado at Boulder. Rocks were broken into small fragments and crushed in a jaw crusher to pebble size and a 30 g portion of this material was saved for whole-rock dissolution. The majority of the sample was then crushed in a disk mill and sifted through a 600 µm sieve. Both jaw crusher and disk mill were cleaned thoroughly with wire brush and air hose between each sample.

Sedimentary samples were processed using a Wilfley table tilted at 20° and adjusted flow rates so that <5% of each sample was sorted into the heaviest bin, and all bins were saved and air dried on drying racks. Care was taken to clean the Wilfley table after each sample using water and air to remove residual grains.

Magnetic Separation

Preliminary magnetic separation was done using a hand magnet to remove the bulk portion of magnetic separates. A Frantz magnetic separator was used in two stages: prior to heavy liquid separation and after heavy liquid separation. Samples were fed into the Frantz separator slowly, with the tilt at 20° and the current set at 0.35 A. The magnetic portion was removed, and the sample was processed again at 20° with the current at 0.6 A. The nonmagnetic portion from this step was used for heavy liquid separation in lithium metatungstate (ρ = 2.85 g/cm^3) discussed below. After heavy liquid separation, the remaining sample was fed through the Frantz until the non-magnetic portion was small enough to pick zircons under binocular microscopes. The final separation parameters were 20° at 1.0 A, 20° at 1.4 A, and decreasing slopes down to 1° until sufficiently sorted. All separates were retained in individual containers.

Heavy Liquid Separation

For each sample, 10 ml of crushed sample was put into a 50 ml test tube. Multiple tubes were required for most samples, and the total number varied depending on amount of sample and zircon fertility. These test tubes were then filled to 45 ml with lithium metatungstate (LMT) at a density of 2.85 g/cm^3. Test tubes were shaken and centrifuged to accelerate density separation.

After density separation, the heavy minerals in the bottom of the test tube were frozen in place using liquid nitrogen. The light, floating mineral separate was dumped into filter paper, rinsed in distilled deionized H_2O (DDI H_2O), and dried at room temperature overnight. The heavy separate was thawed and rinsed into a different filter before drying. LMT was recovered by multiple filtering stages and evaporated until solution was measured at the original density.

Methylene iodide (MEI), at a density of ~ 3.3 g/cm^3, was used in small volume constriction tubes for low yield or poorly separated samples. MEI was poured in a test tube, with the constriction tube inside of it. Sample was then poured inside the constriction tube and allowed to settle. Light minerals were separated by plugging the small hole in the constriction tube and removing it from the test tube. Both separates were rinsed with acetone.

ICP-MS and HR-MC-ICP-MS

Zircon separates were sent to the Arizona LaserChron Center at the University of Arizona in Tucson. Analytical methods for LaserChron analyses can be found in the Analytical Methods Appendix of Gehrels and Pecha (2014). U-Pb measurements were made using a Thermo Element2 single collector ICP-MS (Inductively Coupled Plasma – Mass Spectrometer). U-Pb data tables can be found in Appendix A, Table A-2. Detrital zircon U-Pb data is presented in the following sections as probability density functions, where the area under each curve equals a probability of 100%. Analyses that are >20% discordant or >5% reverse discordant are not included in the results and interpretation.

For Hf isotopic analyses (Table 3.2), zircon were ablated using a Photon Machines Analyte G2 excimer laser coupled to a Nu Instruments HR-MC-ICPMS (High Resolution – Multicollector- Inductively Coupled Plasma – Mass Spectrometer). Hf data tables can be seen in Appendix A, Table A-4. Hf data for all samples are displayed in a rank order diagram in Figure 3.4.

Detrital Zircon U-Pb and Hf Results

Lamotte Sandstone

Detrital zircon in the Lamotte Sandstone (14MO-LMT) [n= 21, where n are number of grains] show a single age peak at 1096 ± 22 Ma, with one grain yielding an older age of 1691.6 ± 18.8 Ma (Figure 3.5). Hafnium isotopic analyses from the Grenvillian detrital zircon show a limited range of ε_{Hf} (0) values ranging from -20.0 to -27.4 with a typical 2σ error of ± 2 ε_{Hf} units.

Flathead Sandstone

Three hundred and thirteen zircon from sample 14WY-FH-2 yielded a dominant U-Pb age population at 1779 Ma that tails towards 1800-1900 Ma (Figure 3.5). An Archean zircon population [n = 19] also exists and forms distinct peaks at 2700 Ma (n=13) and at 2500 Ma. There is one younger zircon

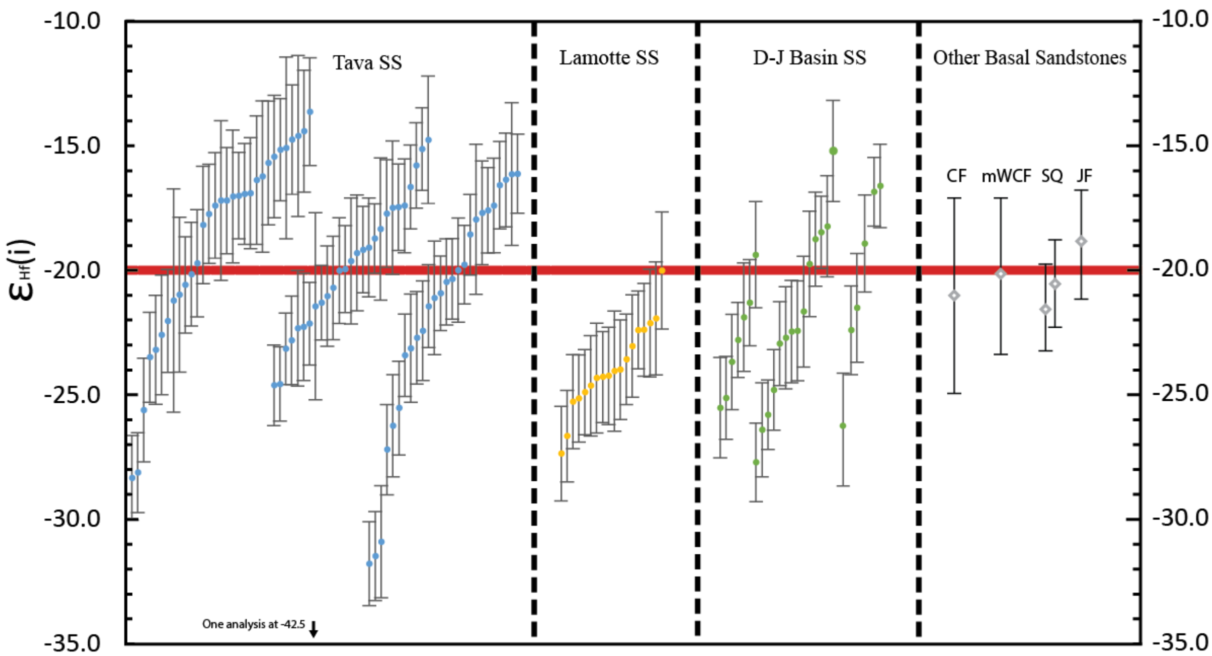

Figure 3.4. Rank order diagram of ε_{Hf} values for Grenvillian zircons from basal sandstones. Tava Sandstone (SH324-BD, SH324-VE, SH324-HO), Lamotte Sandstone (14MO-LMT), and Colorado Cores (14CO-BS, 14CO-T, 14CO-JH) data can be found in Appendix A, Table A-4. Red line denotes "high" and "low" ε_{Hf} at $\varepsilon_{Hf}(i)$= -20. Other detrital zircon values: CF = Campito Formation; mWCF = middle member of the Wood Canyon Formation; SQ = Stirling Quartzite; JF = Johnnie Formation; modified from Howard et al (2015).

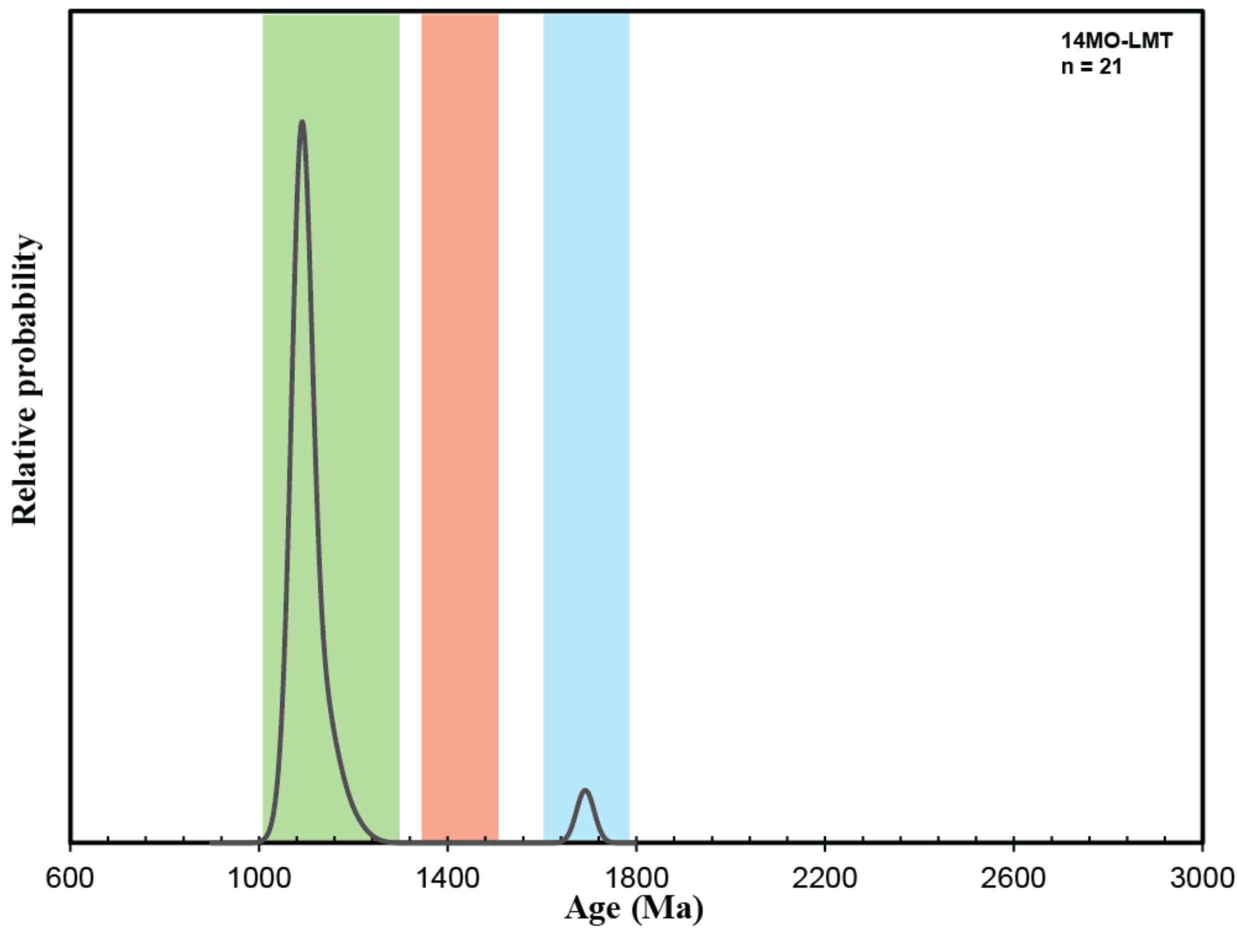

Figure 3.5. Probability Density Function for the Lamotte Sandstone near Farmington, Missouri. Area under each curve totals to 100%. Crystalline basement ages indicated by colors: Green- Grenville Orogeny, Red- Granite-Rhyolite Province, Blue- Yavapai/Mazatzal Provinces.

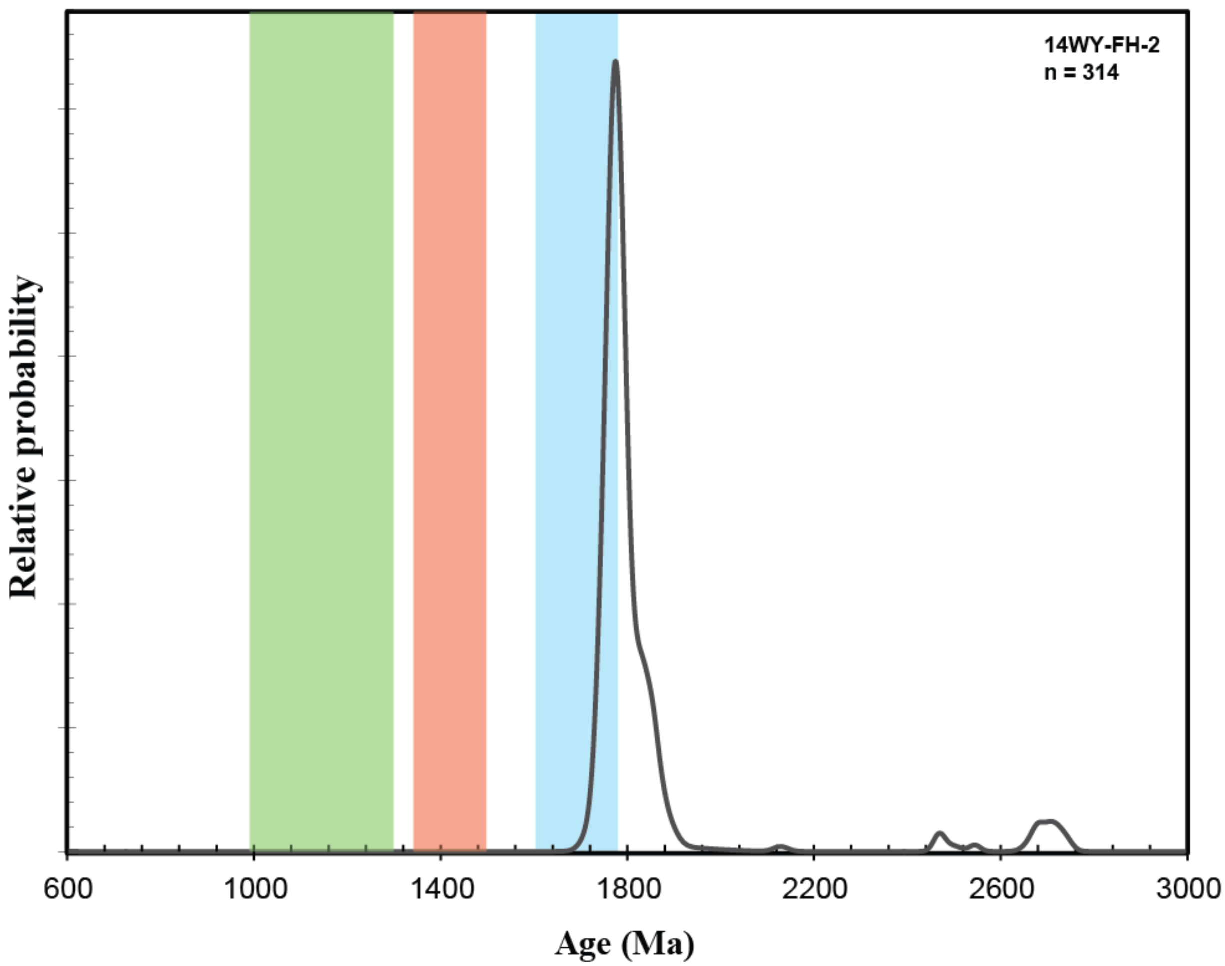

Figure 3.6. Probability Density Functions for the Flathead Sandstone in the Owl Creek Mountains. Area under each curve totals to 100%. Crystalline basement ages indicated by colors: Green- Grenville Orogeny, Red- Granite-Rhyolite Province, Blue- Yavapai/Mazatzal Provinces.

(2128.7 ± 15. 8 Ma) and one older zircon (3324.9 ± 13.1 Ma) that are outside of these age clusters. No Grenvillian detrital zircon were identified, so no zircon Hf isotopic data were obtained for this sample.

D-J Basin Cores

Only two samples (14CO-BS-3 and 14CO-T-3) yielded a sufficient number of zircon grains for the calculation of an age spectra analysis (Figure 3.7a, b, c). Only sample 14CO-BS-3 yielded more than one hundred zircon grains (n = 105), the minimum number most workers suggest is required for the determination of statistically robust age probability function (Vermeesch, 2004). This sample has a dominant age peak at 1378.2 ± 24.1 Ma, and secondary peaks at 1153 ± 28.4 Ma, and 1678.1 ±19.5 Ma. A few older grains are found in this samples, including an Archean zircon (2068.3 ± 17.8 Ma). Sample 14CO-T-3 (n = 60) has prominent age peaks at 1096.4 ± 30.6 Ma, 1411.6 ± 25.1 Ma, and 1722.7 ± 19.6 Ma. For this sample, the age peaks at 1411 Ma and 1722 Ma are subequal, and dominate the zircon population. Zircon yields from the remaining six core samples were low and these grains were combined for the purposes of the U-Pb analyses (n_{total}=69). Zircons in this aggregate sample (14CO-Core) yield age peaks at 1103.7 ± 25.6 Ma, 1370.6 ± 24.2 Ma, and 1688.9 ±22.0 Ma, similar to the two individual samples (Figure 3.7c).

Fourteen Grenvillian zircon grains from sample 14CO-BS-3 were selected for Hf isotopic analysis and yielded ε_{Hf} (0) values from -15.2 to -27.7 with a typical 2σ error of ± 1.9. Seven Grenvillian zircon grains from Taos core sample (14CO-T-3) have ε_{Hf} (0) values from -19.4 to -25.5 with a typical 2σ error of ± 1.9 (Figure 3.4). Six Grenvillian zircon grains from the combined core samples were have ε_{Hf} (0) values from -19.4 to -25.5 (± 2, 2σ).

Tava Sandstone Injectite

The U-Pb ages for the three previously analyzed Tava samples are shown in Figure 3.6 a-c ([SH324-HO] from Siddoway and Gehrels, 2014; and [SH324-BD and SH324-VE] from Siddoway,

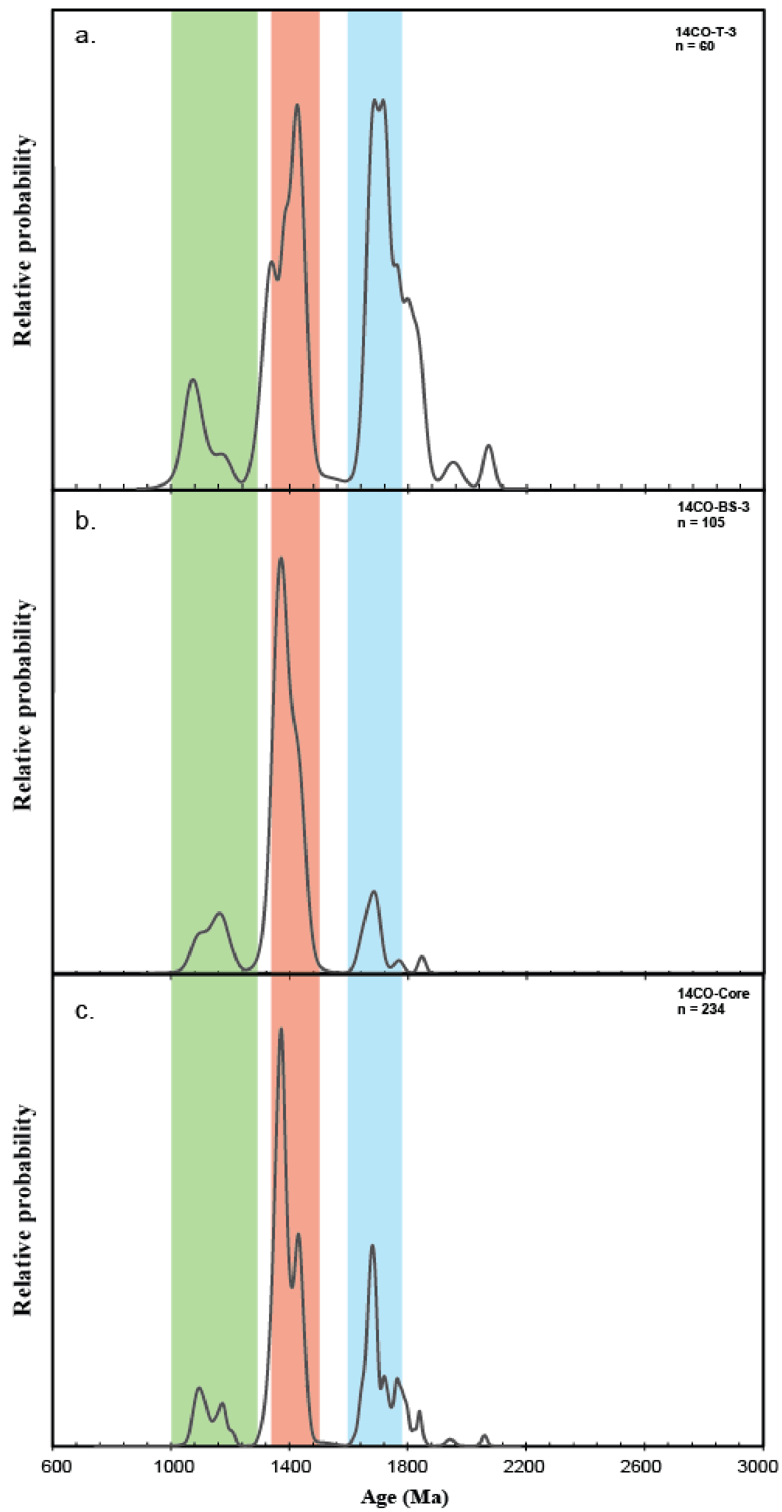

Figure 3.7. Probability Density Function for the cores from the Denver Basin basement drilled cores from Lincoln Country, Colorado. Area under each curve totals to 100%. a. 14CO-BS-3 b. 14CO-T-3 c. 14CO-Cores Crystalline basement ages indicated by colors: Green- Grenville Orogeny, Red- Granite-Rhyolite Province, Blue- Yavapai/Mazatzal Provinces.

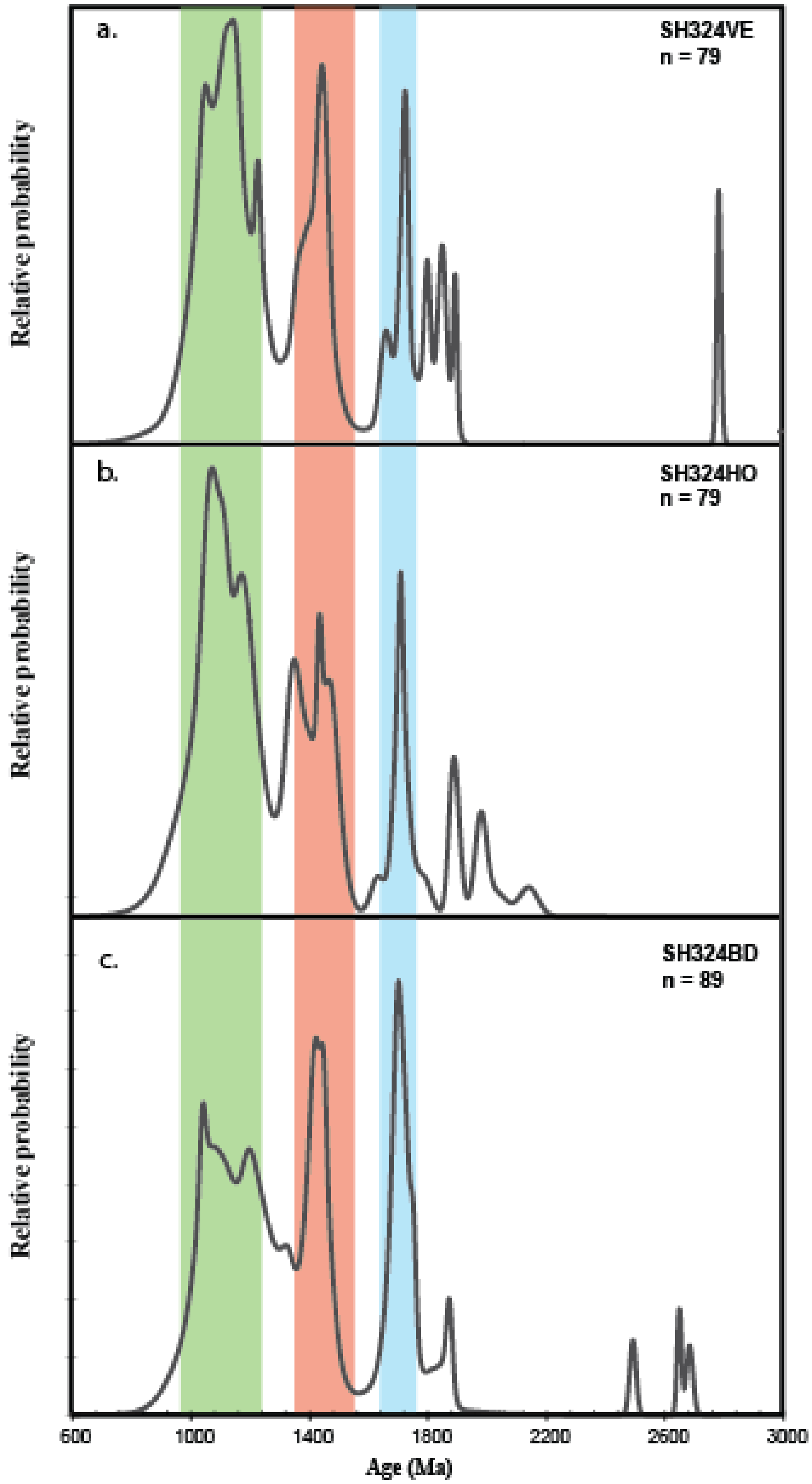

Figure 3.8. Probability Density Functions for Tava Sandstone samples. Area under each curve totals to 100%. Crystalline basement ages indicated by colors: Green- Grenville Orogeny, Red- Granite-Rhyolite Province, Blue- Yavapai/Mazatzal Provinces. SH324BD from Siddoway and Gehrels, 2014. SH324HO and SH324VE from Siddoway, unpublished data.

unpublished data). Grenvillian zircon [n= 84] between the ages of 962 to 1289 Ma were selected for Hf isotopic analyses. The ranges of ε_{Hf} (0) in the zircon grains from the three samples are very similar. Virtually all Grenvillian zircons (n = 83) span a range of ε_{Hf} (0) = -14.4 to -31.8 (± 2, 2σ), with one grain at ε_{Hf} = -42.5 (U-Pb age = 1233 Ma).

Discussion

The main concern of this project is to determine the source regions of Grenvillian zircon in the basal sandstones studied, based on both U-Pb and Hf isotopic data, and to assess the significance of changes in the relative abundances of Grenvillian detrital zircon in the sandstones in terms of the Cambrian paleogeography of southern Laurentia. One overall observation is that most of the sampled sandstones have Grenvillian, as well other ~1.4 Ga and ~1.7 Ga, as the prominent detrital zircon populations. Zircon derived from Archean crustal sources are, where present, only minor contributors to the total detrital zircon load of these sediments. These observations suggest that the primary sources of the detrital zircon deposited above the Great Unconformity were from Paleoproterozoic and Mesoproterozoic crustal sources within or at the margins of southern Laurentia. Archean crustal provinces, which constitute much of the northern half of Laurentia, were either not actively eroding during this time or sediments produced from the exhumation of this older crust were not being transported to the southern half of the continent. In contrast, because of the widespread occurrence of Grenvillian detrital zircon in the basal sandstones, it seems likely that crustal provinces of this age were actively exhuming during the Neoproterozoic and Cambrian and sediments were being transport across southern Laurentia. It should be emphasized, however, that the low clay and feldspar content of these basal sandstones, and the presence of well-rounded and sorted sand grains, suggests that these sediments likely underwent considerable weathering and, potentially, multiple cycles of transport and deposition prior to reaching their final depositional site (Schumm, 1968; Rainbird et al., 2012). Therefore, there is clearly a lag between the time of crustal source exhumation and erosion and sediment deposition, although this time lag does not affect the conclusions reached in the following text regarding the location from which the Grenvillian zircon were ultimately derived.

The second main observation is that although most of the basal sandstones contain Grenvillian zircon, the mode and range of Hf isotopic compositions vary between samples and suggest that multiple sources of Grenvillian zircon exist, as discussed in detail in the following text.

Lamotte Sandstone

The Lamotte sandstone sample is unique among the basal sandstones studied because it contains almost exclusively Grenvillian zircon (1096 ± 22 Ma) with a relatively narrow range of ε_{Hf} (0) values (~-25). These low ε_{Hf} (0) identify these zircon as likely products of erosion of Grenvillian basement rocks in the southern Appalachian Mountains, the latter having low ε_{Hf} (0) values compared to other rocks within the Grenville Province and to Grenvillian rocks in the Llano Uplift in central Texas (Howard et al., 2015). This result reveals that detrital zircon in the upper portions of the Lamotte Sandstone could not have been dominantly sourced either from the local ~1.4 Ga basement, or from Archean and Proterozoic rocks of the Canadian Shield to the north as previous workers speculated (Houseknecht and Ethridge, 1978). Instead, both the U-Pb and Hf isotopic data provide clear evidence that the upper Lamotte sands were transported almost exclusively from the east before being deposited on the shore face developing in southern Missouri during the transgression of Sauk Sea in the upper Cambrian. The narrow range of ε_{Hf} (0) for the detrital zircons in the upper Lamotte suggests that basement source rocks in the present-day southern Appalachian were the only sources of detrital zircon in the original sands, which suggest that either this was the only region actively undergoing exhumation or erosion along the eastern margin of Laurentia in the upper Cambrian, or more likely, that the fluvial systems providing sediments to the Sauk Sea shoreline in this region tapped a small catchment area that was restricted spatially to the southern Appalachians.

Flathead Sandstone

The Flathead sandstone sample is unique among the basal sandstones because it contains no Grenvillian detrital zircon. The lack of Grenvillian zircon in the Flathead Sandstone suggests that east-west directed continental river systems bearing Grenvillian zircon by-passed this region. The source of the main detrital zircon age population at ~1779 Ma in the Flathead Sandstone is enigmatic because rocks of this age are not found in the Precambrian basement of Wyoming (Frost et al., 2006). Detrital zircon with similar Paleoproterozoic ages were also reported for the Flathead Sandstone by May et al. (2013), who suggest a southeastern source from the Yavapai Province. However, the Yavapai Province is riddled with ~1.4 Ga intrusive units, an age which is not expressed in the detrital zircon record of the Flathead Sandstone. The Great Falls Tectonic Zone to the northwest of the Flathead Sandstone depositional area, however, is dominantly composed of 1.8-1.9 Ga intrusive and metamorphic rocks associated with the Big Sky Orogeny during the Paleoproterozoic (Condit et al., 2015). The lack of ~1.4 Ga detrital zircon in the upper Flathead Sandstone suggests that the Great Falls Tectonic Zone may have been the dominant zircon source.

Denver-Julesburg (D-J) Basin

Grenvillian detrital zircons in the D-J Basin cores vary over a significantly larger range, and trend to higher ε_{Hf} (0) values, than detrital zircon grains in the Lamotte Sandstone. The majority of Grenvillian detrital zircon in the D-J Basin sandstones have ε_{Hf} (0) values between -25 and -21, but show no correlation between U-Pb age and ε_{Hf} (0). The distinction between the Hf isotopic characteristics of Grenvillian detrital zircon in the D-J basin and Lamotte Sandstone samples precludes the possibility that zircon in these rocks could have been derived exclusively from the same source rocks in the southern Appalachians. The low ε_{Hf} (0) Grenvillian zircon in the D-J basin cores could share this same Appalachian source, but the higher (>-25) grains must have sources in higher ε_{Hf} (0) Grenvillian basement rocks. One possibility is the local, Mesoproterozoic Pikes Peak batholith, which does range to higher ε_{Hf} (0) values than granitic rocks in the Batholith (Fig. 3.9). More likely sources of older (>1.1 Ga) higher ε_{Hf} (0) zircons in the D-J Basin are the

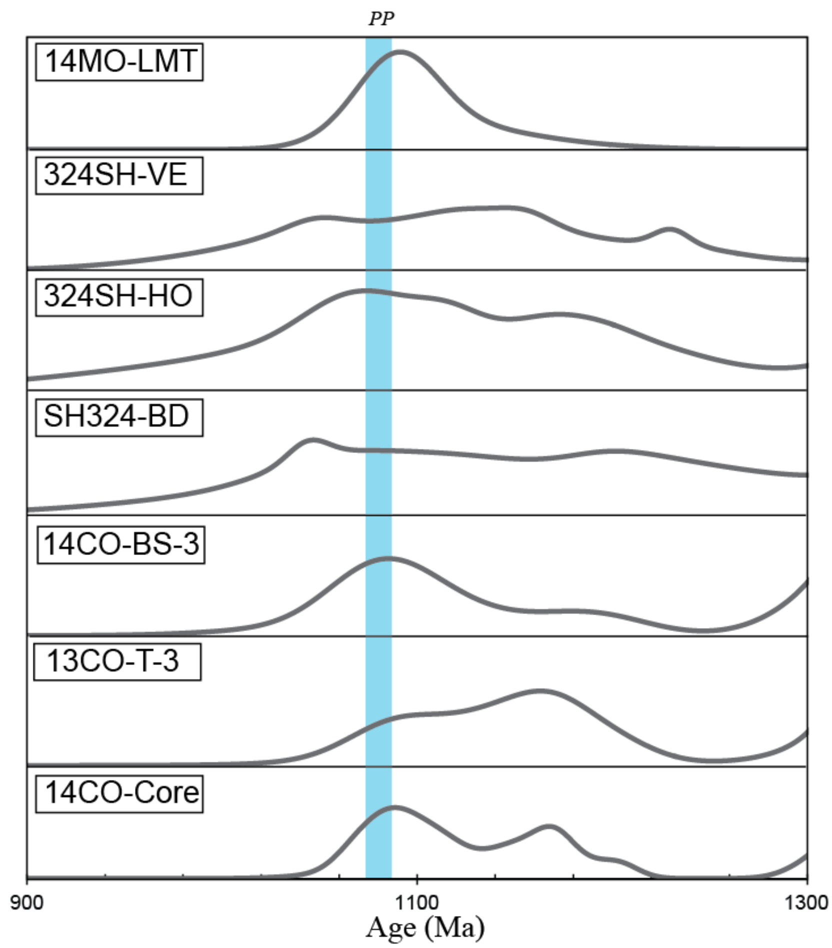

Figure 3.9. Age distribution diagram restricted to Grenville-Age detrital zircon. Blue region (PP) represents age of Pike Peak Batholith data from Howard et al., 2015.

Grenvillian rocks of Llano Uplift or Franklin Mountains to the south, as concluded for detrital zircon with similar Hf isotopic composition found in Cambrian sandstones exposed in the Mojave Desert region (Howard et al., 2015).

Another important question is whether or not the D-J Basin sandstones were deposited contemporaneously with the Sawatch Sandstone exposed in central Colorado (Myrow et al., 2003). The two sedimentary rocks do share lithologic similarities, but no absolute age determinations exist for the D-J Basin sandstone to assess their depositional age. The relative ages of the two sedimentary units is of interest however because, unlike the D-J Basin sandstones, the Sawatch Sandstone apparently contains no Grenvillian detrital zircon and is dominated by ~1.7 Ga and ~1.4 Ga detrital zircon (Siddoway and Gehrels, 2014). A possible explanation for this observation is that the D-J Basin sandstone was not deposited contemporaneously with Sawatch Sandstone, despite their lithologic similarities, and that the sources of detrital zircon delivered to present-day Colorado changed through time. An alternative possibility is that the two sandstones share the same depositional age, but a physical barrier prevented Grenvillian zircon from reaching the western depocenters of Sawatch Sandstone, as discussed further in a following section.

Tava Sandstone Injectite

Grenvillian detrital zircon in the Tava Sandstone Injectite display a wide range of U-Pb ages and Hf isotopic compositions (ε_{Hf} (0) = -14.4 to -31.8), similar to that observed for Grenvillian detrital zircon in the D-J Basin core samples (Figure 3.9). Previous interpretations of the detrital zircon U-Pb ages in the injectites suggested that Grenvillian detrital zircon with ages ~1.1 Ga peak were sourced from the local Pikes Peak Batholith, while grains with older ages (up to 1.33 Ga) were more likely derived from the Grenville Province at the eastern margin of Laurentia (Siddoway and Gehrels, 2014). The new Hf isotopic data are compatible, but require that the low ε_{Hf} (0) (< -20) zircon be derived from the local Pikes Peak batholith, not the southern Appalachians as concluded for the Lamotte sandstone, while the higher ε_{Hf} (0) zircon be derived from more distal sources, such as the Llano uplift area (but not the southern

Appalachians). Zircon sources in basement rocks in the Llano uplift and vicinity could also account for the older (>1.1 Ga) Grenvillian detrital zircon in the Tava Sandstone, given that rocks in the 1.2 to 1.3 Ga age range are found in central Texas (Barker and Reed, 2010). It is important to note that the Neoproterozoic Tava Sandstone is interpreted to record the sediment composition at the surface during the latest Proterozoic (Siddoway and Gehrels, 2014). The similarity between the detrital zircon age populations and isotopic compositions in the Tava Sandstones and those from the D-J Basin cores suggests that sediment transport paths across the southern margin of Laurentia were similar during and just after the breakup of Rodinia, and at both times siliciclastic sediment deposited in present day Colorado contained far-travelled and multi-cycle detrital zircons.

Regional Implications

The provenance information obtained for Grenvillian detrital zircon from these basal sandstones demonstrate that the range in $\varepsilon_{Hf}(0)$ of the Grenvillian detrital zircon population increases with distance from their presumed source regions in eastern Laurentia (Figure 3.10). This is particularly evident when comparing Grenvillian detrital zircon from the eastern and western basal sandstones. Grenvillian detrital zircon from the Upper Lamotte Sandstone, the easternmost sample in this study, contain a narrow range of low $\varepsilon_{Hf}(0)$ Grenvillian zircon. Another example of a locally derived basal sandstone is the El Arpa Formation deposited directly above the ~1.1 Ga Aibo Granite in Sonora, Mexico (Figure 3.10; Howard et al., 2015). Grenvillian detrital zircon from this unit exhibit a restricted range of Hf isotopic compositions identical to that of the Aibo Granite, suggesting that short transport distances prevented mixing of multiple zircon populations (Howard et al., 2015).

In contrast, the Grenvillian detrital zircon found in the Tava sandstone, and D-J Basin sandstone samples from Colorado, show a wider range of $\varepsilon_{Hf}(0)$ values, as well as a wider range of U-Pb ages than the Lamotte Sandstone. This suggests that sediment transport was not exclusively along east-to-west

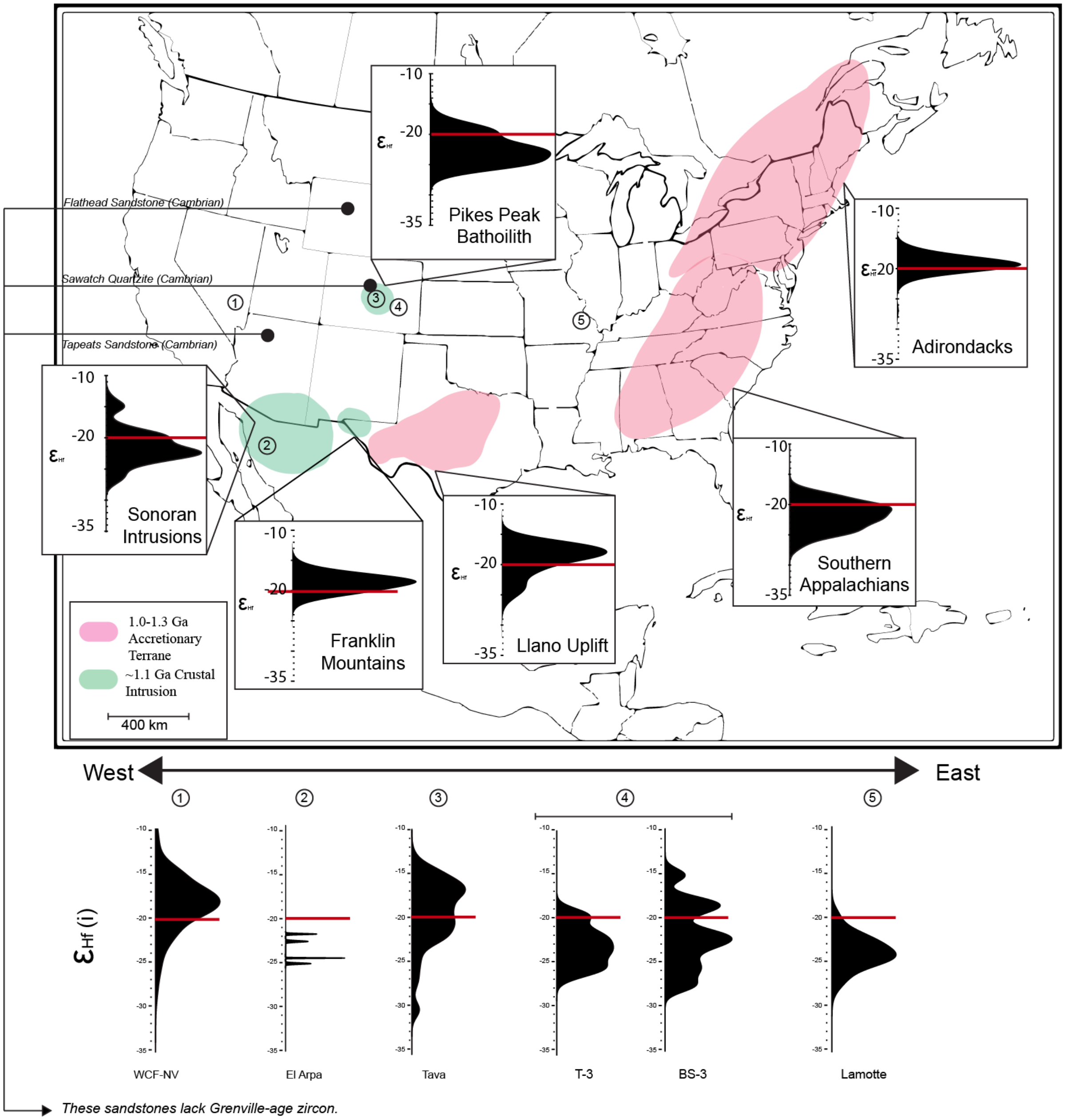

Figure 3.10. Map showing general source regions for Grenvilleian zircon and the observed range of their zircon Hf isotopic compositions. εHf (i) values plotted as probability density plots with 2σ error included. Area under each curve totals to 1. Sample locations are indicated with a number which corresponds to εHf (i) plots below. Red line denotes "high" and "low" εHf at εHf(i)= -20 Samples from this study: Tava Sandstone, BS-3, T-3, Lamotte Sandstone, and Flathead Sandstone. Campito Formation, El Arpa Formation, and Wood Canyon Formation - Nevada (WCF- NV), Franklin Mountains, Llano Uplift, Southern Appalachians (S. Appalachians), Pikes Peak Batholith, and some Sonoran Intrusions data from Howard et al (2015). Adirondack data from Bickford (2010). Sawatch Quartzite data from Siddoway and Gehrels (2014). Tapeats Sandstone data from Stewart et al (2001).

sediment transport vectors, but that south-to-north transport sediment transport was also required to create the observed diversity in detrital zircon $\varepsilon_{Hf}(0)$ values.

The Neoproterozoic-Cambrian Middle Member of the Wood Canyon Formation (MMWCF) in the Mojave Desert region also represents an example of a basal sandstone potentially comprised of distally-derived sediment (Schoenborn et al., 2012; Howard et al., 2015). Grenvillian detrital zircon recovered from the MMWCF exhibit a wide range of $\varepsilon_{Hf}(0)$, interpreted to be due to the mixing of distal zircons from accreted Grenville terranes along the eastern and southern margins of Laurentia with local zircons from intrusive rocks embedded in the Paleoproterozoic crust. (Figure 3.10; Howard et al., 2015).

Assuming that the Grenvillian detrital zircon Hf and U-Pb isotopic data requires sediment transport from both the present-day southern and eastern margins of Laurentia implies that areas of active crustal exhumation and erosion may have been limited to these regions during the Neoproterozoic and earlier Cambrian. One possibility is that the breakup of the Rodinian supercontinent produced uplift along the eastern and southern rifted margins of Laurentia at this time (Thomas, 1991; 2011; Li et al., 2008). If so, then sediments from the erosion of these rift flank uplifts were transported through a braided stream system across the plant-free continent, mixing with sediment from other sources prior to deposition.

Finally, despite a nearly ubiquitous presence of Grenvillian detrital zircon in basal sandstones, these zircon were discontinuously delivered to western Laurentia as a function of time and/or geographic position. The lack of Grenvillian detrital zircon in the Flathead sandstone is evidence for this, and it is supported by an absence of zircon of this age in other basal sandstones, namely the Tapeats Sandstone in Arizona and the Sawatch Sandstone in Colorado (Figure 3.10; Amato and Mack, 2012; Siddoway and Gehrels, 2014). One explanation for this observation is that a physical barrier existed between Grenvillian source rocks and the Flathead Sandstone depositional area, preventing influx of Grenvillian sediments. A NE-SW trending Paleozoic structural high, termed the “Transcontinental Arch” has been proposed on the basis of sediment thickness maps and U-Pb detrital zircon provenance studies (Ross and Tweto, 1980; Carlson, 1999; Amato and Mack, 2012). The transport of Grenvillian sediment would be cut off for sandstones deposited to the west of this proposed topographic high, which could explain the lack of zircons of this age in the Flathead Sandstones. Similarly, the lack of Grenvillian zircon in the Tapeats Sandstone in Arizona has been attributed to the formation of the Transcontinental Arch (Amato and Mack, 2012). This could also explain the lack of Grenvillian zircon found in the Sawatch Sandstone in Colorado, while the Tava Sandstone Injectite and basal sandstones from the D-J Basin must have been deposited to the east of such an arch.

However, the existence of a Transcontinental Arch is not universally accepted. While the Sawatch Sandstone contains no Grenvillian zircons, detailed sedimentologic analysis suggests that such a proposed structural high in Colorado is an artifact of miscorrelation of the Paleozoic section in the region (Myrow et al., 2003; Siddoway and Gehrels, 2014). One alternative to the proposed Transcontinental Arch is the transgression of the Sauk Sea across the continent during the Cambrian, which could have the same effect in the detrital zircon record (Sloss, 1988). Progressive inundation of Laurentia by the Sauk Sea may have "shut off" the transport of Grenvillian detrital zircon to the depocenters of the Tapeats, Sawatch, and Flathead Sandstones. In this case, the presence or absence of Grenvillian detrital zircon in basal Cambrian sandstones could provide information on the paleogeography of the Sauk Sea transgression through time.

Conclusions

Provenance determinations of basal sandstones from the midcontinent and comparisons with preexisting data are interpreted to determine the following conclusions.

1. The increase of the observed range of $\varepsilon_{Hf}(0)$ values of Grenvillian detrital zircon records the mixing of multiple zircon sources with westward transport distance from the Grenville Terrane in eastern Laurentia.

2. Grenvillian detrital zircon found Neoproterozoic to Cambrian basal sandstones in western Laurentia originated from both the southern and eastern margins of Laurentia. This suggests that

topographic highs were present in these regions during the sedimentation during or just after the breakup of Rodinia, which is consistent with rift-related uplift during the late-Proterozoic.

3. External forcing cut off the supply of Grenville-age zircon to the midcontinent during sandstone deposition during Sauk Sea transgression. Restriction of sediment transport from Grenville-age sources was restricted by a topographic barrier such as the Transcontinental Arch, or by spatial and/or temporal variability in the transgressive episodes of the Sauk Sea that intervened between depocenters in the west and sediment sources in the east or south.

References

Amato, J.M., Lawton, F.T., Mauel, D.J., Leggett, W.J., Gonzalez-Leon, C.M., Farmer, G.L., Wooden, J.L., 2009, Testing the Mojave-Sonora megashear hypothesis: Evidence from Paleoproterozoic igneous rocks and deformed Mesozoic strata in Sonora, Mexico: *Geology*, v. 37, p. 75-78.

Amato, J.M., Mack, G.H., 2012, Detrital zircon geochronology from the Cambrian-Ordovician Bliss Sandstone, New Mexico: Evidence for contrasting Grenville-age Cambrian sources on opposite sides of the Transcontinental Arch: *GSA Bulletin*, v. 124, p. 1826-1840.

Amelin, Y., Lee, D-C., Halliday, A.N., Pidgeon, R.T., 1999, Nature of the Earth's earliest crust from hafnium isotopes in single detrital zircons: *Nature*, v. 399, p. 252-255.

Andersen, T., 2005, Detrital zircons as tracers of sedimentary provenance: limiting conditions from statistics and numerical simulation: *Chemical Geology*, v. 216, no. 3-4, p. 249-270.

Anderson, T.H, Silver, L.T., 1981, An overview of Precambrian rocks in Sonora: *Revistas Mexicanas de ciencias geologicas*, v.5, no. 2, p. 131-139.

Anderson, T.H., Silver, L.T., 2005, The Mojave-Sonora megashear—Field and analytical studies leading to the conception and evolution of the hypothesis: *Geological Society of America Special Paper*, v. 393, p. 1-50.

Barker, D.S., Reed, R.M., 2010, Proterozoic granites of the Llano Uplift, Texas: A collision-related suite containing rapakivi and topaz granites: *GSA Bulletin*, v. 122, p. 253-264.

Barovich, K.M., Patchett, P.J., Peterman, Z.E., Sims, P.K., 1989, Nd isotopes and the origin of 1.9-1.7 Ga Penokean continental crust of the Lake Superior region: *GSA Bulletin*, v. 101, no. 3, p. 333-338.

Beebee, R.A., Cox, R., 1998, Dynamics of marine transgression onto a non-linear shoreline: the Middle Cambrian Flathead Sandstone, Clarks Fork Valley, Wyoming: *The Mountain Geologist*, v. 35, No. 3, p. 91-101.

Bell, L.H., 1970, Depositional History of the Flathead Sandstone: *Wyoming Geological Association: 22nd Annual Field Conference Guidebook,* p. 115-131.

Bell, L.H., Middleton, L.T., 1978, An introduction to the Cambrian Flathead Sandstone, Wind River basin, Wyoming: *Wyoming Geological Association: 30th Annual Field Conference Guidebook*, p. 79-88.

Bennett, V.C., DePaolo, D.J., 1987, Proterozoic crustal history of the western United States as determined by neodymium isotopic mapping: *GSA Bulletin*, v. 99, no. 5, p. 674-685.

Bickford, M.E., Mclelland, J.M., Mueller, P.A., Kamenov, G.D., and Neadle, M., 2010, Hafnium isotopic compositions of zircon from Adirondack AMCG suites: Implications for the petrogenesis of anorthosites, gabbros, and granitic members of the suites: *The Canadian Mineralogist*, v. 48, p. 751-761.

Blichert-Toft, J., Albarede, F., 1997, The Lu-Hf isotope geochemistry of chondrites and the evolution of the mantle-crust system: *earth and Planetary Science Letters*, v. 148, 243-258.

Bouvier, A., Vervoort, J.D., Patchett, P.J., 2008, The LU-Hf and Sm-Nd isotopic composition of CHUR: Constraints from unequilibrated chondrites and implications for the bulk composition of terrestrial planets: *Earth and Planetary Science Letters*, v. 273, p. 48-57.

Bowen, B.B., Ochoa, R.I., Wilkens, N.D., Brophy, J., Lovell, T.R., Fishieto, N., Medina, C.R., Rupp, J.A., 2009, Deposition and diagenetic variability within the Cambrian Mount Simon Sandstone: Implications for carbon dioxide sequestration, *Environmental Geosciences*, v. 13, no. 2, p. 69-89.

Bybee, G.M., Ashwal, L.D., 2015, Isotopic disequilibrium and lower crustal contamination in slowly ascending magmas: Insights from Proterozoic anorthosites: *Geochimica et Cosmochimica Acta*, v. 167, p. 286-300.

Carlson, M.P., 1999, Transcontinental Arch – a pattern formed by rejuvenation of local features across central North America: *tectonophysics*, v. 305, p. 225-233.

Condit, C.B., Mahan, K.H., Ault, A.K., Flowers, R.M., 2015, Foreland-directed propagation of high-grade tectonism in the deep roots of a Paleoproterozoic collisional orogen, SW Montana, USA: *Lithosphere*, v. 7, no. 6, p. 625-645.

Cullen, J., 2014, Sedimentology and Depositional history of the Riley Formation in the Northwestern Llano Uplift near Pontotoc, San Saba County, Texas (Abstract): *Gulf Coast Association of Geological Societies Transacions*, v. 64, p. 675.

DePaolo, D.J., 1981, Trace element and isotopic effects of combined wallrock assimilation and fractional crystallization: *Earth and Planetary Science Letters*, v. 53. p. 189-202.

Dickinson, W.R., 2008, Impact of differential zircon fertility of granitoid basement rocks in North America on age populations of detrital zircons and implications for granite petrogenesis: *Earth and Planetary Science Letters*, v. 275, p. 80-92.

Duchesne, J.C., Liegeois, J.P., Vander Auwera, J., Longhi, J., 1999, The crustal tongue melting model and the origin of massive anorthosites: *Terra Nova*, v. 11, no. 2-3, p. 100-105.

Emslie, R.F., Hamilton, M.A., Theriault, R.J., 1994, Petrogensis of a Mid-Proterozoic Anorthosite-Mangerite-Charnockite-Granite (AMCG) Complex: Isotopic and chemical evidence from the Nain Plutonic Suite: *The Journal of Geology*, v. 102, no.5, p. 539-558.

Enriquez-Castillo, M.A., Iriondo, A., Chavez-Cabello, G., Kunk, M.J., 2009, Interaccion termal entre magmas graníticos laramidicos y rocas encajonantes mesoproterozoicasL historia de enriamento de intrusivo de la Sierrita Blanca, NW Sonora: *Boletin de la Sociedad Geológica Mexicana*, v. 61, no. 3, p451-483.

Farmer, G.L., DePaolo, D.J., 1983, Origin of Mesoproerozoic and Tertiary Granite in the Western United States, and Implications for Pre-Mesozoic Crustal Structure 1: Nd and Sr Isotopic studies in the Geocline of the Northern Great Basin: *Journal of geophysical Research*, v. 88, no. 84, p. 3379-3401.

Farmer, G.L., DePaolo, D.J., 1984, Origin of Mesoproerozoic and Tertiary Granite in the Western United States, and Implications for Pre-Mesozoic Crustal Structure 2: Nd and Sr isotopic studies of Unmineralized and Cu- and Mo- Mineralized granite in the Precambrian Craton: *Journal of Geophysical Research*, v. 89, no. B12, p. 10141-10160.

Farmer, G.L., Broxton, D.E., Warren, R.G., Pickthorn, W., 1991, Nd, Sr, and O isotopic variations in metaluminous ashflow tuffs and related volcanic rocks at the Timber Mountain/Oasis Valley Caldera Complex, SW Nevada: implications for the origin and evolution of large-volume silicic magma bodies: *Contributions to Mineralogy and Petrology*, v. 109, p. 53-68.

Farmer, G.L., 1992, Magmas as tracers of lower crustal composition: an isotopic approach: *Lower Crustal developments in Geotectonics*, ch. 23, p. 363-390.

Farmer, G.L., Bowring, S.A., Matzel, J., 2005, Paleoproterozoic Mojave province in northwestern Mexico? Isotopic and U-Pb zircon geochronologic studies of Precambrian and Cambrian crystalline and sedimentary rocks, Caborca, Sonora: *Geological Society of America Special Papers*, v. 393, p. 183-198.

Famer, G.L., Bowring, S.A., Williams, M.L., Christensen, N.I., Matzel, J.P., Stevens, L., 2005b, Contrasting lower crustal evolution across an Archean-Proterozoic suture: Physical, Chemical, and Geochronologic studies of lower crustal zenoliths in southern Wyoming and northern Colorado: *The Rocky Mountain Region: An Evolving Lithosphere, Geophysical Monograph 154*, p. 139- 162.

Fedo, C,M., Cooper, J.D., 2001, Sedimentology and sequence stratigraphy of Neoproterozoic and Cambrian units across a craton-margin hinge zone, southeastern California, and implications for the early evolution of the Cordilleran margin: *Sedimentary Geology*, v. 141-142, p. 501-522.

Fedo, C.M., Sircombe, K.N., Rainbird, R.H., 2003, Detrital zircon analysis of the sedimentary record: *Reviews in Mineralogy and Geochemistry*, v. 53, p. 277-303.

Frost, C.D., Frost, B.R., Kirkwood, R., Chamberlain, K.R., 2006, The tonalite-trondhjemite-granodiotire (TTG) to ganodiorite-granite (GG) transition in the late Archean plutonic rocks of the central Wyoming Province: *Canadian Journal of Earth Sciences*, v. 43, no. 10, p. 1419-1444.

Gehrels, G.E., Blakey, R., Karlstrom, K.E., Timmons, J.M., Dickinson, B., Pecha, M.E., 2011, Detrital zircon U-Pb geochronology of Paleozoic strata in the Grand canyon, Arizona: *Lithosphere*, v. 2, no.3, p.183-200.

Gehrels, G.E., Pecha, M,E., 2014, Detrital zircon U-Pb geochronology and Hf isotope geochemistry of Paleozoic and Triassic passive margin strata of western North America: *geosphere*, v. 10, p. 49-65.

Harms, J.C., 1965, Sandstone dikes in relation to Laramide faults and stress distribution in the Southern Front Range, Colorado: *GSA Bulletin*, v. 76, p. 981-1002.

Hereford, R., 1977, Deposition of the Tapeats Sandstone (Cambrian) in central Arizona: *GSA Bulletin*, v. 88, p. 199-241.

Hiess, J., Condon, D.J., McLean, N., Noble, S.R., 2012, $^{238}U/^{235}U$ systematics in terrestrial uranium-bearing minerals: *Science*, v. 235, p. 1610-1614.

Houseknecht, D.W., Ethridge, F.G., 1978, Depositional history of the Lamotte Sandstone of southeastern Missouri: *Journal of Sedimentary Petrology*, v. 48. No, 2, p 575-586.

Howard, A.L., 2013, Hafnium Isotope evidence on the provenance of ~1.1 Ga detrital zircons from western North America, *Master's Thesis*, University of Colorado at Boulder, Howard, A.L., Farmer, G.L., Amato, J.M., Fedo, C.M., 2015 Zircon U-Pb ages and Hf isotopi compostion indicate multiple sources for ~1.1 Ga detrital zircon deposited in western Laurentia: *Earth and Planetary Science Letters*, v. 432, p. 300-310.

Hynes, A., Rivers, T., 2010, Protracted continental collision – evidence from the Grenville Orogen: *Canadian Journal of Earth Science*, v. 47, p. 591-620.

Iriondo, A, Premo, W.R., 2003, The cabora Block: an inhomogenous pice of Poterozoic crust in Sonora: *Geological Society of America Abstract with Programs*, v. 35, no. 4, p. 67.

Iriondo, A., Premo, W.R., Martinez-Torres, L.M., Budahn, J.R., Atkinson Jr., W.W., Siems, D.F., Gonzalez-Guarias, B., 2004, Isotopic, geochemical, and temporal characterization of Proterozoic basement rocks in the Quitovac region, northwestern Sonora, Mexico: Implications for the reconstruction of the southwestern margin of Laurentia: *GSA Bulletin*, v. 115, no. 1-2, p. 154-170.

Jaffey, A.H., Flynn, K.F., Glendenin, L.F., Bentley, W.C., Essling, A.M., 1971, Precision measurement of half-lives and specific activities of 235Uand 238U: *Physical Review*, v. C4, p. 1889-1906.

Johnson, J.H., 1944, Paleozoic Sratigraphy o the Sawatch Range, Colorado: *GSA Bulletin*, v. 55, p. 303-378.

Jones, J.V., Thrane, K., 2012, Correlating Proterozoic synorogenic metasedimentary successions in southwestern Laurentia: New insights from detrital zircon U-Pb geochronology of Paleoproterozoic quartzite and metaconglomerate in central and northern Colorado, USA: *Rocky Mountain Geology*. V. 47, p. 1-35.

Kempton, P.D., Harmon, R.S., Hawkesworth, C.J., Moorbath, S., 1990, Petrology and geochemistry of lower crustal granulites from the Geronimo Volcanic Field, southeastern Arizona: *Geochimica et Cosmochimica Acta*, v. 54, no. 12, p. 3401-3426.

Kinny, P.D, Maas, R., 2003, Lu-Hf and Sm-Nd isotopic systems in zircon: *Reviews in Mineralogy and Geochemistry*, v. 53, p. 327-341.

Li, Z.X., Bogdanova, S.V., Collins, A.S., Davidson, A., De Waele, B., Ernst, R.E., Fitzsimons, I.C.W., Fuck, R.A., Gladkochub, D.P., Jacobs, J., Karlstrom, K.E., Lu, S., Natapov, L.M., Pease, V., Pisarevsky, S.A., Thrane, K., Vernikovsky, V., 2008, Assembly, configuration, and break-up history of Rodinia: A synthesis: *Precambrian Research*, v. 160, p. 179-210.

Lambiase, J.J., Bosworth, W., 1995, Structural controls on sedimentation in continental rifts: *Geological Society of London, Special Publications*, v. 80, p. 117-144.

Lovell, T.R., Bowen, B.B., 2013, Fluctuations in Sedimentary Provenance of the Upper Cambrian Mount Simon Sandstone, Illinois Basin, United States: *he Journal of Geology*, v. 121, no. 2, p. 129-154.

MacLachlan, J.C., 1961, Cambrian, Ordovician, and Devonian systems, eastern Colorado subsurface: *The Mountain Geologist*, Rocky Mountain Association of Geologists, p. 41-52

May, S.R., Graym G.G., Summa, L.L., stewart, N.R., Gehrels, G.E., Pecha, M.E., 2013, Detrital zircon geochronology from the Bighorn Basin, Wyoming, USA: Implications for tectonostratigraphic evolution and paleogeography: *GSA Bulletin*, v. 125, p. 1403-1422.

McElroy, M.N., 1965, Lithologic and stratigraphic relationships between the Reagan Sandstone (Upper Cambrian) and sub-Reagan and supra-Reagan rocks in western Kansas. Dissertation Abstracts, vol 26, no. 6, p. 3249.

McLelland, J.M., Bickford, M.E., Hill, B.M., Clechenko, C.C., Valley, J.W., Hamilton, M.A., 2004, Direct dating of Adirondack massif anorthosite by U-Pb SHRIMP analysis of igneous zircon: Implications for AMCG complexs: *GSA Bulletin*, v. 116, no. 11-12, p. 1299-1317.

Menuge, J.F., Brewer, T.S., Seeger, C.M., 2002, Petrogenesis of metaluminous A-type rhyolites from the St Francois Mountains, Missouri and the Mesoproterozoic evolution of the southern Laurentian margin: *Precambrian Research*, v. 113, p. 269-291.

Molina-Garza, R.S., Iriondo, A., 2007, The Mojave-Sonora megashear: The hypothesis, the controversy, and the current state of knowledge*: Geological Society of America Special Papers*, v. 422, p. 233-259.

Morel, M.L.A., Nebel, O., Nebel-Jacobsen, Y.J., Miller, J.S., Vroon, P.Z., 2008, Hafnium isotope characterization of the GJ-1 zircon reference material by solution and laser-ablation MC-ICPMS: *Chemical Geology,* v. 255, p. 231-235.

Mueller, P.A., Peterman, Z.E., Granath, J.W., 1985, A bimodal Archean volcanic series, Owl Creek Mountains, Wyoming: *Journal of Geology,* v. 93, no. 6, p. 701-712.

Mueller, P.A., Foster, D.A., Mogk, D.W., Wooden, J.L., Kamenov, G.D., Vogt, J.J., 2007, Detrital mineral chronology of the Uinta Mountain Group: Implications for the Grenville flood in southwestern Laurentia: *Geology*, v. 35, no. 5, p. 431-434.

Myrow, P.M., 1998, Transgressive stratigraphy and depositional framework of Cambrian tidal dune deposits, Peerless Formation, central Colorado, USA: *SEPM Special Publication*, no. 62, p. 143-154.

Myrow, P.M., Taylor, J.F., Miller, J.F., Ethington, R, L., Ripperdan, R.L., Allen, J., 2003, Fallen arches: Dispelling myths concerning Cambrian and Ordovician paleogeography of the Rocky Mountain region: *GSA Bulletin*, v. 115, no. 5, p. 695-713.

Nealy, L.D., Unruh, D.M., 1991, Geochemistry and isotopic characteristics of deep crustal xenoliths from Tule Tank, San Francisco volcanic field, northern Arizona: *Proterozoic geology and ore deposits of Arizona: Arizona Geological Society Digest*, v. 19, p. 153-163.

Nelson, B.K., DePaolo, D.J., 1985, Rapid production of continental crust 1.7 to 1.9 b.y. ago: Nd isotopic evidence from the basement of the North American mid-continent: *GSA Bulletin*, v. 96, p. 746-754.

Ojakangas, R.W., 1963, Petrology and sedimentation of the Upper Cambrian Lamotte Sandstone in Missouri: *Journal of Sedimentary Petrology*, v. 33, no. 4, p. 860-873.

Patchett, P.J., 1983, Importance of the Lu-Hf isotopic system in studies of planetary chronology and chemical evolution: *Geochimica et Cosmochimica Acta*: v. 47, p. 81-91.

Patchett, P.J., Ruiz, J., 1989, Nd Isotopes and the origin of Grenville-Age Rocks in Texas: Implications for Proterozoic evolution of the United States Mid-Continent Region*: Journal of Geology*, v. 97, no. 6, p. 685-695.

Peters, S.E., Gaines, R.R., 2012, Formation of the 'Great Unconformity' as a trigger for the Cambrian explosion: *Nature,*v. 484, p. 363- 366.

Rainbird, R.H., Heaman, L.M., Young, G., 1992, Sampling Laurentia: Detrial zircon geochronology offers evidence for an extensive Neoproterozoic river system originating from the Grenville orogen: *Geology*, v. 20, p. 351-354.

Rainbird, R.H., McNicoll, V.J., Theriault, R.J., Heaman, L.M., Abott, J.G., Long, D.G.F., Thorkelson, D.J., 1997, Pan-continental river system draining Grenville Orogen recorded by U-Pb and Sm-Nd Geochronology of Neoproterozoic quartzarenites and mudrocks, northwestern Canada: *The Journal of Geology*, v. 105, no.1, p. 1-17.

Rainbird, R.H., Cawood, P., Gehrels, G.E., 2012, The great Grenvillian sedimentation episode: record of supercontinent Rodinia's assembly: *Tectonics of Sedimentary Basins: Recent Advances,*1st Edition, Edited by Busby and Azor. Blackwell Publishing Ltd, p. 583-601.

Ross, R.J., Jr., and Tweto, O., 1980, Lower Paleozoic sediments and tectonics in Colorado, in Kent, H.C., and Porter, K.W., *eds.*, Colorado geology: Denver, Colorado, Rocky Mountain Association of Geologists- 1980 Symposium, p. 47-56.

Scherer, E.E., Whitehouse, M.J., Munker, C., 2007, Zircon as a Monitor of Crustal Growth: *Elements*, v. 3, p. 19-24.

Schoenborn, W.A., Fedo, C.M., Farmer, G.L., 2012, Provenance of the Neoproterozoic Johnnie formation and Sitrling Quartzite, southeastern California, determined by etrital zircon geochronology and Nd isotope geochemistry: *Precambrian Research*, v. 206-207, p. 182-199.

Schumm, S.A., 1968, Speculations concerning paleohydrologic controls of terrestrial sedimentation: *GSA Bulletin*, v. 79, p. 1573-1588.

Siddoway, C.S., Gehrels, G.E., 2014, Basement-hosted sandstone injectites of Colorado: A vestige of the Neoproterozoic revealed through detrital zircon provenance analysis: *Lithosphere*, v. 6, no. 6, p. 403-408.

Sloss, L.L., 1963, Sequences in the Cratonic Interior of North America: *GSA Bulletin*, v. 74, p. 93-114.

Sloss, L.L., 1988, Tectonic evolution of the craton during Phanerozoic time: *The Geology of North America*, vol. D-2: Sedimentary Cover-North American Craton: U.S., The Geological Society of America, p. 25-51.

Smith, D.R., Noblett, J., Wobus, R.A., Unruh, D., Douglass, J., Beane, R., Davis, C., Goldman, S., Kay, G., Gustavson, B., Saltoun, B., Stewart, J., 1999, Petrology and geochemistry of late-stage intrusions of the A-type, mid-Proterozoic Pikes Peak batholith (Central Colorado, USA): implications for petrogenetic models: *Precambrian Research*, v. 98, p. 271-305.

Spencer, C.J., Hoiland, C.W., Harris, R.A., Link, P.K., Balgord, E.A., 2012, Constraining the timing and provenance of the Neoproterozoic Little Willow and Big Cottonwood Formations, Utah: Expanding the sedimentary record for early rifting of Rodinia: *Precambrian Research*m, v. 204-205, p. 57-65.

Spencer, C.J., Prave, A.R., Cawood, P.A., Roberts, N.M.W., 2014, Detrital ziron geochronology of the Grenville/Llano foreland and basal Sauk Sequence in west Texas, USA: *GSA Bulletin*, v. 126, p. 1117-1128.

Stevenson, R.K., Patchett, P.J., 1990, Implications for the evolution of continental crust from Hf isotope systematics of Archean detrital zircons*: Geochimica et Cosmochimca Acta*, v. 54, p. 1683-1697.

Stewart, J.H., Gehrels, G.E., Barth, A.P., Link, P.K., Christie-Blick, N., Wrucke, C.T., 2001, Detrital zircon provenance of Mesoproterozoic to Cambrian arenites in the western united States and northwestern Mexico: *GSA Bulletin*, v. 113, no. 10, p. 1343-1356.

Stewart, J.H., Amaya-Martinez, R., Palmer, A.R., 2002, Neoproterozoic and Cambrian strata of Sonora, Mexico: Rodinian supercontinent to Laurentian Cordilleran margin: *Geological Society of America Special Paper*, v. 365, p. 5-48.

Thomas, W.A., 1991, The Appalachian-Ouachita rifted margin of southeastern North America: *GSA Bulletin,* v. 103, no. 3, p. 415-431.

Thomas, W.A., 2001, Detrital-zircon geochronology and sedimentary provenance: *Lithosphere,* v. 3, no. 4, p.304-308.

Thomas, W.A., 2011, The Iapetan rifted margin of southern Laurentia: *Geosphere*, v. 7, p. 97-120.

Turner, S.P., Foden, J.D., Morrison, R.S., 1992, Derivation of some A-type magmas by fractionation of basaltic magma: An example from the Padthaway Ridge, South Australia*: Lithos*, v. 28, p. 151-179.

Van Schmus, W.R., et al., 1993, Transcontinental Proerozoic Provinces, *Precambrian: Conterminous U.S.*: Boulder, Colorado, Geological Society of America, Ch. 2, p. 171-334

Vermeesch, P., 2004, How many grains are needed for a provenance study? *Earth and Planetary Science Letters*,v. 224, p. 441-451.

Vervoort, J.D., Patchett, P.J., 1996, Behavior of hafnium and neodymium isotopes in the crust: Constraints from Precambrian crustally derived granites: *Geochemica et Cosmochimica Acta*, v. 60. No. 19, p. 3717-3733.

Vervoort, J.D., Patchett, P.J., Gehrels, G.E., Nutman, A.P., 1996, Constraints on early Earth differentiation from hafnium and neodymium isotopes: *Nature,* v. 379, p.624-627.

Vervoort, J.D., Blichert-Toft, J., 1999, Evolution of the depleted mantle: Hf isotopic evidence from juvenile rocks through time: *Geochimica et Cosmochimica Acta,* v. 63, no. 3-4, p. 533-556.

Vitanage, P.W., 1954, Sandstone dikes in the South Platte Area, Colorado: *The Journal of Geology*, v. 62, no. 5, p. 493-500.

Wetherill, G.W., 1956, Discordant uranium-lead ages: *Eos, American Geophysical Union Transactions*, v. 37, no. 3, p. 320-326.

Whitmeyer, S.J., Karlstrom, K.E., 2007, Tectonic model for the Proterozoic growth of North America: *Geosphere*, v. 3. No. 4, p. 220-259.

Appendix A: Data Tables

Table A-1. LA-ICP-MS U-Pb data for igneous samples from Sonora, Mexico. Uncertainties include both random and systematic error. Analysis with >10% measurement error, >20% discordance, or >5% reverse discordance were discarded.

Analysis	U (ppm)	206Pb 204Pb	U/Th	206Pb* 207Pb*	± (%)	207Pb* 235U*	± (%)	206Pb* 238U	± (%)	error corr.	206Pb* 238U*	± (Ma)	207Pb* 235U	± (Ma)	206Pb* 207Pb*	± (Ma)	Best age (Ma)	± (Ma)	Concordance (%)
CP-3-Spot 104	448	33118	1.8	13.0109	1.1	1.8803	2.1	0.1774	1.7	0.85	1052.9	16.9	1074.2	13.6	1117.5	21.8	**1117.5**	**21.8**	94.2
CP-3-Spot 24	524	72439	0.5	13.3340	0.7	1.7720	1.3	0.1714	1.1	0.85	1019.6	10.7	1035.3	8.6	1068.4	14.0	**1068.4**	**14.0**	95.4
CP-3-Spot 36	545	244325	2.7	13.0819	1.2	1.6793	3.0	0.1593	2.7	0.91	953.1	24.2	1000.7	19.0	1106.6	24.1	**1106.6**	**24.1**	86.1
CP-3-Spot 46	154	56655	1.4	11.0590	1.3	3.1633	2.1	0.2537	1.6	0.77	1457.6	20.6	1448.2	15.9	1434.5	25.1	**1434.5**	**25.1**	101.6
CP-3-Spot 47	595	94390	2.2	13.2023	0.5	2.0067	1.5	0.1921	1.4	0.93	1133.0	14.0	1117.8	9.8	1088.3	10.7	**1088.3**	**10.7**	104.1
CP-3-Spot 59	365	83602	1.6	13.1734	0.8	1.8243	2.5	0.1743	2.4	0.95	1035.8	22.8	1054.2	16.4	1092.7	15.2	**1092.7**	**15.2**	94.8
CP-3-Spot 76	1255	494613	1.7	13.1562	1.0	1.9586	1.6	0.1869	1.3	0.79	1104.5	12.9	1101.4	10.8	1095.4	19.7	**1095.4**	**19.7**	100.8
QTV-1-Spot 17	247	77583	2.1	13.2890	1.3	1.8482	2.3	0.1781	1.9	0.82	1056.7	18.2	1062.8	14.9	1075.2	25.7	**1075.2**	**25.7**	98.3
QTV-1-Spot 21	135	57970	2.3	13.3204	1.4	1.8744	2.1	0.1811	1.6	0.76	1072.9	15.7	1072.1	13.9	1070.5	27.5	**1070.5**	**27.5**	100.2
QTV-1-Spot 56	1173	343460	2.9	13.1523	0.8	1.6866	3.9	0.1609	3.8	0.98	961.7	33.8	1003.5	24.6	1095.9	15.5	**1095.9**	**15.5**	87.8
QTV-1-Spot 65	395	139192	1.9	12.9806	0.9	1.8828	1.8	0.1773	1.6	0.88	1051.9	15.6	1075.0	12.1	1122.2	17.4	**1122.2**	**17.4**	93.7
QTV-1-Spot 68	149	64024	3.2	13.1788	1.3	1.9300	1.9	0.1845	1.4	0.74	1091.4	14.3	1091.6	12.8	1091.9	25.6	**1091.9**	**25.6**	100.0
QTV-2-Spot 13	1353	161760	1.8	13.2349	0.5	1.8870	1.5	0.1811	1.4	0.95	1073.1	13.8	1076.5	9.7	1083.4	9.3	**1083.4**	**9.3**	99.1
QTV-2-Spot 18	951	61237	3.6	13.2454	0.7	1.8512	3.0	0.1778	2.9	0.97	1055.1	28.2	1063.9	19.7	1081.8	14.3	**1081.8**	**14.3**	97.5
QTV-2-Spot 2	145	62451	3.0	12.9003	1.6	1.6325	2.0	0.1527	1.2	0.58	916.3	10.0	982.8	12.7	1134.5	32.8	**1134.5**	**32.8**	80.8
QTV-2-Spot 26	278	33656	1.7	13.1373	1.0	1.8742	1.9	0.1786	1.6	0.86	1059.2	15.8	1072.0	12.5	1098.2	19.1	**1098.2**	**19.1**	96.4
QTV-2-Spot 28	420	62238	5.7	13.1164	0.8	1.7702	1.9	0.1684	1.7	0.90	1003.3	15.9	1034.6	12.4	1101.4	16.9	**1101.4**	**16.9**	91.1
QTV-2-Spot 34	1070	152449	1.9	13.2535	0.9	1.8506	1.6	0.1779	1.3	0.83	1055.4	12.9	1063.6	10.6	1080.6	18.1	**1080.6**	**18.1**	97.7
QTV-2-Spot 44	444	63517	2.3	13.0220	1.0	1.8714	1.8	0.1767	1.5	0.83	1049.2	14.5	1071.0	11.9	1115.8	20.0	**1115.8**	**20.0**	94.0
QTV-2-Spot 55	805	68123	1.8	13.0706	1.0	1.8047	1.5	0.1711	1.1	0.76	1018.1	10.6	1047.2	9.7	1108.4	19.1	**1108.4**	**19.1**	91.9
QTV-2-Spot 62	440	134684	1.9	13.1102	1.6	1.9249	3.6	0.1830	3.3	0.90	1083.5	32.6	1089.8	24.4	1102.4	32.2	**1102.4**	**32.2**	98.3
QTV-2-Spot 63	492	236017	2.2	13.0643	1.2	1.7855	3.1	0.1692	2.8	0.92	1007.6	26.1	1040.2	19.9	1109.3	24.6	**1109.3**	**24.6**	90.8
QTV-2-Spot 67	2347	1274108	1.8	13.1211	0.6	1.9442	1.1	0.1850	0.9	0.83	1094.3	9.5	1096.5	7.7	1100.7	12.8	**1100.7**	**12.8**	99.4
QTV-2-Spot 77	134	37825	3.0	13.2069	1.0	1.8930	1.6	0.1813	1.3	0.81	1074.2	13.2	1078.6	10.9	1087.6	19.3	**1087.6**	**19.3**	98.8
QTV-2-Spot 78	499	180974	1.8	13.1470	1.3	1.7907	3.5	0.1707	3.3	0.93	1016.2	30.7	1042.1	22.8	1096.7	25.3	**1096.7**	**25.3**	92.7
QTV-2-Spot 79	271	46292	1.9	13.2285	1.2	1.8766	2.0	0.1800	1.7	0.82	1067.2	16.4	1072.9	13.5	1084.4	23.4	**1084.4**	**23.4**	98.4
QTV-2-Spot 88	750	203898	2.0	13.0779	1.1	1.9142	1.6	0.1816	1.1	0.73	1075.5	11.3	1086.0	10.5	1107.3	21.7	**1107.3**	**21.7**	97.1
QTV-2-Spot 94	570	118790	1.7	13.2168	1.0	1.8409	1.8	0.1765	1.5	0.85	1047.6	14.8	1060.2	11.9	1086.1	19.3	**1086.1**	**19.3**	96.5
QTV-2-Spot 27	184	133447	0.9	12.9472	1.0	1.8453	3.6	0.1733	3.5	0.96	1030.1	33.0	1061.8	23.8	1127.3	19.7	**1127.3**	**19.7**	91.4
QTV-2-Spot 45	1104	196328	1.6	13.3108	0.8	1.9215	1.4	0.1855	1.1	0.80	1097.0	11.2	1088.6	9.3	1071.9	16.8	**1071.9**	**16.8**	102.3

Analysis	U	206Pb	U/Th	206Pb*	±	207Pb*	±	206Pb*	±	error	206Pb*	±	207Pb*	±	206Pb*	±	Best age	±	Concordance
	(ppm)	204Pb		207Pb*	(%)	235U*	(%)	238U	(%)	corr.	238U*	(Ma)	235U	(Ma)	207Pb*	(Ma)	(Ma)	(Ma)	(%)
QTV-3-Spot 12	1445	177700	1.7	13.1481	1.2	1.8096	2.3	0.1726	2.0	0.86	1026.2	18.9	1048.9	15.2	1096.6	23.8	**1096.6**	**23.8**	93.6
QTV-3-Spot 14	216	31809	2.4	13.2279	0.8	1.9674	1.5	0.1887	1.2	0.84	1114.6	12.6	1104.4	9.9	1084.5	16.2	**1084.5**	**16.2**	102.8
QTV-3-Spot 20	425	196825	3.3	13.2983	1.0	1.9134	1.8	0.1845	1.5	0.84	1091.8	15.3	1085.8	12.1	1073.8	19.8	**1073.8**	**19.8**	101.7
QTV-3-Spot 22	880	58987	2.1	13.1645	1.3	1.8472	2.1	0.1764	1.7	0.80	1047.1	16.4	1062.4	14.0	1094.1	25.4	**1094.1**	**25.4**	95.7
QTV-3-Spot 25	1730	58757	1.6	13.3250	0.9	1.8627	1.4	0.1800	1.1	0.80	1067.0	11.2	1067.9	9.4	1069.8	17.1	**1069.8**	**17.1**	99.7
QTV-3-Spot 30	1260	52322	1.9	13.3027	0.8	1.8889	1.4	0.1822	1.2	0.85	1079.2	12.1	1077.2	9.5	1073.1	15.2	**1073.1**	**15.2**	100.6
QTV-3-Spot 32	492	2550289	3.1	13.1258	1.1	1.8366	2.4	0.1748	2.1	0.89	1038.7	20.3	1058.6	15.6	1100.0	21.5	**1100.0**	**21.5**	94.4
QTV-3-Spot 33	960	120829	5.5	13.2710	0.5	1.8488	1.2	0.1779	1.0	0.89	1055.7	10.2	1063.0	7.8	1077.9	10.6	**1077.9**	**10.6**	97.9
QTV-3-Spot 38	202	69909	2.5	13.1558	1.3	1.9066	2.3	0.1819	1.9	0.83	1077.4	19.2	1083.4	15.5	1095.4	25.6	**1095.4**	**25.6**	98.4
QTV-3-Spot 89	168	132543	2.8	13.2366	1.6	1.9046	2.0	0.1828	1.2	0.59	1082.5	11.7	1082.7	13.2	1083.1	32.1	**1083.1**	**32.1**	99.9
QTV-3-Spot 9	1704	160202	2.4	13.2092	0.6	1.9136	1.4	0.1833	1.3	0.89	1085.1	12.5	1085.8	9.4	1087.3	13.0	**1087.3**	**13.0**	99.8
QTV-3-Spot 91	1081	93304	2.4	12.9416	1.7	1.9718	2.2	0.1851	1.4	0.63	1094.7	13.9	1105.9	14.8	1128.2	33.9	**1128.2**	**33.9**	97.0
QTV-3-Spot 96	643	63264	2.6	12.9419	1.2	1.7519	2.6	0.1644	2.4	0.90	981.4	21.6	1027.9	17.1	1128.1	23.5	**1128.1**	**23.5**	87.0
QTV-3-Spot 103	1103	206527	3.3	13.1237	1.0	1.9112	1.6	0.1819	1.3	0.81	1077.4	13.2	1085.0	10.9	1100.3	19.0	**1100.3**	**19.0**	97.9
QTV-3-Spot 31	360	128315	2.1	13.2276	1.2	1.8666	1.7	0.1791	1.3	0.72	1061.9	12.2	1069.3	11.4	1084.5	24.0	**1084.5**	**24.0**	97.9
QTV-3-Spot 39	1212	99910	2.0	13.1255	0.8	1.9691	1.6	0.1874	1.4	0.86	1107.5	14.1	1105.0	10.8	1100.0	16.1	**1100.0**	**16.1**	100.7
QTV-3-Spot 43	1063	188093	1.7	13.2453	0.9	1.9042	1.3	0.1829	1.0	0.74	1082.9	9.9	1082.6	8.9	1081.8	18.0	**1081.8**	**18.0**	100.1
QTV-3-Spot 57	220	75402	1.7	13.1634	1.2	1.9258	1.6	0.1839	1.1	0.67	1088.0	10.6	1090.1	10.5	1094.2	23.4	**1094.2**	**23.4**	99.4
QTV-3-Spot 99	849	147640	1.7	12.7352	1.0	1.8221	2.8	0.1683	2.7	0.93	1002.7	24.6	1053.4	18.7	1160.1	20.7	**1160.1**	**20.7**	86.4
QTV-3-Spot 41	546	69650	3.8	12.9263	1.5	1.8907	2.3	0.1772	1.7	0.75	1051.9	16.4	1077.8	15.0	1130.5	30.0	**1130.5**	**30.0**	93.0

Table A-2. LA-ICP-MS U-Pb data for detrital zircon recovered from siliciclastic units from the central United States. Uncertainties include both random and systematic error. Analysis with >10% measurement error, >20% discordance, or >5% reverse discordance were discarded.

Analysis	U (ppm)	206Pb 204Pb	U/Th	206Pb* 207Pb*	± (%)	207Pb* 235U*	± (%)	206Pb* 238U	± (%)	error corr.	206Pb* 238U*	± (Ma)	207Pb* 235U	± (Ma)	206Pb* 207Pb*	± (Ma)	Best age (Ma)	± (Ma)	Conc (%)
14MO-LMT-Spot 2	429	102286	3.4	12.7699	1.3	1.9944	1.9	0.1847	1.4	0.74	1092.7	14.2	1113.6	12.9	1154.7	25.6	**1154.7**	**25.6**	94.6
14MO-LMT-Spot 4	118	33553	3.1	13.2173	1.0	1.8814	1.9	0.1804	1.6	0.84	1068.9	15.8	1074.6	12.6	1086.0	20.7	**1086.0**	**20.7**	98.4
14MO-LMT-Spot 9	2117	75989	1.3	13.2392	0.9	1.7625	1.6	0.1692	1.3	0.81	1007.9	12.0	1031.8	10.3	1082.7	18.6	**1082.7**	**18.6**	93.1
14MO-LMT-Spot 11	149	95151	2.0	9.6419	1.0	4.2798	3.4	0.2993	3.2	0.95	1687.8	47.7	1689.5	27.8	1691.6	18.8	**1691.6**	**18.8**	99.8
14MO-LMT-Spot 14	600	66814	2.2	13.2635	1.2	1.8305	2.8	0.1761	2.6	0.91	1045.5	25.1	1056.4	18.7	1079.1	23.6	**1079.1**	**23.6**	96.9
14MO-LMT-Spot 17	248	133374	2.0	13.0914	1.2	1.8757	1.8	0.1781	1.4	0.74	1056.5	13.2	1072.5	12.1	1105.2	24.7	**1105.2**	**24.7**	95.6
14MO-LMT-Spot 20	479	91042	2.8	13.0541	0.8	1.9011	1.4	0.1800	1.1	0.80	1066.9	10.9	1081.5	9.3	1110.9	16.8	**1110.9**	**16.8**	96.0
14MO-LMT-Spot 38	434	115308	2.4	13.1394	1.4	1.9469	1.9	0.1855	1.3	0.69	1097.1	13.3	1097.4	12.9	1097.9	28.0	**1097.9**	**28.0**	99.9
14MO-LMT-Spot 40	1092	203101	1.8	13.1740	0.9	1.9281	1.4	0.1842	1.0	0.74	1090.0	10.2	1090.9	9.2	1092.6	18.6	**1092.6**	**18.6**	99.8
14MO-LMT-Spot 43	1253	141877	1.8	13.2103	0.8	1.9010	3.3	0.1821	3.2	0.97	1078.6	32.0	1081.5	22.1	1087.1	16.1	**1087.1**	**16.1**	99.2
14MO-LMT-Spot 47	215	152673	2.9	13.3120	1.2	1.7328	1.8	0.1673	1.3	0.75	997.2	12.2	1020.8	11.3	1071.7	23.3	**1071.7**	**23.3**	93.0
14MO-LMT-Spot 49	277	76772	2.5	12.8835	1.3	1.9331	3.1	0.1806	2.8	0.91	1070.4	27.7	1092.6	20.6	1137.1	25.1	**1137.1**	**25.1**	94.1
14MO-LMT-Spot 51	819	159548	2.0	13.2915	0.9	1.8552	1.8	0.1788	1.6	0.86	1060.6	15.6	1065.3	12.2	1074.8	18.7	**1074.8**	**18.7**	98.7
14MO-LMT-Spot 53	232	29790	2.9	12.5875	1.7	1.8655	2.4	0.1703	1.6	0.67	1013.8	14.9	1069.0	15.6	1183.2	34.3	**1183.2**	**34.3**	85.7
14MO-LMT-Spot 57	1292	419089	2.1	13.2169	0.8	1.8964	1.5	0.1818	1.2	0.85	1076.7	12.4	1079.8	9.7	1086.1	15.2	**1086.1**	**15.2**	99.1
14MO-LMT-Spot 61	608	187411	4.8	13.1063	0.7	1.9903	1.6	0.1892	1.5	0.90	1117.0	15.0	1112.2	11.0	1102.9	14.4	**1102.9**	**14.4**	101.3
14MO-LMT-Spot 75	280	139658	2.8	13.0691	1.5	1.9280	1.8	0.1827	0.9	0.53	1082.0	9.2	1090.8	11.7	1108.6	29.8	**1108.6**	**29.8**	97.6
14MO-LMT-Spot 77	285	197906	3.1	13.1528	0.9	1.9113	2.9	0.1823	2.8	0.95	1079.7	27.7	1085.0	19.6	1095.8	18.7	**1095.8**	**18.7**	98.5
14MO-LMT-Spot 79	282	71169	2.2	13.2050	1.5	1.9045	2.0	0.1824	1.3	0.67	1080.1	13.3	1082.7	13.2	1087.9	29.5	**1087.9**	**29.5**	99.3
14MO-LMT-Spot 92	180	41792	2.4	13.0518	1.2	1.9372	2.3	0.1834	1.9	0.84	1085.4	19.4	1094.0	15.4	1111.2	24.5	**1111.2**	**24.5**	97.7
14MO-LMT-Spot 98	1492	290882	2.0	13.2197	0.9	1.9698	1.6	0.1889	1.4	0.83	1115.2	14.0	1105.2	11.0	1085.7	18.0	**1085.7**	**18.0**	102.7
14CO-Core1-Spot 3	109	34529	4.1	13.2055	1.4	1.9765	1.8	0.1893	1.2	0.65	1117.6	11.8	1107.5	12.0	1087.9	27.2	**1087.9**	**27.2**	102.7
14CO-Core1-Spot 4	184	73812	1.4	9.7671	1.2	4.2113	1.7	0.2983	1.3	0.73	1683.0	18.8	1676.2	14.2	1667.8	21.7	**1667.8**	**21.7**	100.9
14CO-Core1-Spot 6	435	172788	2.0	9.3199	0.7	4.5537	1.7	0.3078	1.5	0.90	1729.9	22.9	1740.8	14.0	1754.0	13.6	**1754.0**	**13.6**	98.6
14CO-Core1-Spot 8	106	122529	1.4	9.8018	1.4	4.0798	2.0	0.2900	1.3	0.68	1641.7	19.3	1650.3	15.9	1661.2	26.4	**1661.2**	**26.4**	98.8
14CO-Core1-Spot 9	76	40840	1.3	11.7574	1.4	2.7734	3.6	0.2365	3.4	0.93	1368.5	41.4	1348.4	27.0	1316.7	26.2	**1316.7**	**26.2**	103.9
14CO-Core1-Spot 12	202	71854	1.7	9.6927	0.9	4.3793	1.5	0.3079	1.3	0.83	1730.1	19.4	1708.4	12.7	1681.9	15.8	**1681.9**	**15.8**	102.9
14CO-Core1-Spot 14	113	23199	1.6	13.3684	2.0	0.7323	4.0	0.0710	3.5	0.87	442.2	14.9	557.9	17.2	1063.2	39.9	**442.2**	**14.9**	41.6
14CO-Core1-Spot 15	165	59570	1.1	11.5279	1.2	2.7984	1.9	0.2340	1.6	0.80	1355.3	19.2	1355.1	14.6	1354.8	22.3	**1354.8**	**22.3**	100.0
14CO-Core1-Spot 16	144	210613	1.4	9.6671	1.2	4.2763	2.6	0.2998	2.3	0.88	1690.4	34.3	1688.8	21.6	1686.8	23.1	**1686.8**	**23.1**	100.2
14CO-Core1-Spot 18	163	55264	1.2	11.4338	1.0	2.9122	2.1	0.2415	1.8	0.88	1394.5	22.9	1385.1	15.7	1370.6	19.0	**1370.6**	**19.0**	101.7
14CO-Core1-Spot 19	57	45658	1.4	11.6790	1.5	2.7285	2.1	0.2311	1.4	0.67	1340.4	16.8	1336.3	15.4	1329.7	30.0	**1329.7**	**30.0**	100.8
14CO-Core1-Spot 22	249	52146	2.1	9.7192	1.0	4.1387	2.1	0.2917	1.8	0.88	1650.2	26.8	1662.0	17.2	1676.9	18.7	**1676.9**	**18.7**	98.4

Analysis	U	206Pb	U/Th	206Pb*	±	207Pb*	±	206Pb*	±	error	206Pb*	±	207Pb*	±	206Pb*	±	Best age	±	Conc
	(ppm)	204Pb		207Pb*	(%)	235U*	(%)	238U	(%)	corr.	238U*	(Ma)	235U	(Ma)	207Pb*	(Ma)	(Ma)	(Ma)	(%)
14CO-Core1-Spot 30	159	52276	1.3	11.4380	0.9	2.8271	1.6	0.2345	1.4	0.84	1358.2	16.8	1362.7	12.2	1369.9	16.8	**1369.9**	**16.8**	99.1
14CO-Core1-Spot 38	230	131870	1.5	11.2263	1.0	2.9629	1.7	0.2412	1.3	0.78	1393.2	16.3	1398.2	12.7	1405.8	19.9	**1405.8**	**19.9**	99.1
14CO-Core1-Spot 39	97	31218	1.5	11.3657	1.8	2.8470	3.5	0.2347	3.1	0.87	1359.0	37.6	1368.0	26.6	1382.1	33.8	**1382.1**	**33.8**	98.3
14CO-Core1-Spot 40	179	79651	1.8	11.5044	1.3	2.8466	2.4	0.2375	2.0	0.83	1373.8	24.5	1367.9	17.9	1358.8	25.3	**1358.8**	**25.3**	101.1
14CO-Core1-Spot 42	162	74179	1.5	11.5126	1.1	2.8690	1.8	0.2396	1.4	0.78	1384.4	17.8	1373.8	13.8	1357.4	22.0	**1357.4**	**22.0**	102.0
14CO-Core1-Spot 43	88	21427	0.8	9.7751	0.9	4.2296	1.8	0.2999	1.6	0.86	1690.6	23.4	1679.8	15.0	1666.3	17.0	**1666.3**	**17.0**	101.5
14CO-Core1-Spot 45	241	54259	2.0	9.8548	1.0	4.1930	1.9	0.2997	1.5	0.82	1689.8	22.7	1672.7	15.2	1651.2	19.4	**1651.2**	**19.4**	102.3
14CO-Core1-Spot 48	172	48063	0.6	11.2995	1.4	2.9794	3.6	0.2442	3.3	0.92	1408.3	41.8	1402.4	27.4	1393.3	27.7	**1393.3**	**27.7**	101.1
14CO-Core1-Spot 49	148	41819	1.0	9.9997	1.1	3.9129	3.0	0.2838	2.8	0.92	1610.4	39.2	1616.4	24.1	1624.1	21.4	**1624.1**	**21.4**	99.2
14CO-Core1-Spot 50	108	20700	2.0	13.1385	1.7	2.0163	2.5	0.1921	1.9	0.75	1132.9	19.6	1121.0	17.0	1098.0	33.0	**1098.0**	**33.0**	103.2
14CO-Core1-Spot 53	137	26945	1.9	11.5524	1.3	2.8430	1.8	0.2382	1.3	0.70	1377.3	15.8	1367.0	13.6	1350.7	24.8	**1350.7**	**24.8**	102.0
14CO-Core1-Spot 54	176	49858	1.7	11.4670	1.1	2.8957	1.7	0.2408	1.2	0.74	1391.0	15.2	1380.8	12.5	1365.0	21.5	**1365.0**	**21.5**	101.9
14CO-Core1-Spot 60	131	46242	1.4	11.5288	1.6	2.8009	2.1	0.2342	1.5	0.68	1356.4	17.9	1355.8	16.0	1354.7	30.1	**1354.7**	**30.1**	100.1
14CO-Core1-Spot 61	226	98833	1.9	13.3397	1.1	1.8582	1.7	0.1798	1.3	0.77	1065.7	12.8	1066.3	11.2	1067.6	21.8	**1067.6**	**21.8**	99.8
14CO-Core1-Spot 62	186	33446	2.1	9.7009	1.1	4.1982	1.4	0.2954	1.0	0.68	1668.3	14.4	1673.7	11.8	1680.4	19.4	**1680.4**	**19.4**	99.3
14CO-Core1-Spot 63	240	55526	2.3	11.4452	0.9	2.8535	1.9	0.2369	1.7	0.88	1370.4	20.7	1369.7	14.4	1368.7	17.8	**1368.7**	**17.8**	100.1
14CO-Core1-Spot 67	359	248897	1.7	11.4411	1.0	2.8192	1.7	0.2339	1.4	0.83	1355.1	17.3	1360.7	12.9	1369.4	18.6	**1369.4**	**18.6**	99.0
14CO-Core1-Spot 68	270	188062	3.8	11.3908	1.2	2.8657	1.9	0.2367	1.4	0.76	1369.7	17.9	1372.9	14.3	1377.9	23.7	**1377.9**	**23.7**	99.4
14CO-Core1-Spot 71	71	41963	1.4	11.6261	1.4	2.8400	2.3	0.2395	1.9	0.80	1383.9	23.2	1366.2	17.5	1338.5	26.8	**1338.5**	**26.8**	103.4
14CO-Core1-Spot 74	106	70028	1.4	9.6436	1.4	4.2215	2.2	0.2953	1.7	0.77	1667.8	25.5	1678.2	18.4	1691.3	26.2	**1691.3**	**26.2**	98.6
14CO-Core1-Spot 77	105	47520	1.2	10.8963	1.3	3.0297	2.4	0.2394	2.1	0.85	1383.7	25.7	1415.1	18.6	1462.7	24.3	**1462.7**	**24.3**	94.6
14CO-Core1-Spot 78	150	42693	1.6	11.4557	1.3	2.9028	2.4	0.2412	1.9	0.82	1392.8	24.2	1382.7	17.8	1366.9	25.8	**1366.9**	**25.8**	101.9
14CO-Core1-Spot 83	194	148562	1.8	11.1560	1.2	3.0900	1.7	0.2500	1.2	0.72	1438.5	15.8	1430.2	13.1	1417.8	22.9	**1417.8**	**22.9**	101.5
14CO-Core1-Spot 85	29	121814	1.4	11.6364	1.7	2.7730	3.8	0.2340	3.4	0.89	1355.6	41.3	1348.3	28.3	1336.8	33.4	**1336.8**	**33.4**	101.4
14CO-Core1-Spot 88	212	5584946	2.7	9.8136	1.2	4.1696	2.0	0.2968	1.6	0.81	1675.3	24.2	1668.1	16.7	1659.0	22.4	**1659.0**	**22.4**	101.0
14CO-Core1-Spot 92	82	30285	1.2	11.5687	1.3	2.6022	2.8	0.2183	2.5	0.89	1273.1	29.1	1301.2	20.6	1348.0	24.3	**1348.0**	**24.3**	94.4
14CO-Core1-Spot 96	220	94200	1.2	11.3871	1.3	3.0183	2.7	0.2493	2.4	0.88	1434.7	30.7	1412.3	20.6	1378.5	24.2	**1378.5**	**24.2**	104.1
14CO-Core1-Spot 97	299	254530	1.2	11.2745	1.1	2.7584	2.1	0.2256	1.8	0.85	1311.2	20.9	1344.4	15.4	1397.6	20.7	**1397.6**	**20.7**	93.8
14CO-Core1-Spot 100	276	33954	1.1	9.2442	3.6	4.3071	3.8	0.2888	1.4	0.37	1635.4	20.7	1694.7	31.6	1768.9	65.1	**1768.9**	**65.1**	92.5
14CO-Core1-Spot 101	38	34031	1.2	9.3760	3.1	4.4865	3.5	0.3051	1.6	0.45	1716.5	24.1	1728.5	29.3	1743.0	57.7	**1743.0**	**57.7**	98.5
14CO-Core1-Spot 104	73	100428	1.4	11.5494	1.8	2.8088	2.4	0.2353	1.7	0.69	1362.1	20.5	1357.9	18.1	1351.2	33.9	**1351.2**	**33.9**	100.8
14CO-Core1-Spot 106	286	126882	2.3	11.3868	0.9	2.8342	2.4	0.2341	2.2	0.92	1355.7	27.0	1364.6	17.9	1378.6	17.5	**1378.6**	**17.5**	98.3
14CO-Core1-Spot 108	53	43586	1.4	11.4813	1.8	2.8608	2.4	0.2382	1.6	0.65	1377.4	19.3	1371.6	18.0	1362.6	35.0	**1362.6**	**35.0**	101.1
14CO-Core1-Spot 109	266	84505	1.2	11.3680	1.1	2.5613	1.7	0.2112	1.2	0.74	1235.1	14.0	1289.7	12.4	1381.7	21.9	**1381.7**	**21.9**	89.4
14CO-Core-2-Spot 2	305	58179	2.2	9.5984	0.8	4.2624	1.2	0.2967	0.9	0.77	1675.1	13.5	1686.1	9.7	1699.9	13.8	**1699.9**	**13.8**	98.5
14CO-Core-2-Spot 3	119	32109	1.3	11.3471	1.3	2.8661	1.8	0.2359	1.3	0.70	1365.2	15.4	1373.1	13.6	1385.3	24.8	**1385.3**	**24.8**	98.6
14CO-Core-2-Spot 5	174	40244	0.9	9.7292	0.9	4.2229	1.6	0.2980	1.3	0.80	1681.3	18.6	1678.5	12.8	1675.0	17.2	**1675.0**	**17.2**	100.4
14CO-Core-2-Spot 10	79	13438	4.0	10.9663	1.0	3.0785	1.6	0.2448	1.3	0.78	1411.9	16.0	1427.4	12.4	1450.5	19.3	**1450.5**	**19.3**	97.3
14CO-Core-2-Spot 13	155	44179	2.4	9.6560	1.0	4.3170	1.8	0.3023	1.5	0.84	1702.9	22.7	1696.6	14.8	1688.9	17.8	**1688.9**	**17.8**	100.8
14CO-Core-2-Spot 20	216	39791	1.7	11.7208	1.3	2.3762	2.0	0.2020	1.5	0.74	1186.0	15.8	1235.5	14.1	1322.8	25.8	**1322.8**	**25.8**	89.7
14CO-Core-2-Spot 25	139	164465	2.1	9.6975	1.0	4.1974	1.5	0.2952	1.1	0.71	1667.6	15.6	1673.5	12.2	1681.0	19.3	**1681.0**	**19.3**	99.2

Analysis	U (ppm)	206Pb 204Pb	U/Th	206Pb* 207Pb*	± (%)	207Pb* 235U*	± (%)	206Pb* 238U	± (%)	error corr.	206Pb* 238U*	± (Ma)	207Pb* 235U	± (Ma)	206Pb* 207Pb*	± (Ma)	Best age (Ma)	± (Ma)	Conc (%)
14CO-Core-2-Spot 35	56	17199	2.9	11.1296	1.4	3.0509	1.9	0.2463	1.3	0.68	1419.2	16.5	1420.4	14.5	1422.3	26.6	**1422.3**	**26.6**	99.8
14CO-Core-2-Spot 39	175	44238	1.7	9.2037	0.8	4.6363	1.6	0.3095	1.3	0.86	1738.2	20.3	1755.8	13.0	1776.9	14.7	**1776.9**	**14.7**	97.8
14CO-Core-2-Spot 46	366	65079	1.8	9.2296	0.9	3.6747	1.7	0.2460	1.4	0.83	1417.7	17.4	1565.9	13.2	1771.8	17.0	**1771.8**	**17.0**	80.0
14CO-Core-2-Spot 59	262	63544	2.4	9.8853	1.1	4.0206	1.6	0.2883	1.2	0.74	1632.8	16.9	1638.4	12.9	1645.5	20.0	**1645.5**	**20.0**	99.2
14CO-Core-2-Spot 70	181	105705	2.0	11.3975	1.0	2.8126	1.5	0.2325	1.2	0.75	1347.6	14.0	1358.9	11.5	1376.7	19.7	**1376.7**	**19.7**	97.9
14CO-Core-2-Spot 73	95	39157	2.2	9.5821	1.1	4.2804	1.8	0.2975	1.4	0.79	1678.8	20.7	1689.6	14.7	1703.1	20.3	**1703.1**	**20.3**	98.6
14CO-Core-2-Spot 76	290	55196	3.9	9.1667	0.9	4.7160	1.6	0.3135	1.3	0.82	1758.1	20.0	1770.1	13.3	1784.3	16.5	**1784.3**	**16.5**	98.5
14CO-Core-2-Spot 83	213	57436	2.5	11.0237	1.4	3.0740	1.9	0.2458	1.4	0.72	1416.6	17.8	1426.2	14.9	1440.6	25.9	**1440.6**	**25.9**	98.3
14CO-Core-2-Spot 84	344	100270	2.9	9.3805	0.9	4.5785	1.3	0.3115	0.9	0.69	1748.0	13.8	1745.4	10.9	1742.1	17.2	**1742.1**	**17.2**	100.3
14CO-Core-2-Spot 87	213	98944	1.8	11.4161	1.1	2.8068	1.7	0.2324	1.3	0.76	1347.0	15.5	1357.3	12.6	1373.6	21.2	**1373.6**	**21.2**	98.1
14CO-Core-2-Spot 95	216	200899	1.7	9.6448	1.2	4.1033	1.8	0.2870	1.4	0.77	1626.7	20.4	1655.0	15.0	1691.1	21.4	**1691.1**	**21.4**	96.2
14CO-Core-2-Spot 98	186	46458	2.3	11.4536	1.2	2.8405	1.7	0.2360	1.1	0.67	1365.7	13.7	1366.3	12.5	1367.3	23.7	**1367.3**	**23.7**	99.9
14CO-Core-2-Spot 101	400	54801	2.8	9.1557	0.8	4.6501	1.7	0.3088	1.5	0.89	1734.7	22.4	1758.3	13.9	1786.5	14.0	**1786.5**	**14.0**	97.1
14CO-Core-2-Spot 104	120	37531	1.8	13.0639	1.5	1.9611	1.8	0.1858	1.1	0.58	1098.6	10.7	1102.3	12.3	1109.4	29.9	**1109.4**	**29.9**	99.0
14CO-Core-2-Spot 106	231	84678	1.0	9.6489	1.0	4.2418	1.8	0.2968	1.5	0.85	1675.6	22.8	1682.2	15.0	1690.3	17.9	**1690.3**	**17.9**	99.1
14CO-Core-2-Spot 107	317	99130	1.6	11.1512	1.1	3.0176	1.7	0.2441	1.2	0.72	1407.7	15.0	1412.1	12.6	1418.6	22.0	**1418.6**	**22.0**	99.2
14CO-BS-3–Spot 1	326	102108	1.0	11.4236	0.8	2.6396	1.6	0.2187	1.3	0.85	1275.0	15.5	1311.7	11.6	1372.3	15.7	**1372.3**	**15.7**	92.9
14CO-BS-3–Spot 2	138	49501	3.4	9.8207	1.2	3.9677	2.1	0.2826	1.7	0.80	1604.5	23.7	1627.6	16.9	1657.6	23.0	**1657.6**	**23.0**	96.8
14CO-BS-3–Spot 3	349	75979	0.8	11.3701	0.8	2.5964	1.4	0.2141	1.2	0.83	1250.7	13.5	1299.6	10.5	1381.4	15.2	**1381.4**	**15.2**	90.5
14CO-BS-3–Spot 4	120	43477	1.9	11.1127	1.4	3.1019	2.3	0.2500	1.9	0.79	1438.5	23.9	1433.2	18.0	1425.2	27.6	**1425.2**	**27.6**	100.9
14CO-BS-3–Spot 5	293	31922	3.2	12.6648	0.9	2.1346	1.3	0.1961	0.9	0.70	1154.2	9.6	1160.1	8.9	1171.1	18.1	**1171.1**	**18.1**	98.6
14CO-BS-3–Spot 6	101	32025	3.1	11.0628	1.4	3.1435	1.9	0.2522	1.3	0.66	1449.9	16.2	1443.4	14.6	1433.8	27.3	**1433.8**	**27.3**	101.1
14CO-BS-3–Spot 7	147	42755	1.9	11.3100	1.1	2.7762	2.5	0.2277	2.3	0.90	1322.6	27.2	1349.2	18.9	1391.6	21.2	**1391.6**	**21.2**	95.0
14CO-BS-3–Spot 9	57	20055	1.9	13.0386	3.1	2.0030	3.6	0.1894	1.8	0.52	1118.2	18.9	1116.5	24.2	1113.3	61.2	**1113.3**	**61.2**	100.4
14CO-BS-3--Spot 10	129	144682	1.3	9.6919	1.1	4.1590	1.3	0.2923	0.7	0.56	1653.2	10.6	1666.0	10.7	1682.1	20.0	**1682.1**	**20.0**	98.3
14CO-BS-3--Spot 11	508	119636	2.6	11.2640	0.9	3.0402	1.3	0.2484	1.0	0.77	1430.1	13.2	1417.8	10.2	1399.4	16.4	**1399.4**	**16.4**	102.2
14CO-BS-3--Spot 12	115	95130	1.9	11.4653	1.1	2.8390	1.8	0.2361	1.5	0.81	1366.3	18.4	1365.9	13.9	1365.3	21.1	**1365.3**	**21.1**	100.1
14CO-BS-3--Spot 13	216	27093	1.0	11.4169	1.3	2.8593	1.8	0.2368	1.3	0.72	1369.8	16.0	1371.3	13.7	1373.5	24.4	**1373.5**	**24.4**	99.7
14CO-BS-3--Spot 14	207	30539	2.6	11.1116	1.3	3.1097	3.8	0.2506	3.6	0.94	1441.6	46.1	1435.1	29.2	1425.4	24.7	**1425.4**	**24.7**	101.1
14CO-BS-3--Spot 15	215	42811	1.5	11.5637	1.2	2.8047	1.7	0.2352	1.2	0.72	1361.8	15.2	1356.8	12.9	1348.9	23.1	**1348.9**	**23.1**	101.0
14CO-BS-3--Spot 16	289	78711	1.2	11.5084	0.8	2.8827	1.2	0.2406	0.9	0.76	1389.9	11.8	1377.4	9.3	1358.1	15.5	**1358.1**	**15.5**	102.3
14CO-BS-3--Spot 17	105	26114	1.7	11.3797	1.0	2.8164	1.4	0.2324	1.0	0.71	1347.3	12.2	1359.9	10.6	1379.8	19.0	**1379.8**	**19.0**	97.6
14CO-BS-3--Spot 18	548	231718	3.8	9.2476	0.9	4.7024	1.2	0.3154	0.8	0.68	1767.2	12.6	1767.7	10.0	1768.2	16.0	**1768.2**	**16.0**	99.9
14CO-BS-3--Spot 19	87	22091	0.6	11.3765	1.2	2.7979	2.0	0.2309	1.6	0.80	1339.0	19.8	1355.0	15.3	1380.3	23.4	**1380.3**	**23.4**	97.0
14CO-BS-3--Spot 20	137	64398	0.6	11.3197	1.2	2.8065	1.7	0.2304	1.1	0.68	1336.6	13.8	1357.3	12.6	1389.9	23.9	**1389.9**	**23.9**	96.2
14CO-BS-3--Spot 21	133	109775	3.4	10.9220	1.0	3.0864	1.7	0.2445	1.3	0.79	1410.0	16.6	1429.3	12.8	1458.2	19.4	**1458.2**	**19.4**	96.7
14CO-BS-3--Spot 22	152	46776	1.6	11.4193	1.1	2.8913	1.7	0.2395	1.3	0.76	1383.9	16.1	1379.6	12.9	1373.1	21.5	**1373.1**	**21.5**	100.8
14CO-BS-3--Spot 23	190	31959	1.2	12.4508	1.0	2.2416	1.7	0.2024	1.4	0.82	1188.3	15.4	1194.2	12.2	1204.7	19.7	**1204.7**	**19.7**	98.6
14CO-BS-3--Spot 24	197	63932	1.5	11.3984	0.9	2.9488	2.0	0.2438	1.8	0.89	1406.3	22.5	1394.6	15.1	1376.6	17.3	**1376.6**	**17.3**	102.2
14CO-BS-3--Spot 25	244	73621	2.5	11.4378	1.2	2.8260	1.7	0.2344	1.2	0.71	1357.7	14.4	1362.4	12.4	1370.0	22.4	**1370.0**	**22.4**	99.1

Analysis	U	206Pb	U/Th	206Pb*	±	207Pb*	±	206Pb*	±	error	206Pb*	±	207Pb*	±	206Pb*	±	Best age	±	Conc
	(ppm)	204Pb		207Pb*	(%)	235U*	(%)	238U	(%)	corr.	238U*	(Ma)	235U	(Ma)	207Pb*	(Ma)	(Ma)	(Ma)	(%)
14CO-BS-3--Spot 26	67	25421	1.6	11.3313	1.4	2.8424	1.9	0.2336	1.2	0.65	1353.3	15.0	1366.8	14.2	1387.9	27.7	**1387.9**	**27.7**	97.5
14CO-BS-3--Spot 27	95	24829	1.6	11.5123	1.2	2.8302	2.2	0.2363	1.8	0.83	1367.5	22.3	1363.6	16.5	1357.5	23.9	**1357.5**	**23.9**	100.7
14CO-BS-3--Spot 28	216	47039	1.5	11.4273	0.9	2.8457	1.2	0.2359	0.8	0.67	1365.1	9.7	1367.7	8.9	1371.7	16.9	**1371.7**	**16.9**	99.5
14CO-BS-3--Spot 29	166	92479	0.7	11.5039	1.2	2.8432	1.7	0.2372	1.3	0.74	1372.2	16.0	1367.0	13.1	1358.9	22.6	**1358.9**	**22.6**	101.0
14CO-BS-3--Spot 30	96	16998	1.3	11.5767	1.5	2.7524	2.0	0.2311	1.3	0.66	1340.3	16.3	1342.7	15.1	1346.7	29.2	**1346.7**	**29.2**	99.5
14CO-BS-3--Spot 31	106	211973	1.1	11.1349	1.4	2.9192	3.5	0.2358	3.2	0.91	1364.6	39.4	1386.9	26.6	1421.4	27.6	**1421.4**	**27.6**	96.0
14CO-BS-3--Spot 32	422	46259	1.2	13.1927	1.1	2.0255	1.5	0.1938	1.0	0.68	1142.0	10.8	1124.1	10.3	1089.8	22.2	**1089.8**	**22.2**	104.8
14CO-BS-3--Spot 33	91	49848	1.5	11.3059	1.3	2.7936	2.3	0.2291	1.9	0.81	1329.6	22.4	1353.8	17.1	1392.2	25.5	**1392.2**	**25.5**	95.5
14CO-BS-3--Spot 34	138	39683	4.0	11.1133	0.8	3.0851	1.4	0.2487	1.2	0.83	1431.6	15.1	1429.0	10.8	1425.1	14.9	**1425.1**	**14.9**	100.5
14CO-BS-3--Spot 35	295	103723	1.4	11.4800	1.0	2.7621	3.5	0.2300	3.4	0.96	1334.4	40.6	1345.4	26.3	1362.9	19.9	**1362.9**	**19.9**	97.9
14CO-BS-3--Spot 36	600	93785	2.6	11.0313	0.8	3.0849	1.4	0.2468	1.1	0.80	1422.0	13.7	1428.9	10.4	1439.3	15.6	**1439.3**	**15.6**	98.8
14CO-BS-3--Spot 37	187	60600	2.0	9.9039	1.1	3.9947	1.5	0.2869	1.0	0.68	1626.2	14.1	1633.1	11.8	1642.0	19.8	**1642.0**	**19.8**	99.0
14CO-BS-3--Spot 38	205	58591	1.4	9.6264	0.7	4.2026	1.5	0.2934	1.3	0.88	1658.6	19.4	1674.5	12.5	1694.6	13.5	**1694.6**	**13.5**	97.9
14CO-BS-3--Spot 39	129	117874	2.2	9.6038	1.4	4.2389	1.9	0.2953	1.2	0.65	1667.7	18.3	1681.6	15.6	1698.9	26.5	**1698.9**	**26.5**	98.2
14CO-BS-3--Spot 40	364	57843	1.8	12.8367	1.1	2.0183	2.7	0.1879	2.5	0.92	1110.0	25.7	1121.7	18.7	1144.3	21.8	**1144.3**	**21.8**	97.0
14CO-BS-3--Spot 41	76	34487	1.4	11.2011	1.7	2.8579	3.5	0.2322	3.1	0.88	1345.9	37.8	1370.9	26.6	1410.1	32.3	**1410.1**	**32.3**	95.4
14CO-BS-3--Spot 42	139	105532	2.1	12.7202	1.3	1.9952	1.7	0.1841	1.0	0.60	1089.2	10.0	1113.9	11.2	1162.4	26.3	**1162.4**	**26.3**	93.7
14CO-BS-3--Spot 43	172	61766	2.4	9.8902	0.9	4.0044	1.6	0.2872	1.3	0.82	1627.7	18.9	1635.1	13.0	1644.6	17.1	**1644.6**	**17.1**	99.0
14CO-BS-3--Spot 44	158	37199	1.0	11.3321	1.4	2.8648	2.1	0.2355	1.5	0.73	1363.0	18.4	1372.7	15.4	1387.8	26.9	**1387.8**	**26.9**	98.2
14CO-BS-3--Spot 45	100	34946	1.4	11.4078	1.3	2.8425	3.9	0.2352	3.7	0.94	1361.6	45.4	1366.8	29.5	1375.0	25.4	**1375.0**	**25.4**	99.0
14CO-BS-3--Spot 46	201	44919	1.1	11.4334	0.9	2.8546	1.9	0.2367	1.7	0.89	1369.6	20.8	1370.0	14.2	1370.7	16.5	**1370.7**	**16.5**	99.9
14CO-BS-3--Spot 47	302	29310	2.7	11.0764	1.2	3.0665	1.6	0.2463	1.1	0.67	1419.6	13.6	1424.4	12.2	1431.5	22.6	**1431.5**	**22.6**	99.2
14CO-BS-3--Spot 48	243	33223	3.6	10.9686	1.4	3.1047	2.5	0.2470	2.0	0.82	1422.9	25.7	1433.9	19.0	1450.1	27.1	**1450.1**	**27.1**	98.1
14CO-BS-3--Spot 49	182	34133	2.7	11.1252	1.0	3.0746	1.8	0.2481	1.4	0.81	1428.6	18.2	1426.4	13.5	1423.1	19.7	**1423.1**	**19.7**	100.4
14CO-BS-3--Spot 50	197	30404	1.4	11.4653	1.3	2.8904	1.8	0.2403	1.3	0.71	1388.5	16.2	1379.4	13.7	1365.3	24.5	**1365.3**	**24.5**	101.7
14CO-BS-3--Spot 51	140	76411	1.6	12.7004	1.6	2.1051	2.2	0.1939	1.5	0.69	1142.5	15.5	1150.5	14.8	1165.5	31.1	**1165.5**	**31.1**	98.0
14CO-BS-3--Spot 52	85	27649	1.9	12.6400	1.1	2.0733	1.8	0.1901	1.4	0.78	1121.7	14.3	1140.0	12.2	1175.0	22.2	**1175.0**	**22.2**	95.5
14CO-BS-3--Spot 53	106	25751	1.0	11.4405	1.1	2.8491	1.4	0.2364	0.8	0.60	1368.0	10.4	1368.6	10.5	1369.5	21.4	**1369.5**	**21.4**	99.9
14CO-BS-3--Spot 54	142	55555	1.6	11.2402	1.6	2.8917	3.3	0.2357	2.9	0.88	1364.5	35.2	1379.8	24.6	1403.4	30.0	**1403.4**	**30.0**	97.2
14CO-BS-3--Spot 55	129	207596	1.2	11.3919	0.9	2.8290	1.7	0.2337	1.4	0.84	1354.1	17.6	1363.3	12.9	1377.7	18.1	**1377.7**	**18.1**	98.3
14CO-BS-3--Spot 56	259	27327	1.7	11.5222	0.9	2.9151	1.6	0.2436	1.3	0.82	1405.4	16.9	1385.8	12.2	1355.8	17.7	**1355.8**	**17.7**	103.7
14CO-BS-3--Spot 58	285	94688	1.8	9.7406	1.0	4.2148	1.6	0.2978	1.2	0.77	1680.2	17.7	1676.9	12.7	1672.8	18.2	**1672.8**	**18.2**	100.4
14CO-BS-3--Spot 59	129	193154	1.5	11.2722	1.2	2.8512	1.9	0.2331	1.5	0.78	1350.7	18.1	1369.1	14.3	1398.0	22.6	**1398.0**	**22.6**	96.6
14CO-BS-3--Spot 60	134	52058	2.4	9.7410	1.1	4.2473	1.7	0.3001	1.3	0.76	1691.6	19.2	1683.2	13.9	1672.7	20.2	**1672.7**	**20.2**	101.1
14CO-BS-3--Spot 61	98	86193	1.6	11.3889	1.8	2.8203	2.4	0.2330	1.6	0.67	1350.0	19.4	1360.9	17.8	1378.2	33.9	**1378.2**	**33.9**	98.0
14CO-BS-3--Spot 62	166	184314	1.4	11.2752	1.1	2.8235	2.7	0.2309	2.5	0.92	1339.2	30.2	1361.8	20.3	1397.5	20.3	**1397.5**	**20.3**	95.8
14CO-BS-3--Spot 63	129	92735	1.1	11.3785	1.2	2.8541	1.7	0.2355	1.2	0.70	1363.4	14.8	1369.9	13.0	1380.0	23.8	**1380.0**	**23.8**	98.8
14CO-BS-3--Spot 64	219	64906	1.4	11.4393	1.2	2.8862	2.5	0.2395	2.2	0.89	1383.8	27.7	1378.3	18.9	1369.7	22.2	**1369.7**	**22.2**	101.0
14CO-BS-3--Spot 65	263	120885	2.7	11.0319	1.2	3.0616	1.7	0.2450	1.2	0.72	1412.4	15.7	1423.1	13.2	1439.2	22.9	**1439.2**	**22.9**	98.1
14CO-BS-3--Spot 66	192	26051	1.1	11.4316	1.1	2.8462	2.9	0.2360	2.7	0.93	1365.7	33.2	1367.8	21.8	1371.0	20.7	**1371.0**	**20.7**	99.6
14CO-BS-3--Spot 67	113	91296	2.0	11.4705	1.8	2.8255	2.1	0.2351	1.1	0.52	1361.0	13.3	1362.3	15.6	1364.5	34.0	**1364.5**	**34.0**	99.7

Analysis	U (ppm)	206Pb 204Pb	U/Th	206Pb* 207Pb*	± (%)	207Pb* 235U*	± (%)	206Pb* 238U	± (%)	error corr.	206Pb* 238U*	± (Ma)	207Pb* 235U	± (Ma)	206Pb* 207Pb*	± (Ma)	Best age (Ma)	± (Ma)	Conc (%)
14CO-BS-3--Spot 68	164	39544	3.6	13.0423	1.5	2.0671	2.1	0.1955	1.5	0.71	1151.2	15.6	1138.0	14.3	1112.7	29.7	**1112.7**	**29.7**	103.5
14CO-BS-3--Spot 69	207	81653	2.2	8.8610	0.7	5.1750	1.4	0.3326	1.2	0.88	1850.9	19.5	1848.5	11.8	1845.9	12.1	**1845.9**	**12.1**	100.3
14CO-BS-3--Spot 70	39	13482	1.2	11.6105	2.5	2.7814	2.8	0.2342	1.4	0.50	1356.5	17.3	1350.6	21.3	1341.1	47.8	**1341.1**	**47.8**	101.2
14CO-BS-3--Spot 71	297	109192	4.4	12.7147	1.3	2.0792	2.4	0.1917	2.0	0.84	1130.8	21.1	1142.0	16.5	1163.3	25.6	**1163.3**	**25.6**	97.2
14CO-BS-3--Spot 72	195	49577	1.6	11.5313	0.9	2.8321	1.7	0.2369	1.4	0.84	1370.3	17.6	1364.1	12.8	1354.3	18.0	**1354.3**	**18.0**	101.2
14CO-BS-3--Spot 73	81	22149	1.0	11.3326	1.7	2.8787	3.0	0.2366	2.5	0.83	1369.0	30.8	1376.4	22.7	1387.7	32.4	**1387.7**	**32.4**	98.7
14CO-BS-3--Spot 74	241	68986	2.9	11.0276	1.1	3.0663	1.8	0.2452	1.5	0.79	1413.9	18.5	1424.3	14.0	1439.9	21.2	**1439.9**	**21.2**	98.2
14CO-BS-3--Spot 75	326	99037	3.9	10.9790	0.8	3.0770	1.6	0.2450	1.4	0.86	1412.7	17.8	1427.0	12.6	1448.3	16.2	**1448.3**	**16.2**	97.5
14CO-BS-3--Spot 76	177	163799	2.6	12.7759	1.7	2.0913	5.0	0.1938	4.7	0.94	1141.8	48.7	1145.9	34.2	1153.8	34.5	**1153.8**	**34.5**	99.0
14CO-BS-3--Spot 77	67	30065	1.0	11.2129	2.9	2.8897	3.3	0.2350	1.7	0.51	1360.6	20.8	1379.2	25.2	1408.1	55.2	**1408.1**	**55.2**	96.6
14CO-BS-3--Spot 78	190	26379	1.0	11.5376	1.1	2.8268	1.9	0.2365	1.5	0.82	1368.7	18.9	1362.7	14.0	1353.2	20.5	**1353.2**	**20.5**	101.1
14CO-BS-3--Spot 80	149	25487	3.0	11.0497	1.0	3.1492	1.7	0.2524	1.4	0.80	1450.7	17.6	1444.8	13.0	1436.1	19.1	**1436.1**	**19.1**	101.0
14CO-BS-3--Spot 81	380	50564	2.9	9.7128	1.0	4.3437	4.1	0.3060	3.9	0.97	1720.9	59.6	1701.7	33.6	1678.1	18.8	**1678.1**	**18.8**	102.6
14CO-BS-3--Spot 82	126	49687	2.1	9.6736	1.1	4.1669	2.7	0.2923	2.5	0.91	1653.2	36.4	1667.5	22.5	1685.6	21.2	**1685.6**	**21.2**	98.1
14CO-BS-3--Spot 83	427	65346	2.6	11.0661	0.9	3.1079	2.7	0.2494	2.5	0.94	1435.6	32.6	1434.7	20.6	1433.3	16.8	**1433.3**	**16.8**	100.2
14CO-BS-3--Spot 85	71	14339	1.5	11.7092	1.6	2.8213	2.1	0.2396	1.3	0.63	1384.6	16.7	1361.2	15.9	1324.7	31.7	**1324.7**	**31.7**	104.5
14CO-BS-3--Spot 86	154	59466	1.4	11.4791	1.1	2.8350	1.5	0.2360	1.1	0.72	1366.0	13.4	1364.8	11.4	1363.0	20.4	**1363.0**	**20.4**	100.2
14CO-BS-3--Spot 87	366	243563	1.4	11.5467	3.3	2.6249	3.4	0.2198	1.0	0.30	1280.9	12.2	1307.6	25.3	1351.7	63.3	**1351.7**	**63.3**	94.8
14CO-BS-3--Spot 88	27	12798	2.6	10.8951	2.7	3.0842	3.8	0.2437	2.7	0.71	1406.0	34.2	1428.8	29.2	1462.9	51.1	**1462.9**	**51.1**	96.1
14CO-BS-3--Spot 89	166	19075	2.6	13.2540	1.1	1.9382	2.6	0.1863	2.4	0.91	1101.4	24.3	1094.4	17.7	1080.5	22.1	**1080.5**	**22.1**	101.9
14CO-BS-3--Spot 90	108	25298	1.7	9.6215	0.9	4.2656	1.4	0.2977	1.1	0.77	1679.7	15.9	1686.8	11.4	1695.5	16.3	**1695.5**	**16.3**	99.1
14CO-BS-3--Spot 91	177	33363	1.6	11.6344	1.3	2.8164	3.0	0.2377	2.7	0.91	1374.5	33.3	1359.9	22.2	1337.1	24.2	**1337.1**	**24.2**	102.8
14CO-BS-3--Spot 92	159	28244	1.9	11.2413	1.2	2.8934	3.4	0.2359	3.1	0.93	1365.3	38.5	1380.2	25.4	1403.2	23.7	**1403.2**	**23.7**	97.3
14CO-BS-3--Spot 93	187	62010	1.6	11.5581	0.8	2.8181	1.2	0.2362	0.9	0.76	1367.1	11.7	1360.4	9.3	1349.8	15.6	**1349.8**	**15.6**	101.3
14CO-BS-3--Spot 94	245	49531	2.1	11.1475	1.0	3.0568	1.7	0.2471	1.4	0.80	1423.7	17.3	1421.9	12.9	1419.3	19.4	**1419.3**	**19.4**	100.3
14CO-BS-3--Spot 95	120	29708	1.1	11.4940	1.5	2.8174	2.2	0.2349	1.6	0.73	1360.0	19.4	1360.2	16.3	1360.5	28.6	**1360.5**	**28.6**	100.0
14CO-BS-3--Spot 96	121	98264	1.7	11.4560	1.3	2.8564	1.8	0.2373	1.3	0.70	1372.8	15.6	1370.5	13.6	1366.9	25.0	**1366.9**	**25.0**	100.4
14CO-BS-3--Spot 97	42	11650	1.6	13.1568	1.8	1.9769	2.2	0.1886	1.3	0.58	1114.0	13.0	1107.7	14.8	1095.3	36.0	**1095.3**	**36.0**	101.7
14CO-BS-3--Spot 98	181	31861	2.4	11.1187	1.1	3.0568	1.9	0.2465	1.6	0.81	1420.4	19.8	1421.9	14.6	1424.2	21.2	**1424.2**	**21.2**	99.7
14CO-BS-3--Spot 99	207	112567	2.2	11.4368	1.2	2.8579	1.8	0.2371	1.4	0.78	1371.4	17.6	1370.9	13.8	1370.1	22.3	**1370.1**	**22.3**	100.1
14CO-BS-3--Spot 100	208	60288	2.0	11.3785	1.3	2.8757	1.9	0.2373	1.4	0.74	1372.7	17.8	1375.6	14.6	1380.0	24.8	**1380.0**	**24.8**	99.5
14CO-BS-3--Spot 101	299	50014	3.0	11.1008	1.1	3.0972	2.9	0.2494	2.7	0.93	1435.2	34.7	1432.0	22.2	1427.3	20.1	**1427.3**	**20.1**	100.6
14CO-BS-3--Spot 102	209	34485	2.0	11.6142	1.0	2.7645	1.5	0.2329	1.1	0.74	1349.5	13.3	1346.0	11.1	1340.4	19.3	**1340.4**	**19.3**	100.7
14CO-BS-3--Spot 103	180	231196	2.1	11.5846	1.1	2.8167	1.8	0.2367	1.4	0.77	1369.3	16.7	1360.0	13.2	1345.4	21.7	**1345.4**	**21.7**	101.8
14CO-BS-3--Spot 105	112	201635	1.2	11.4292	1.6	2.8231	2.2	0.2340	1.6	0.70	1355.5	19.1	1361.7	16.7	1371.4	30.6	**1371.4**	**30.6**	98.8
14CO-BS-3--Spot 106	91	32205	0.8	11.5717	1.7	2.7284	2.2	0.2290	1.4	0.62	1329.2	16.4	1336.2	16.2	1347.5	33.0	**1347.5**	**33.0**	98.6
14CO-BS-3--Spot 107	187	45463	2.1	11.1665	0.8	3.0805	1.5	0.2495	1.3	0.85	1435.8	16.4	1427.8	11.5	1416.0	14.9	**1416.0**	**14.9**	101.4
14CO-BS-3--Spot 108	306	32717	1.8	11.5021	1.1	2.8828	1.5	0.2405	1.0	0.65	1389.2	12.1	1377.4	11.3	1359.2	22.0	**1359.2**	**22.0**	102.2
14CO-BS-3--Spot 109	298	96905	3.3	13.0384	1.3	2.0375	2.0	0.1927	1.5	0.75	1135.8	16.1	1128.1	13.9	1113.3	26.8	**1113.3**	**26.8**	102.0
14CO-BS-3--Spot 110	206	43224	1.4	11.4774	1.1	2.8192	1.9	0.2347	1.5	0.80	1359.0	18.6	1360.7	14.3	1363.3	22.1	**1363.3**	**22.1**	99.7

Analysis	U	206Pb	U/Th	206Pb*	±	207Pb*	±	206Pb*	±	error	206Pb*	±	207Pb*	±	206Pb*	±	Best age	±	Conc
	(ppm)	204Pb		207Pb*	(%)	235U*	(%)	238U	(%)	corr.	238U*	(Ma)	235U	(Ma)	207Pb*	(Ma)	(Ma)	(Ma)	(%)
14CO-T-3-Spot 7	189	78213	1.2	9.6273	1.1	4.4143	1.8	0.3082	1.4	0.80	1731.9	21.5	1715.0	14.7	1694.4	19.8	**1694.4**	**19.8**	102.2
14CO-T-3-Spot 8	291	55113	1.6	9.4386	1.0	4.2530	2.5	0.2911	2.3	0.92	1647.2	33.5	1684.3	20.7	1730.8	18.5	**1730.8**	**18.5**	95.2
14CO-T-3-Spot 14	68	24003	3.3	9.4770	0.9	4.4372	1.4	0.3050	1.1	0.79	1716.0	17.3	1719.3	12.0	1723.4	16.2	**1723.4**	**16.2**	99.6
14CO-T-3-Spot 15	207	79883	7.1	9.0749	1.1	4.8775	1.9	0.3210	1.5	0.81	1794.7	23.7	1798.4	15.7	1802.6	19.7	**1802.6**	**19.7**	99.6
14CO-T-3-Spot 16	51	23763	2.8	9.0981	1.4	4.8176	1.8	0.3179	1.3	0.68	1779.4	19.5	1788.0	15.6	1797.9	24.7	**1797.9**	**24.7**	99.0
14CO-T-3-Spot 17	285	216362	3.2	9.4804	0.8	4.5709	1.2	0.3143	0.8	0.70	1761.8	12.5	1744.0	9.6	1722.7	15.1	**1722.7**	**15.1**	102.3
14CO-T-3-Spot 18	37	9563	1.3	13.3465	2.5	1.9048	2.9	0.1844	1.5	0.51	1090.9	15.0	1082.8	19.3	1066.5	50.1	**1066.5**	**50.1**	102.3
14CO-T-3-Spot 19	151	36599	0.9	11.2114	1.2	3.1260	1.8	0.2542	1.4	0.75	1460.0	17.7	1439.1	13.9	1408.3	22.8	**1408.3**	**22.8**	103.7
14CO-T-3-Spot 20	80	33709	3.3	9.7745	1.2	4.1871	4.2	0.2968	4.0	0.96	1675.6	59.1	1671.5	34.4	1666.4	22.7	**1666.4**	**22.7**	100.6
14CO-T-3-Spot 21	114	45615	3.2	9.5387	1.4	4.3576	2.3	0.3015	1.9	0.81	1698.6	27.7	1704.3	19.0	1711.4	25.1	**1711.4**	**25.1**	99.2
14CO-T-3-Spot 22	201	37425	1.4	11.0956	1.3	3.1209	1.9	0.2511	1.4	0.74	1444.4	17.9	1437.8	14.4	1428.2	24.1	**1428.2**	**24.1**	101.1
14CO-T-3-Spot 23	103	34069	1.3	13.2182	1.3	1.9046	4.1	0.1826	3.9	0.95	1081.1	38.4	1082.7	27.1	1085.9	25.4	**1085.9**	**25.4**	99.6
14CO-T-3-Spot 24	30	30769	3.4	9.7797	1.5	4.0619	2.0	0.2881	1.3	0.63	1632.1	18.1	1646.7	16.2	1665.4	28.4	**1665.4**	**28.4**	98.0
14CO-T-3-Spot 25	101	26678	1.2	11.1735	1.5	3.0858	2.3	0.2501	1.8	0.77	1438.8	23.0	1429.2	17.8	1414.8	28.3	**1414.8**	**28.3**	101.7
14CO-T-3-Spot 26	63	91907	4.1	12.9487	1.8	2.0368	2.4	0.1913	1.6	0.66	1128.3	16.2	1127.9	16.2	1127.1	35.7	**1127.1**	**35.7**	100.1
14CO-T-3-Spot 28	270	102977	1.7	8.9536	0.8	5.0437	1.3	0.3275	1.1	0.81	1826.4	16.8	1826.7	11.1	1827.0	13.9	**1827.0**	**13.9**	100.0
14CO-T-3-Spot 29	107	58276	2.0	11.0908	1.4	3.0649	2.0	0.2465	1.4	0.72	1420.6	18.4	1424.0	15.3	1429.0	26.5	**1429.0**	**26.5**	99.4
14CO-T-3-Spot 30	56	28597	2.7	10.5687	3.4	3.0857	4.5	0.2365	2.9	0.65	1368.6	36.3	1429.1	34.7	1520.5	64.7	**1520.5**	**64.7**	90.0
14CO-T-3-Spot 31	43	13508	1.4	11.8488	1.3	2.6744	1.9	0.2298	1.4	0.74	1333.6	17.2	1321.4	14.2	1301.7	25.1	**1301.7**	**25.1**	102.5
14CO-T-3-Spot 32	236	113674	1.8	9.2696	0.9	4.1982	3.0	0.2822	2.9	0.95	1602.6	41.1	1673.7	24.9	1763.9	16.7	**1763.9**	**16.7**	90.9
14CO-T-3-Spot 34	79	32347	1.4	11.0736	1.4	3.0629	2.1	0.2460	1.6	0.74	1417.8	20.1	1423.5	16.3	1432.0	27.2	**1432.0**	**27.2**	99.0
14CO-T-3-Spot 44	93	26219	1.8	13.1488	1.3	1.9304	1.7	0.1841	1.0	0.60	1089.3	10.2	1091.7	11.3	1096.4	26.9	**1096.4**	**26.9**	99.3
14CO-T-3-Spot 50	136	29845	0.9	11.6018	1.5	2.7883	2.0	0.2346	1.4	0.69	1358.7	17.0	1352.4	15.1	1342.5	28.3	**1342.5**	**28.3**	101.2
14CO-T-3-Spot 51	114	210084	1.8	11.6481	1.1	2.8422	1.6	0.2401	1.1	0.71	1387.3	14.4	1366.7	12.2	1334.8	22.1	**1334.8**	**22.1**	103.9
14CO-T-3-Spot 52	176	54725	2.2	8.3589	1.6	4.8272	2.2	0.2926	1.5	0.69	1654.8	22.4	1789.7	18.8	1950.7	29.1	**1950.7**	**29.1**	84.8
14CO-T-3-Spot 53	115	38073	2.5	8.8192	1.1	5.0889	2.0	0.3255	1.6	0.83	1816.5	25.9	1834.3	16.8	1854.4	20.2	**1854.4**	**20.2**	98.0
14CO-T-3-Spot 54	168	236021	2.1	9.2626	0.6	4.6874	1.5	0.3149	1.4	0.91	1764.7	21.1	1765.0	12.6	1765.3	11.7	**1765.3**	**11.7**	100.0
14CO-T-3-Spot 55	139	32257	2.6	9.4973	0.7	4.3295	1.9	0.2982	1.8	0.93	1682.5	26.3	1699.0	15.8	1719.4	13.1	**1719.4**	**13.1**	97.9
14CO-T-3-Spot 56	387	71376	3.5	9.0887	0.9	4.8397	2.2	0.3190	2.0	0.92	1785.0	31.9	1791.8	18.7	1799.8	15.6	**1799.8**	**15.6**	99.2
14CO-T-3-Spot 58	86	34083	0.9	13.3172	1.2	1.8858	1.8	0.1821	1.4	0.76	1078.6	13.6	1076.1	12.0	1071.0	23.8	**1071.0**	**23.8**	100.7
14CO-T-3-Spot 60	179	78858	1.8	10.9217	1.1	3.1511	2.5	0.2496	2.2	0.89	1436.4	28.9	1445.3	19.3	1458.3	21.5	**1458.3**	**21.5**	98.5
14CO-T-3-Spot 62	180	166206	3.0	9.6688	1.0	4.2368	1.6	0.2971	1.2	0.75	1676.9	17.1	1681.2	12.8	1686.5	19.1	**1686.5**	**19.1**	99.4
14CO-T-3-Spot 63	145	84730	3.1	10.9813	1.2	3.1322	2.2	0.2495	1.8	0.83	1435.7	23.7	1440.6	17.1	1447.9	23.4	**1447.9**	**23.4**	99.2
14CO-T-3-Spot 65	106	55967	1.4	11.0153	1.4	3.1492	3.6	0.2516	3.3	0.92	1446.7	43.3	1444.8	27.9	1442.0	26.7	**1442.0**	**26.7**	100.3
14CO-T-3-Spot 66	54	36015	2.0	12.5402	1.4	2.2977	2.0	0.2090	1.4	0.71	1223.4	15.5	1211.6	13.9	1190.7	27.5	**1190.7**	**27.5**	102.7
14CO-T-3-Spot 67	121	711556	1.7	9.7301	1.0	4.1651	2.9	0.2939	2.7	0.94	1661.1	39.4	1667.2	23.5	1674.8	18.6	**1674.8**	**18.6**	99.2
14CO-T-3-Spot 68	56	31154	3.8	9.4615	1.5	4.4056	2.0	0.3023	1.3	0.65	1702.8	19.5	1713.4	16.6	1726.4	27.9	**1726.4**	**27.9**	98.6
14CO-T-3-Spot 70	149	57807	1.9	11.3215	0.6	2.8610	1.1	0.2349	0.9	0.83	1360.2	11.1	1371.7	8.2	1389.6	11.6	**1389.6**	**11.6**	97.9
14CO-T-3-Spot 71	111	119155	1.2	11.0294	1.0	3.1637	4.1	0.2531	3.9	0.97	1454.3	51.2	1448.4	31.3	1439.6	19.4	**1439.6**	**19.4**	101.0
14CO-T-3-Spot 73	142	27329	1.4	11.5699	0.9	2.8041	1.5	0.2353	1.2	0.81	1362.2	14.8	1356.6	11.1	1347.8	16.7	**1347.8**	**16.7**	101.1
14CO-T-3-Spot 74	96	27553	1.7	11.0768	1.1	3.1356	1.7	0.2519	1.2	0.74	1448.3	16.1	1441.5	12.9	1431.4	21.5	**1431.4**	**21.5**	101.2

Analysis	U	206Pb	U/Th	206Pb*	±	207Pb*	±	206Pb*	±	error	206Pb*	±	207Pb*	±	206Pb*	±	Best age	±	Conc
	(ppm)	204Pb		207Pb*	(%)	235U*	(%)	238U	(%)	corr.	238U*	(Ma)	235U	(Ma)	207Pb*	(Ma)	(Ma)	(Ma)	(%)
14CO-T-3-Spot 77	120	29485	3.9	9.4256	0.8	4.4042	2.9	0.3011	2.7	0.96	1696.6	40.8	1713.1	23.7	1733.3	15.5	**1733.3**	**15.5**	97.9
14CO-T-3-Spot 78	57	31638	2.1	11.6191	1.5	2.7135	2.1	0.2287	1.5	0.71	1327.5	18.2	1332.1	15.9	1339.6	29.2	**1339.6**	**29.2**	99.1
14CO-T-3-Spot 80	67	42242	1.2	11.2638	1.4	3.0071	1.8	0.2457	1.2	0.65	1416.1	14.9	1409.4	13.7	1399.4	26.3	**1399.4**	**26.3**	101.2
14CO-T-3-Spot 81	256	113847	1.1	11.0713	0.8	3.0610	2.5	0.2458	2.3	0.95	1416.7	29.8	1423.0	19.0	1432.4	15.3	**1432.4**	**15.3**	98.9
14CO-T-3-Spot 83	84	27439	1.7	11.4687	1.4	2.8385	1.9	0.2361	1.3	0.68	1366.4	16.0	1365.8	14.4	1364.8	27.1	**1364.8**	**27.1**	100.1
14CO-T-3-Spot 84	170	54942	3.3	9.6597	1.0	4.1686	1.6	0.2920	1.2	0.77	1651.8	17.8	1667.9	12.9	1688.2	18.4	**1688.2**	**18.4**	97.8
14CO-T-3-Spot 85	198	59404	1.1	9.0772	1.2	4.7157	1.7	0.3105	1.2	0.70	1743.0	18.5	1770.0	14.4	1802.1	22.3	**1802.1**	**22.3**	96.7
14CO-T-3-Spot 88	218	65138	2.1	9.3959	1.2	4.4092	2.4	0.3005	2.1	0.86	1693.6	30.6	1714.1	19.8	1739.1	22.4	**1739.1**	**22.4**	97.4
14CO-T-3-Spot 89	162	108069	2.8	8.8730	0.8	5.1242	2.4	0.3298	2.2	0.94	1837.2	35.5	1840.1	20.0	1843.4	14.1	**1843.4**	**14.1**	99.7
14CO-T-3-Spot 91	75	30641	1.1	11.4476	1.3	2.7369	4.2	0.2272	4.0	0.95	1320.0	47.9	1338.5	31.3	1368.3	24.5	**1368.3**	**24.5**	96.5
14CO-T-3-Spot 95	139	152552	3.0	11.0797	1.2	3.0859	1.8	0.2480	1.3	0.71	1428.0	16.1	1429.2	13.6	1430.9	23.8	**1430.9**	**23.8**	99.8
14CO-T-3-Spot 96	139	63400	4.0	9.6763	0.9	4.2009	1.6	0.2948	1.3	0.81	1665.5	19.3	1674.2	13.2	1685.0	17.3	**1685.0**	**17.3**	98.8
14CO-T-3-Spot 97	100	37239	3.0	9.6744	1.1	4.1584	1.5	0.2918	1.0	0.65	1650.4	14.3	1665.9	12.3	1685.4	21.0	**1685.4**	**21.0**	97.9
14CO-T-3-Spot 99	35	45501	1.0	7.8229	1.0	6.5160	1.8	0.3697	1.5	0.84	2028.0	26.7	2048.1	16.2	2068.3	17.8	**2068.3**	**17.8**	98.0
14CO-T-3-Spot 100	102	50796	3.9	9.2126	1.3	4.6142	1.6	0.3083	0.9	0.60	1732.4	14.3	1751.8	13.2	1775.2	23.1	**1775.2**	**23.1**	97.6
14CO-T-3-Spot 104	106	66278	2.0	11.3652	1.4	2.8059	2.0	0.2313	1.5	0.72	1341.2	17.6	1357.1	15.2	1382.2	27.1	**1382.2**	**27.1**	97.0
14CO-T-3-Spot 107	167	162589	2.2	9.6246	1.0	4.1948	1.6	0.2928	1.2	0.78	1655.6	18.0	1673.0	12.9	1694.9	18.2	**1694.9**	**18.2**	97.7
14CO-T-3-Spot 108	26	87673	3.6	9.7547	1.1	4.1571	2.2	0.2941	1.9	0.87	1662.0	28.1	1665.6	18.0	1670.1	20.0	**1670.1**	**20.0**	99.5
14CO-T-3-Spot 110	68	59752	2.2	11.6745	1.0	2.5594	2.5	0.2167	2.2	0.91	1264.5	25.6	1289.1	18.0	1330.4	20.0	**1330.4**	**20.0**	95.0
14WY-FH-2-Spot 1	275	109903	1.4	9.3974	1.7	4.6982	2.9	0.3202	2.3	0.79	1790.8	35.6	1766.9	24.0	1738.8	31.8	**1738.8**	**31.8**	103.0
14WY-FH-2-Spot 2	79	65419	2.1	9.1992	0.9	4.8923	1.3	0.3264	0.8	0.66	1821.0	13.3	1800.9	10.7	1777.8	17.3	**1777.8**	**17.3**	102.4
14WY-FH-2-Spot 3	226	174322	1.8	9.2793	0.8	4.6913	1.5	0.3157	1.2	0.84	1768.8	19.2	1765.7	12.4	1762.0	14.6	**1762.0**	**14.6**	100.4
14WY-FH-2-Spot 4	444	91406	4.4	9.0529	2.1	4.4005	2.3	0.2889	0.9	0.37	1636.2	12.5	1712.4	19.2	1807.0	39.1	**1807.0**	**39.1**	90.5
14WY-FH-2-Spot 5	301	56753	3.2	9.3591	0.6	4.6344	1.2	0.3146	1.0	0.85	1763.2	15.6	1755.5	10.0	1746.3	11.6	**1746.3**	**11.6**	101.0
14WY-FH-2-Spot 6	131	197104	1.4	9.2442	1.0	4.9685	1.6	0.3331	1.2	0.75	1853.5	18.8	1814.0	13.1	1768.9	18.7	**1768.9**	**18.7**	104.8
14WY-FH-2-Spot 7	56	50387	8.3	8.9546	1.2	5.0222	2.3	0.3262	2.0	0.86	1819.8	31.5	1823.1	19.6	1826.8	21.6	**1826.8**	**21.6**	99.6
14WY-FH-2-Spot 8	258	51327	2.7	9.2638	0.9	4.5152	1.5	0.3034	1.2	0.77	1708.0	17.3	1733.8	12.4	1765.0	17.2	**1765.0**	**17.2**	96.8
14WY-FH-2-Spot 9	312	171818	3.2	9.1642	0.8	4.6708	1.2	0.3104	1.0	0.77	1742.9	14.6	1762.0	10.4	1784.8	14.4	**1784.8**	**14.4**	97.7
14WY-FH-2-Spot 10	233	155006	2.3	8.8935	0.6	5.0394	1.3	0.3251	1.2	0.91	1814.3	19.3	1826.0	11.4	1839.2	10.2	**1839.2**	**10.2**	98.6
14WY-FH-2-Spot 11	164	65855	2.6	9.3268	0.7	4.6639	1.3	0.3155	1.1	0.85	1767.6	17.0	1760.8	10.9	1752.6	12.6	**1752.6**	**12.6**	100.9
14WY-FH-2-Spot 12	472	54966	5.2	9.2582	0.9	4.7598	1.5	0.3196	1.2	0.82	1787.8	19.2	1777.8	12.6	1766.1	15.9	**1766.1**	**15.9**	101.2
14WY-FH-2-Spot 13	253	172963	3.2	9.2495	0.7	4.6310	2.0	0.3107	1.9	0.93	1744.0	28.5	1754.9	16.7	1767.9	12.9	**1767.9**	**12.9**	98.6
14WY-FH-2-Spot 14	248	97544	1.7	9.2136	0.8	4.3352	1.7	0.2897	1.5	0.88	1640.0	21.6	1700.1	14.0	1775.0	14.9	**1775.0**	**14.9**	92.4
14WY-FH-2-Spot 16	141	93212	1.1	9.1210	0.9	4.8910	1.3	0.3235	0.9	0.71	1807.0	14.7	1800.7	11.1	1793.4	17.0	**1793.4**	**17.0**	100.8
14WY-FH-2-Spot 17	193	205192	3.1	9.1305	1.0	4.7649	1.6	0.3155	1.2	0.77	1767.9	18.6	1778.7	13.1	1791.5	18.2	**1791.5**	**18.2**	98.7
14WY-FH-2-Spot 19	176	71701	3.4	9.2212	1.2	4.7586	1.5	0.3182	0.9	0.59	1781.2	13.9	1777.6	12.8	1773.5	22.6	**1773.5**	**22.6**	100.4
14WY-FH-2-Spot 20	136	232488	2.1	9.0720	1.1	4.7551	1.6	0.3129	1.2	0.73	1754.8	17.9	1777.0	13.3	1803.2	19.6	**1803.2**	**19.6**	97.3
14WY-FH-2-Spot 21	517	1400914	3.7	9.2737	0.8	4.8142	1.4	0.3238	1.1	0.82	1808.2	17.7	1787.4	11.6	1763.1	14.5	**1763.1**	**14.5**	102.6
14WY-FH-2-Spot 22	83	94012	1.2	9.3685	1.1	4.5744	1.5	0.3108	1.0	0.69	1744.7	15.9	1744.6	12.6	1744.5	20.1	**1744.5**	**20.1**	100.0
14WY-FH-2-Spot 26	94	42929	3.0	8.8458	1.2	5.0751	1.5	0.3256	0.9	0.60	1817.0	14.2	1832.0	12.8	1849.0	21.8	**1849.0**	**21.8**	98.3

Analysis	U	206Pb	U/Th	206Pb*	±	207Pb*	±	206Pb*	±	error	206Pb*	±	207Pb*	±	206Pb*	±	Best age	±	Conc
	(ppm)	204Pb		207Pb*	(%)	235U*	(%)	238U	(%)	corr.	238U*	(Ma)	235U	(Ma)	207Pb*	(Ma)	(Ma)	(Ma)	(%)
14WY-FH-2-Spot 27	155	55787	3.1	8.6255	1.0	5.4374	4.4	0.3402	4.3	0.97	1887.4	70.1	1890.8	37.7	1894.4	17.6	**1894.4**	**17.6**	99.6
14WY-FH-2-Spot 28	190	50958	2.0	9.4251	0.6	4.5458	1.4	0.3107	1.3	0.89	1744.4	19.5	1739.4	11.9	1733.4	11.7	**1733.4**	**11.7**	100.6
14WY-FH-2-Spot 29	313	884844	3.9	9.2236	0.8	4.7358	1.7	0.3168	1.5	0.89	1774.1	23.6	1773.6	14.3	1773.0	14.1	**1773.0**	**14.1**	100.1
14WY-FH-2-Spot 30	229	79923	3.5	9.1949	0.8	4.6966	1.6	0.3132	1.4	0.85	1756.4	20.8	1766.6	13.2	1778.7	15.0	**1778.7**	**15.0**	98.8
14WY-FH-2-Spot 31	373	134911	2.7	9.1624	0.6	4.7243	1.9	0.3139	1.8	0.94	1760.0	28.3	1771.6	16.3	1785.1	11.6	**1785.1**	**11.6**	98.6
14WY-FH-2-Spot 32	61	73015	2.5	9.1588	1.0	4.8445	1.7	0.3218	1.4	0.83	1798.5	22.5	1792.7	14.6	1785.8	17.7	**1785.8**	**17.7**	100.7
14WY-FH-2-Spot 33	113	65926	3.0	8.1724	3.2	5.5575	3.3	0.3294	1.0	0.29	1835.5	15.4	1909.5	28.6	1990.9	56.5	**1990.9**	**56.5**	92.2
14WY-FH-2-Spot 34	75	93868	4.2	8.8933	1.0	5.0504	1.8	0.3258	1.4	0.81	1817.8	22.9	1827.8	15.0	1839.3	18.6	**1839.3**	**18.6**	98.8
14WY-FH-2-Spot 35	317	171508	3.0	9.1986	0.9	4.6912	1.2	0.3130	0.8	0.62	1755.3	11.6	1765.7	10.1	1777.9	17.3	**1777.9**	**17.3**	98.7
14WY-FH-2-Spot 36	281	150390	7.3	8.9756	0.6	5.0402	0.8	0.3281	0.6	0.74	1829.2	9.8	1826.1	7.0	1822.6	10.1	**1822.6**	**10.1**	100.4
14WY-FH-2-Spot 37	155	140238	3.4	9.1426	0.9	4.7473	1.2	0.3148	0.8	0.68	1764.2	13.1	1775.6	10.4	1789.1	16.6	**1789.1**	**16.6**	98.6
14WY-FH-2-Spot 38	165	61293	2.4	9.2627	0.9	4.5751	2.8	0.3074	2.6	0.95	1727.7	40.0	1744.7	23.1	1765.3	15.6	**1765.3**	**15.6**	97.9
14WY-FH-2-Spot 39	199	165534	2.4	9.2621	0.6	4.6898	1.6	0.3150	1.4	0.91	1765.5	22.0	1765.4	13.0	1765.4	11.5	**1765.4**	**11.5**	100.0
14WY-FH-2-Spot 40	270	137045	2.1	9.2783	0.8	4.8369	1.2	0.3255	0.9	0.75	1816.5	14.2	1791.3	10.1	1762.2	14.7	**1762.2**	**14.7**	103.1
14WY-FH-2-Spot 41	132	85548	0.8	9.2054	0.9	4.6223	1.3	0.3086	0.9	0.69	1733.8	13.5	1753.3	10.6	1776.6	16.7	**1776.6**	**16.7**	97.6
14WY-FH-2-Spot 42	75	136658	1.3	9.1771	0.8	4.8198	1.3	0.3208	1.0	0.80	1793.6	16.3	1788.4	10.9	1782.2	14.0	**1782.2**	**14.0**	100.6
14WY-FH-2-Spot 43	445	59087	4.0	9.2782	0.7	4.7251	1.3	0.3180	1.1	0.84	1779.7	17.1	1771.7	10.9	1762.2	12.9	**1762.2**	**12.9**	101.0
14WY-FH-2-Spot 44	102	171521	2.4	8.8004	1.0	5.2355	2.8	0.3342	2.6	0.93	1858.5	41.4	1858.4	23.6	1858.3	18.7	**1858.3**	**18.7**	100.0
14WY-FH-2-Spot 45	152	88319	0.8	9.0529	0.8	4.8337	1.2	0.3174	0.8	0.68	1776.9	12.4	1790.8	9.8	1807.0	15.4	**1807.0**	**15.4**	98.3
14WY-FH-2-Spot 46	127	50147	5.3	8.8770	1.0	4.4517	1.7	0.2866	1.4	0.81	1624.6	20.0	1722.0	14.3	1842.6	18.4	**1842.6**	**18.4**	88.2
14WY-FH-2-Spot 47	67	102765	2.4	9.1904	0.7	5.0225	1.5	0.3348	1.3	0.87	1861.5	21.1	1823.1	12.8	1779.6	13.6	**1779.6**	**13.6**	104.6
14WY-FH-2-Spot 48	547	71496	3.4	9.1915	0.7	4.3010	1.2	0.2867	0.9	0.77	1625.1	12.8	1693.5	9.5	1779.4	13.5	**1779.4**	**13.5**	91.3
14WY-FH-2-Spot 49	281	123816	7.3	9.1666	0.7	4.7675	1.4	0.3170	1.2	0.86	1774.8	19.2	1779.2	12.1	1784.3	13.4	**1784.3**	**13.4**	99.5
14WY-FH-2-Spot 50	382	133016	3.1	9.1760	0.7	4.6433	1.2	0.3090	0.9	0.82	1735.8	14.4	1757.1	9.6	1782.4	12.1	**1782.4**	**12.1**	97.4
14WY-FH-2-Spot 51	371	121448	3.8	9.2475	0.7	4.7378	1.1	0.3178	0.9	0.79	1778.8	14.0	1773.9	9.5	1768.2	12.6	**1768.2**	**12.6**	100.6
14WY-FH-2-Spot 52	314	143643	1.6	9.1688	0.8	4.6502	1.4	0.3092	1.1	0.82	1736.9	17.3	1758.3	11.6	1783.8	14.6	**1783.8**	**14.6**	97.4
14WY-FH-2-Spot 53	221	185457	1.8	9.1837	0.7	4.6941	1.5	0.3127	1.3	0.89	1753.8	20.0	1766.2	12.3	1780.9	12.3	**1780.9**	**12.3**	98.5
14WY-FH-2-Spot 54	300	392438	2.4	9.1708	0.7	4.7226	2.1	0.3141	1.9	0.93	1760.9	29.6	1771.2	17.3	1783.5	13.6	**1783.5**	**13.6**	98.7
14WY-FH-2-Spot 55	72	49513	2.1	9.1993	1.1	4.8338	3.4	0.3225	3.2	0.95	1802.0	50.3	1790.8	28.4	1777.8	19.5	**1777.8**	**19.5**	101.4
14WY-FH-2-Spot 56	76	34269	2.2	9.3216	1.2	4.6430	2.0	0.3139	1.6	0.80	1759.8	25.0	1757.0	17.1	1753.7	22.6	**1753.7**	**22.6**	100.4
14WY-FH-2-Spot 57	160	84466	3.8	9.2103	0.8	4.7759	1.7	0.3190	1.5	0.87	1785.0	23.2	1780.7	14.3	1775.6	15.1	**1775.6**	**15.1**	100.5
14WY-FH-2-Spot 58	239	53076	2.3	9.1564	0.7	4.6513	1.2	0.3089	1.0	0.83	1735.2	14.7	1758.5	9.8	1786.3	12.0	**1786.3**	**12.0**	97.1
14WY-FH-2-Spot 59	183	91337	2.1	9.1996	0.8	4.7492	3.2	0.3169	3.1	0.97	1774.4	48.4	1776.0	27.0	1777.7	14.7	**1777.7**	**14.7**	99.8
14WY-FH-2-Spot 60	51	62387	4.9	9.1075	1.4	4.9377	2.1	0.3262	1.6	0.75	1819.7	24.7	1808.7	17.5	1796.1	24.9	**1796.1**	**24.9**	101.3
14WY-FH-2-Spot 61	120	84386	1.7	9.1343	0.8	4.6995	3.6	0.3113	3.5	0.97	1747.3	53.2	1767.2	29.9	1790.7	15.1	**1790.7**	**15.1**	97.6
14WY-FH-2-Spot 62	321	95288	5.3	9.2231	0.8	4.5341	2.7	0.3033	2.6	0.96	1707.6	38.7	1737.2	22.4	1773.1	14.2	**1773.1**	**14.2**	96.3
14WY-FH-2-Spot 63	151	230801	1.5	9.1598	0.8	4.8560	1.5	0.3226	1.3	0.86	1802.4	20.7	1794.7	12.9	1785.6	14.3	**1785.6**	**14.3**	100.9
14WY-FH-2-Spot 65	96	133259	3.0	9.0922	1.0	4.9269	1.6	0.3249	1.2	0.76	1813.6	19.1	1806.9	13.4	1799.1	18.8	**1799.1**	**18.8**	100.8
14WY-FH-2-Spot 66	243	90553	2.1	9.3851	0.9	4.6511	1.4	0.3166	1.0	0.75	1773.0	15.8	1758.5	11.4	1741.2	16.5	**1741.2**	**16.5**	101.8
14WY-FH-2-Spot 67	190	113990	3.4	9.2322	0.6	4.7474	1.2	0.3179	1.0	0.84	1779.4	15.4	1775.6	9.9	1771.3	11.5	**1771.3**	**11.5**	100.5
14WY-FH-2-Spot 68	114	138676	4.8	5.4690	0.7	12.9627	1.2	0.5142	1.0	0.83	2674.4	22.0	2676.9	11.4	2678.9	11.2	**2678.9**	**11.2**	99.8

Analysis	U	206Pb	U/Th	206Pb*	±	207Pb*	±	206Pb*	±	error	206Pb*	±	207Pb*	±	206Pb*	±	Best age	±	Conc
	(ppm)	204Pb		207Pb*	(%)	235U*	(%)	238U	(%)	corr.	238U*	(Ma)	235U	(Ma)	207Pb*	(Ma)	(Ma)	(Ma)	(%)
14WY-FH-2-Spot 69	126	136649	3.9	8.9417	0.7	5.1089	1.4	0.3313	1.2	0.86	1844.8	19.0	1837.6	11.7	1829.4	12.6	**1829.4**	**12.6**	100.8
14WY-FH-2-Spot 70	226	193210	1.9	9.1791	0.8	4.6735	1.5	0.3111	1.3	0.84	1746.2	19.2	1762.5	12.5	1781.8	14.7	**1781.8**	**14.7**	98.0
14WY-FH-2-Spot 73	147	224004	1.7	9.2458	1.0	4.6208	1.5	0.3099	1.1	0.74	1740.0	16.6	1753.0	12.3	1768.6	18.0	**1768.6**	**18.0**	98.4
14WY-FH-2-Spot 74	124	106327	2.9	8.9334	1.1	5.0584	2.0	0.3277	1.6	0.82	1827.4	25.9	1829.2	16.9	1831.1	20.8	**1831.1**	**20.8**	99.8
14WY-FH-2-Spot 75	248	57292	2.7	6.2040	0.7	10.3658	1.3	0.4664	1.1	0.85	2467.8	23.0	2468.0	12.2	2468.1	11.5	**2468.1**	**11.5**	100.0
14WY-FH-2-Spot 76	75	46681	5.5	8.7233	1.0	5.3062	4.6	0.3357	4.5	0.98	1866.0	73.2	1869.9	39.6	1874.1	18.4	**1874.1**	**18.4**	99.6
14WY-FH-2-Spot 77	244	169818	2.1	9.2299	1.0	4.6666	2.7	0.3124	2.6	0.94	1752.5	39.4	1761.3	23.0	1771.7	17.7	**1771.7**	**17.7**	98.9
14WY-FH-2-Spot 78	295	50215	3.4	9.3118	0.9	4.6478	1.3	0.3139	1.0	0.75	1759.8	14.7	1757.9	10.7	1755.6	15.6	**1755.6**	**15.6**	100.2
14WY-FH-2-Spot 79	93	73297	3.2	8.8879	0.9	5.1429	2.3	0.3315	2.1	0.91	1845.7	34.2	1843.2	19.8	1840.4	17.1	**1840.4**	**17.1**	100.3
14WY-FH-2-Spot 80	147	128217	3.1	9.0927	0.9	4.8335	1.2	0.3187	0.8	0.65	1783.6	11.9	1790.7	9.8	1799.0	16.2	**1799.0**	**16.2**	99.1
14WY-FH-2-Spot 81	238	143212	1.3	9.1242	0.7	4.7202	1.2	0.3124	0.9	0.78	1752.3	14.1	1770.8	9.8	1792.7	13.2	**1792.7**	**13.2**	97.7
14WY-FH-2-Spot 82	103	58746	1.1	9.2600	0.9	4.7390	1.3	0.3183	0.9	0.71	1781.3	14.7	1774.2	11.2	1765.8	17.3	**1765.8**	**17.3**	100.9
14WY-FH-2-Spot 83	364	86672	2.1	9.1895	0.9	4.1792	2.0	0.2785	1.8	0.90	1584.0	24.7	1670.0	16.1	1779.7	15.7	**1779.7**	**15.7**	89.0
14WY-FH-2-Spot 84	174	234793	3.9	9.1539	0.8	4.7456	1.3	0.3151	1.0	0.77	1765.6	15.5	1775.3	10.9	1786.8	15.0	**1786.8**	**15.0**	98.8
14WY-FH-2-Spot 85	296	541473	4.0	9.3318	0.8	4.7045	1.1	0.3184	0.8	0.69	1781.9	12.1	1768.0	9.5	1751.7	15.1	**1751.7**	**15.1**	101.7
14WY-FH-2-Spot 86	187	65142	4.5	8.9766	0.8	5.0460	1.2	0.3285	0.9	0.77	1831.2	15.1	1827.1	10.4	1822.4	14.3	**1822.4**	**14.3**	100.5
14WY-FH-2-Spot 87	375	78658	4.6	9.3026	1.1	4.5640	1.6	0.3079	1.2	0.74	1730.5	17.8	1742.7	13.2	1757.4	19.6	**1757.4**	**19.6**	98.5
14WY-FH-2-Spot 88	93	40137	1.0	9.3620	0.8	4.5357	1.3	0.3080	1.1	0.80	1730.7	16.2	1737.5	11.1	1745.7	14.5	**1745.7**	**14.5**	99.1
14WY-FH-2-Spot 89	214	102381	1.9	9.2223	0.9	4.6226	1.7	0.3092	1.4	0.84	1736.7	21.6	1753.4	14.1	1773.2	16.7	**1773.2**	**16.7**	97.9
14WY-FH-2-Spot 90	189	70264	1.5	9.1972	0.8	4.6117	1.5	0.3076	1.3	0.85	1729.0	19.3	1751.4	12.6	1778.2	14.6	**1778.2**	**14.6**	97.2
14WY-FH-2-Spot 91	263	815928	3.4	9.2093	0.7	4.7332	1.5	0.3161	1.3	0.87	1770.8	19.9	1773.1	12.4	1775.8	13.5	**1775.8**	**13.5**	99.7
14WY-FH-2-Spot 92	172	519214	1.9	8.7674	0.7	5.3470	4.0	0.3400	3.9	0.98	1886.7	63.6	1876.4	33.8	1865.0	13.0	**1865.0**	**13.0**	101.2
14WY-FH-2-Spot 93	422	198081	3.9	9.0931	0.6	4.6244	2.4	0.3050	2.3	0.97	1715.9	35.2	1753.7	20.1	1799.0	10.4	**1799.0**	**10.4**	95.4
14WY-FH-2-Spot 94	152	51725	2.7	8.9281	0.8	4.9047	2.5	0.3176	2.3	0.95	1778.0	36.3	1803.1	20.8	1832.2	14.6	**1832.2**	**14.6**	97.0
14WY-FH-2-Spot 95	177	141856	4.3	8.8259	0.9	5.1995	2.6	0.3328	2.4	0.94	1852.1	38.9	1852.5	21.9	1853.0	15.7	**1853.0**	**15.7**	99.9
14WY-FH-2-Spot 96	217	170118	1.8	9.1692	0.7	4.6572	2.5	0.3097	2.4	0.96	1739.3	36.0	1759.6	20.7	1783.8	13.4	**1783.8**	**13.4**	97.5
14WY-FH-2-Spot 97	218	122520	1.5	9.1696	0.7	4.6554	1.5	0.3096	1.3	0.87	1738.7	19.7	1759.3	12.5	1783.7	13.5	**1783.7**	**13.5**	97.5
14WY-FH-2-Spot 98	310	229341	3.1	8.9067	0.7	4.1395	1.5	0.2674	1.3	0.89	1527.6	18.2	1662.1	12.3	1836.5	12.2	**1836.5**	**12.2**	83.2
14WY-FH-2-Spot 99	194	87733	3.2	9.1980	0.7	4.8726	1.2	0.3251	1.0	0.84	1814.4	16.5	1797.5	10.5	1778.0	12.3	**1778.0**	**12.3**	102.0
14WY-FH-2-Spot 100	387	239431	3.5	9.1833	1.0	4.6199	1.5	0.3077	1.0	0.72	1729.4	15.9	1752.9	12.1	1781.0	18.3	**1781.0**	**18.3**	97.1
14WY-FH-2-Spot 101	129	90036	1.8	9.1872	0.9	4.6845	1.5	0.3121	1.2	0.79	1751.2	18.0	1764.5	12.5	1780.2	16.8	**1780.2**	**16.8**	98.4
14WY-FH-2-Spot 102	62	51991	2.5	5.3378	0.9	14.0115	2.7	0.5424	2.5	0.94	2793.6	57.3	2750.5	25.5	2719.0	15.1	**2719.0**	**15.1**	102.7
14WY-FH-2-Spot 103	241	168760	2.8	9.2859	0.6	4.5467	1.4	0.3062	1.2	0.89	1722.0	18.2	1739.6	11.3	1760.7	11.6	**1760.7**	**11.6**	97.8
14WY-FH-2-Spot 104	225	79109	3.4	9.2087	0.6	4.6866	1.5	0.3130	1.4	0.91	1755.5	20.9	1764.9	12.5	1775.9	11.5	**1775.9**	**11.5**	98.9
14WY-FH-2-Spot 105	107	124833	2.7	5.3691	1.1	13.3689	2.2	0.5206	1.9	0.87	2701.7	41.6	2706.1	20.5	2709.3	17.6	**2709.3**	**17.6**	99.7
14WY-FH-2-Spot 106	459	15755616	4.4	9.1249	0.7	4.0981	1.1	0.2712	0.9	0.79	1547.0	12.2	1653.9	9.1	1792.6	12.4	**1792.6**	**12.4**	86.3
14WY-FH-2-Spot 107	305	729171	7.1	8.8170	0.8	4.8320	1.9	0.3090	1.7	0.91	1735.7	26.4	1790.5	16.0	1854.9	13.8	**1854.9**	**13.8**	93.6
14WY-FH-2-Spot 108	263	112749	4.0	9.1278	0.7	4.9226	1.5	0.3259	1.4	0.89	1818.4	21.7	1806.1	13.0	1792.0	13.1	**1792.0**	**13.1**	101.5
14WY-FH-2-Spot 109	231	55152	3.0	9.2721	0.6	4.6359	1.0	0.3118	0.8	0.77	1749.3	11.9	1755.8	8.4	1763.4	11.8	**1763.4**	**11.8**	99.2
14WY-FH-2-Spot 110	263	896582	5.1	9.1529	0.7	4.7154	1.3	0.3130	1.0	0.80	1755.6	15.4	1770.0	10.5	1787.0	13.6	**1787.0**	**13.6**	98.2
14WY-FH-2-Spot 111	76	33086	17.7	8.8189	1.4	5.2049	4.0	0.3329	3.7	0.94	1852.5	60.2	1853.4	33.9	1854.5	24.7	**1854.5**	**24.7**	99.9

Analysis	U	206Pb	U/Th	206Pb*	±	207Pb*	±	206Pb*	±	error	206Pb*	±	207Pb*	±	206Pb*	±	Best age	±	Conc
	(ppm)	204Pb		207Pb*	(%)	235U*	(%)	238U	(%)	corr.	238U*	(Ma)	235U	(Ma)	207Pb*	(Ma)	(Ma)	(Ma)	(%)
14WY-FH-2-Spot 112	280	78331	2.3	8.9364	0.9	4.9916	1.3	0.3235	0.9	0.72	1806.9	14.4	1817.9	10.8	1830.5	16.0	**1830.5**	**16.0**	98.7
14WY-FH-2-Spot 113	189	118961	2.7	9.0992	1.0	4.8438	1.5	0.3197	1.2	0.76	1788.1	18.2	1792.5	12.9	1797.7	18.1	**1797.7**	**18.1**	99.5
14WY-FH-2-Spot 114	252	49409	1.9	9.1224	0.8	4.3749	1.3	0.2895	1.1	0.82	1638.8	15.8	1707.6	11.0	1793.1	13.8	**1793.1**	**13.8**	91.4
14WY-FH-2-Spot 115	723	58893	2.2	9.3935	0.5	4.6042	1.3	0.3137	1.2	0.92	1758.8	19.0	1750.0	11.2	1739.6	9.8	**1739.6**	**9.8**	101.1
14WY-FH-2-Spot 116	256	80001	2.6	9.2236	0.7	4.8529	1.1	0.3246	0.9	0.76	1812.3	13.5	1794.1	9.5	1773.0	13.5	**1773.0**	**13.5**	102.2
14WY-FH-2-Spot 117	185	65960	2.7	9.0104	0.9	5.0143	1.4	0.3277	1.1	0.76	1827.1	17.1	1821.7	11.9	1815.6	16.5	**1815.6**	**16.5**	100.6
14WY-FH-2-Spot 118	377	235216	1.8	9.3054	0.8	4.7408	1.3	0.3200	1.1	0.81	1789.5	16.5	1774.5	10.9	1756.8	13.8	**1756.8**	**13.8**	101.9
14WY-FH-2-Spot 119	592	121928	1.7	9.4512	0.8	4.6495	1.8	0.3187	1.6	0.89	1783.4	25.4	1758.2	15.3	1728.4	15.2	**1728.4**	**15.2**	103.2
14WY-FH-2-Spot 120	276	179161	3.0	9.2628	0.7	4.7302	2.6	0.3178	2.5	0.96	1778.9	38.9	1772.6	21.8	1765.2	12.9	**1765.2**	**12.9**	100.8
14WY-FH-2-Spot 122	362	158059	0.9	9.2628	0.8	4.6675	1.3	0.3136	1.0	0.78	1758.2	15.2	1761.4	10.6	1765.2	14.6	**1765.2**	**14.6**	99.6
14WY-FH-2-Spot 123	430	896176	8.8	9.0419	0.8	5.0541	1.4	0.3314	1.1	0.80	1845.4	17.5	1828.4	11.6	1809.2	15.1	**1809.2**	**15.1**	102.0
14WY-FH-2-Spot 124	113	28241	2.3	9.1995	1.1	4.6718	2.4	0.3117	2.1	0.89	1749.1	32.2	1762.2	19.8	1777.7	20.0	**1777.7**	**20.0**	98.4
14WY-FH-2-Spot 125	165	48673	4.9	8.8249	1.1	5.1156	1.8	0.3274	1.4	0.80	1825.9	23.0	1838.7	15.3	1853.2	19.4	**1853.2**	**19.4**	98.5
14WY-FH-2-Spot 126	150	405632	2.3	8.9023	1.0	5.0561	3.5	0.3264	3.4	0.95	1821.1	53.3	1828.8	29.8	1837.4	19.0	**1837.4**	**19.0**	99.1
14WY-FH-2-Spot 127	259	63852	3.9	8.8455	0.8	5.2150	2.4	0.3346	2.3	0.95	1860.5	36.7	1855.1	20.4	1849.0	13.9	**1849.0**	**13.9**	100.6
14WY-FH-2-Spot 128	282	96283	2.1	9.3526	0.8	4.6059	1.5	0.3124	1.3	0.85	1752.6	19.6	1750.3	12.6	1747.6	14.7	**1747.6**	**14.7**	100.3
14WY-FH-2-Spot 129	207	38879	3.2	9.1496	0.8	4.7704	1.8	0.3166	1.6	0.89	1772.9	25.2	1779.7	15.2	1787.7	14.8	**1787.7**	**14.8**	99.2
14WY-FH-2-Spot 130	112	37734	2.7	8.8246	0.9	5.1314	1.5	0.3284	1.2	0.78	1830.7	18.4	1841.3	12.6	1853.3	16.6	**1853.3**	**16.6**	98.8
14WY-FH-2-Spot 131	339	63970	1.9	8.9463	0.7	5.1658	1.3	0.3352	1.1	0.86	1863.5	17.8	1847.0	10.9	1828.5	11.9	**1828.5**	**11.9**	101.9
14WY-FH-2-Spot 132	176	86663	3.5	9.1340	1.0	4.9262	1.5	0.3263	1.1	0.74	1820.6	17.5	1806.8	12.6	1790.8	18.4	**1790.8**	**18.4**	101.7
14WY-FH-2-Spot 133	79	78255	2.0	9.1350	1.5	4.6076	2.8	0.3053	2.4	0.84	1717.4	36.2	1750.7	23.8	1790.6	27.8	**1790.6**	**27.8**	95.9
14WY-FH-2-Spot 134	324	428404	0.7	9.3250	1.0	4.6842	1.6	0.3168	1.3	0.78	1774.1	19.5	1764.4	13.4	1753.0	18.2	**1753.0**	**18.2**	101.2
14WY-FH-2-Spot 135	530	50425	2.4	9.2357	0.6	4.5905	2.8	0.3075	2.8	0.98	1728.3	41.9	1747.5	23.5	1770.6	10.4	**1770.6**	**10.4**	97.6
14WY-FH-2-Spot 136	439	466737	3.7	9.0268	0.7	4.9634	1.2	0.3249	1.0	0.79	1813.8	15.1	1813.1	10.2	1812.3	13.4	**1812.3**	**13.4**	100.1
14WY-FH-2-Spot 137	466	305623	2.9	8.8347	0.8	4.6184	2.6	0.2959	2.5	0.95	1671.1	36.2	1752.6	21.7	1851.2	15.3	**1851.2**	**15.3**	90.3
14WY-FH-2-Spot 138	78	77084	1.3	5.2633	0.8	13.3657	1.4	0.5102	1.1	0.80	2657.5	24.8	2705.8	13.4	2742.1	13.9	**2742.1**	**13.9**	96.9
14WY-FH-2-Spot 140	198	94497	1.7	9.2232	1.0	4.7372	1.3	0.3169	0.7	0.57	1774.5	11.2	1773.8	10.6	1773.1	18.9	**1773.1**	**18.9**	100.1
14WY-FH-2-Spot 141	217	125693	2.3	8.9358	0.7	5.1747	1.5	0.3354	1.3	0.88	1864.3	21.6	1848.5	12.9	1830.6	13.1	**1830.6**	**13.1**	101.8
14WY-FH-2-Spot 142	250	43385	0.7	9.2069	1.2	4.6827	1.8	0.3127	1.4	0.76	1753.9	21.3	1764.2	15.3	1776.3	21.7	**1776.3**	**21.7**	98.7
14WY-FH-2-Spot 143	309	108563	2.7	9.2736	0.7	4.7412	1.3	0.3189	1.2	0.86	1784.3	18.0	1774.5	11.3	1763.1	12.4	**1763.1**	**12.4**	101.2
14WY-FH-2-Spot 144	926	111074	6.6	9.2392	0.6	4.1944	1.3	0.2811	1.2	0.88	1596.7	16.6	1672.9	10.9	1769.9	11.5	**1769.9**	**11.5**	90.2
14WY-FH-2-Spot 145	624	51520	3.5	8.7767	0.9	4.1754	1.3	0.2658	0.9	0.72	1519.4	12.4	1669.2	10.5	1863.1	16.0	**1863.1**	**16.0**	81.5
14WY-FH-2-Spot 146	146	212159	1.2	9.2804	1.1	4.6726	1.5	0.3145	1.1	0.69	1762.8	16.4	1762.3	12.8	1761.8	20.1	**1761.8**	**20.1**	100.1
14WY-FH-2-Spot 147	190	152816	0.9	9.2795	1.0	4.7058	1.4	0.3167	0.9	0.68	1773.6	14.3	1768.3	11.4	1761.9	18.3	**1761.9**	**18.3**	100.7
14WY-FH-2-Spot 148	163	54941	2.2	9.3634	0.7	4.6024	1.7	0.3125	1.5	0.90	1753.2	23.0	1749.7	13.8	1745.5	12.9	**1745.5**	**12.9**	100.4
14WY-FH-2-Spot 149	200	11860672	1.9	9.2012	0.9	4.8062	2.0	0.3207	1.7	0.88	1793.3	27.1	1786.0	16.6	1777.4	17.2	**1777.4**	**17.2**	100.9
14WY-FH-2-Spot 150	308	111541	0.7	9.2989	0.8	4.7537	1.5	0.3206	1.2	0.83	1792.7	19.0	1776.8	12.2	1758.1	14.7	**1758.1**	**14.7**	102.0
14WY-FH-2-Spot 151	310	59605	2.5	9.2560	1.1	4.5692	1.5	0.3067	1.1	0.72	1724.6	16.6	1743.7	12.7	1766.6	19.2	**1766.6**	**19.2**	97.6
14WY-FH-2-Spot 152	143	72370	2.6	9.1412	0.9	4.6978	1.7	0.3115	1.4	0.82	1747.9	21.0	1766.8	14.0	1789.4	17.2	**1789.4**	**17.2**	97.7
14WY-FH-2-Spot 153	281	313745	2.6	9.2418	0.9	4.7540	1.5	0.3186	1.3	0.83	1783.1	19.6	1776.8	12.8	1769.4	15.6	**1769.4**	**15.6**	100.8
14WY-FH-2-Spot 154	312	113298	2.8	9.2725	0.8	4.8769	1.5	0.3280	1.3	0.84	1828.5	20.1	1798.3	12.7	1763.3	15.2	**1763.3**	**15.2**	103.7

Analysis	U	206Pb	U/Th	206Pb*	±	207Pb*	±	206Pb*	±	error	206Pb*	±	207Pb*	±	206Pb*	±	Best age	±	Conc
	(ppm)	204Pb		207Pb*	(%)	235U*	(%)	238U	(%)	corr.	238U*	(Ma)	235U	(Ma)	207Pb*	(Ma)	(Ma)	(Ma)	(%)
14WY-FH-2-Spot 155	92	26781	1.5	8.8468	1.5	4.2407	2.3	0.2721	1.8	0.77	1551.4	24.5	1681.9	19.1	1848.8	27.0	**1848.8**	**27.0**	83.9
14WY-FH-2-Spot 156	246	75826	2.0	9.3086	1.0	4.6671	3.9	0.3151	3.8	0.97	1765.7	58.5	1761.4	32.8	1756.2	18.5	**1756.2**	**18.5**	100.5
14WY-FH-2-Spot157	386	176551	5.1	9.3103	0.6	4.8728	1.5	0.3290	1.4	0.93	1833.7	22.7	1797.6	12.9	1755.9	10.4	**1755.9**	**10.4**	104.4
14WY-FH-2-Spot 158	428	188148	3.6	9.3640	0.9	4.8210	1.5	0.3274	1.2	0.78	1825.8	18.4	1788.6	12.5	1745.3	17.1	**1745.3**	**17.1**	104.6
14WY-FH-2-Spot 159	184	102886	3.6	9.0125	1.0	5.0336	1.9	0.3290	1.6	0.84	1833.6	25.4	1825.0	16.1	1815.1	18.7	**1815.1**	**18.7**	101.0
14WY-FH-2-Spot 160	493	142879	3.3	9.3888	0.8	4.6781	1.5	0.3186	1.3	0.84	1782.7	19.7	1763.3	12.6	1740.5	14.9	**1740.5**	**14.9**	102.4
14WY-FH-2-Spot 161	97	311604	2.3	9.2987	1.1	4.6448	2.0	0.3132	1.6	0.83	1756.7	25.0	1757.4	16.4	1758.2	20.0	**1758.2**	**20.0**	99.9
14WY-FH-2-Spot 162	321	114887	1.4	9.2056	1.0	4.8050	2.8	0.3208	2.6	0.94	1793.7	41.1	1785.8	23.6	1776.5	18.0	**1776.5**	**18.0**	101.0
14WY-FH-2-Spot 163	257	49096	3.3	9.2898	0.8	4.6630	1.8	0.3142	1.6	0.89	1761.2	24.6	1760.6	15.0	1759.9	14.9	**1759.9**	**14.9**	100.1
14WY-FH-2-Spot 164	57	36814	1.9	9.2386	1.7	3.8452	2.2	0.2576	1.4	0.64	1477.8	18.4	1602.3	17.4	1770.0	30.2	**1770.0**	**30.2**	83.5
14WY-FH-2-Spot 165	177	182571	2.7	9.2834	1.0	4.8985	1.5	0.3298	1.1	0.77	1837.5	18.2	1802.0	12.6	1761.2	17.5	**1761.2**	**17.5**	104.3
14WY-FH-2-Spot 166	302	207152	2.7	9.3044	0.9	4.4022	1.3	0.2971	1.0	0.75	1676.7	14.9	1712.7	11.2	1757.0	16.4	**1757.0**	**16.4**	95.4
14WY-FH-2-Spot 167	218	72045	1.6	9.3776	0.9	4.6502	1.4	0.3163	1.1	0.77	1771.5	17.1	1758.3	12.0	1742.7	16.8	**1742.7**	**16.8**	101.7
14WY-FH-2-Spot 168	257	100849	1.7	9.2704	1.0	4.6983	1.4	0.3159	0.9	0.67	1769.6	14.5	1766.9	11.7	1763.7	19.0	**1763.7**	**19.0**	100.3
14WY-FH-2-Spot 169	283	122501	0.7	9.3876	1.0	4.7078	1.7	0.3205	1.4	0.81	1792.3	21.2	1768.6	14.0	1740.8	17.9	**1740.8**	**17.9**	103.0
14WY-FH-2-Spot 170	604	74628	1.5	9.5548	0.8	4.4941	1.2	0.3114	0.9	0.75	1747.7	13.4	1729.9	9.7	1708.3	14.3	**1708.3**	**14.3**	102.3
14WY-FH-2-Spot 171	381	71114	1.2	9.2793	1.1	4.2008	1.8	0.2827	1.4	0.80	1605.0	19.9	1674.2	14.4	1762.0	19.2	**1762.0**	**19.2**	91.1
14WY-FH-2-Spot 172	339	100007	3.2	9.3589	0.7	4.6864	1.1	0.3181	0.9	0.81	1780.4	14.1	1764.8	9.4	1746.4	12.1	**1746.4**	**12.1**	102.0
14WY-FH-2-Spot 173	194	36846	2.3	9.2240	1.0	4.6070	1.6	0.3082	1.3	0.78	1731.9	19.2	1750.5	13.5	1772.9	18.6	**1772.9**	**18.6**	97.7
14WY-FH-2-Spot 174	117	69355	1.4	9.1377	0.8	4.6974	2.7	0.3113	2.5	0.95	1747.2	38.8	1766.8	22.3	1790.0	15.0	**1790.0**	**15.0**	97.6
14WY-FH-2-Spot 175	759	87354	7.3	9.0047	0.8	4.7345	1.6	0.3092	1.4	0.87	1736.8	21.8	1773.4	13.8	1816.7	14.8	**1816.7**	**14.8**	95.6
14WY-FH-2-Spot 176	185	94601	1.7	5.9290	0.7	10.4099	1.3	0.4476	1.1	0.84	2384.7	22.2	2471.9	12.3	2544.4	12.0	**2544.4**	**12.0**	93.7
14WY-FH-2-Spot 177	124	81718	3.3	9.2343	1.0	4.7922	1.3	0.3210	0.9	0.67	1794.4	13.6	1783.5	10.9	1770.9	17.5	**1770.9**	**17.5**	101.3
14WY-FH-2-Spot 178	214	37325	0.4	9.1817	1.1	4.7593	1.8	0.3169	1.5	0.82	1774.7	23.3	1777.8	15.5	1781.3	19.4	**1781.3**	**19.4**	99.6
14WY-FH-2-Spot 179	215	137453	1.7	9.2054	0.9	4.8078	2.3	0.3210	2.1	0.92	1794.5	32.8	1786.3	19.2	1776.6	16.3	**1776.6**	**16.3**	101.0
14WY-FH-2-Spot 181	567	147942	5.9	9.1717	0.8	4.9297	3.1	0.3279	3.0	0.97	1828.3	48.0	1807.4	26.3	1783.3	14.5	**1783.3**	**14.5**	102.5
14WY-FH-2-Spot 182	257	41090	4.0	8.9325	0.7	5.2049	1.3	0.3372	1.1	0.86	1873.2	18.3	1853.4	11.2	1831.3	12.1	**1831.3**	**12.1**	102.3
14WY-FH-2-Spot 183	248	75940	2.8	9.1957	1.0	4.7656	2.5	0.3178	2.3	0.91	1779.2	35.2	1778.9	20.9	1778.5	18.9	**1778.5**	**18.9**	100.0
14WY-FH-2-Spot 184	540	217204	1.7	9.3853	0.7	4.7066	1.9	0.3204	1.8	0.93	1791.6	27.8	1768.4	16.0	1741.2	12.8	**1741.2**	**12.8**	102.9
14WY-FH-2-Spot 186	104	66186	1.0	9.0979	1.2	4.8232	3.1	0.3183	2.9	0.92	1781.2	44.4	1788.9	26.1	1798.0	22.0	**1798.0**	**22.0**	99.1
14WY-FH-2-Spot 187	344	172029	3.0	9.2329	0.9	4.7764	1.9	0.3198	1.7	0.90	1789.0	27.1	1780.8	16.2	1771.1	15.7	**1771.1**	**15.7**	101.0
14WY-FH-2-Spot 188	405	65397	4.6	9.3131	0.9	4.7627	2.3	0.3217	2.1	0.92	1798.0	32.8	1778.4	19.1	1755.3	16.7	**1755.3**	**16.7**	102.4
14WY-FH-2-Spot 189	478	273739	2.5	9.2852	0.8	4.7308	1.4	0.3186	1.2	0.82	1782.8	18.4	1772.7	12.1	1760.8	15.3	**1760.8**	**15.3**	101.2
14WY-FH-2-Spot 190	333	58499	1.9	8.9402	1.1	5.2238	1.8	0.3387	1.4	0.78	1880.5	22.3	1856.5	15.0	1829.7	20.1	**1829.7**	**20.1**	102.8
14WY-FH-2-Spot 192	231	247102	1.1	9.1741	0.8	4.8651	2.7	0.3237	2.6	0.96	1807.8	41.5	1796.2	23.1	1782.8	13.8	**1782.8**	**13.8**	101.4
14WY-FH-2-Spot 193	404	69640	4.8	9.2716	0.9	4.6350	2.2	0.3117	2.1	0.92	1749.0	31.9	1755.6	18.8	1763.5	15.7	**1763.5**	**15.7**	99.2
14WY-FH-2-Spot 194	201	47037	2.0	9.2132	0.9	4.7134	2.0	0.3150	1.7	0.89	1765.0	27.0	1769.6	16.6	1775.0	16.8	**1775.0**	**16.8**	99.4
14WY-FH-2-Spot 195	495	236261	1.0	9.3361	0.9	4.7457	1.7	0.3213	1.4	0.86	1796.3	22.5	1775.4	14.0	1750.8	15.8	**1750.8**	**15.8**	102.6
14WY-FH-2-Spot 196	106	33865	1.3	9.2981	1.1	4.5537	1.8	0.3071	1.5	0.80	1726.4	22.3	1740.8	15.3	1758.3	20.1	**1758.3**	**20.1**	98.2
14WY-FH-2-Spot 197	364	84895	2.0	7.5586	0.9	5.8591	3.2	0.3212	3.0	0.96	1795.6	47.6	1955.2	27.5	2128.7	15.8	**2128.7**	**15.8**	84.4
14WY-FH-2-Spot 198	586	158653	2.9	9.2928	1.2	4.7066	1.7	0.3172	1.3	0.74	1776.1	20.2	1768.4	14.6	1759.3	21.4	**1759.3**	**21.4**	101.0

Analysis	U	206Pb	U/Th	206Pb*	±	207Pb*	±	206Pb*	±	error	206Pb*	±	207Pb*	±	206Pb*	±	Best age	±	Conc
	(ppm)	204Pb		207Pb*	(%)	235U*	(%)	238U	(%)	corr.	238U*	(Ma)	235U	(Ma)	207Pb*	(Ma)	(Ma)	(Ma)	(%)
14WY-FH-2-Spot 199	129	26545	1.2	9.2393	0.8	4.6962	1.4	0.3147	1.1	0.81	1763.7	17.1	1766.6	11.5	1769.9	14.6	**1769.9**	**14.6**	99.7
14WY-FH-2-Spot 200	186	54108	3.9	8.9492	1.0	5.1551	1.5	0.3346	1.2	0.76	1860.6	18.6	1845.2	12.9	1827.9	17.8	**1827.9**	**17.8**	101.8
14WY-FH-2-Spot 201	264	103430	2.8	9.2419	0.9	4.8237	1.7	0.3233	1.4	0.85	1806.0	22.3	1789.0	14.0	1769.4	16.0	**1769.4**	**16.0**	102.1
14WY-FH-2-Spot 202	607	195105	7.3	9.3264	0.7	4.5055	1.6	0.3048	1.4	0.90	1714.8	21.7	1732.0	13.3	1752.7	13.0	**1752.7**	**13.0**	97.8
14WY-FH-2-Spot 203	72	32602	1.8	8.9140	1.1	5.0232	1.3	0.3248	0.8	0.57	1812.9	12.2	1823.2	11.4	1835.1	19.9	**1835.1**	**19.9**	98.8
14WY-FH-2-Spot 204	154	43240	1.0	9.2090	0.7	4.7641	1.3	0.3182	1.1	0.82	1780.9	16.8	1778.6	11.0	1775.9	13.5	**1775.9**	**13.5**	100.3
14WY-FH-2-Spot 205	274	209948	1.3	9.2500	1.0	4.9216	1.7	0.3302	1.4	0.82	1839.2	22.5	1806.0	14.4	1767.8	17.8	**1767.8**	**17.8**	104.0
14WY-FH-2-Spot 206	295	57076	1.0	9.1950	0.9	4.8100	3.5	0.3208	3.3	0.96	1793.5	52.2	1786.6	29.1	1778.7	17.0	**1778.7**	**17.0**	100.8
14WY-FH-2-Spot 207	129	111749	1.4	9.1901	0.7	4.6800	1.5	0.3119	1.3	0.88	1750.2	20.4	1763.7	12.7	1779.6	13.1	**1779.6**	**13.1**	98.3
14WY-FH-2-Spot 208	118	38735	7.6	8.7164	1.4	5.2660	2.0	0.3329	1.5	0.73	1852.4	23.7	1863.4	17.1	1875.6	24.6	**1875.6**	**24.6**	98.8
14WY-FH-2-Spot 209	96	134582	2.3	8.9939	1.4	4.8237	2.8	0.3147	2.5	0.87	1763.6	37.8	1789.0	23.8	1818.9	25.6	**1818.9**	**25.6**	97.0
14WY-FH-2-Spot 210	119	30692	4.9	8.9460	1.3	5.0702	1.7	0.3290	1.1	0.66	1833.4	18.3	1831.1	14.7	1828.6	23.7	**1828.6**	**23.7**	100.3
14WY-FH-2-Spot 212	266	50464	1.2	9.2144	0.9	4.8143	1.7	0.3217	1.4	0.86	1798.2	22.3	1787.4	13.9	1774.8	15.5	**1774.8**	**15.5**	101.3
14WY-FH-2-Spot 213	264	78076	3.2	9.2013	0.9	4.8828	3.4	0.3259	3.2	0.96	1818.2	51.4	1799.3	28.4	1777.4	16.7	**1777.4**	**16.7**	102.3
14WY-FH-2-Spot 214	275	171193	2.0	9.3072	0.9	4.6575	1.7	0.3144	1.4	0.85	1762.3	21.9	1759.6	14.0	1756.5	16.1	**1756.5**	**16.1**	100.3
14WY-FH-2-Spot 215	352	59096	2.6	9.2673	0.8	4.7557	1.5	0.3196	1.2	0.83	1788.0	19.5	1777.1	12.7	1764.3	15.5	**1764.3**	**15.5**	101.3
14WY-FH-2-Spot 216	342	144417	3.9	9.3058	1.0	4.8284	1.3	0.3259	0.9	0.70	1818.4	14.8	1789.9	11.2	1756.8	17.5	**1756.8**	**17.5**	103.5
14WY-FH-2-Spot 217	420	74645	3.2	8.9918	1.1	4.9835	1.5	0.3250	1.0	0.67	1814.1	16.3	1816.5	13.0	1819.3	20.5	**1819.3**	**20.5**	99.7
14WY-FH-2-Spot 218	577	61687	2.8	9.2497	0.7	4.8140	2.9	0.3229	2.8	0.97	1804.1	43.9	1787.3	24.2	1767.8	13.2	**1767.8**	**13.2**	102.1
14WY-FH-2-Spot 219	155	74455	5.5	9.0287	0.8	5.1273	1.4	0.3357	1.2	0.83	1866.2	19.0	1840.6	12.1	1811.9	14.5	**1811.9**	**14.5**	103.0
14WY-FH-2-Spot 220	288	2166176	2.0	9.2782	1.1	4.7784	3.9	0.3215	3.8	0.96	1797.3	58.9	1781.1	32.9	1762.2	20.2	**1762.2**	**20.2**	102.0
14WY-FH-2-Spot 221	148	66521	1.4	9.2855	1.0	4.6057	1.8	0.3102	1.5	0.83	1741.6	22.3	1750.3	14.7	1760.8	18.1	**1760.8**	**18.1**	98.9
14WY-FH-2-Spot 222	193	55460	0.5	9.0765	0.7	4.6463	2.3	0.3059	2.2	0.95	1720.3	32.8	1757.6	19.1	1802.3	12.9	**1802.3**	**12.9**	95.5
14WY-FH-2-Spot 223	95	74792	2.0	5.2891	0.9	13.6352	1.6	0.5231	1.3	0.83	2712.1	29.9	2724.7	15.5	2734.1	15.2	**2734.1**	**15.2**	99.2
14WY-FH-2-Spot 224	304	117886	2.2	9.1866	0.8	4.6763	3.8	0.3116	3.7	0.98	1748.4	57.1	1763.0	32.0	1780.3	15.3	**1780.3**	**15.3**	98.2
14WY-FH-2-Spot 225	268	106383	2.5	9.1607	0.6	4.6832	1.5	0.3111	1.4	0.91	1746.4	21.1	1764.2	12.7	1785.5	11.5	**1785.5**	**11.5**	97.8
14WY-FH-2-Spot 226	93	896390	1.5	9.1179	0.9	4.6259	2.0	0.3059	1.8	0.89	1720.5	26.7	1753.9	16.5	1794.0	16.3	**1794.0**	**16.3**	95.9
14WY-FH-2-Spot 227	149	71604	1.2	9.2304	1.1	4.6955	1.7	0.3143	1.3	0.77	1762.0	20.4	1766.4	14.5	1771.6	20.2	**1771.6**	**20.2**	99.5
14WY-FH-2-Spot 228	196	82641	3.0	9.1142	0.8	4.7306	2.0	0.3127	1.8	0.91	1754.0	27.9	1772.7	16.7	1794.7	15.0	**1794.7**	**15.0**	97.7
14WY-FH-2-Spot 229	80	34140	1.0	9.1803	1.1	4.6468	1.6	0.3094	1.1	0.70	1737.7	16.9	1757.7	13.3	1781.6	20.7	**1781.6**	**20.7**	97.5
14WY-FH-2-Spot 230	124	30524	1.0	9.2797	1.3	4.6643	1.8	0.3139	1.2	0.67	1760.0	18.2	1760.9	14.8	1761.9	24.2	**1761.9**	**24.2**	99.9
14WY-FH-2-Spot 231	462	69326	2.7	9.3272	0.8	4.6202	1.7	0.3125	1.5	0.89	1753.2	23.7	1752.9	14.4	1752.6	14.1	**1752.6**	**14.1**	100.0
14WY-FH-2-Spot 232	484	140546	2.8	9.2117	0.7	4.2435	1.9	0.2835	1.8	0.94	1609.0	25.4	1682.5	15.7	1775.3	12.3	**1775.3**	**12.3**	90.6
14WY-FH-2-Spot 233	199	85337	1.4	5.4702	0.9	12.7972	1.3	0.5077	0.9	0.69	2646.8	18.8	2664.8	11.8	2678.5	14.9	**2678.5**	**14.9**	98.8
14WY-FH-2-Spot 234	77	107040	1.2	5.3294	1.1	13.1836	1.8	0.5096	1.4	0.77	2654.8	29.7	2692.9	16.7	2721.5	18.7	**2721.5**	**18.7**	97.5
14WY-FH-2-Spot 235	225	47126	2.3	9.2021	0.7	4.7173	1.6	0.3148	1.5	0.91	1764.4	23.0	1770.3	13.7	1777.2	12.1	**1777.2**	**12.1**	99.3
14WY-FH-2-Spot 236	145	70698	2.6	9.1835	1.1	4.6611	2.5	0.3105	2.3	0.89	1742.9	34.4	1760.3	21.1	1780.9	20.9	**1780.9**	**20.9**	97.9
14WY-FH-2-Spot 237	196	91227	1.3	9.1931	1.0	4.7916	1.8	0.3195	1.5	0.83	1787.2	23.4	1783.4	15.1	1779.0	18.2	**1779.0**	**18.2**	100.5
14WY-FH-2-Spot 238	38	27791	1.1	9.2174	1.6	4.6708	2.9	0.3122	2.5	0.84	1751.8	38.0	1762.0	24.5	1774.2	28.7	**1774.2**	**28.7**	98.7
14WY-FH-2-Spot 239	413	115235	3.2	9.2206	0.8	4.7939	2.1	0.3206	2.0	0.93	1792.6	31.2	1783.8	18.0	1773.6	14.2	**1773.6**	**14.2**	101.1
14WY-FH-2-Spot 240	80	31546	1.3	5.4976	1.1	12.5520	2.7	0.5005	2.5	0.92	2615.8	53.4	2646.6	25.5	2670.2	18.0	**2670.2**	**18.0**	98.0

Analysis	U	206Pb	U/Th	206Pb*	±	207Pb*	±	206Pb*	±	error	206Pb*	±	207Pb*	±	206Pb*	±	Best age	±	Conc
	(ppm)	204Pb		207Pb*	(%)	235U*	(%)	238U	(%)	corr.	238U*	(Ma)	235U	(Ma)	207Pb*	(Ma)	(Ma)	(Ma)	(%)
14WY-FH-2-Spot 241	406	155982	2.1	8.9008	1.1	4.6931	1.6	0.3030	1.2	0.72	1706.0	17.6	1766.0	13.6	1837.8	20.3	**1837.8**	**20.3**	92.8
14WY-FH-2-Spot 242	138	220871	0.9	9.2080	0.6	4.7011	2.1	0.3140	2.0	0.95	1760.1	30.2	1767.4	17.3	1776.1	11.7	**1776.1**	**11.7**	99.1
14WY-FH-2-Spot 244	208	156638	1.9	9.1256	0.9	4.7164	2.4	0.3122	2.2	0.93	1751.3	33.6	1770.2	19.8	1792.5	16.0	**1792.5**	**16.0**	97.7
14WY-FH-2-Spot 245	264	199072	2.5	8.7507	0.9	5.1215	1.4	0.3250	1.1	0.78	1814.3	17.5	1839.7	12.1	1868.5	16.2	**1868.5**	**16.2**	97.1
14WY-FH-2-Spot 246	85	36336	2.1	9.3059	1.3	4.5994	1.8	0.3104	1.3	0.71	1742.8	20.1	1749.2	15.4	1756.8	23.7	**1756.8**	**23.7**	99.2
14WY-FH-2-Spot 247	608	152623	4.3	9.2907	0.6	4.7263	1.2	0.3185	1.0	0.85	1782.3	16.1	1771.9	10.2	1759.7	11.8	**1759.7**	**11.8**	101.3
14WY-FH-2-Spot 248	84	48194	1.6	9.1609	1.1	4.7528	1.5	0.3158	1.1	0.71	1769.1	17.1	1776.6	13.0	1785.4	19.8	**1785.4**	**19.8**	99.1
14WY-FH-2-Spot 249	368	155441	2.2	9.2339	1.1	4.6808	2.0	0.3135	1.7	0.83	1757.8	25.8	1763.8	17.0	1770.9	20.8	**1770.9**	**20.8**	99.3
14WY-FH-2-Spot 250	55	61113	1.5	5.3899	1.0	13.1872	3.2	0.5155	3.1	0.95	2680.1	67.5	2693.1	30.7	2702.9	17.2	**2702.9**	**17.2**	99.2
14WY-FH-2-Spot 251	74	114891	3.4	8.6950	1.0	5.2293	1.6	0.3298	1.2	0.77	1837.3	19.3	1857.4	13.3	1880.0	17.8	**1880.0**	**17.8**	97.7
14WY-FH-2-Spot 252	220	190758	3.0	8.9323	1.1	5.0254	2.6	0.3256	2.4	0.91	1816.8	37.8	1823.6	22.3	1831.3	19.9	**1831.3**	**19.9**	99.2
14WY-FH-2-Spot 253	179	109246	0.7	9.2569	0.5	4.6680	1.0	0.3134	0.9	0.90	1757.4	14.0	1761.5	8.5	1766.4	8.3	**1766.4**	**8.3**	99.5
14WY-FH-2-Spot 254	48	42933	1.1	9.1754	1.5	4.5488	2.9	0.3027	2.4	0.85	1704.7	36.3	1739.9	23.7	1782.5	27.5	**1782.5**	**27.5**	95.6
14WY-FH-2-Spot 255	77	32105	0.9	9.1396	1.3	4.7733	1.6	0.3164	1.0	0.61	1772.2	14.9	1780.2	13.3	1789.7	22.9	**1789.7**	**22.9**	99.0
14WY-FH-2-Spot 256	169	72658	2.4	5.3647	0.9	11.2983	1.7	0.4396	1.4	0.83	2348.9	27.6	2548.1	15.7	2710.7	15.4	**2710.7**	**15.4**	86.7
14WY-FH-2-Spot 257	130	42660	1.7	9.2915	0.8	4.6634	1.4	0.3143	1.2	0.84	1761.6	18.6	1760.7	12.0	1759.6	14.4	**1759.6**	**14.4**	100.1
14WY-FH-2-Spot 258	401	51220	2.9	9.2554	0.9	4.7163	1.7	0.3166	1.4	0.83	1773.0	21.4	1770.1	14.0	1766.7	17.3	**1766.7**	**17.3**	100.4
14WY-FH-2-Spot 259	384	125512	6.3	9.1474	0.8	4.5469	1.6	0.3017	1.4	0.86	1699.5	20.8	1739.6	13.5	1788.1	15.0	**1788.1**	**15.0**	95.0
14WY-FH-2-Spot 260	332	68172	2.7	9.2431	1.0	4.7799	1.4	0.3204	1.0	0.71	1791.8	15.9	1781.4	11.9	1769.1	18.2	**1769.1**	**18.2**	101.3
14WY-FH-2-Spot 261	111	167611	1.7	6.0845	1.0	10.4202	1.6	0.4598	1.3	0.81	2438.8	26.8	2472.8	15.1	2500.9	16.0	**2500.9**	**16.0**	97.5
14WY-FH-2-Spot 262	236	71660	2.8	9.1472	1.0	4.7569	1.9	0.3156	1.7	0.87	1768.1	25.6	1777.3	16.0	1788.1	17.4	**1788.1**	**17.4**	98.9
14WY-FH-2-Spot 263	101	71260	0.8	3.6594	0.8	25.5718	1.3	0.6787	0.9	0.75	3339.3	24.5	3330.3	12.3	3324.9	13.1	**3324.9**	**13.1**	100.4
14WY-FH-2-Spot 264	464	62875	4.3	9.2379	0.8	4.6961	1.8	0.3146	1.6	0.90	1763.5	25.2	1766.5	15.2	1770.2	14.7	**1770.2**	**14.7**	99.6
14WY-FH-2-Spot 265	192	79556	2.8	6.2099	0.7	10.4358	1.5	0.4700	1.3	0.87	2483.6	25.9	2474.2	13.4	2466.5	12.2	**2466.5**	**12.2**	100.7
14WY-FH-2-Spot 266	320	196013	2.1	9.2641	1.0	4.7554	1.5	0.3195	1.1	0.76	1787.4	17.7	1777.1	12.6	1765.0	17.9	**1765.0**	**17.9**	101.3
14WY-FH-2-Spot 267	60	40097	1.3	9.4243	1.4	4.5407	2.0	0.3104	1.4	0.71	1742.5	21.7	1738.5	16.6	1733.6	25.8	**1733.6**	**25.8**	100.5
14WY-FH-2-Spot 268	413	244291	2.4	9.2098	0.8	4.7211	1.6	0.3154	1.3	0.84	1767.0	20.1	1771.0	13.0	1775.7	15.4	**1775.7**	**15.4**	99.5
14WY-FH-2-Spot 269	353	141102	1.3	9.1995	0.6	4.5928	1.5	0.3064	1.4	0.91	1723.1	21.1	1748.0	12.8	1777.7	11.7	**1777.7**	**11.7**	96.9
14WY-FH-2-Spot 270	105	52354	1.6	5.4448	1.0	13.0301	2.4	0.5145	2.2	0.91	2676.0	47.9	2681.8	22.7	2686.2	16.7	**2686.2**	**16.7**	99.6
14WY-FH-2-Spot 271	102	53847	2.1	8.9540	1.3	5.0611	2.1	0.3287	1.6	0.78	1831.9	25.8	1829.6	17.6	1827.0	23.7	**1827.0**	**23.7**	100.3
14WY-FH-2-Spot 272	35	29808	2.3	9.1231	1.6	4.7839	2.2	0.3165	1.5	0.69	1772.8	23.3	1782.1	18.2	1793.0	28.3	**1793.0**	**28.3**	98.9
14WY-FH-2-Spot 273	720	195128	3.4	9.2500	0.8	4.7649	1.7	0.3197	1.5	0.89	1788.1	23.0	1778.7	13.9	1767.8	13.9	**1767.8**	**13.9**	101.2
14WY-FH-2-Spot 274	162	58262	0.7	6.1837	0.9	9.7446	1.4	0.4370	1.1	0.79	2337.3	21.8	2410.9	13.0	2473.7	14.6	**2473.7**	**14.6**	94.5
14WY-FH-2-Spot 275	451	65321	2.8	9.1831	0.9	4.7067	1.7	0.3135	1.5	0.85	1757.8	22.3	1768.4	14.2	1781.0	16.1	**1781.0**	**16.1**	98.7
14WY-FH-2-Spot 277	361	104846	5.4	9.2804	0.7	4.6876	1.7	0.3155	1.5	0.92	1767.8	23.7	1765.0	14.0	1761.8	12.3	**1761.8**	**12.3**	100.3
14WY-FH-2-Spot 278	308	561874	6.2	9.1303	0.7	4.7575	2.2	0.3150	2.1	0.94	1765.4	31.8	1777.4	18.4	1791.5	13.6	**1791.5**	**13.6**	98.5
14WY-FH-2-Spot 279	158	55975	1.2	9.1535	1.3	4.7642	3.8	0.3163	3.6	0.94	1771.6	55.1	1778.6	31.7	1786.9	22.9	**1786.9**	**22.9**	99.1
14WY-FH-2-Spot 280	241	120573	3.0	9.1820	0.9	4.8043	1.6	0.3199	1.4	0.85	1789.4	22.0	1785.6	13.9	1781.2	15.6	**1781.2**	**15.6**	100.5
14WY-FH-2-Spot 276	214	104633	2.3	9.1131	1.2	4.7902	1.9	0.3166	1.4	0.77	1773.1	22.2	1783.2	15.7	1794.9	21.8	**1794.9**	**21.8**	98.8
14WY-FH-2-Spot 281	236	68173	3.1	9.0863	0.8	4.8425	1.3	0.3191	1.0	0.79	1785.4	16.0	1792.3	10.9	1800.3	14.4	**1800.3**	**14.4**	99.2
14WY-FH-2-Spot 282	132	158142	2.9	5.3933	0.9	13.4178	2.5	0.5248	2.3	0.93	2719.7	51.1	2709.5	23.4	2701.9	15.0	**2701.9**	**15.0**	100.7

Analysis	U	206Pb	U/Th	206Pb*	±	207Pb*	±	206Pb*	±	error	206Pb*	±	207Pb*	±	206Pb*	±	Best age	±	Conc
	(ppm)	204Pb		207Pb*	(%)	235U*	(%)	238U	(%)	corr.	238U*	(Ma)	235U	(Ma)	207Pb*	(Ma)	(Ma)	(Ma)	(%)
14WY-FH-2-Spot 284	86	65580	5.4	8.8834	1.1	5.0934	2.0	0.3282	1.6	0.83	1829.5	26.0	1835.0	16.6	1841.3	19.6	**1841.3**	**19.6**	99.4
14WY-FH-2-Spot 285	92	37454	3.0	8.8021	1.0	5.2134	1.9	0.3328	1.6	0.84	1852.0	25.7	1854.8	16.2	1857.9	18.6	**1857.9**	**18.6**	99.7
14WY-FH-2-Spot 286	222	72333	2.7	9.1624	0.8	4.7807	1.6	0.3177	1.4	0.85	1778.4	21.0	1781.5	13.3	1785.1	15.0	**1785.1**	**15.0**	99.6
14WY-FH-2-Spot 287	213	84140	0.9	9.0662	1.0	4.7920	1.6	0.3151	1.2	0.76	1765.7	18.8	1783.5	13.4	1804.3	18.9	**1804.3**	**18.9**	97.9
14WY-FH-2-Spot 288	315	59196	2.3	9.1079	0.9	4.6403	1.8	0.3065	1.5	0.85	1723.6	23.0	1756.6	14.9	1796.0	17.1	**1796.0**	**17.1**	96.0
14WY-FH-2-Spot 289	47	42148	2.6	8.9527	1.4	4.9916	2.0	0.3241	1.4	0.71	1809.8	22.3	1817.9	16.7	1827.2	25.1	**1827.2**	**25.1**	99.0
14WY-FH-2-Spot 290	398	222161	1.1	8.7748	1.0	4.2040	1.8	0.2675	1.5	0.83	1528.3	20.6	1674.8	15.0	1863.5	18.4	**1863.5**	**18.4**	82.0
14WY-FH-2-Spot 291	161	70012	1.5	5.5187	1.0	12.8861	1.7	0.5158	1.4	0.80	2681.2	29.7	2671.4	15.9	2663.9	16.8	**2663.9**	**16.8**	100.6
14WY-FH-2-Spot 292	649	213050	8.1	9.2803	0.9	4.6518	1.7	0.3131	1.4	0.82	1755.9	20.8	1758.6	13.8	1761.8	17.3	**1761.8**	**17.3**	99.7
14WY-FH-2-Spot 293	121	51826	1.3	9.1097	0.8	4.7577	3.8	0.3143	3.7	0.98	1762.0	57.3	1777.5	31.9	1795.6	14.3	**1795.6**	**14.3**	98.1
14WY-FH-2-Spot 294	229	90319	1.6	9.1447	0.9	4.7885	1.5	0.3176	1.2	0.79	1777.9	18.3	1782.9	12.6	1788.6	16.9	**1788.6**	**16.9**	99.4
14WY-FH-2-Spot 295	58	34166	2.3	9.3233	0.9	4.6008	1.7	0.3111	1.5	0.85	1746.1	22.3	1749.4	14.3	1753.3	16.5	**1753.3**	**16.5**	99.6
14WY-FH-2-Spot 297	319	87506	1.8	9.1035	0.9	4.6332	2.0	0.3059	1.8	0.89	1720.5	27.2	1755.3	17.0	1796.9	17.2	**1796.9**	**17.2**	95.8
14WY-FH-2-Spot 298	309	205334	4.1	9.2199	1.0	4.6065	1.7	0.3080	1.4	0.81	1731.0	20.9	1750.5	14.2	1773.7	18.2	**1773.7**	**18.2**	97.6
14WY-FH-2-Spot 299	487	218117	2.3	8.8106	0.5	5.0294	1.6	0.3214	1.5	0.95	1796.5	23.8	1824.3	13.5	1856.2	9.0	**1856.2**	**9.0**	96.8
14WY-FH-2-Spot 300	34	75581	2.5	9.2175	1.7	4.6157	3.2	0.3086	2.7	0.84	1733.7	40.4	1752.1	26.4	1774.2	31.4	**1774.2**	**31.4**	97.7
14WY-FH-2-Spot 301	386	59224	5.1	9.2380	0.9	4.8023	1.8	0.3218	1.6	0.87	1798.3	24.5	1785.3	15.2	1770.1	16.5	**1770.1**	**16.5**	101.6
14WY-FH-2-Spot 302	48	57408	2.0	8.6475	1.4	5.2556	2.3	0.3296	1.9	0.81	1836.5	30.0	1861.7	19.8	1889.9	24.4	**1889.9**	**24.4**	97.2
14WY-FH-2-Spot 303	129	31258	2.8	9.0960	1.1	4.7759	1.6	0.3151	1.1	0.73	1765.6	17.7	1780.7	13.3	1798.4	19.8	**1798.4**	**19.8**	98.2
14WY-FH-2-Spot 304	431	140775	2.2	8.9566	1.2	4.4212	2.1	0.2872	1.7	0.83	1627.5	24.9	1716.3	17.3	1826.4	21.2	**1826.4**	**21.2**	89.1
14WY-FH-2-Spot 305	547	121041	1.7	9.2389	0.6	4.7518	1.3	0.3184	1.1	0.89	1781.9	17.5	1776.4	10.6	1770.0	10.4	**1770.0**	**10.4**	100.7
14WY-FH-2-Spot 306	253	232809	3.6	9.2003	0.9	4.6440	2.0	0.3099	1.8	0.90	1740.1	27.7	1757.2	16.9	1777.6	16.3	**1777.6**	**16.3**	97.9
14WY-FH-2-Spot 307	330	32312	2.6	8.4794	3.2	4.7127	3.4	0.2898	1.1	0.33	1640.6	16.3	1769.5	28.7	1925.1	57.9	**1925.1**	**57.9**	85.2
14WY-FH-2-Spot 308	23	16750	1.0	8.5331	2.2	5.2063	2.6	0.3222	1.4	0.52	1800.5	21.2	1853.6	22.0	1913.8	39.6	**1913.8**	**39.6**	94.1
14WY-FH-2-Spot 309	250	988819	1.0	9.1709	0.7	4.7847	1.5	0.3182	1.3	0.89	1781.2	21.0	1782.2	12.8	1783.4	12.7	**1783.4**	**12.7**	99.9
14WY-FH-2-Spot 310	244	91056	1.3	9.1816	0.7	4.7764	1.3	0.3181	1.0	0.81	1780.3	15.9	1780.8	10.6	1781.3	13.7	**1781.3**	**13.7**	99.9
14WY-FH-2-Spot 311	120	46605	1.6	9.3178	1.0	4.8299	1.6	0.3264	1.2	0.76	1820.9	18.8	1790.1	13.1	1754.4	18.3	**1754.4**	**18.3**	103.8
14WY-FH-2-Spot 312	144	39213	1.5	8.6354	0.9	5.4307	3.3	0.3401	3.2	0.96	1887.3	52.1	1889.7	28.4	1892.4	16.3	**1892.4**	**16.3**	99.7
14WY-FH-2-Spot 313	333	66328	2.2	9.1361	0.7	4.7642	1.5	0.3157	1.4	0.88	1768.6	21.0	1778.6	13.0	1790.4	13.4	**1790.4**	**13.4**	98.8
14WY-FH-2-Spot 314	297	247495	2.5	9.2165	0.9	4.7821	2.6	0.3197	2.4	0.93	1788.1	37.2	1781.8	21.5	1774.4	17.0	**1774.4**	**17.0**	100.8
14WY-FH-2-Spot 315	230	70543	3.2	9.1774	0.9	4.7227	1.4	0.3143	1.0	0.75	1762.1	15.7	1771.3	11.4	1782.1	16.5	**1782.1**	**16.5**	98.9
14WY-FH-2-Spot 316	256	71537	2.9	8.8375	0.6	5.2671	1.2	0.3376	1.0	0.85	1875.1	16.3	1863.6	10.1	1850.7	11.2	**1850.7**	**11.2**	101.3
14WY-FH-2-Spot 317	200	245586	3.3	9.1780	1.0	4.7698	1.6	0.3175	1.3	0.80	1777.5	20.1	1779.6	13.7	1782.0	17.9	**1782.0**	**17.9**	99.7
14WY-FH-2-Spot 318	168	155704	4.9	8.8840	1.0	5.2590	1.7	0.3389	1.4	0.82	1881.2	22.8	1862.2	14.5	1841.2	17.4	**1841.2**	**17.4**	102.2
14WY-FH-2-Spot 319	231	77982	1.1	9.1543	1.1	4.5766	3.3	0.3039	3.1	0.94	1710.4	46.5	1745.0	27.4	1786.7	20.0	**1786.7**	**20.0**	95.7
14WY-FH-2-Spot 320	403	219280	3.1	9.3048	1.1	4.4915	1.6	0.3031	1.2	0.76	1706.7	18.3	1729.4	13.4	1757.0	19.2	**1757.0**	**19.2**	97.1
14WY-FH-2-Spot 321	137	47923	1.0	8.7678	0.9	5.1409	1.4	0.3269	1.1	0.76	1823.4	16.7	1842.9	11.8	1865.0	16.3	**1865.0**	**16.3**	97.8
14WY-FH-2-Spot 322	211	62688	2.8	9.1556	1.3	4.8410	3.5	0.3215	3.3	0.93	1796.8	51.2	1792.1	29.7	1786.5	24.3	**1786.5**	**24.3**	100.6
14WY-FH-2-Spot 323	97	130075	1.7	9.2404	1.0	4.7202	1.5	0.3163	1.1	0.76	1771.8	17.4	1770.8	12.4	1769.7	17.4	**1769.7**	**17.4**	100.1
14WY-FH-2-Spot 324	125	50150	1.8	9.1541	1.0	4.8078	1.5	0.3192	1.1	0.74	1785.8	17.6	1786.3	12.8	1786.8	18.5	**1786.8**	**18.5**	99.9
14WY-FH-2-Spot 325	139	38567	2.6	8.8876	0.9	5.2370	1.5	0.3376	1.2	0.79	1875.0	19.9	1858.7	13.2	1840.4	17.1	**1840.4**	**17.1**	101.9

Analysis	U	206Pb	U/Th	206Pb*	±	207Pb*	±	206Pb*	±	error	206Pb*	±	207Pb*	±	206Pb*	±	Best age	±	Conc
	(ppm)	204Pb		207Pb*	(%)	235U*	(%)	238U	(%)	corr.	238U*	(Ma)	235U	(Ma)	207Pb*	(Ma)	(Ma)	(Ma)	(%)
14WY-FH-2-Spot 326	234	117460	2.2	9.1649	0.8	4.7782	1.3	0.3176	0.9	0.74	1778.0	14.4	1781.1	10.5	1784.6	15.5	**1784.6**	**15.5**	99.6
14WY-FH-2-Spot 327	189	124078	2.8	9.2391	1.0	4.7991	4.2	0.3216	4.0	0.97	1797.4	63.4	1784.7	35.0	1769.9	18.5	**1769.9**	**18.5**	101.6
14WY-FH-2-Spot 328	220	113082	1.4	9.2241	1.0	4.8371	1.5	0.3236	1.2	0.77	1807.3	18.2	1791.4	12.6	1772.9	17.4	**1772.9**	**17.4**	101.9
14WY-FH-2-Spot 329	192	151432	3.5	9.1906	1.1	4.8940	1.6	0.3262	1.3	0.77	1820.0	19.9	1801.2	13.8	1779.5	19.2	**1779.5**	**19.2**	102.3
14WY-FH-2-Spot 330	184	217514	2.9	9.1029	0.8	4.9428	1.3	0.3263	1.0	0.75	1820.5	15.2	1809.6	10.8	1797.0	15.3	**1797.0**	**15.3**	101.3
SH324BD-Spot 33	73	42660	1.4	13.9240	3.3	1.6153	3.6	0.1631	1.4	0.39	974.1	12.5	976.2	22.5	980.8	67.4	**980.8**	**67.4**	99.3
SH324BD-Spot 15	69	45997	1.2	13.9010	2.9	1.6152	3.1	0.1628	1.2	0.39	972.5	11.0	976.1	19.5	984.2	58.3	**984.2**	**58.3**	98.8
SH324BD-Spot 76	317	37496	4.1	13.4957	0.5	1.6358	1.1	0.1601	1.0	0.89	957.4	8.9	984.1	7.1	1044.1	10.2	**1044.1**	**10.2**	91.7
SH324BD-Spot 79	103	79615	2.7	13.4942	2.0	1.8164	2.6	0.1778	1.7	0.64	1054.8	16.1	1051.4	16.9	1044.3	39.8	**1044.3**	**39.8**	101.0
SH324BD-Spot 99	132	63538	1.8	13.4940	1.4	1.8416	1.6	0.1802	0.8	0.49	1068.3	7.6	1060.4	10.4	1044.4	27.8	**1044.4**	**27.8**	102.3
SH324BD-Spot 34	104	62321	1.2	13.4606	2.7	1.8722	2.8	0.1828	0.5	0.19	1082.1	5.2	1071.3	18.4	1049.4	55.1	**1049.4**	**55.1**	103.1
SH324BD-Spot 84	67	36543	3.5	13.3963	3.0	1.7089	3.2	0.1660	0.9	0.29	990.3	8.6	1011.9	20.4	1059.0	61.4	**1059.0**	**61.4**	93.5
SH324BD-Spot 92	126	63395	1.6	13.3770	1.5	1.8951	1.7	0.1839	0.7	0.40	1088.0	6.8	1079.4	11.2	1061.9	31.0	**1061.9**	**31.0**	102.5
SH324BD-Spot 101	36	43274	1.7	13.3697	4.8	1.8763	5.2	0.1819	2.1	0.39	1077.6	20.5	1072.8	34.7	1063.0	96.8	**1063.0**	**96.8**	101.4
SH324BD-Spot 86	114	43015	2.1	13.3470	1.6	1.7165	2.3	0.1662	1.7	0.73	990.9	15.3	1014.7	14.6	1066.5	31.4	**1066.5**	**31.4**	92.9
SH324BD-Spot 59	49	30498	0.5	13.3379	3.6	1.8608	3.7	0.1800	0.9	0.23	1067.0	8.6	1067.3	24.7	1067.8	73.1	**1067.8**	**73.1**	99.9
SH324BD-Spot 13	22	12164	0.4	13.3349	5.2	1.9249	5.6	0.1862	2.2	0.39	1100.6	22.5	1089.8	37.8	1068.3	104.4	**1068.3**	**104.4**	103.0
SH324BD-Spot 102	58	25594	1.1	13.3104	3.3	1.7627	6.1	0.1702	5.1	0.84	1013.0	47.7	1031.8	39.4	1072.0	66.9	**1072.0**	**66.9**	94.5
SH324BD-Spot 65	87	76940	2.0	13.2207	2.2	1.7913	2.3	0.1718	0.8	0.36	1021.8	8.0	1042.3	15.3	1085.5	44.0	**1085.5**	**44.0**	94.1
SH324BD-Spot 107	72	43028	1.1	13.1581	3.5	2.0008	3.7	0.1909	1.3	0.36	1126.4	13.7	1115.8	25.1	1095.1	69.3	**1095.1**	**69.3**	102.9
SH324BD-Spot 109	83	83170	2.1	13.1100	2.0	1.9853	2.2	0.1888	0.8	0.38	1114.7	8.4	1110.5	14.7	1102.4	40.3	**1102.4**	**40.3**	101.1
SH324BD-Spot 16	30	24399	0.5	13.0634	7.7	2.0005	7.9	0.1895	1.8	0.23	1118.9	18.5	1115.7	53.5	1109.5	153.9	**1109.5**	**153.9**	100.8
SH324BD-Spot 41	86	79677	1.2	13.0465	2.2	1.9225	2.3	0.1819	0.7	0.29	1077.4	6.5	1089.0	15.2	1112.0	43.4	**1112.0**	**43.4**	96.9
SH324BD-Spot 6	27	17578	0.7	13.0251	5.4	2.0514	5.9	0.1938	2.4	0.40	1141.9	25.0	1132.8	40.4	1115.3	108.2	**1115.3**	**108.2**	102.4
SH324BD-Spot 108	69	52050	1.9	13.0167	3.0	1.9421	4.0	0.1833	2.7	0.68	1085.2	27.3	1095.7	27.0	1116.7	59.0	**1116.7**	**59.0**	97.2
SH324BD-Spot 90	125	64233	2.2	12.9895	1.6	2.0378	1.9	0.1920	0.9	0.49	1132.1	9.4	1128.2	12.7	1120.8	32.5	**1120.8**	**32.5**	101.0
SH324BD-Spot 73	40	38814	0.9	12.9858	6.4	1.9505	6.8	0.1837	2.3	0.35	1087.2	23.5	1098.6	45.5	1121.4	126.8	**1121.4**	**126.8**	96.9
SH324BD-Spot 38	73	34743	2.2	12.9425	1.7	1.9569	2.0	0.1837	0.9	0.48	1087.1	9.4	1100.8	13.2	1128.1	34.5	**1128.1**	**34.5**	96.4
SH324BD-Spot 74	55	42561	1.4	12.8587	3.6	2.0622	4.2	0.1923	2.0	0.49	1133.9	21.1	1136.3	28.6	1141.0	72.5	**1141.0**	**72.5**	99.4
SH324BD-Spot 45	27	24339	0.5	12.8052	6.2	2.0720	6.5	0.1924	2.0	0.31	1134.5	20.7	1139.6	44.6	1149.2	123.3	**1149.2**	**123.3**	98.7
SH324BD-Spot 12	60	39248	0.6	12.6733	2.7	2.1681	3.1	0.1993	1.5	0.49	1171.5	16.5	1170.9	21.6	1169.8	53.6	**1169.8**	**53.6**	100.1
SH324BD-Spot 60	60	81041	1.2	12.6488	2.6	2.1529	2.8	0.1975	1.0	0.35	1161.9	10.3	1166.0	19.3	1173.6	51.5	**1173.6**	**51.5**	99.0
SH324BD-Spot 40	78	121867	0.6	12.5538	2.2	2.2755	2.3	0.2072	0.7	0.29	1213.8	7.3	1204.7	16.2	1188.5	43.4	**1188.5**	**43.4**	102.1
SH324BD-Spot 96	60	36051	0.9	12.5191	2.6	2.2122	3.0	0.2009	1.4	0.47	1180.0	15.2	1184.9	20.9	1194.0	51.8	**1194.0**	**51.8**	98.8
SH324BD-Spot 100	193	12232	2.2	12.5005	1.1	1.8984	3.5	0.1721	3.4	0.95	1023.7	31.9	1080.5	23.5	1196.9	21.1	**1196.9**	**21.1**	85.5
SH324BD-Spot 46	56	29562	1.4	12.4482	1.9	2.3356	2.1	0.2109	0.9	0.41	1233.4	9.7	1223.2	14.8	1205.2	37.4	**1205.2**	**37.4**	102.3
SH324BD-Spot 80	53	38965	1.6	12.3624	2.9	2.3473	3.1	0.2105	1.1	0.36	1231.3	12.5	1226.7	22.1	1218.8	57.0	**1218.8**	**57.0**	101.0
SH324BD-Spot 95	178	58446	0.9	12.3404	1.5	1.9868	2.0	0.1778	1.3	0.66	1055.1	12.6	1111.0	13.3	1222.3	29.1	**1222.3**	**29.1**	86.3
SH324BD-Spot 22	40	25605	1.3	12.2742	3.0	2.2689	6.4	0.2020	5.6	0.88	1186.0	61.2	1202.7	45.0	1232.9	58.3	**1232.9**	**58.3**	96.2
SH324BD-Spot 51	56	26204	1.2	12.2493	2.6	2.3923	2.7	0.2125	0.9	0.31	1242.3	9.7	1240.3	19.7	1236.8	51.1	**1236.8**	**51.1**	100.4

Analysis	U (ppm)	206Pb 204Pb	U/Th	206Pb* 207Pb*	± (%)	207Pb* 235U*	± (%)	206Pb* 238U	± (%)	error corr.	206Pb* 238U*	± (Ma)	207Pb* 235U	± (Ma)	206Pb* 207Pb*	± (Ma)	Best age (Ma)	± (Ma)	Conc (%)
SH324BD-Spot 81	85	23723	1.9	12.1953	1.9	2.2651	2.0	0.2003	0.6	0.29	1177.2	6.3	1201.5	14.3	1245.5	38.1	**1245.5**	**38.1**	94.5
SH324BD-Spot 25	36	28667	0.5	12.1934	2.9	2.3993	3.1	0.2122	1.1	0.36	1240.4	12.4	1242.4	21.9	1245.8	55.9	**1245.8**	**55.9**	99.6
SH324BD-Spot 44	43	22473	1.1	12.0389	5.2	2.3041	6.9	0.2012	4.5	0.66	1181.6	48.9	1213.5	48.7	1270.7	100.9	**1270.7**	**100.9**	93.0
SH324BD-Spot 85	33	18022	1.1	11.9850	2.0	2.5107	2.2	0.2182	1.1	0.48	1272.6	12.4	1275.1	16.3	1279.5	38.3	**1279.5**	**38.3**	99.5
SH324BD-Spot 19	66	26045	1.5	11.9293	2.8	2.6213	2.9	0.2268	1.0	0.35	1317.7	12.2	1306.6	21.7	1288.5	53.8	**1288.5**	**53.8**	102.3
SH324BD-Spot 77	149	7354	1.4	11.8276	3.0	1.1130	7.5	0.0955	6.9	0.92	587.8	38.6	759.6	40.1	1305.2	58.2	**1305.2**	**58.2**	45.0
SH324BD-Spot 52	108	129911	2.4	11.7750	2.1	2.6868	2.2	0.2295	0.7	0.30	1331.6	7.9	1324.8	16.0	1313.8	39.8	**1313.8**	**39.8**	101.4
SH324BD-Spot 67	37	38173	1.0	11.7071	3.5	2.6812	3.7	0.2277	1.3	0.35	1322.2	15.7	1323.3	27.4	1325.0	67.2	**1325.0**	**67.2**	99.8
SH324BD-Spot 97	156	72064	2.2	11.6575	1.1	2.7192	3.6	0.2299	3.4	0.96	1334.0	41.2	1333.7	26.6	1333.3	20.4	**1333.3**	**20.4**	100.1
SH324BD-Spot 62	64	60821	1.6	11.5660	2.2	2.8127	2.4	0.2359	1.0	0.40	1365.6	12.0	1358.9	18.2	1348.5	43.1	**1348.5**	**43.1**	101.3
SH324BD-Spot 106	31	20907	2.4	11.4296	3.8	2.8719	4.3	0.2381	1.9	0.44	1376.6	23.4	1374.6	32.1	1371.3	73.4	**1371.3**	**73.4**	100.4
SH324BD-Spot 57	52	28591	1.9	11.3035	1.7	3.0448	2.4	0.2496	1.7	0.70	1436.5	21.6	1418.9	18.3	1392.7	32.7	**1392.7**	**32.7**	103.1
SH324BD-Spot 54	127	141401	2.1	11.2851	1.0	2.9167	1.2	0.2387	0.6	0.55	1380.1	8.1	1386.3	8.9	1395.8	19.0	**1395.8**	**19.0**	98.9
SH324BD-Spot 31	29	1140	0.7	11.2451	7.9	2.6471	8.4	0.2159	2.9	0.34	1260.1	33.3	1313.8	62.2	1402.6	151.9	**1402.6**	**151.9**	89.8
SH324BD-Spot 36	62	41997	1.2	11.2051	1.7	3.0922	1.8	0.2513	0.7	0.38	1445.1	8.9	1430.8	13.8	1409.4	31.8	**1409.4**	**31.8**	102.5
SH324BD-Spot 42	60	28581	0.9	11.1753	2.9	2.7197	3.2	0.2204	1.4	0.43	1284.2	16.0	1333.9	23.5	1414.5	54.6	**1414.5**	**54.6**	90.8
SH324BD-Spot 35	99	86869	2.9	11.1524	0.7	2.9925	1.3	0.2420	1.1	0.84	1397.3	14.1	1405.7	10.2	1418.4	13.9	**1418.4**	**13.9**	98.5
SH324BD-Spot 32	99	73260	1.0	11.1268	1.1	3.0981	1.4	0.2500	0.8	0.59	1438.6	10.4	1432.2	10.4	1422.8	20.9	**1422.8**	**20.9**	101.1
SH324BD-Spot 82	165	174335	3.0	11.0710	0.8	3.1405	1.3	0.2522	0.9	0.75	1449.6	12.2	1442.7	9.6	1432.4	15.7	**1432.4**	**15.7**	101.2
SH324BD-Spot 50	73	95301	0.6	11.0697	1.2	3.1173	1.9	0.2503	1.5	0.78	1439.9	19.1	1437.0	14.6	1432.6	22.7	**1432.6**	**22.7**	100.5
SH324BD-Spot 2	90	64872	1.2	11.0627	1.7	3.0669	2.0	0.2461	1.0	0.53	1418.2	13.3	1424.5	15.0	1433.8	31.7	**1433.8**	**31.7**	98.9
SH324BD-Spot 28	138	50541	2.1	11.0601	1.5	2.4424	6.1	0.1959	5.9	0.97	1153.4	62.0	1255.2	43.7	1434.3	29.0	**1434.3**	**29.0**	80.4
SH324BD-Spot 30	57	10204	0.8	11.0120	2.8	3.0565	2.9	0.2441	0.8	0.28	1408.0	10.5	1421.9	22.3	1442.6	53.3	**1442.6**	**53.3**	97.6
SH324BD-Spot 20	106	478581	0.7	11.0084	1.5	3.1458	1.8	0.2512	0.9	0.48	1444.5	11.0	1444.0	13.6	1443.2	29.3	**1443.2**	**29.3**	100.1
SH324BD-Spot 26	101	89037	1.2	10.9630	1.4	3.2942	1.8	0.2619	1.2	0.66	1499.7	16.0	1479.7	14.1	1451.1	25.8	**1451.1**	**25.8**	103.4
SH324BD-Spot 56	199	43114	3.1	10.9482	0.5	2.8359	1.8	0.2252	1.7	0.96	1309.2	20.0	1365.1	13.2	1453.7	9.0	**1453.7**	**9.0**	90.1
SH324BD-Spot 17	97	87416	1.3	10.9017	1.4	3.2020	1.6	0.2532	0.8	0.47	1454.8	10.0	1457.7	12.6	1461.8	27.3	**1461.8**	**27.3**	99.5
SH324BD-Spot 58	101	91613	1.2	10.8457	1.2	3.1750	3.0	0.2497	2.7	0.91	1437.2	35.4	1451.1	23.3	1471.5	23.4	**1471.5**	**23.4**	97.7
SH324BD-Spot 93	48	48685	0.6	10.7203	2.1	3.3225	2.8	0.2583	1.8	0.65	1481.3	23.7	1486.4	21.6	1493.6	39.8	**1493.6**	**39.8**	99.2
SH324BD-Spot 70	42	58076	0.6	10.0964	3.0	3.7524	3.1	0.2748	0.9	0.29	1565.0	12.7	1582.6	25.0	1606.2	55.7	**1606.2**	**55.7**	97.4
SH324BD-Spot 66	63	128942	1.1	9.7660	2.3	4.1777	2.4	0.2959	0.7	0.30	1671.0	10.6	1669.7	19.5	1668.0	42.0	**1668.0**	**42.0**	100.2
SH324BD-Spot 27	63	59808	1.2	9.7358	1.4	4.1901	1.7	0.2959	1.0	0.59	1670.8	14.5	1672.1	13.8	1673.7	25.1	**1673.7**	**25.1**	99.8
SH324BD-Spot 11	138	144762	2.7	9.6730	1.3	4.0150	6.3	0.2817	6.1	0.98	1599.8	86.5	1637.2	50.9	1685.7	24.4	**1685.7**	**24.4**	94.9
SH324BD-Spot 24	61	47027	2.0	9.6317	1.4	4.3157	1.7	0.3015	0.9	0.55	1698.6	13.9	1696.4	14.0	1693.6	26.3	**1693.6**	**26.3**	100.3
SH324BD-Spot 8	73	135819	2.8	9.6303	0.8	4.2466	1.1	0.2966	0.7	0.68	1674.5	10.6	1683.1	8.7	1693.8	14.4	**1693.8**	**14.4**	98.9
SH324BD-Spot 91	104	99972	1.9	9.6107	0.9	4.0594	1.3	0.2830	1.0	0.75	1606.2	13.9	1646.2	10.6	1697.6	15.9	**1697.6**	**15.9**	94.6
SH324BD-Spot 98	161	97975	1.5	9.5781	0.6	3.8425	5.5	0.2669	5.5	0.99	1525.2	74.7	1601.7	44.6	1703.8	10.4	**1703.8**	**10.4**	89.5
SH324BD-Spot 37	148	147309	1.5	9.5394	0.9	4.4263	1.0	0.3062	0.5	0.45	1722.2	6.9	1717.3	8.5	1711.3	16.8	**1711.3**	**16.8**	100.6
SH324BD-Spot 3	44	23367	1.0	9.5331	1.4	4.3986	2.2	0.3041	1.7	0.78	1711.7	25.8	1712.1	18.3	1712.5	25.6	**1712.5**	**25.6**	100.0
SH324BD-Spot 5	23	14906	2.7	9.5168	3.1	4.3258	3.9	0.2986	2.3	0.61	1684.2	34.8	1698.3	31.8	1715.7	56.2	**1715.7**	**56.2**	98.2
SH324BD-Spot 110	107	269154	1.3	9.4891	0.8	4.3759	0.9	0.3012	0.4	0.43	1697.0	5.8	1707.8	7.4	1721.0	14.8	**1721.0**	**14.8**	98.6

Analysis	U	206Pb	U/Th	206Pb*	±	207Pb*	±	206Pb*	±	error	206Pb*	±	207Pb*	±	206Pb*	±	Best age	±	Conc
	(ppm)	204Pb		207Pb*	(%)	235U*	(%)	238U	(%)	corr.	238U*	(Ma)	235U	(Ma)	207Pb*	(Ma)	(Ma)	(Ma)	(%)
SH324BD-Spot 75	66	91152	1.9	9.4883	1.2	4.6103	1.6	0.3173	1.0	0.66	1776.4	16.2	1751.1	13.1	1721.2	21.6	1721.2	21.6	103.2
SH324BD-Spot 78	81	100400	1.2	9.4450	2.0	4.1892	3.9	0.2870	3.3	0.85	1626.4	47.0	1671.9	31.6	1729.6	37.3	1729.6	37.3	94.0
SH324BD-Spot 9	112	136418	1.6	9.4312	0.7	4.4795	0.9	0.3064	0.5	0.57	1723.0	7.6	1727.2	7.3	1732.3	13.3	1732.3	13.3	99.5
SH324BD-Spot 69	64	71378	0.9	9.4147	1.4	4.5332	2.1	0.3095	1.6	0.75	1738.4	24.3	1737.1	17.7	1735.5	25.9	1735.5	25.9	100.2
SH324BD-Spot 39	41	67645	1.8	9.3782	1.6	4.4757	1.8	0.3044	0.7	0.41	1713.2	11.0	1726.5	14.8	1742.6	29.9	1742.6	29.9	98.3
SH324BD-Spot 55	184	37446	3.2	9.3101	0.5	3.9721	1.9	0.2682	1.8	0.97	1531.7	24.7	1628.5	15.2	1755.9	8.8	1755.9	8.8	87.2
SH324BD-Spot 14	67	97625	0.9	8.9918	1.4	4.9431	1.7	0.3224	1.0	0.57	1801.3	15.0	1809.6	14.1	1819.3	24.8	1819.3	24.8	99.0
SH324BD-Spot 21	16	16015	0.2	8.9451	7.6	5.0373	7.7	0.3268	1.1	0.15	1822.8	17.8	1825.6	65.2	1828.8	138.1	1828.8	138.1	99.7
SH324BD-Spot 89	86	66622	2.4	8.7743	1.2	5.2523	1.5	0.3342	0.9	0.63	1858.9	15.2	1861.1	12.8	1863.6	21.0	1863.6	21.0	99.7
SH324BD-Spot 43	143	276301	2.2	8.7066	0.5	5.3770	0.9	0.3395	0.7	0.80	1884.4	12.0	1881.2	7.8	1877.6	9.9	1877.6	9.9	100.4
SH324BD-Spot 23	190	490567	4.2	6.1020	0.6	10.4404	1.2	0.4620	1.1	0.87	2448.6	21.9	2474.6	11.5	2496.1	10.4	2496.1	10.4	98.1
SH324BD-Spot 64	86	143935	1.1	5.5569	0.4	12.5356	0.6	0.5052	0.4	0.66	2636.2	8.4	2645.4	5.5	2652.5	7.3	2652.5	7.3	99.4
SH324BD-Spot 87	75	105477	0.6	5.4398	0.7	12.7979	0.9	0.5049	0.6	0.66	2634.9	12.9	2664.9	8.5	2687.7	11.2	2687.7	11.2	98.0
SH324HO-Spot 46	75	95170	1.3	14.0556	2.8	1.5673	2.9	0.1598	0.8	0.26	955.5	6.7	957.4	17.9	961.6	56.8	961.6	56.8	99.4
SH324HO-Spot 17	63	20535	2.0	14.0502	3.6	1.6185	3.8	0.1649	1.4	0.37	984.1	12.9	977.4	24.1	962.4	73.1	962.4	73.1	102.3
SH324HO-Spot 6	118	80911	2.1	13.9719	2.6	1.6415	2.7	0.1663	0.9	0.35	991.9	8.7	986.3	17.2	973.8	52.2	973.8	52.2	101.9
SH324HO-Spot 82	47	19968	1.6	13.7625	5.8	1.7757	6.1	0.1772	1.8	0.30	1051.9	17.5	1036.6	39.4	1004.5	117.5	1004.5	117.5	104.7
SH324HO-Spot 58	37	14770	1.3	13.6844	6.3	1.7637	6.5	0.1750	1.8	0.27	1039.9	17.1	1032.2	42.2	1016.0	127.0	1016.0	127.0	102.3
SH324HO-Spot 73	57	41456	0.7	13.6144	2.7	1.7319	4.0	0.1710	3.0	0.74	1017.6	27.9	1020.4	25.9	1026.4	55.1	1026.4	55.1	99.1
SH324HO-Spot 24	163	30563	2.3	13.5236	1.7	1.4483	2.2	0.1421	1.4	0.65	856.3	11.3	909.2	13.0	1039.9	33.4	1039.9	33.4	82.3
SH324HO-Spot 36	43	28772	1.6	13.5213	6.9	1.8517	10.2	0.1816	7.6	0.74	1075.6	74.9	1064.0	67.7	1040.3	139.7	1040.3	139.7	103.4
SH324HO-Spot 4	92	56369	1.5	13.5106	2.0	1.8214	2.8	0.1785	2.0	0.71	1058.7	19.9	1053.2	18.7	1041.9	40.3	1041.9	40.3	101.6
SH324HO-Spot 44	50	34460	0.6	13.4866	3.4	1.7538	4.5	0.1715	2.9	0.65	1020.6	27.5	1028.6	29.2	1045.5	69.3	1045.5	69.3	97.6
SH324HO-Spot 95	65	42565	2.4	13.4759	3.7	1.7190	4.0	0.1680	1.6	0.40	1001.2	14.7	1015.7	25.6	1047.1	73.9	1047.1	73.9	95.6
SH324HO-Spot 71	82	26253	1.5	13.4577	2.3	1.7348	6.0	0.1693	5.5	0.92	1008.4	51.3	1021.5	38.4	1049.8	46.4	1049.8	46.4	96.1
SH324HO-Spot 22	197	153010	3.1	13.4481	1.0	1.8757	4.8	0.1829	4.8	0.98	1083.0	47.4	1072.5	32.1	1051.3	19.5	1051.3	19.5	103.0
SH324HO-Spot 18	162	124621	3.4	13.3990	1.1	1.8066	1.2	0.1756	0.6	0.49	1042.7	5.7	1047.9	7.9	1058.6	21.2	1058.6	21.2	98.5
SH324HO-Spot 41	47	26880	0.9	13.3545	5.4	1.8928	6.5	0.1833	3.7	0.57	1085.1	36.9	1078.5	43.3	1065.3	108.1	1065.3	108.1	101.9
SH324HO-Spot 57	283	15477	4.0	13.2880	1.0	1.6988	3.6	0.1637	3.5	0.96	977.4	31.6	1008.1	23.1	1075.4	19.3	1075.4	19.3	90.9
SH324HO-Spot 31	172	75601	2.7	13.2751	1.2	1.8978	2.1	0.1827	1.8	0.83	1081.8	17.6	1080.3	14.2	1077.3	24.1	1077.3	24.1	100.4
SH324HO-Spot 90	89	65295	1.4	13.2732	2.4	1.8913	2.5	0.1821	0.7	0.28	1078.3	7.0	1078.1	16.6	1077.6	48.2	1077.6	48.2	100.1
SH324HO-Spot 35	67	44613	0.8	13.2143	1.9	1.7262	6.3	0.1654	6.0	0.95	986.9	55.0	1018.3	40.6	1086.5	38.8	1086.5	38.8	90.8
SH324HO-Spot 50	91	29290	1.5	13.1844	1.6	1.9085	2.3	0.1825	1.6	0.70	1080.6	16.2	1084.1	15.4	1091.0	32.9	1091.0	32.9	99.0
SH324HO-Spot 56	100	87444	1.4	13.1692	1.3	2.0003	1.8	0.1911	1.3	0.68	1127.1	13.0	1115.6	12.5	1093.3	26.9	1093.3	26.9	103.1
SH324HO-Spot 30	53	47667	1.4	13.1315	5.0	1.9398	5.2	0.1847	1.2	0.23	1092.8	11.7	1094.9	34.6	1099.1	100.6	1099.1	100.6	99.4
SH324HO-Spot 34	89	61387	1.6	13.1052	1.8	1.9842	2.1	0.1886	1.1	0.52	1113.8	11.3	1110.2	14.3	1103.1	36.1	1103.1	36.1	101.0
SH324HO-Spot 39	259	136104	2.4	13.0341	0.8	1.9744	0.9	0.1866	0.5	0.56	1103.2	5.3	1106.8	6.3	1113.9	15.3	1113.9	15.3	99.0
SH324HO-Spot 87	22	31706	2.2	13.0170	4.1	2.0915	4.8	0.1975	2.6	0.53	1161.7	27.1	1146.0	33.1	1116.6	81.7	1116.6	81.7	104.0
SH324HO-Spot 78	59	35842	1.1	13.0076	3.4	1.9252	3.7	0.1816	1.4	0.39	1075.9	14.3	1089.9	24.6	1118.0	67.6	1118.0	67.6	96.2
SH324HO-Spot 43	99	47451	1.1	12.9750	1.5	1.9822	1.8	0.1865	1.0	0.53	1102.6	9.7	1109.5	12.2	1123.0	30.7	1123.0	30.7	98.2

Analysis	U	206Pb	U/Th	206Pb*	±	207Pb*	±	206Pb*	±	error	206Pb*	±	207Pb*	±	206Pb*	±	Best age	±	Conc
	(ppm)	204Pb		207Pb*	(%)	235U*	(%)	238U	(%)	corr.	238U*	(Ma)	235U	(Ma)	207Pb*	(Ma)	(Ma)	(Ma)	(%)
SH324HO-Spot 84	23	20336	30.5	12.8450	7.3	2.1771	8.0	0.2028	3.2	0.40	1190.5	34.6	1173.8	55.4	1143.1	145.1	**1143.1**	**145.1**	104.1
SH324HO-Spot 99	32	15651	1.3	12.8307	5.4	2.1283	10.8	0.1981	9.3	0.86	1164.9	99.1	1158.0	74.4	1145.3	107.5	**1145.3**	**107.5**	101.7
SH324HO-Spot 9	106	368178	2.2	12.7460	2.0	2.1720	2.4	0.2008	1.4	0.58	1179.5	15.1	1172.1	16.7	1158.4	38.7	**1158.4**	**38.7**	101.8
SH324HO-Spot 96	89	50237	2.2	12.7261	2.4	2.1199	2.9	0.1957	1.7	0.57	1152.0	17.7	1155.3	20.2	1161.5	47.7	**1161.5**	**47.7**	99.2
SH324HO-Spot 48	163	66117	1.6	12.6958	0.8	2.1542	1.3	0.1984	1.0	0.78	1166.5	10.8	1166.4	9.1	1166.2	16.4	**1166.2**	**16.4**	100.0
SH324HO-Spot 26	98	41549	2.3	12.6880	1.9	2.1907	2.1	0.2016	0.9	0.42	1183.9	9.4	1178.1	14.4	1167.5	37.0	**1167.5**	**37.0**	101.4
SH324HO-Spot 53	65	39538	1.3	12.6589	3.4	2.2329	5.0	0.2050	3.6	0.73	1202.1	39.5	1191.4	34.8	1172.1	67.7	**1172.1**	**67.7**	102.6
SH324HO-Spot 28	80	76227	2.0	12.6396	2.7	2.1508	3.1	0.1972	1.5	0.50	1160.1	16.2	1165.3	21.2	1175.1	52.6	**1175.1**	**52.6**	98.7
SH324HO-Spot 15	60	46711	1.9	12.6141	2.8	2.0616	3.9	0.1886	2.7	0.69	1113.8	27.3	1136.1	26.6	1179.1	55.9	**1179.1**	**55.9**	94.5
SH324HO-Spot 77	72	30303	2.1	12.5913	2.8	2.2316	3.6	0.2038	2.3	0.63	1195.7	24.8	1191.0	25.3	1182.6	55.4	**1182.6**	**55.4**	101.1
SH324HO-Spot 91	73	63040	0.4	12.5459	1.9	2.2735	3.1	0.2069	2.5	0.79	1212.1	27.2	1204.1	21.9	1189.8	37.3	**1189.8**	**37.3**	101.9
SH324HO-Spot 74	161	94954	3.8	12.5319	0.9	2.2227	1.9	0.2020	1.7	0.89	1186.2	18.8	1188.2	13.7	1192.0	17.6	**1192.0**	**17.6**	99.5
SH324HO-Spot 64	43	34538	0.4	12.5067	2.8	2.3213	3.7	0.2106	2.4	0.64	1231.8	26.7	1218.8	26.3	1195.9	56.0	**1195.9**	**56.0**	103.0
SH324HO-Spot 60	62	34479	1.8	12.3459	1.4	2.3591	1.9	0.2112	1.2	0.64	1235.4	13.6	1230.3	13.4	1221.4	28.5	**1221.4**	**28.5**	101.1
SH324HO-Spot 10	115	46106	0.9	12.2284	1.8	2.3670	3.4	0.2099	2.9	0.85	1228.4	32.2	1232.7	24.2	1240.2	34.8	**1240.2**	**34.8**	99.1
SH324HO-Spot 3	27	18178	3.0	11.9430	7.5	2.3149	8.2	0.2005	3.3	0.41	1178.1	35.9	1216.8	58.2	1286.3	146.1	**1286.3**	**146.1**	91.6
SH324HO-Spot 88	96	54599	2.9	11.7955	1.6	2.2760	6.0	0.1947	5.8	0.96	1146.9	60.8	1204.9	42.4	1310.4	31.1	**1310.4**	**31.1**	87.5
SH324HO-Spot 79	60	63436	1.9	11.7380	1.8	2.5186	3.0	0.2144	2.4	0.80	1252.3	27.1	1277.4	21.7	1319.9	34.7	**1319.9**	**34.7**	94.9
SH324HO-Spot 27	234	80152	1.8	11.6835	0.9	2.6739	1.5	0.2266	1.2	0.81	1316.5	14.3	1321.3	10.9	1328.9	16.6	**1328.9**	**16.6**	99.1
SH324HO-Spot 11	103	75320	0.6	11.5645	1.4	2.7440	2.2	0.2301	1.7	0.77	1335.3	20.2	1340.5	16.2	1348.7	26.9	**1348.7**	**26.9**	99.0
SH324HO-Spot 2	68	97666	1.0	11.5555	0.9	2.8797	1.2	0.2413	0.8	0.65	1393.7	9.5	1376.6	8.8	1350.2	17.1	**1350.2**	**17.1**	103.2
SH324HO-Spot 83	143	209295	0.5	11.5206	1.1	2.7396	2.4	0.2289	2.1	0.90	1328.8	25.8	1339.3	17.8	1356.1	20.4	**1356.1**	**20.4**	98.0
SH324HO-Spot 67	35	21513	1.6	11.3864	3.0	2.8824	3.7	0.2380	2.1	0.57	1376.5	26.2	1377.3	27.8	1378.6	58.2	**1378.6**	**58.2**	99.8
SH324HO-Spot 1	59	50243	1.2	11.3710	1.6	2.9298	2.4	0.2416	1.7	0.73	1395.1	21.8	1389.6	18.1	1381.2	31.5	**1381.2**	**31.5**	101.0
SH324HO-Spot 37	105	85229	1.4	11.3441	1.2	2.8278	1.7	0.2327	1.3	0.73	1348.4	15.5	1362.9	13.1	1385.8	23.0	**1385.8**	**23.0**	97.3
SH324HO-Spot 14	108	87988	1.5	11.2441	1.2	3.0649	3.8	0.2499	3.6	0.94	1438.2	45.9	1424.0	28.9	1402.8	23.9	**1402.8**	**23.9**	102.5
SH324HO-Spot 40	34	20993	1.7	11.1562	3.7	3.0505	4.4	0.2468	2.5	0.55	1422.1	31.3	1420.4	33.9	1417.8	70.7	**1417.8**	**70.7**	100.3
SH324HO-Spot 61	190	31155	2.7	11.0700	0.4	2.6797	2.6	0.2151	2.6	0.99	1256.2	29.8	1322.9	19.6	1432.6	8.0	**1432.6**	**8.0**	87.7
SH324HO-Spot 47	59	32092	0.8	10.9781	2.4	3.1550	3.6	0.2512	2.7	0.76	1444.7	35.4	1446.2	27.9	1448.5	44.9	**1448.5**	**44.9**	99.7
SH324HO-Spot 94	74	49018	1.1	10.9440	2.3	3.1182	2.8	0.2475	1.6	0.57	1425.6	20.5	1437.2	21.5	1454.4	43.6	**1454.4**	**43.6**	98.0
SH324HO-Spot 81	70	77775	0.6	10.9414	1.9	2.9032	3.4	0.2304	2.8	0.82	1336.5	33.6	1382.8	25.7	1454.9	37.0	**1454.9**	**37.0**	91.9
SH324HO-Spot 55	86	54911	0.6	10.9360	1.6	3.2550	3.1	0.2582	2.7	0.86	1480.5	35.6	1470.4	24.2	1455.8	30.0	**1455.8**	**30.0**	101.7
SH324HO-Spot 38	109	120623	2.3	10.8941	1.5	3.2058	2.2	0.2533	1.6	0.73	1455.4	20.8	1458.6	16.8	1463.1	28.0	**1463.1**	**28.0**	99.5
SH324HO-Spot 25	170	236004	1.7	10.8704	1.2	3.2406	2.0	0.2555	1.6	0.81	1466.7	21.2	1466.9	15.5	1467.2	22.4	**1467.2**	**22.4**	100.0
SH324HO-Spot 32	81	95850	3.8	10.8038	1.7	3.1768	3.1	0.2489	2.5	0.82	1432.9	32.4	1451.5	23.7	1478.9	33.1	**1478.9**	**33.1**	96.9
SH324HO-Spot 23	69	43854	1.6	10.7810	1.6	3.2827	1.9	0.2567	1.0	0.50	1472.8	12.5	1477.0	14.7	1482.9	30.9	**1482.9**	**30.9**	99.3
SH324HO-Spot 89	82	84811	1.5	9.9790	1.3	3.8821	2.0	0.2810	1.5	0.77	1596.2	21.7	1610.0	16.1	1628.0	23.6	**1628.0**	**23.6**	98.1
SH324HO-Spot 97	65	35231	2.6	9.6495	1.1	3.7256	5.8	0.2607	5.6	0.98	1493.6	75.2	1576.9	46.1	1690.1	21.0	**1690.1**	**21.0**	88.4
SH324HO-Spot 93	99	101553	3.0	9.6239	1.0	4.4097	1.7	0.3078	1.4	0.81	1729.8	21.0	1714.2	14.2	1695.1	18.8	**1695.1**	**18.8**	102.1
SH324HO-Spot 51	132	29400	1.8	9.6188	0.8	3.6428	2.7	0.2541	2.6	0.95	1459.7	34.0	1558.9	21.8	1696.0	15.3	**1696.0**	**15.3**	86.1
SH324HO-Spot 45	97	300928	2.6	9.5727	0.4	4.3385	2.7	0.3012	2.7	0.99	1697.3	40.5	1700.7	22.7	1704.9	7.8	**1704.9**	**7.8**	99.6

Analysis	U (ppm)	206Pb 204Pb	U/Th	206Pb* 207Pb*	± (%)	207Pb* 235U*	± (%)	206Pb* 238U	± (%)	error corr.	206Pb* 238U*	± (Ma)	207Pb* 235U	± (Ma)	206Pb* 207Pb*	± (Ma)	Best age (Ma)	± (Ma)	Conc (%)
SH324HO-Spot 19	150	23387	2.2	9.5141	0.8	3.6869	7.3	0.2544	7.2	0.99	1461.2	94.5	1568.5	58.2	1716.2	15.3	**1716.2**	**15.3**	85.1
SH324HO-Spot 72	99	55316	2.2	9.4995	1.5	4.4569	1.9	0.3071	1.2	0.62	1726.2	18.1	1723.0	16.0	1719.0	27.9	**1719.0**	**27.9**	100.4
SH324HO-Spot 29	72	139740	1.5	9.4614	1.3	4.4404	1.9	0.3047	1.4	0.73	1714.6	20.6	1719.9	15.6	1726.4	23.5	**1726.4**	**23.5**	99.3
SH324HO-Spot 12	74	74187	3.8	9.1696	1.4	4.8216	2.4	0.3207	2.0	0.82	1792.9	31.4	1788.7	20.5	1783.7	25.2	**1783.7**	**25.2**	100.5
SH324HO-Spot 16	76	78204	0.4	8.7047	0.9	5.4448	1.3	0.3437	0.9	0.71	1904.6	15.2	1891.9	11.1	1878.0	16.3	**1878.0**	**16.3**	101.4
SH324HO-Spot 42	79	82097	1.3	8.6837	0.8	5.3797	3.0	0.3388	2.9	0.96	1881.0	47.4	1881.6	25.8	1882.4	14.3	**1882.4**	**14.3**	99.9
SH324HO-Spot 100	77	85831	2.3	8.6254	1.0	5.5588	3.4	0.3477	3.2	0.96	1923.8	53.3	1909.7	28.8	1894.5	17.7	**1894.5**	**17.7**	101.6
SH324HO-Spot 52	65	163012	1.9	8.2760	1.2	5.5432	4.1	0.3327	3.9	0.96	1851.5	63.5	1907.3	35.4	1968.5	20.7	**1968.5**	**20.7**	94.1
SH324HO-Spot 5	58	77555	1.4	8.2434	1.0	5.9551	2.2	0.3560	2.0	0.89	1963.4	33.0	1969.3	19.1	1975.6	17.8	**1975.6**	**17.8**	99.4
SH324HO-Spot 70	32	32238	1.5	8.0364	2.1	6.4963	2.9	0.3786	2.1	0.71	2069.9	36.8	2045.4	25.8	2020.7	36.6	**2020.7**	**36.6**	102.4
SH324HO-Spot 33	20	29540	1.2	7.5360	1.8	6.9183	3.1	0.3781	2.6	0.82	2067.5	45.5	2101.0	27.8	2133.9	31.5	**2133.9**	**31.5**	96.9
SH324VE-Spot 78	110	20546	1.5	13.9736	1.9	1.4942	7.1	0.1514	6.9	0.97	909.0	58.2	928.0	43.3	973.5	37.9	**973.5**	**37.9**	93.4
SH324VE-Spot 17	32	26400	0.9	13.9692	5.7	1.6392	5.9	0.1661	1.8	0.30	990.5	16.3	985.4	37.5	974.2	115.8	**974.2**	**115.8**	101.7
SH324VE-Spot 90	157	64040	3.8	13.6019	2.3	1.8072	2.4	0.1783	0.9	0.36	1057.6	8.5	1048.1	15.9	1028.3	45.7	**1028.3**	**45.7**	102.9
SH324VE-Spot 60	112	94098	1.7	13.5789	2.0	1.7492	2.2	0.1723	1.0	0.42	1024.6	9.0	1026.9	14.5	1031.7	41.2	**1031.7**	**41.2**	99.3
SH324VE-Spot 43	75	28115	1.4	13.5579	2.6	1.7371	3.3	0.1708	2.0	0.60	1016.6	18.4	1022.4	21.1	1034.8	53.1	**1034.8**	**53.1**	98.2
SH324VE-Spot 92	107	77304	1.4	13.5541	1.9	1.7690	2.0	0.1739	0.8	0.41	1033.6	7.9	1034.2	13.3	1035.4	37.8	**1035.4**	**37.8**	99.8
SH324VE-Spot 6	25	10930	2.1	13.4811	9.9	1.7806	10.3	0.1741	2.6	0.25	1034.6	24.6	1038.4	66.8	1046.3	200.9	**1046.3**	**200.9**	98.9
SH324VE-Spot 94	86	44327	3.2	13.4800	1.3	1.7798	1.4	0.1740	0.6	0.44	1034.1	6.0	1038.1	9.2	1046.5	25.7	**1046.5**	**25.7**	98.8
SH324VE-Spot 44	186	118822	3.6	13.4701	0.7	1.7930	1.1	0.1752	0.8	0.74	1040.5	7.5	1042.9	6.9	1048.0	14.3	**1048.0**	**14.3**	99.3
SH324VE-Spot 47	28	20989	0.9	13.4670	6.7	1.7778	7.3	0.1736	2.7	0.37	1032.2	25.9	1037.4	47.3	1048.4	136.2	**1048.4**	**136.2**	98.4
SH324VE-Spot 76	78	38910	3.2	13.4505	1.8	1.8595	1.9	0.1814	0.4	0.22	1074.6	3.9	1066.8	12.2	1050.9	36.5	**1050.9**	**36.5**	102.3
SH324VE-Spot 81	39	36478	0.7	13.4398	4.8	1.8787	4.9	0.1831	1.1	0.22	1084.0	10.9	1073.6	32.4	1052.5	96.1	**1052.5**	**96.1**	103.0
SH324VE-Spot 34	78	68914	1.4	13.4372	2.3	1.8325	2.6	0.1786	1.3	0.50	1059.3	12.9	1057.2	17.2	1052.9	45.7	**1052.9**	**45.7**	100.6
SH324VE-Spot 4	70	59947	1.5	13.3526	2.5	1.8978	3.8	0.1838	2.8	0.74	1087.6	27.8	1080.3	25.0	1065.6	51.0	**1065.6**	**51.0**	102.1
SH324VE-Spot 68	35	44792	1.6	13.2774	5.6	1.8914	5.8	0.1821	1.4	0.25	1078.7	14.3	1078.1	38.6	1077.0	113.0	**1077.0**	**113.0**	100.2
SH324VE-Spot 85	68	35714	1.6	13.2134	2.1	1.9790	2.3	0.1897	0.9	0.41	1119.5	9.8	1108.4	15.7	1086.7	42.7	**1086.7**	**42.7**	103.0
SH324VE-Spot 49	126	101437	2.1	13.1687	1.4	1.9850	1.6	0.1896	0.7	0.46	1119.1	7.5	1110.4	10.8	1093.5	28.4	**1093.5**	**28.4**	102.3
SH324VE-Spot 58	107	74340	2.0	13.1302	2.5	1.9559	2.7	0.1863	1.0	0.38	1101.1	10.4	1100.5	18.0	1099.3	49.6	**1099.3**	**49.6**	100.2
SH324VE-Spot 87	157	96214	3.1	13.0742	1.0	2.0238	5.4	0.1919	5.3	0.98	1131.7	54.8	1123.5	36.6	1107.8	20.8	**1107.8**	**20.8**	102.2
SH324VE-Spot 64	41	30350	3.2	13.0560	2.9	1.9046	5.9	0.1803	5.2	0.87	1068.9	50.7	1082.7	39.5	1110.6	58.8	**1110.6**	**58.8**	96.2
SH324VE-Spot 5	92	66943	1.4	13.0507	2.6	1.9746	3.3	0.1869	2.0	0.61	1104.6	20.7	1106.9	22.5	1111.4	52.7	**1111.4**	**52.7**	99.4
SH324VE-Spot 18	70	91738	0.9	13.0288	1.8	1.9980	2.4	0.1888	1.7	0.69	1114.8	17.3	1114.8	16.6	1114.8	35.4	**1114.8**	**35.4**	100.0
SH324VE-Spot 32	200	60625	1.6	12.9457	0.8	2.1106	1.1	0.1982	0.6	0.60	1165.5	6.8	1152.3	7.3	1127.5	16.9	**1127.5**	**16.9**	103.4
SH324VE-Spot 98	50	60721	2.4	12.9450	3.3	2.0761	3.5	0.1949	1.0	0.28	1148.0	10.4	1141.0	23.9	1127.6	66.7	**1127.6**	**66.7**	101.8
SH324VE-Spot 82	79	55268	2.9	12.9042	2.8	2.0803	3.0	0.1947	1.0	0.34	1146.8	10.6	1142.3	20.3	1133.9	55.4	**1133.9**	**55.4**	101.1
SH324-VE-Spot 86	39	41039	0.8	12.8789	3.9	2.0578	4.6	0.1922	2.4	0.52	1133.3	24.5	1134.9	31.2	1137.9	77.9	**1137.9**	**77.9**	99.6
SH324VE-Spot 80	65	31842	1.2	12.8726	2.1	2.0731	2.3	0.1935	0.9	0.39	1140.5	9.1	1139.9	15.4	1138.8	41.3	**1138.8**	**41.3**	100.2
SH324VE-Spot 89	70	60267	2.3	12.8355	2.4	2.1520	2.5	0.2003	0.9	0.37	1177.1	10.1	1165.7	17.6	1144.5	47.0	**1144.5**	**47.0**	102.8
SH324VE-Spot 71	144	108019	2.0	12.7969	1.2	2.1564	1.3	0.2001	0.5	0.40	1176.1	5.6	1167.1	8.9	1150.5	23.4	**1150.5**	**23.4**	102.2

Analysis	U	206Pb	U/Th	206Pb*	±	207Pb*	±	206Pb*	±	error	206Pb*	±	207Pb*	±	206Pb*	±	Best age	±	Conc
	(ppm)	204Pb		207Pb*	(%)	235U*	(%)	238U	(%)	corr.	238U*	(Ma)	235U	(Ma)	207Pb*	(Ma)	(Ma)	(Ma)	(%)
SH324VE-Spot 41	51	43150	1.3	12.7946	1.6	2.1670	2.4	0.2011	1.7	0.73	1181.2	18.6	1170.5	16.4	1150.9	32.1	1150.9	32.1	102.6
SH324VE-Spot 40	207	130358	1.8	12.7616	0.7	2.1184	0.8	0.1961	0.4	0.55	1154.2	4.6	1154.8	5.4	1156.0	12.9	1156.0	12.9	99.8
SH324VE-Spot 2	318	15313	2.5	12.7204	1.4	2.0602	7.2	0.1901	7.1	0.98	1121.7	73.1	1135.7	49.5	1162.4	27.1	1162.4	27.1	96.5
SH324VE-Spot 1	67	47161	1.5	12.7082	2.5	2.2118	4.4	0.2039	3.6	0.83	1196.0	39.3	1184.8	30.5	1164.3	48.7	1164.3	48.7	102.7
SH324VE-Spot 42	38	30936	1.4	12.6068	3.0	2.1092	3.4	0.1929	1.7	0.49	1136.8	17.2	1151.8	23.4	1180.2	58.6	1180.2	58.6	96.3
SH324VE-Spot 65	64	46225	1.0	12.5893	2.3	2.2556	2.5	0.2059	1.0	0.38	1207.2	10.6	1198.5	17.8	1183.0	46.2	1183.0	46.2	102.0
SH324VE-Spot 91	114	72513	1.1	12.4239	1.3	2.3547	1.5	0.2122	0.9	0.58	1240.4	10.0	1229.0	10.9	1209.0	24.6	1209.0	24.6	102.6
SH324VE-Spot 72	26	24316	1.1	12.3630	7.7	2.2884	7.9	0.2052	1.7	0.22	1203.2	19.2	1208.7	56.0	1218.7	152.0	1218.7	152.0	98.7
SH324VE-Spot 24	170	70089	3.0	12.2910	0.5	2.3949	0.8	0.2135	0.7	0.83	1247.4	7.6	1241.1	5.8	1230.2	8.9	1230.2	8.9	101.4
SH324VE-Spot 59	70	125251	1.3	12.2213	2.5	2.3394	3.7	0.2074	2.8	0.75	1214.7	30.9	1224.3	26.6	1241.3	48.6	1241.3	48.6	97.9
SH324VE-Spot 63	86	67230	1.9	12.2028	1.3	2.4575	1.5	0.2175	0.8	0.53	1268.6	9.5	1259.6	11.1	1244.3	25.6	1244.3	25.6	102.0
SH324VE-Spot 22	121	158097	2.1	12.1820	1.4	2.3687	2.1	0.2093	1.6	0.74	1225.0	17.5	1233.2	15.1	1247.6	27.8	1247.6	27.8	98.2
SH324VE-Spot 97	23	25850	2.4	11.9473	5.5	2.6409	5.6	0.2288	1.1	0.19	1328.4	13.0	1312.1	41.1	1285.6	106.6	1285.6	106.6	103.3
SH324VE-Spot 14	67	44800	1.0	11.7147	1.6	2.7147	1.9	0.2307	1.2	0.59	1337.9	13.9	1332.5	14.4	1323.8	30.3	1323.8	30.3	101.1
SH324VE-Spot 100	64	101381	0.9	11.5572	2.1	2.8530	2.4	0.2391	1.1	0.48	1382.2	14.0	1369.6	17.8	1349.9	40.1	1349.9	40.1	102.4
SH324VE-Spot 29	161	203444	2.7	11.4828	0.8	2.8761	1.1	0.2395	0.8	0.71	1384.2	10.1	1375.7	8.6	1362.4	15.6	1362.4	15.6	101.6
SH324VE-Spot 3	87	86605	1.7	11.3440	1.4	2.8804	1.6	0.2370	0.7	0.47	1371.0	9.2	1376.8	12.0	1385.8	27.1	1385.8	27.1	98.9
SH324VE-Spot 33	98	112129	1.8	11.3141	1.1	2.9805	1.4	0.2446	0.8	0.58	1410.4	10.1	1402.7	10.5	1390.9	21.6	1390.9	21.6	101.4
SH324VE-Spot 77	98	93624	1.0	11.2547	0.9	3.0052	1.4	0.2453	1.0	0.76	1414.2	13.3	1408.9	10.5	1400.9	17.3	1400.9	17.3	100.9
SH324VE-Spot 83	20	19592	1.1	11.2430	5.4	3.0761	5.5	0.2508	1.1	0.21	1442.7	14.7	1426.7	42.5	1402.9	104.0	1402.9	104.0	102.8
SH324VE-Spot 57	67	54034	2.1	11.1817	2.0	3.1317	2.1	0.2540	0.6	0.30	1458.9	8.1	1440.5	16.0	1413.4	37.9	1413.4	37.9	103.2
SH324VE-Spot 75	26	20408	1.6	11.1129	4.6	2.9946	5.1	0.2414	2.2	0.43	1393.8	27.3	1406.3	38.7	1425.2	87.8	1425.2	87.8	97.8
SH324VE-Spot 99	104	135406	1.4	11.0483	0.9	3.1861	1.1	0.2553	0.7	0.63	1465.7	9.2	1453.8	8.7	1436.3	16.7	1436.3	16.7	102.0
SH324VE-Spot 74	135	159790	1.4	11.0134	1.0	3.1732	1.2	0.2535	0.6	0.50	1456.3	7.8	1450.7	9.1	1442.4	19.5	1442.4	19.5	101.0
SH324VE-Spot 69	147	98465	1.6	10.9955	0.8	2.6343	3.0	0.2101	2.8	0.96	1229.2	31.8	1310.3	21.9	1445.5	16.1	1445.5	16.1	85.0
SH324VE-Spot 12	78	33388	1.9	10.9907	0.9	3.3144	5.9	0.2642	5.8	0.99	1511.3	77.9	1484.4	45.7	1446.3	17.4	1446.3	17.4	104.5
SH324VE-Spot 15	63	57383	1.6	10.9619	2.1	3.0677	4.3	0.2439	3.8	0.87	1406.9	47.7	1424.7	33.1	1451.3	39.9	1451.3	39.9	96.9
SH324VE-Spot 51	137	153590	3.3	10.9341	0.8	3.2169	0.9	0.2551	0.5	0.57	1464.8	7.1	1461.2	7.3	1456.1	14.7	1456.1	14.7	100.6
SH324VE-Spot 19	65	44556	0.8	10.9213	1.7	3.2072	2.3	0.2540	1.6	0.69	1459.3	21.2	1458.9	18.1	1458.3	32.1	1458.3	32.1	100.1
SH324VE-Spot 67	74	222913	2.9	10.8926	1.7	2.8255	1.9	0.2232	0.8	0.44	1298.9	10.0	1362.3	14.4	1463.3	32.9	1463.3	32.9	88.8
SH324VE-Spot 21	33	30851	4.4	10.8559	2.8	3.0911	3.0	0.2434	0.9	0.31	1404.2	11.8	1430.5	23.0	1469.8	54.0	1469.8	54.0	95.5
SH324VE-Spot 10	32	10715	1.1	9.8754	3.1	3.7770	3.6	0.2705	1.8	0.51	1543.4	25.1	1587.9	28.8	1647.3	57.3	1647.3	57.3	93.7
SH324VE-Spot 84	91	94254	1.3	9.8471	0.9	4.1444	1.0	0.2960	0.5	0.52	1671.4	8.1	1663.1	8.5	1652.7	16.5	1652.7	16.5	101.1
SH324VE-Spot 50	86	146012	1.0	9.7533	0.9	4.2212	1.1	0.2986	0.7	0.62	1684.3	9.9	1678.1	8.9	1670.4	15.8	1670.4	15.8	100.8
SH324VE-Spot 96	79	116994	3.0	9.5506	0.8	4.3656	1.5	0.3024	1.2	0.84	1703.2	18.7	1705.9	12.3	1709.1	14.9	1709.1	14.9	99.7
SH324VE-Spot 45	105	102240	1.6	9.5096	0.7	4.4872	1.3	0.3095	1.1	0.83	1738.1	16.3	1728.6	10.7	1717.1	13.3	1717.1	13.3	101.2
SH324VE-Spot 95	124	109132	1.7	9.4679	0.5	4.4859	0.7	0.3080	0.5	0.75	1731.0	8.3	1728.4	6.1	1725.1	8.9	1725.1	8.9	100.3
SH324VE-Spot 66	132	109438	1.4	9.4674	1.1	4.5296	1.3	0.3110	0.7	0.54	1745.7	10.3	1736.4	10.4	1725.2	19.4	1725.2	19.4	101.2
SH324VE-Spot 88	144	178200	0.7	9.4343	0.5	4.4721	1.0	0.3060	0.9	0.88	1721.0	13.2	1725.8	8.2	1731.6	8.5	1731.6	8.5	99.4
SH324VE-Spot 46	44	64694	0.8	9.3196	2.2	4.7518	2.5	0.3212	1.2	0.48	1795.5	18.6	1776.4	20.7	1754.0	39.7	1754.0	39.7	102.4
SH324VE-Spot 23	46	72517	0.9	9.2793	1.4	4.5845	1.8	0.3085	1.1	0.61	1733.5	16.5	1746.4	14.8	1762.0	25.6	1762.0	25.6	98.4

Analysis	U	206Pb	U/Th	206Pb*	±	207Pb*	±	206Pb*	±	error	206Pb*	±	207Pb*	±	206Pb*	±	Best age	±	Conc
	(ppm)	204Pb		207Pb*	(%)	235U*	(%)	238U	(%)	corr.	238U*	(Ma)	235U	(Ma)	207Pb*	(Ma)	(Ma)	(Ma)	(%)
SH324VE-Spot 7	85	114523	2.5	9.0881	0.8	4.9539	1.6	0.3265	1.5	0.89	1821.5	23.1	1811.5	13.9	1799.9	13.8	**1799.9**	**13.8**	101.2
SH324VE-Spot 55	131	135489	3.5	9.0776	0.5	4.7713	1.0	0.3141	0.9	0.85	1761.0	13.1	1779.9	8.4	1802.1	9.7	**1802.1**	**9.7**	97.7
SH324VE-Spot 11	59	109283	1.0	8.8818	1.1	5.3511	2.3	0.3447	2.1	0.89	1909.2	34.3	1877.1	20.0	1841.6	19.2	**1841.6**	**19.2**	103.7
SH324VE-Spot 26	112	189934	4.0	8.8726	0.7	5.2389	1.0	0.3371	0.7	0.72	1872.8	11.6	1859.0	8.5	1843.5	12.5	**1843.5**	**12.5**	101.6
SH324VE-Spot 77	114	319995	0.8	8.8146	0.6	5.0725	0.8	0.3243	0.5	0.64	1810.6	7.6	1831.5	6.4	1855.4	10.5	**1855.4**	**10.5**	97.6
SH324VE-Spot 93	56	72058	1.3	8.7038	1.1	5.2622	1.4	0.3322	0.8	0.57	1848.9	12.6	1862.8	11.7	1878.2	20.4	**1878.2**	**20.4**	98.4
SH324VE-Spot 20	214	130626	2.3	8.6218	0.4	5.3971	1.5	0.3375	1.4	0.97	1874.6	22.8	1884.4	12.4	1895.2	6.5	**1895.2**	**6.5**	98.9
SH324VE-Spot 38	75	209239	1.2	5.1316	0.4	14.7613	0.6	0.5494	0.5	0.77	2822.6	10.5	2800.0	5.6	2783.7	6.1	**2783.7**	**6.1**	101.4
SH324VE-Spot 39	59	66954	1.3	5.1266	0.5	14.7609	1.1	0.5488	1.0	0.90	2820.3	23.2	2800.0	10.8	2785.3	8.2	**2785.3**	**8.2**	101.3

Table A-3. LA-HR-MC-ICP-MS Hf isotopic data for Grenville-age zircon recovered from intrusive units in Sonora, Mexico. Uncertainties include both random and systematic error reported at 2σ. Samples on zircon with poor age data omitted.

Sample	(^{176}Yb + ^{176}Lu) / ^{176}Hf (%)	Volts Hf	$^{176}Hf/^{177}Hf$	± (2σ)	$^{176}Lu/^{177}Hf$	$^{176}Hf/^{177}Hf$ (T)	E-Hf (0)	E-Hf (0) ± (2σ)	E-Hf (T)	Age (Ma)
13S-CP-3-24	33.4	5.7	0.282076	0.000030	0.001885	0.282038	**-25.1**	**1.1**	-2.5	1068
13S-CP-3-36	9.6	6.6	0.282120	0.000041	0.000596	0.282108	**-23.5**	**1.5**	0.9	1110
13S-CP-3-59	15.5	6.4	0.282152	0.000040	0.000958	0.282132	**-22.4**	**1.4**	1.4	1093
13S-QTV-1-21	9.1	5.0	0.282078	0.000044	0.000539	0.282067	**-25.0**	**1.6**	-1.4	1071
13S-QTV-1-17	14.7	4.4	0.282085	0.000038	0.000790	0.282069	**-24.8**	**1.3**	-1.2	1075
13S-QTV-1-68	16.3	4.5	0.282087	0.000044	0.000877	0.282069	**-24.7**	**1.5**	-0.9	1092
13S-QTV-1-65	14.8	4.9	0.282094	0.000045	0.000801	0.282077	**-24.4**	**1.6**	0.1	1122
13S-QTV-1-36	12.7	4.6	0.282145	0.000038	0.000706	0.282130	**-22.6**	**1.3**	1.6	1107
13S-QTV-2-2	38.8	5.4	0.282065	0.000054	0.002044	0.282021	**-25.5**	**1.9**	-1.6	1135
13S-QTV-2-18	14.2	5.0	0.282073	0.000044	0.000789	0.282057	**-25.2**	**1.6**	-1.5	1082
13S-QTV-2-67	29.9	5.3	0.282078	0.000046	0.001596	0.282044	**-25.0**	**1.6**	-1.5	1101
13S-QTV-2-55	21.4	4.7	0.282097	0.000041	0.001209	0.282071	**-24.3**	**1.5**	-0.4	1108
13S-QTV-2-25	17.1	4.3	0.282110	0.000062	0.000988	0.282090	**-23.9**	**2.2**	-0.6	1070
13S-QTV-2-94	21.7	4.5	0.282111	0.000039	0.001177	0.282087	**-23.8**	**1.4**	-0.4	1086
13S-QTV-2-44	20.5	4.4	0.282112	0.000066	0.001109	0.282088	**-23.8**	**2.3**	0.4	1116
13S-QTV-2-79	23.1	4.4	0.282122	0.000057	0.001214	0.282097	**-23.4**	**2.0**	0.0	1084
13S-QTV-2-62	11.7	4.7	0.282125	0.000042	0.000640	0.282111	**-23.4**	**1.5**	0.9	1102
13S-QTV-2-63	14.7	4.9	0.282141	0.000041	0.000866	0.282123	**-22.8**	**1.4**	1.4	1109
13S-QTV-2-13	29.0	5.2	0.282142	0.000045	0.001556	0.282110	**-22.7**	**1.6**	0.4	1083
13S-QTV-2-77	10.6	4.5	0.282151	0.000067	0.000586	0.282139	**-22.4**	**2.4**	1.5	1088

Sample	(^{176}Yb + ^{176}Lu) / ^{176}Hf (%)	Volts Hf	$^{176}Hf/^{177}Hf$	± (2σ)	$^{176}Lu/^{177}Hf$	$^{176}Hf/^{177}Hf$ (T)	E-Hf (0)	E-Hf (0) ± (2σ)	E-Hf (T)	Age (Ma)
13S-QTV-2-34	19.5	4.9	0.282166	0.000042	0.001069	0.282144	**-21.9**	**1.5**	1.5	1081
13S-QTV-2-28	21.6	4.6	0.282169	0.000059	0.001216	0.282144	**-21.8**	**2.1**	2.0	1101
13S-QTV-2-78	13.3	4.0	0.282186	0.000041	0.000739	0.282170	**-21.2**	**1.4**	2.9	1097
13S-QTV-2-58	13.0	4.4	0.282189	0.000050	0.000751	0.282174	**-21.1**	**1.8**	3.0	1100
13S-QTV-3-91	25.7	5.3	0.282075	0.000047	0.001361	0.282046	**-25.1**	**1.6**	-0.8	1128
13S-QTV-3-89	19.7	4.6	0.282081	0.000055	0.001064	0.282060	**-24.9**	**1.9**	-1.4	1083
13S-QTV-3-25	46.9	4.5	0.282088	0.000060	0.002544	0.282036	**-24.7**	**2.1**	-2.5	1070
13S-QTV-3-12	32.7	4.7	0.282088	0.000065	0.001746	0.282052	**-24.6**	**2.3**	-1.3	1097
13S-QTV-3-9	27.7	5.4	0.282091	0.000051	0.001444	0.282061	**-24.6**	**1.8**	-1.2	1087
13S-QTV-3-96	16.6	4.3	0.282091	0.000059	0.000938	0.282071	**-24.5**	**2.1**	0.0	1128
13S-QTV-3-30	30.7	5.0	0.282095	0.000046	0.001607	0.282062	**-24.4**	**1.6**	-1.5	1073
13S-QTV-3-43	30.3	4.9	0.282103	0.000059	0.001641	0.282070	**-24.1**	**2.1**	-1.1	1082
13S-QTV-3-20	33.3	4.8	0.282109	0.000049	0.001737	0.282072	**-23.9**	**1.7**	0.2	1135
13S-QTV-3-32	14.0	4.4	0.282111	0.000053	0.000774	0.282095	**-23.8**	**1.9**	0.3	1100
13S-QTV-3-38	11.5	4.5	0.282127	0.000054	0.000647	0.282114	**-23.3**	**1.9**	0.8	1095
13S-QTV-3-31	15.9	4.1	0.282128	0.000052	0.000878	0.282110	**-23.2**	**1.8**	0.5	1085
13S-QTV-3-33	10.1	5.3	0.282145	0.000048	0.000600	0.282133	**-22.6**	**1.7**	1.1	1078
13S-QTV-3-22	26.7	4.7	0.282128	0.000053	0.001492	0.282097	**-23.2**	**1.9**	0.2	1094

Table A-4. LA-HR-MC-ICP-MS Hf isotopic data for Grenville-age detrital zircon recovered from siliclastic rocks from the central United States. Uncertainties include both random and systematic error reported at 2σ. Samples on zircon with poor age data omitted. Samples listed in red are valid analyses from zircons outside the 1.0-1.3 Ga age range.

Sample	(^{176}Yb + ^{176}Lu) / ^{176}Hf (%)	Volts Hf	^{176}Hf/^{177}Hf	± (2σ)	^{176}Lu/^{177}Hf	^{176}Hf/^{177}Hf (T)	E-Hf (0)	E-Hf (0) ± (2σ)	E-Hf (T)	Age (Ma)
14CO-CORE-1-3	13.7	4.0	0.282177	0.000062	0.000725	0.282162	-21.5	**2.2**	**2.4**	1088
14CO-CORE-1-9	17.1	3.7	0.282151	0.000050	0.001002	0.282126	-22.4	**1.8**	**6.3**	1317
14CO-CORE-1-50	21.5	4.6	0.282309	0.000039	0.001374	0.282280	-16.8	**1.4**	**6.8**	1098
14CO-CORE-1-61	12.2	5.4	0.282315	0.000047	0.000767	0.282300	-16.6	**1.7**	**6.8**	1068
14CO-CORE-2-20	19.5	4.9	0.282088	0.000077	0.001108	0.282060	-24.7	**2.7**	**4.1**	1323
14CO-CORE-2-104	24.1	3.9	0.282250	0.000055	0.001287	0.282223	-18.9	**1.9**	**5.0**	1109
14CO-T-3-23	11.6	4.7	0.282140	0.000043	0.000661	0.282127	-22.8	**1.5**	**1.1**	1086
14CO-T-3-18	9.8	4.2	0.282115	0.000054	0.000561	0.282104	-23.7	**1.9**	**-0.2**	1067
14CO-T-3-58	23.3	4.2	0.282075	0.000047	0.001259	0.282049	-25.1	**1.7**	**-2.0**	1071
14CO-T-3-44	40.7	3.2	0.282237	0.000060	0.002100	0.282193	-19.4	**2.1**	**3.7**	1096
14CO-T-3-26	10.6	3.2	0.282183	0.000049	0.000613	0.282170	-21.3	**1.7**	**3.5**	1127
14CO-T-3-31	15.5	4.3	0.282063	0.000057	0.000887	0.282042	-25.5	**2.0**	**3.0**	1302
14CO-T-3-66	18.0	3.9	0.282166	0.000062	0.001034	0.282143	-21.9	**2.2**	**4.0**	1191
14CO-BS-3-5	30.4	3.9	0.282269	0.000057	0.001627	0.282233	-18.2	**2.0**	**6.8**	1171
14CO-BS-3-9	13.2	4.5	0.282084	0.000046	0.000764	0.282068	-24.8	**1.6**	**-0.4**	1113
14CO-BS-3-23	10.8	4.6	0.282001	0.000045	0.000599	0.281988	-27.7	**1.6**	**-1.2**	1205
14CO-BS-3-32	70.5	3.7	0.282173	0.000063	0.003582	0.282099	-21.7	**2.2**	**0.2**	1090
14CO-BS-3-40	17.4	3.3	0.282255	0.000053	0.000998	0.282233	-18.7	**1.9**	**6.2**	1144
14CO-BS-3-42	9.4	4.9	0.282263	0.000041	0.000517	0.282251	-18.5	**1.5**	**7.2**	1162

Sample	(^{176}Yb + ^{176}Lu) / ^{176}Hf (%)	Volts Hf	$^{176}Hf/^{177}Hf$	± (2σ)	$^{176}Lu/^{177}Hf$	$^{176}Hf/^{177}Hf$ (T)	E-Hf (0)	E-Hf (0) ± (2σ)	E-Hf (T)	Age (Ma)
14CO-BS-3-51	19.3	3.6	0.282227	0.000060	0.001002	0.282205	-19.7	**2.1**	**5.6**	1166
14CO-BS-3-52	12.1	3.8	0.282136	0.000048	0.000679	0.282121	-22.9	**1.7**	**2.9**	1175
14CO-BS-3-68	11.8	4.1	0.282143	0.000058	0.000659	0.282129	-22.7	**2.0**	**1.7**	1113
14CO-BS-3-71	15.2	4.3	0.282151	0.000057	0.000767	0.282134	-22.4	**2.0**	**3.1**	1163
14CO-BS-3-76	19.7	3.2	0.282150	0.000058	0.001102	0.282126	-22.5	**2.0**	**2.6**	1154
14CO-BS-3-89	19.0	4.0	0.282355	0.000057	0.000943	0.282336	-15.2	**2.0**	**8.3**	1081
14CO-BS-3-97	12.5	3.6	0.282038	0.000054	0.000718	0.282024	-26.4	**1.9**	**-2.4**	1095
14CO-BS-3-109	11.8	4.6	0.282055	0.000039	0.000670	0.282041	-25.8	**1.4**	**-1.3**	1113
14MO-LMT-75	11.3	4.7	0.282088	0.000057	0.000637	0.282075	-24.6	**2.0**	**-0.3**	1109
14MO-LMT-77	9.5	4.4	0.282165	0.000064	0.000531	0.282154	-21.9	**2.3**	**2.2**	1096
14MO-LMT-79	16.2	4.5	0.282031	0.000052	0.000890	0.282013	-26.7	**1.8**	**-2.9**	1088
14MO-LMT-14	30.0	4.3	0.282081	0.000048	0.001663	0.282047	-24.9	**1.7**	**-1.9**	1079
14MO-LMT-9	37.7	4.5	0.282097	0.000062	0.002038	0.282056	-24.3	**2.2**	**-1.5**	1083
14MO-LMT-53	17.0	3.9	0.282160	0.000061	0.001054	0.282136	-22.1	**2.2**	**3.6**	1183
14MO-LMT-98	38.9	5.2	0.282074	0.000050	0.002119	0.282030	-25.1	**1.8**	**-2.4**	1086
14MO-LMT-20	12.9	5.0	0.282070	0.000054	0.000708	0.282056	-25.3	**1.9**	**-0.9**	1111
14MO-LMT-49	21.3	4.5	0.282219	0.000067	0.001394	0.282189	-20.0	**2.4**	**4.4**	1137
14MO-LMT-51	26.7	4.2	0.282105	0.000068	0.001462	0.282075	-24.0	**2.4**	**-1.0**	1075
14MO-LMT-38	18.5	4.6	0.282152	0.000044	0.001134	0.282128	-22.4	**1.6**	**1.4**	1098
14MO-LMT-47	18.6	4.8	0.282107	0.000057	0.001095	0.282085	-24.0	**2.0**	**-0.8**	1072
14MO-LMT-40	36.6	4.9	0.282098	0.000052	0.001997	0.282057	-24.3	**1.8**	**-1.3**	1093
14MO-LMT-92	10.9	4.4	0.282133	0.000058	0.000611	0.282121	-23.0	**2.1**	**1.4**	1111
14MO-LMT-61	18.2	5.1	0.282118	0.000051	0.001008	0.282097	-23.6	**1.8**	**0.4**	1103
14MO-LMT-4	9.8	3.7	0.282152	0.000053	0.000566	0.282140	-22.4	**1.9**	**1.5**	1086
14MO-LMT-57	29.5	4.5	0.282011	0.000054	0.001615	0.281978	-27.4	**1.9**	**-4.2**	1086
14MO-LMT-17	12.1	4.8	0.282100	0.000055	0.000685	0.282085	-24.2	**2.0**	**0.0**	1105
SH324BD-22	13.3	4.7	0.281582	0.000053	0.000752	0.281565	-42.5	**1.9**	**-15.5**	1233
SH324BD-19	20.7	4.4	0.282131	0.000062	0.001227	0.282101	-23.1	**2.2**	**4.8**	1289
SH324BD-16	15.6	4.7	0.281886	0.000048	0.000901	0.281868	-31.8	**1.7**	**-7.6**	1110
SH324BD-15	10.0	4.1	0.282287	0.000048	0.000551	0.282277	-17.6	**1.7**	**4.1**	984

Sample	**(^{176}Yb + ^{176}Lu) / ^{176}Hf (%)**	**Volts Hf**	**^{176}Hf/^{177}Hf**	**± (2σ)**	**^{176}Lu/^{177}Hf**	**^{176}Hf/^{177}Hf (T)**	**E-Hf (0)**	**E-Hf (0) ± (2σ)**	**E-Hf (T)**	**Age (Ma)**
SH324BD-13	17.7	4.1	0.282063	0.000053	0.000991	0.282043	-25.5	**1.9**	**-2.3**	1068
SH324BD-12	21.6	3.8	0.282188	0.000064	0.001184	0.282162	-21.1	**2.3**	**4.2**	1170
SH324BD-06	22.7	3.7	0.282016	0.000051	0.001196	0.281991	-27.2	**1.8**	**-3.1**	1115
SH324BD-33	19.7	3.9	0.282322	0.000053	0.001061	0.282303	-16.4	**1.9**	**4.9**	981
SH324BD-34	18.6	4.7	0.282220	0.000059	0.001105	0.282198	-20.0	**2.1**	**2.7**	1049
SH324BD-25	8.5	3.4	0.281911	0.000064	0.000509	0.281899	-30.9	**2.2**	**-3.4**	1246
SH324BD-38	8.4	5.0	0.282316	0.000050	0.000480	0.282306	-16.6	**1.8**	**8.4**	1128
SH324BD-40	14.7	4.6	0.282193	0.000042	0.000887	0.282174	-20.9	**1.5**	**5.1**	1189
SH324BD-41	22.4	3.9	0.282226	0.000045	0.001184	0.282201	-19.8	**1.6**	**4.3**	1112
SH324BD-44	8.4	4.5	0.282123	0.000047	0.000509	0.282111	-23.4	**1.7**	**4.7**	1271
SH324BD-45	12.7	4.1	0.282043	0.000058	0.000799	0.282026	-26.2	**2.0**	**-1.1**	1149
SH324BD-46	17.2	2.7	0.282277	0.000085	0.001226	0.282249	-18.0	**3.0**	**8.1**	1205
SH324BD-51	14.7	4.1	0.282151	0.000056	0.000877	0.282130	-22.4	**2.0**	**4.6**	1237
SH324BD-59	12.8	4.5	0.281895	0.000051	0.000728	0.281881	-31.5	**1.8**	**-8.1**	1068
SH324BD-81	20.2	4.1	0.282143	0.000052	0.001149	0.282116	-22.7	**1.9**	**4.3**	1246
SH324BD-85	9.8	4.7	0.282206	0.000049	0.000596	0.282192	-20.5	**1.7**	**7.8**	1280
SH324BD-84	10.4	4.7	0.282329	0.000045	0.000609	0.282317	-16.1	**1.6**	**7.2**	1059
SH324BD-74	10.4	3.7	0.282260	0.000046	0.000563	0.282248	-18.6	**1.6**	**6.6**	1141
SH324BD-108	9.5	4.4	0.282179	0.000047	0.000523	0.282168	-21.4	**1.7**	**3.2**	1117
SH324BD-109	21.9	2.2	0.282329	0.000081	0.001251	0.282303	-16.1	**2.9**	**7.7**	1102
SH324BD-101	11.2	4.8	0.282210	0.000046	0.000642	0.282197	-20.3	**1.6**	**3.0**	1063
SH324BD-92	22.5	4.3	0.282293	0.000054	0.001195	0.282269	-17.4	**1.9**	**5.6**	1062
SH324BD-99	12.1	4.4	0.282284	0.000059	0.000680	0.282271	-17.7	**2.1**	**5.2**	1044
SH324HO-4	13.7	3.9	0.282284	0.000061	0.000925	0.282266	-17.7	**2.2**	**5.0**	1042
SH324HO-3	23.5	3.2	0.282230	0.000071	0.001284	0.282199	-19.6	**2.5**	**8.2**	1286
SH324HO-6	12.6	3.3	0.282367	0.000072	0.000920	0.282351	-14.8	**2.6**	**6.5**	974
SH324HO-9	32.0	2.0	0.282179	0.000106	0.001912	0.282137	-21.4	**3.8**	**3.1**	1158
SH324HO-79	19.3	3.9	0.282190	0.000057	0.001295	0.282158	-21.0	**2.0**	**7.5**	1320
SH324HO-87	21.4	2.5	0.282290	0.000076	0.001339	0.282262	-17.5	**2.7**	**6.6**	1117
SH324HO-53	22.1	4.4	0.282199	0.000058	0.001233	0.282172	-20.7	**2.1**	**4.6**	1172

Sample	(^{176}Yb + ^{176}Lu) / ^{176}Hf (%)	Volts Hf	^{176}Hf/^{177}Hf	± (2σ)	^{176}Lu/^{177}Hf	^{176}Hf/^{177}Hf (T)	E-Hf (0)	E-Hf (0) ± (2σ)	E-Hf (T)	Age (Ma)
SH324HO-71	25.9	3.1	0.282266	0.000081	0.001619	0.282234	-18.3	**2.9**	**4.0**	1050
SH324HO-73	22.4	3.8	0.282357	0.000047	0.001680	0.282325	-15.1	**1.7**	**6.7**	1026
SH324HO-90	4.9	4.7	0.282182	0.000042	0.000361	0.282175	-21.3	**1.5**	**2.6**	1078
SH324HO-18	16.4	4.0	0.282154	0.000065	0.001155	0.282131	-22.3	**2.3**	**0.6**	1059
SH324HO-17B	11.6	3.9	0.282314	0.000048	0.000662	0.282302	-16.7	**1.7**	**4.5**	962
SH324HO-24	9.4	4.2	0.282089	0.000046	0.000701	0.282075	-24.6	**1.6**	**-1.8**	1040
SH324HO-50	21.7	3.6	0.282293	0.000053	0.001199	0.282268	-17.4	**1.9**	**6.2**	1091
SH324HO-46	14.8	3.5	0.282155	0.000061	0.000947	0.282138	-22.3	**2.2**	**-1.3**	962
SH324HO-58	8.3	3.5	0.282140	0.000050	0.000464	0.282131	-22.8	**1.8**	**-0.4**	1016
SH324HO-74	8.3	4.6	0.282130	0.000041	0.000472	0.282120	-23.1	**1.4**	**3.2**	1192
SH324HO-43	19.9	4.6	0.282243	0.000049	0.001260	0.282216	-19.2	**1.7**	**5.1**	1123
SH324HO-44B	12.5	3.8	0.282090	0.000042	0.000685	0.282077	-24.6	**1.5**	**-1.6**	1046
SH324HO-84	5.3	5.7	0.282159	0.000047	0.000357	0.282151	-22.1	**1.7**	**3.2**	1143
SH324HO-41	21.5	4.1	0.282245	0.000056	0.001358	0.282218	-19.1	**2.0**	**3.8**	1065
SH324HO-39	26.9	3.8	0.282338	0.000048	0.001390	0.282309	-15.8	**1.7**	**8.2**	1114
SH324HO-26	5.7	5.1	0.282219	0.000060	0.000347	0.282211	-20.0	**2.1**	**5.9**	1168
SH324HO-30	16.7	4.5	0.282291	0.000049	0.000994	0.282270	-17.5	**1.7**	**6.5**	1099
SH324HO-34	40.8	2.8	0.282239	0.000066	0.001985	0.282198	-19.3	**2.3**	**4.0**	1103
SH324HO-35	21.5	4.6	0.282256	0.000039	0.001247	0.282230	-18.7	**1.4**	**4.7**	1087
SH324HO-60	11.4	4.0	0.282221	0.000049	0.000643	0.282206	-20.0	**1.7**	**7.4**	1240
SH324VE-1	15.6	3.6	0.282326	0.000086	0.000996	0.282304	-16.2	**3.0**	**9.1**	1164
SH324VE-41	11.9	3.3	0.282162	0.000059	0.000701	0.282147	-22.0	**2.1**	**3.2**	1151
SH324VE-4	20.0	4.0	0.282356	0.000058	0.001301	0.282330	-15.2	**2.1**	**7.8**	1066
SH324VE-6	8.9	4.7	0.282377	0.000069	0.000549	0.282366	-14.4	**2.4**	**8.7**	1046
SH324VE-17	14.4	4.8	0.282399	0.000061	0.000785	0.282385	-13.6	**2.2**	**7.7**	974
SH324VE-18	16.9	4.6	0.282283	0.000056	0.000992	0.282263	-17.7	**2.0**	**6.5**	1115
SH324VE-32	54.2	3.5	0.282227	0.000061	0.002786	0.282168	-19.7	**2.2**	**3.5**	1128
SH324VE-40	20.4	4.5	0.282215	0.000059	0.001042	0.282192	-20.2	**2.1**	**5.0**	1156
SH324VE-34	18.2	3.9	0.282341	0.000070	0.001069	0.282320	-15.7	**2.5**	**7.2**	1053
SH324VE-51	10.7	4.2	0.282061	0.000059	0.000612	0.282044	-25.6	**2.1**	**6.6**	1456

Sample	(^{176}Yb + ^{176}Lu) / ^{176}Hf (%)	Volts Hf	$^{176}Hf/^{177}Hf$	± (2σ)	$^{176}Lu/^{177}Hf$	$^{176}Hf/^{177}Hf$ (T)	E-Hf (0)	E-Hf (0) ± (2σ)	E-Hf (T)	Age (Ma)
SH324VE-44	14.7	4.2	0.282293	0.000060	0.000992	0.282273	-17.4	**2.1**	**5.4**	1048
SH324VE-47	8.9	4.5	0.282304	0.000049	0.000544	0.282293	-17.0	**1.7**	**6.1**	1048
SH324VE-59	28.9	3.2	0.282192	0.000088	0.001854	0.282148	-21.0	**3.1**	**5.4**	1241
SH324VE-24	18.9	4.9	0.281990	0.000045	0.001056	0.281965	-28.1	**1.6**	**-1.4**	1230
SH324VE-58	13.7	4.2	0.282307	0.000063	0.000864	0.282289	-16.9	**2.2**	**7.1**	1099
SH324VE-63	12.0	4.0	0.282129	0.000062	0.000712	0.282112	-23.2	**2.2**	**4.2**	1244
SH324VE-65	26.4	2.1	0.282185	0.000127	0.001676	0.282148	-21.2	**4.5**	**4.0**	1183
SH324VE-68	15.4	4.3	0.282299	0.000060	0.000886	0.282281	-17.2	**2.1**	**6.3**	1077
SH324VE-76	10.6	4.4	0.282322	0.000073	0.000714	0.282308	-16.4	**2.6**	**6.7**	1051
SH324VE-81	21.6	2.6	0.282299	0.000091	0.001495	0.282269	-17.2	**3.2**	**5.3**	1053
SH324VE-82	9.3	2.1	0.282358	0.000103	0.000678	0.282344	-15.1	**3.6**	**9.8**	1134
SH324VE-80	14.3	3.8	0.282303	0.000076	0.000784	0.282286	-17.0	**2.7**	**7.9**	1139
SH324VE-83	17.9	2.0	0.282372	0.000091	0.001270	0.282338	-14.6	**3.2**	**15.8**	1403
SH324VE-86	13.1	4.2	0.282121	0.000051	0.000820	0.282103	-23.5	**1.8**	**1.4**	1138
SH324VE-89	9.4	4.5	0.282146	0.000068	0.000542	0.282134	-22.6	**2.4**	**2.7**	1145
SH324VE-90	12.0	4.8	0.282306	0.000057	0.000651	0.282293	-16.9	**2.0**	**5.7**	1028
SH324VE-97	15.5	3.2	0.282203	0.000055	0.000869	0.282182	-20.6	**1.9**	**7.6**	1286
SH324VE-98	9.8	4.0	0.282271	0.000067	0.000562	0.282259	-18.2	**2.4**	**6.7**	1128
SH324VE-94	19.1	4.1	0.282349	0.000069	0.001230	0.282324	-15.4	**2.5**	**7.2**	1047
SH324VE-85	9.8	4.5	0.282368	0.000062	0.000559	0.282356	-14.8	**2.2**	**9.2**	1087
SH324VE-92	18.3	4.7	0.281984	0.000048	0.001399	0.281956	-28.3	**1.7**	**-6.1**	1035

Appendix B: Core Logs

Here are the detailed core logs of Denver-Julesburg Basin Sandstones provided by Nighthawk Energy, LLC. Core logs have been converted to digital images from hand written assessment of cores. Sample location depths are included. Sedimentary analysis of lithology, grain size, bioturbation, and presence of glauconite was used to make interpretations on the depositional environment. Lithofacies 1 and 2, described in the main text, are marked here (D. Budd, personal communication. Below is the explanation for all core logs. Glc = Glauconite, BT = Bioturbation.

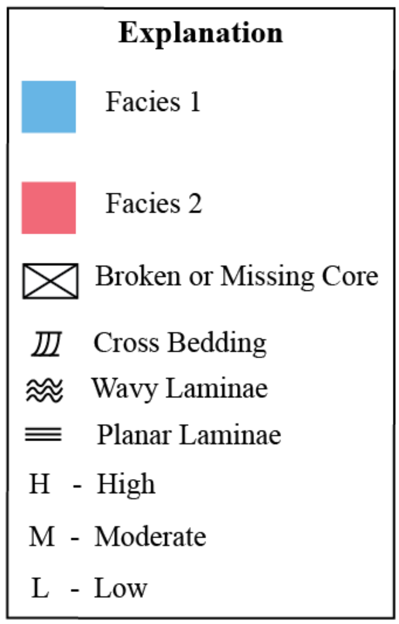

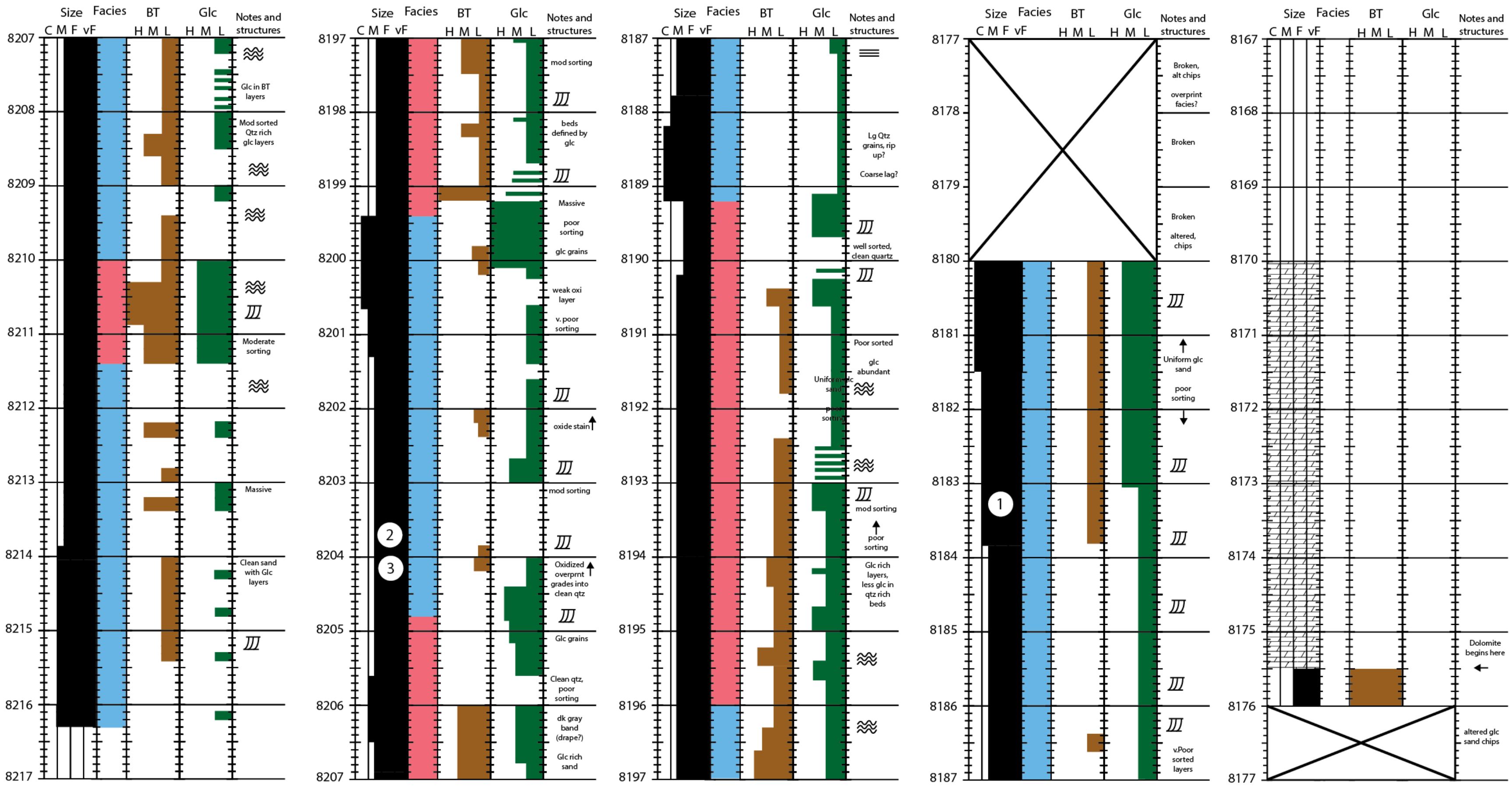

Figure B-1. Schematic core logs for the Big Sky Core from Lincoln County, Colorado. Numbers indicate sample label (14CO-BS-X) and core location.

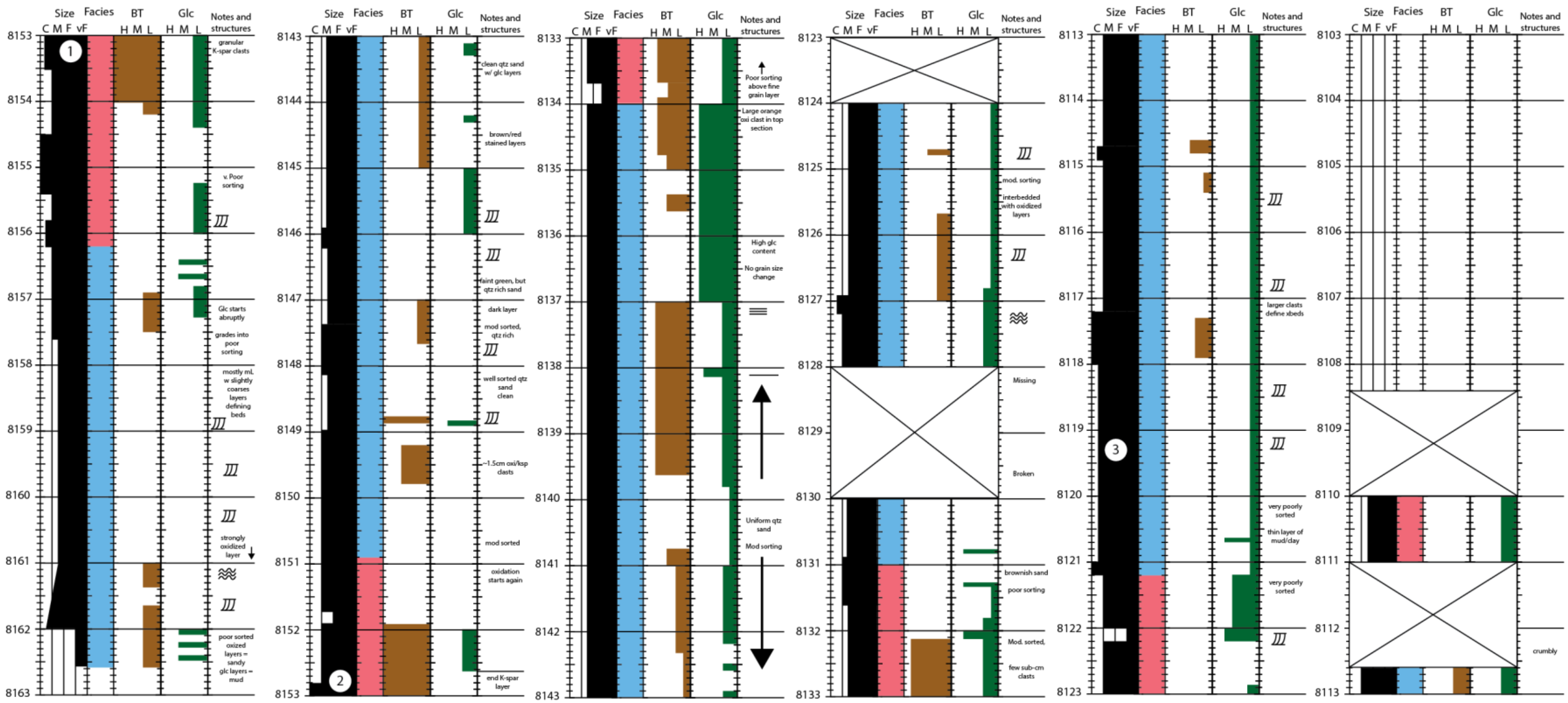

Figure B-2. Schematic core logs for the Taos Core from Lincoln County, Colorado. Numbers indicate sample label (14CO-T-X) and core location.

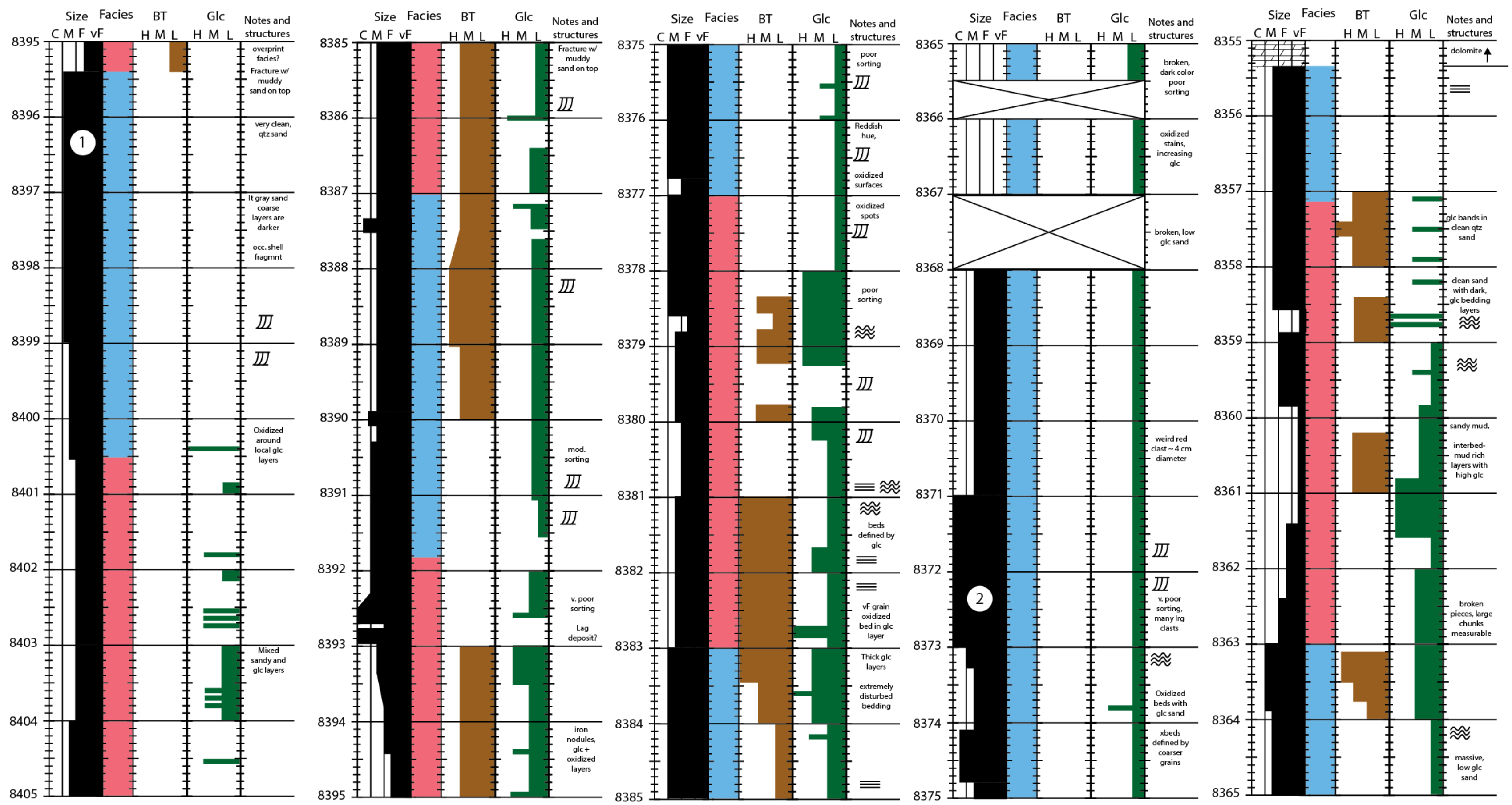

Figure B-3. Schematic core logs for the Jackson Hole Core from Lincoln County, Colorado. Numbers indicate sample label (14CO-JH-X) and core location.